Author:
Fletcher-Jones, Alexandra S

Title:
The C-terminal helix 9 motif in rat cannabinoid receptor type 1 regulates axonal trafficking and surface expression

THE C-TERMINAL HELIX 9 MOTIF IN RAT CANNABINOID RECEPTOR TYPE 1 REGULATES AXONAL TRAFFICKING AND SURFACE EXPRESSION

Alexandra Sian Fletcher-Jones

School of Biochemistry

September 2019

A dissertation submitted to the University of Bristol in accordance with the requirements for award of the degree of Doctor of Philosophy in the Faculty of Life Sciences.

45,377 words

ABSTRACT

The cannabinoid type one receptor (CB1R) is one of the most abundant G-protein coupled receptors (GPCRs) in the central nervous system. CB1R activation at the presynaptic terminal by ligand released retrogradely from the postsynapse dampens down neurotransmitter release. Consistent with its presynaptic role, CB1R is only stably surface expressed in axons. How this tightly regulated axonal surface polarity is established and maintained is unclear.

To address this question, I applied retention using selective hooks (RUSH) to visualise the trafficking of CB1R from biosynthesis to mature polarised localisation in cultured rat hippocampal neurons. I show that axonal surface polarity is initially established through axonally biased delivery of newly synthesized CB1R by the secretory pathway. Axonal surface polarity is subsequently enhanced and maintained by selective removal from the dendritic membrane and stable retention at the axonal surface.

This dual mechanism is mediated by the CB1R C-terminus and involves the Helix 9 (*H9*) domain. Removal of the *H9* domain ($CB1R^{\Delta H9}$) both increases secretory pathway delivery to dendrites and decreases surface stability. Furthermore, $CB1R^{\Delta H9}$ is more sensitive to agonist-induced internalisation and less efficient at downstream signalling than $CB1R^{WT}$.

A screen for *H9* interacting proteins highlighted SH3-containing GRB2-like protein 3-interacting protein 1 (SGIP1), a protein linked to clathrin-mediated endocytosis. SGIP1 stabilises CB1R at the surface, likely through interaction with the *H9* domain.

Together, these results shed new light on how polarity of CB1R is mediated and indicate that the C-terminal *H9* domain plays key roles in this process. This is important because defining the trafficking pathways and protein interactions that mediate axonal CB1R localisation could provide novel targets to enhance or reduce ECS signalling without the need to directly activate or block the receptor.

ACKNOWLEDGEMENTS

First and foremost, I am hugely grateful to Jeremy for being a wonderful supervisor. Your sage advice ("Why don't you just try it and see what happens?") and belief in me have truly built my confidence in myself as a researcher. I have learned a lot during my PhD and enjoyed learning it due to the supportive, humorous, and forgiving environment that you foster.

A big thank you to all the postdocs – Kev, Suko, Ash, Dan, Ruth, and Nadiia – for their advice and support and for answering my stupid questions with a straight face. A special thanks to Suko for somehow holding the lab together by sheer force of will, despite floods and mite infestations (two of them!), cold-rooms-turned-to-saunas and our general collective ineptitude (only in the Henley lab, eh?). A huge thanks Ash, who taught me everything I know about imaging, and a massive thanks to Kev, who taught me everything I know about everything else with a great deal of patience and humour.

To Laura, Sonam, Vanilla, Jodie, and Caroline, thank you for many a coffee morning and tea break – you kept me from going (completely) insane. A special thanks to Laura, the incorrigible troublemaker and my constant tea buddy over the past four years – I'll sorely miss your shenanigans and our tea breaks (I guess this means we'll actually have to do some work now, huh?). Thank you to everyone else in the Henley/Hanley lab, past and present, and my housemates throughout the years – Sonam, Lea, Rachel, Joe, and Maria – for providing tons of guidance, positive encouragement, and entertainment.

To Mummy and Daddy and my (not so) little brother, Huw, thank you for your unwavering love, belief, and support that traverses loudly and clearly across countries and continents (can you hear me now?). This is for you (and I expect you to refer to me as 'Dr' from now on).

AUTHOR'S DECLARATION

Part of the content of this thesis (especially chapters 3 and 4) has been published in a paper in which I am the first author: (Fletcher-Jones A, Hildick KL, Evans AJ, Nakamura Y, Wilkinson KA, Henley JM. 2019. The C-terminal helix 9 motif in rat cannabinoid receptor type 1 regulates axonal trafficking and surface expression. Elife 8. doi:10.7554/eLife.44252). A copy of this publication can be found in Appendix I.

I declare that the work in this dissertation was carried out in accordance with the requirements of the University's Regulations and Code of Practice for Research Degree Programmes and that it has not been submitted for any other academic award. Except where indicated by specific reference in the text, the work is the candidate's own work. Work done in collaboration with, or with the assistance of, others, is indicated as such. Any views expressed in the dissertation are those of the author.

SIGNED: ..... DATE:.....

TABLE OF CONTENTS

LIST OF FIGURES

LIST OF TABLES

ABBREVIATIONS

Δ^9-THC	Δ^9-tetrahydrocannabinoil
2-AG	2-Arachidonoylglycerol
7-TM	7 transmembrane receptor
AC	adenylyl cyclase
AcD	axon carrying dendrite
ACEA	Arachidonyl-2'-chloroethylamide
AIS	axon initial segment
AM281	1-(2,4-Dichlorophenyl)-5-(4-iodophenyl)-4-methyl-N-4-morpholinyl-1H-pyrazole-3-carboxamide
amp	ampicillin
AMPA	γ-amino-3-hydroxy-5-methylisoaxzole-4-propionic
anandamide	N-arachidonoylethanolamine (AEA)
ANOVA	Analysis of variance
AP-1/-2/-3/-4	adaptor protein-1-2/-3/-4
APS	Ammonium persulfate
ATP/ADP	Adenosine tri-/di-phosphate
BFA	Brefeldin A
BHK	Baby hamster kidney
BSA	Bovine serum albumin
C. elegans	Caenorhabditis elegans
Ca^{2+}	calcium ion
cAMP	cyclic adenosine monophosphate
CB1R	cannabinoid receptor type I
CB2R	cannabinoid receptor type I
CBR	cannabinoid receptor
CD4	cluster of differentiation 4
CIP	Calf Intestinal Alkaline Phosphatase
CME	clathrin-mediate endocytosis
CNS	central nervous system
CO_2	carbon dioxide
Co-IP	co-immunoprecipitation
COP-II	coat-protein complex II
COS-7	African Green Monkey Kidney
CRIP1a/b	Cannabinoid receptor interacting protein 1a/1b
ctCB1R	cannabinoid receptor type 1 C-terminal tail
cy-2/-3/-5	cyanine-2/-3/-5
DAG	diacylglycerol
DAGLα/β	diacylglycerol lipases α/β
DAPI	4',6-diamidino-2-phenylindole
dH_2O	distilled water
DIV	days *in vitro*
DMEM	Dulbecco's Modified Eagle's Medium
DN	dominant negative
DNA	deoxyribonucleic acid
dNTPs	deoxynucleotide triphosphates
DO	dendritic origin
E. coli	*Escherichia coli*
E17/18	Embryonic day 17/18
ECACC	European Collection of Cell Cultures
eCB(s)	endocannabinoid(s)
ECL	enhanced chemiluminescence
EGFP	enhanced green fluorescent protein
EGFR	epidermal growth factor receptor
EM	electron microscopy
ER	endoplasmic reticulum

ERES	endoplasmic reticulum exit sites
ERK1/2	extracellular signal-regulated kinases 1/2
ERGIC	ER-Golgi intermediate compartment
FAAH	fatty acid amine hydrolase
FBS	Foetal Bovine serum
GAPDH	Glyceraldehyde 3-phosphate dehydrogenase
GASP1	G-protein coupled receptor associated sorting protein 1
GCA	Golgicide A
GEF	guanine nucleotide exchange factors
GFP	green fluorescent protein
GIRK	G-protein mediated inward rectifying potassium channels
goi	gene of interest
GPCR	G-protein-coupled receptor
GRIP	glutamate receptor interacting protein
GRK	G protein receptor kinase
GST	glutathione-S-transferase
GTP/GDP	guanosine tri-/di-phosphate
H8	Helix 8
H9	Helix 9
HA	Hemagglutinin
HBS	HEPES buffered saline
HBSS	Hank's Balance Salt Solution
HEK293T	Human Embryonic Kidney
HeLa	Henrietta Lacks
HRP	horseradish peroxidase
HS	Horse serum
IgG	Immunoglobulin G
iGluR	ionotropic glutamate receptor
IgY	Immunoglobulin Y
Ins(1,4,5)P3	inositol-1,4,5-trisphosphate (Ins(1,4,5)P3)
IP	immunoprecipitation
K^+	potassium ion
kan	kanamycin
L1/NgCAM	L1/neuron-glia cell adhesion molecule
LAMP1	Lysosome associated sorting protein 1
LB	Luria-Bertani
MAGL	monoacylgylcerol lipase
MAP2	microtubule associated protein 2
MAPK	mitogen-activated protein kinase
mGluR	metabatropic glutamate receptor
$MgSO_4$	magnesium sulphate
MP	membrane phospholipids binding domain
µHD	µ homology domain
Na^+	sodium ion
NaCl	Sodium chloride
N/S	not significant
NH_4Cl	ammonium chloride
O_2	Oxygen
PBS	Phosphate Buffered Solution
PCR	Polymerase Chain Reaction
PDZ	postsynaptic density 95/disc large/zonula occludens-1
PFA	paraformaldehyde
PKA	Protein kinase A
PKC	Protein Kinase C
PLD	phospholipase D
PLL	Poly-L-lysine
PDL	Poly-D-lysine
PRD	proline rich domain
PTM	post translational modification
PTX	pertussis-toxin

PVDF	polyvinylidene difluoride
rER	rough endoplasmic reticulum
RNA	ribonucleic acid
RNase	ribonucleases
RUSH	retention using selective hooks
ROI	region of interest
SBP	streptavidin binding peptide
SCR	scrambled
SDS	sodium dodecyl sulphate
SDS-PAGE	sodium dodecyl sulphate-polyacrylamide gel electrophoresis
SEP	Super-ecliptic pHluorin
SGIP1	SH3-containing GRB2-like protein 3-interacting protein 1
shRNA	short hairpin RNA
SO	somatic origin
SP	signal peptide
SRP	signal recognition particle
Strep	streptavidin
TEMED	Tetramethylethylenediamine
TGN	*trans*-Golgi network
TM	transmembrane
TMT	tandem mass tagging
WT	wild-type
βME	β-mercaptoethanol

µL	microlitre
µM	micromolar
µm	micron
bp	base pairs
g	gram
hr	hour(s)
kb	kilobase
kV	kilovolts
M	Molar
mg	milligram
min	minute(s)
mL	millilitre
mm	millimetre
mM	millimolar
MW	molecular weight
ng	nanogram
rpm	revolutions per minute
RT	room temperature
s	second(s)
Tm	melting temperature
V	Volt
v/v	volume per volume
vol	volume
w/v	weight per volume

Chapter 1 – INTRODUCTION

1.1 NEURONAL POLARITY

Neurons are highly polarised cells with complex morphologies. Neurons generally possess long processes, typically multiple dendrites and a single axon, which extend far from the soma – axons of spinal motor neurons extend up to a meter away from the soma (Bonifacino, 2014). Dendrites receive information, the soma integrates information, and the axon passes on information in the form of an action potential (**Figure 1-1**). Each compartment requires distinct receptors, ion channels, structural proteins, cytosolic proteins, etc. that must be sorted, targeted to, and retained in the correct location, often far away from the cell body, for the proper function of the neuron (Bentley and Banker, 2016). Other specialised structural elements within the compartments – e.g. postsynaptic densities, the axon initial segment, nodes of Ranvier, internodes, presynaptic terminals, and axonal growth cones – also require the strict and accurate control of local composition.

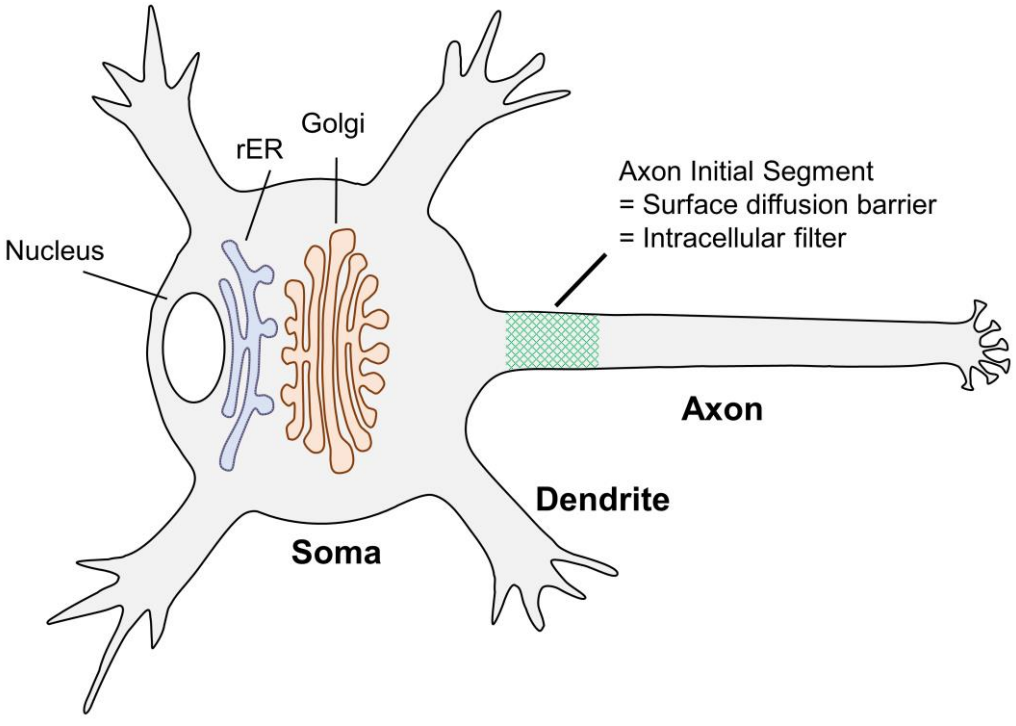

Figure 1-1 Neurons are polarised cells.

Dendrites receive information, the soma integrates information, and the axon passes information on. The axon initial segment acts as a surface diffusion barrier and intracellular filter to separate the somatodendritic compartment from the axon. The secretory pathway machinery – the rough endoplasmic reticulum (rER) and the Golgi apparatus are in the somatodendritic compartment.

1.1.1 Membrane trafficking

Broadly, neurons are separated into the somatodendritic compartment and the axonal compartment, separated by the axon initial segment (AIS; **Figure 1-1**). Transmembrane receptors required for each compartment are trafficked by vesicular transport. *De novo* transmembrane receptors are delivered to the plasma membrane by the secretory pathway, which is located in the somatodendritic compartment (**Figure 1-1** and **Figure 1-2**). Surface expressed transmembrane receptors can be retrieved from the plasma membrane of either compartment by endocytosis (**Figure 1-3** and **Figure 1-4**). The *trans*-Golgi Network (TGN) of the secretory pathway and the endosomal system constitute the main sorting stations for polarised transmembrane proteins.

1.1.1.1 Secretory pathway

1.1.1.1.1 Endoplasmic Reticulum (ER)

Synthesis begins in the rough endoplasmic reticulum (rER), the ribosome studded matrix of ER responsible for protein translation (**Figure 1-2**; (Reid and Nicchitta, 2015). The N-terminus of transmembrane proteins generally comprises of a cleavable signal peptide that is recognised by the signal recognition particle (SRP) as it is emerges from the ribosome (Zheng and Gierasch, 1996; Nyathi et al., 2013; Janda et al., 2010). The SRP then directs the nascent protein to the translocon pore Sec61, which translocates the peptide across the ER membrane co-translationally, threading the transmembrane domains according to its topology (Nyathi et al., 2013; von Heijne, 2006; Janda et al., 2010). After delivery to the translocon, the signal peptide is cleaved to produce the mature protein (Nyathi et al., 2013; Janda et al., 2010; Auclair et al., 2012). N-linked glycosylation, the addition of glycans to asparagine residues, occurs by resident ER enzymes to aid the correct folding and stability of the transmembrane protein (Hanson et al., 2009; Live et al., 1996; Ruiz-Canada et al., 2009). Proteins must be correctly folded to exit the ER or they are sent for degradation by ER associated protein degradation (ERAD; (Guerriero and Brodsky, 2012)). The correctly folded protein then leaves the ER at specialised sites called ER exit sites (ERES; (Langhans et al., 2012)) by vesicular transport in COPII-coated vesicles, traveling via the ER-Golgi intermediate compartment (ERGIC) to the Golgi (Stagg et al., 2006; Fath et al., 2007).

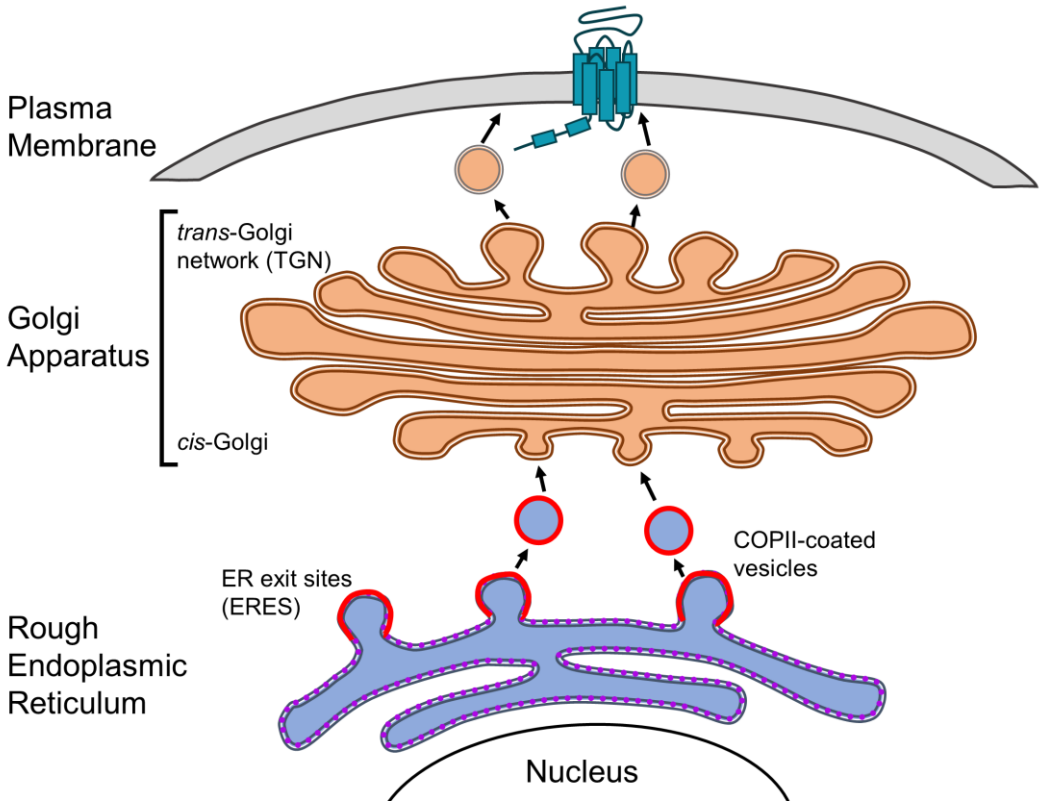

Figure 1-2 Schematic of the canonical secretory pathway.

Plasma membrane proteins are synthesised, processed, and correctly folded in the rough endoplasmic reticulum (rER). Cargo leaves the ER at ER exit sites (ERES) by vesicular transport in COPII-coated vesicles to the *cis* face of the Golgi Apparatus where it is further modified. The *trans* face of the Golgi network (TGN) acts as a sorting station, sending cargo to its proper location in the plasma membrane or endosomal system.

1.1.1.1.2 Golgi Apparatus

Cargo enters the Golgi at the *cis* face, traverses the Golgi cisternae, and exits at the *trans*-Golgi network (TGN) (**Figure 1-2**; (Klumperman, 2011)). Cargo 'matures' as it traverses the cisternae, undergoing additional modifications, including the processing of the glycans added by the ER during N-linked glycosylation, resulting in a mature glycosylation profile (Kornfeld and Kornfeld, 1985). The TGN acts as a central sorting station, sending cargo to the plasma membrane as well as the endosomal system (Rothman and Simons, 1981).

How cargo traffics within the Golgi is controversial and two different models have been proposed: the vesicular transport model and the cisternae maturation model (Martínez-Alonso et al., 2013). The vesicular transport model proposes that cargo is packaged into vesicles to move along to the next static stack following a *cis-medial-trans* trajectory (Martínez-Alonso et al., 2013). The cisternae maturation model suggests that the cisternae themselves are dynamic, moving with their

cargo as a whole to the *trans* side, (Martínez-Alonso et al., 2013). These models are not mutually exclusive and may work in tandem (Pelham and Rothman, 2000; Rabouille and Klumperman, 2005; Luini, 2011).

1.1.1.2 Endocytosis

Transmembrane proteins are removed from the plasma membrane by endocytosis. Several different pathways for of endocytosis exist (see (Doherty and McMahon, 2009) for a review), but clathrin-mediated endocytosis (CME) is the best understood (**Figure 1-3**).

1.1.1.2.1 Clathrin-mediated endocytosis (CME)

During CME, cargo and docking factors (e.g. phosphoinositides) recruit adaptor complex 2 (AP-2), a heterotetrameric complex consisting of α, β2, μ2, and σ2 subunits (Guardia et al., 2018). AP-2 in turn recruits clathrin, a three-legged scaffold protein, forming clathrin-coated pits. The membrane scission protein dynamin pinches off the neck of the pit to form a clathrin coated vesicle. See (Mousavi et al., 2004) for a review.

1.1.1.2.2 The endosomal system

The endosomal system constitutes another complex and interconnected sorting station, sorting cargo either back to the plasma membrane (recycling), back to the TGN, or to lysosomes for degradation (Cullen and Steinberg, 2018; Cullen, 2008). The endosomal system can be functionally compartmentalised into ‘Rab domains’ (**Figure 1-4**). Rab proteins are small GTPases that act as membrane organisers and different Rabs occupy distinct types of endosomal compartments (e.g. Rab5 = early endosome, Rab 7 = late endosome etc.; (Sönnichsen et al., 2000; Zerial and McBride, 2001)).

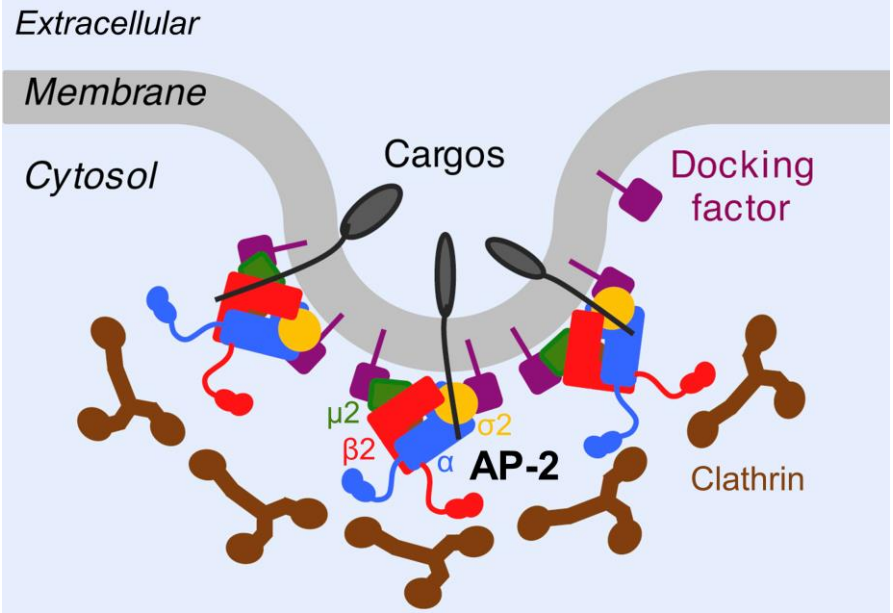

Figure 1-3 Schematic of clathrin mediated endocytosis (CME).

Adaptor protein complex 2 (AP-2) is made up of four subunits: α, β2, μ2, and σ2. AP-2 binds cargo and docking factors (phosphoinositides) and recruits clathrin to form clathrin-coated pits.

Figure adapted from (Guardia et al., 2018).

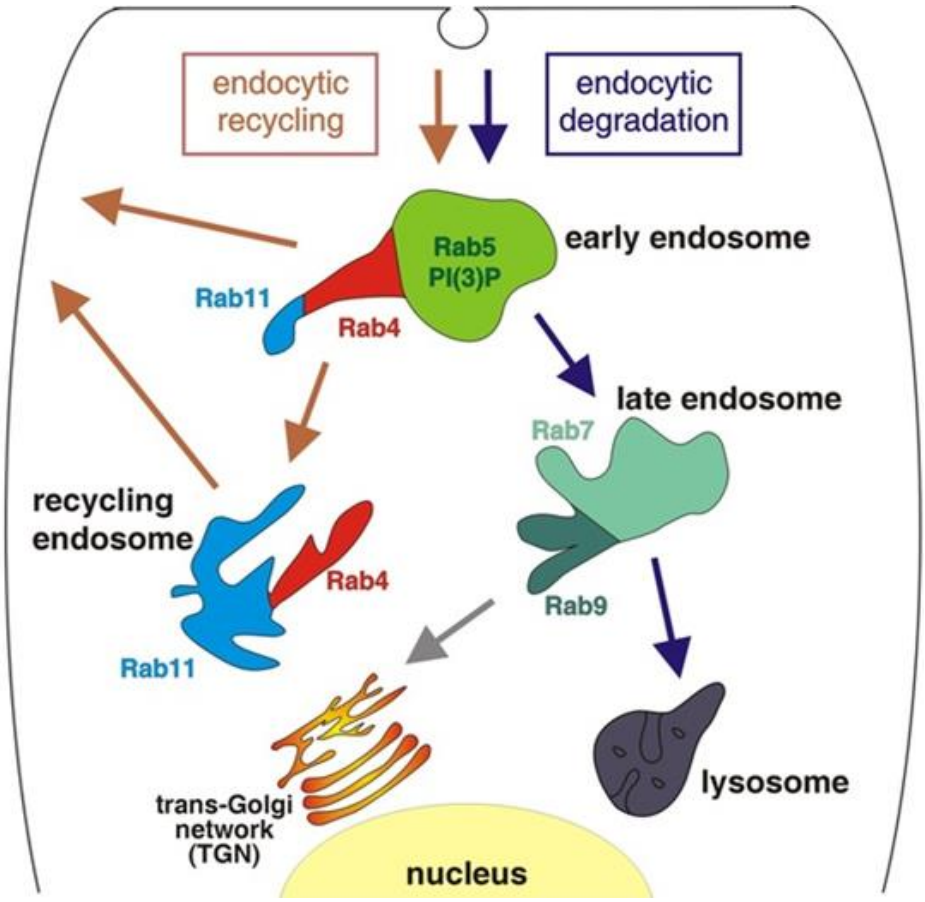

Figure 1-4 The endocytic system compartmentalised by Rab GTPase 'domains'.

Figure from http://zerial.mpi-cbg.de/page/project-rab-gtpases; (Sönnichsen et al., 2000; Zerial and McBride, 2001).

1.1.2 Polarised trafficking

1.1.2.1 Somatodendritic sorting signals

Sorting of polarised cargo in the TGN and endosomal system relies on intrinsic sorting motifs usually located in the C-terminus or intracellular loops of the transmembrane protein. Several canonical dileucine-like and tyrosine sorting motifs and non-canonical motifs have been identified for sorting cargo to dendrites (see (Bentley and Banker, 2016) for a review). Sorting signals for axonal proteins are far less understood and no canonical sorting signals have been identified (Bentley and Banker, 2016).

1.1.2.2 Adaptor proteins sort polarised cargo

Sorting and packaging of axonal and somatodendritic cargo into distinct vesicles occurs via binding of specific adaptor protein complexes to sorting signals (**Figure 1-5**; (Bonifacino, 2014; Guardia et al., 2018)). There are 5 types of adaptor complexes (AP-1 to AP-5), each made up of 4 subunits (see **Figure 1-3** for example), and each with a characteristic distribution, signal recognition ability, and function (Guardia et al., 2018).

AP-1 mediates sorting of somatodendritic proteins, budding off from both the TGN and endosomes in the soma to traffic to the plasma membrane (Margeta et al., 2009; Farías et al., 2012; Dwyer et al., 2001; Li et al., 2016). Furthermore, AP-1 retrieves somatodendritic proteins from the axon by retrograde transport (Margeta et al., 2009). AP-4 also sorts a subset of somatodendritic proteins from the TGN (Matsuda et al., 2008).

Axonal sorting is less well understood, although AP-3 is reported to sort axonal proteins from the TGN in *C. elegans* (Li et al., 2016). AP-3 has other specialised axonal functions including contributing to the generation of synaptic vesicles from synaptic vesicle precursors (Nakatsu et al., 2004; Salazar et al., 2004).

1.1.2.3 Polarised vesicular transport

Once cargo is sorted into somatodendritic or axonal vesicles, the vesicles themselves need to be trafficked to the right compartment. Vesicle trafficking is driven by motors proteins that travel along specific cytoskeletal tracks. The organisation of the neuronal cytoskeleton plays a vital role in establishing and maintaining polarity (see (Kapitein and Hoogenraad, 2011) for a review).

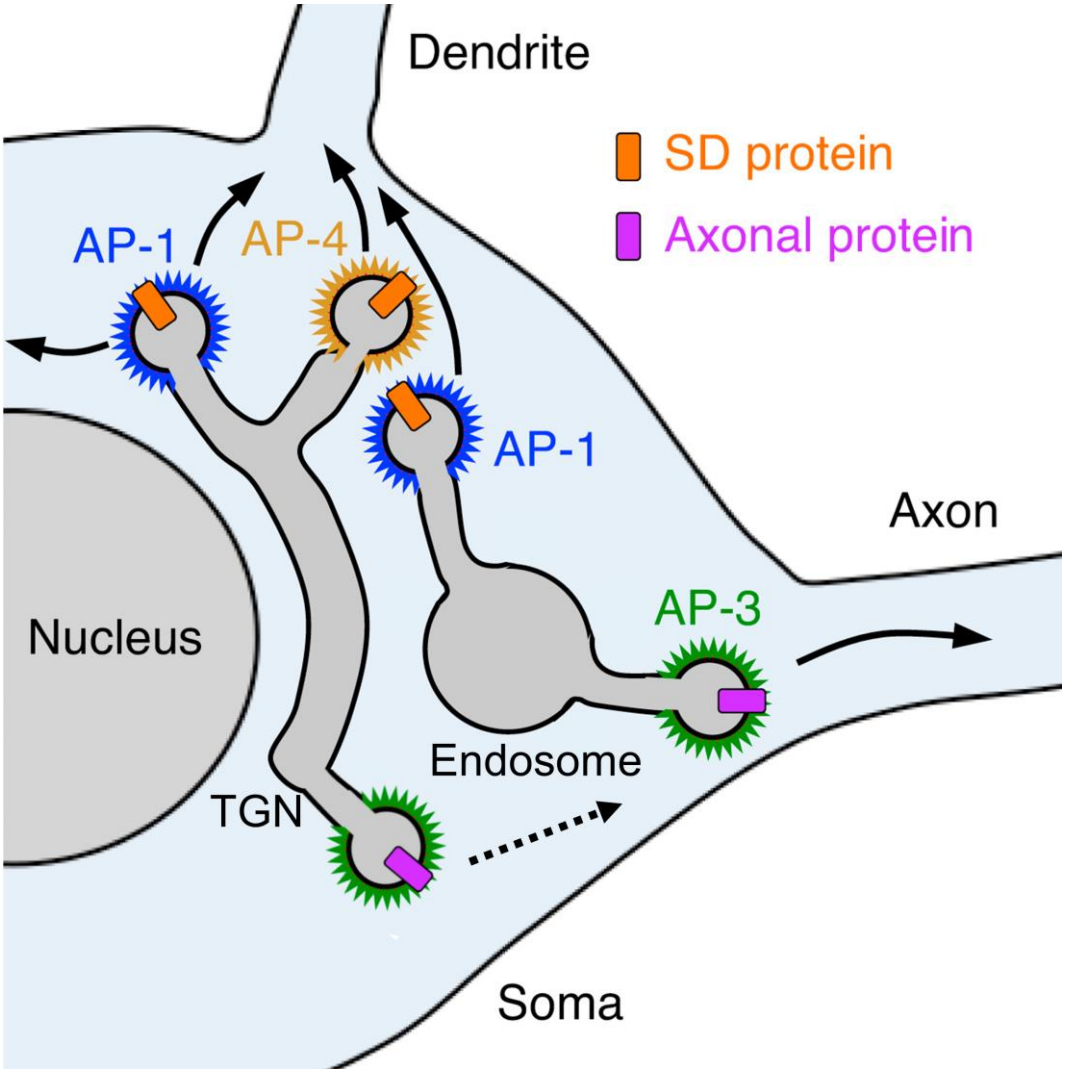

Figure 1-5 Role of adaptor proteins in polarised sorting of cargo.

Adaptor proteins sort cargo from TGN and the endosomal network. Dendritic cargo is sorted by AP-1 and AP-4 whereas axonal cargo is sorted by AP-3. Recent evidence from *C. elegans* suggests that AP-3 can sort axonal cargo from the TGN (dotted line arrow; (Li et al., 2016)).

Figure adapted from (Guardia et al., 2018).

1.1.2.3.1 The axon initial segment (AIS)

The axon initial segment (AIS) is a specialised segment incorporating the first 30-50 µm of the axon that separates the somatodendritic compartment from the axonal compartment. While its main function is cluster and maintain a high density voltage gated ion channels in order to initiate action potentials, the AIS also plays an important function as a surface diffusion barrier and intracellular filter, only allowing in vesicles with axonal motor proteins, and refusing entry for dendritic proteins driven by dendritic motor proteins (**Figure 1-6**; (Leterrier and Dargent, 2014; Song et al., 2009; Farias et al., 2015).

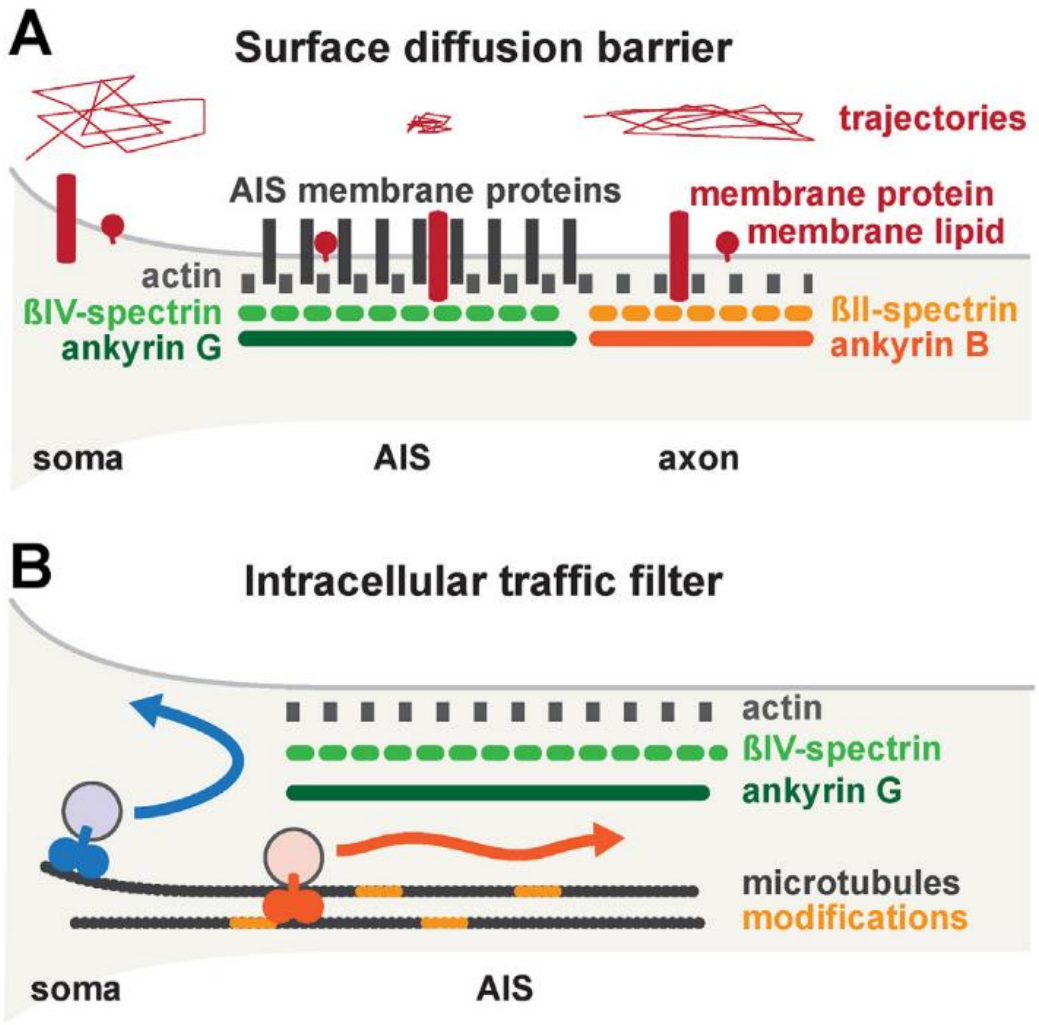

Figure 1-6 The axon initial segment acts as a surface diffusion barrier and intracellular filter.

(**A**) **The AIS diffusion barrier**. Lipids and membrane proteins (red) diffusion is impeded in the AIS, due to corralling from the submembrane scaffold (green) and the concentration of AIS membrane proteins (grey). Diffusion along distal axon and soma is less restricted, as measured from trajectories of individual molecules (above, red), despite the presence of the distal axon ankB/βII-spectrin scaffold (orange).

(**B**) **The AIS traffic filter**. Vesicles containing somatodendritic proteins (blue) are excluded from entering the axon (blue arrow), whereas vesicles transporting axonal proteins (orange) can proceed through the AIS (orange arrow). Specific recruitment of axonal kinesins is helped by cues on microtubule such as post-translational modifications (light orange).

Figure and legend from (Leterrier and Dargent, 2014).

1.1.2.4 Axon sorting

Establishing axonal polarity is more complex than establishing dendritic polarity since axonal cargo cannot be excluded from the somatodendritic compartment due to the simple fact that the secretory pathway components are located in the soma (although see (Luarte et al., 2018; González et al., 2018) for reviews on the possibility of the existence of an axonal local secretory pathway).

Three main routes through the secretory pathway and the endosomal system pathways have been described for generating axonal polarity (**Figure 1-7**; reviewed in (Lasiecka and Winckler, 2011; Bentley and Banker, 2016)).

1) A **direct pathway** whereby cargo is sorted at the TGN and sorted into axonal or somatodendritic secretory vesicles and delivered directly to the correct compartment.
2) **Non-polarized delivery** of secretory vesicles by the TGN followed by **selective retrieval** from the somatodendritic compartment and/or **selective retention** at the axonal compartment.
3) Delivery by TGN of secretory vesicles solely to the dendritic membrane followed by internalisation of axonal cargo and delivery of cargo-containing endosomes to the axonal membrane, a process known as **transcytosis**.

These three pathways are not necessarily mutually exclusive, and multiple pathways have been attributed to the same cargo – for example, both direct (Sampo et al., 2003) and transcytotic (Wisco et al., 2003; Yap et al., 2008b) pathways have been described for the axonally polarised cell adhesion molecule L1/NgCAM.

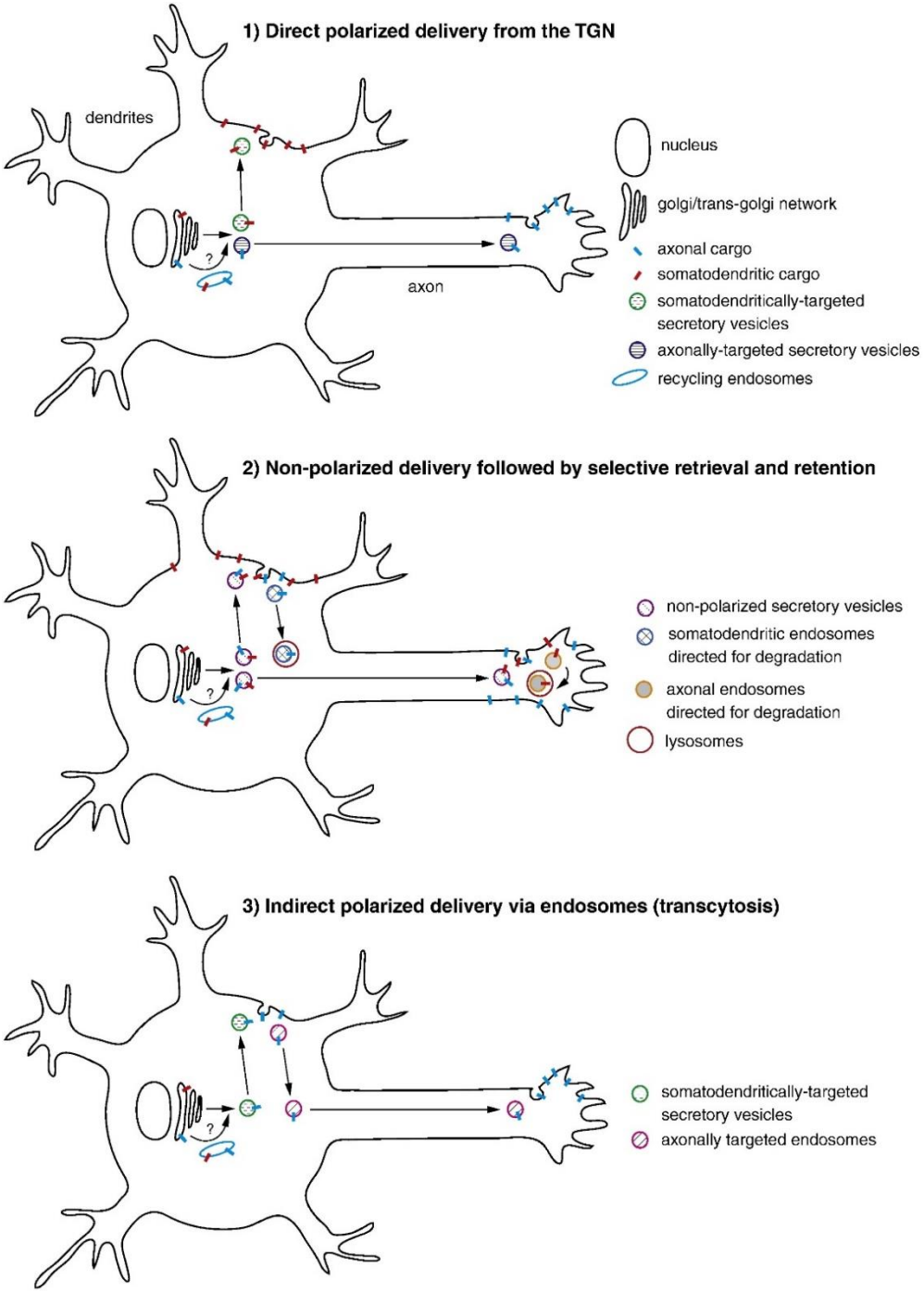

Figure 1-7 Models of 3 pathways of polarised trafficking.

(1) Direct polarized delivery from the TGN. Axonal and somatodendritic proteins are sorted in TGN into axonally- and somatodendritically-targeted secretory vesicles. Those vesicles are transported and fuse with axonal and somatodendritic membranes, respectively.

(2) Non-polarized delivery followed by selective retrieval and retention. Axonal and somatodendritic cargo exits TGN into secretory vesicles, which can fuse with both somatodendritic and axonal membranes. After this initial non-polarized insertion, proper polarized distribution of proteins is achieved by subsequent endocytic removal of missorted proteins (presumably for degradation) and retention of the properly targeted proteins at the plasma membrane.

(3) Indirect polarized delivery via endosomes (transcytosis). Proteins coming out of TGN are sorted into somatodendritically-targeted secretory vesicles, and then inserted into somatodendritic membrane and subsequently endocytosed into axonally-targeted endosomal compartments, which finally fuse with axonal membrane.

Figure and legend from (Lasiecka and Winckler, 2011).

1.2 ENDOCANNABINOID SYSTEM (ECS)

The endocannabinoid system (ECS) is an important neuromodulatory system in the brain that plays a role in a wide range of behaviours, including appetite, pain, and memory (Busquets-Garcia et al., 2015).

1.2.1 Discovery

Cannabis sativa has been used for thousands of years for its medicinal and mind-altering properties. In the past decade there has been a resurgence in interest in cannabis for therapeutic use, with newly legalised medical marijuana and its derivatives being touted as a kind of cure-all for a multitude of diseases and conditions.

The ECS field began in 1964 with the discovery of Δ^9-Tetrahydrocannabinol (Δ^9-THC), a lipophilic compound that is the main psychoactive component of cannabis (Gaoni and Mechoulam, 1964). Almost 30 years later, the cannabinoid type 1 receptor (CB1R) was identified as the receptor that mediates the psychoactive effects of Δ^9-THC (Matsuda et al., 1990). The discovery of a second receptor (CB2R; (Munro et al., 1993)) as well as two lipophilic endogenous cannabinoids (endocannabinoids; eCBs), N-arachidonoylethanolamide (named anandamide, from the Sanskrit word '*ananda'* meaning '*inner bliss*'; (Devane et al., 1992)) and 2-arachidonylglycerol (2-AG; (Sugiura et al., 1995; Mechoulam et al., 1995)) soon followed.

1.2.2 Retrograde transmission

In 2001, it was found that the ECS mediates retrograde signalling at synapses in the central nervous system (CNS; **Figure 1-8**; (Wilson and Nicoll, 2001; Ohno-Shosaku et al., 2001; Maejima et al., 2001; Kreitzer and Regehr, 2001)). Activation of the postsynapse causes the on-demand synthesis of 2-AG which traverses the synaptic cleft retrogradely activating CB1R and dampening down further neurotransmission. Thus, the ECS acts as a negative feedback loop to modulate synaptic activity. For a thorough review see (Kano et al., 2009).

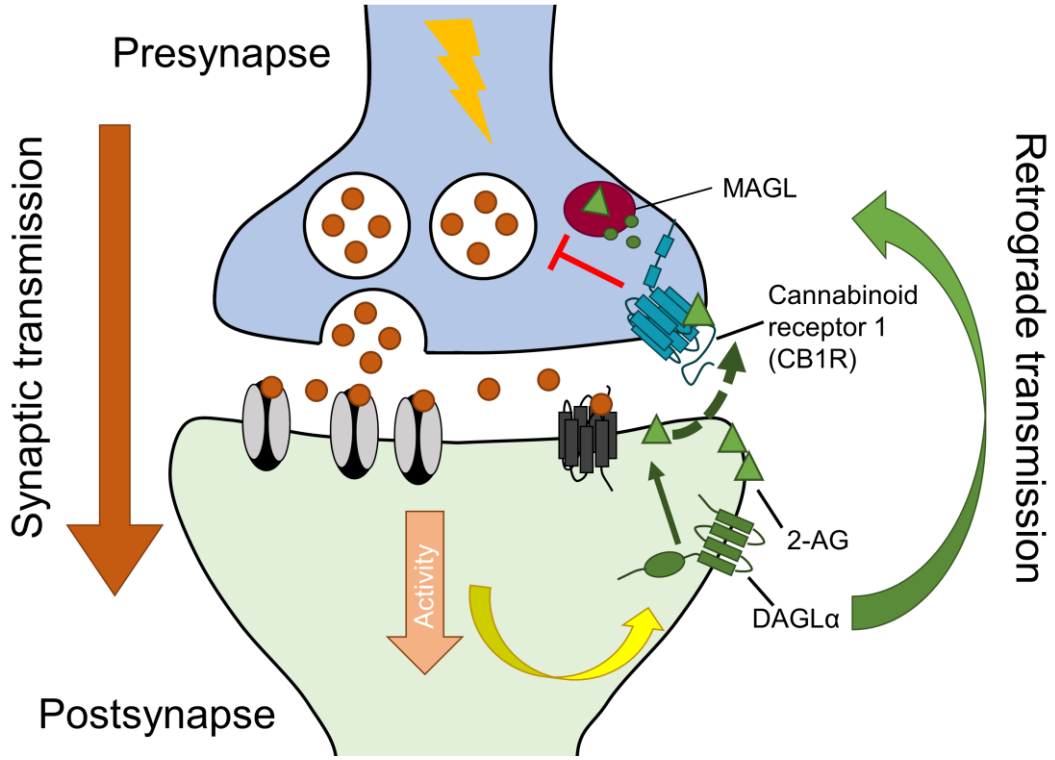

Figure 1-8 The principle of retrograde transmission.

Information transfer at the synapse generally flows anterogradely from presynapse to postsynapse. An action potential (yellow lightning bolt) traveling down the presynaptic axon triggers the release of synaptic vesicles filled with neurotransmitter, which cross the synaptic cleft and bind to ionotropic and metabotropic receptors on the postsynaptic membrane. In certain cases, activation of the postsynapse triggers the production of endocannabinoids such at 2-AG, which is synthesised by diacylglycerol lipase alpha (DAGLα), a plasma membrane protein located at postsynaptic spines. 2-AG then travels retrogradely across the synaptic clef to activate the presynaptically-localised cannabinoid type 1 receptor (CB1R). Activation of CB1R triggers downstream signalling cascades that prevent the release of additional neurotransmitter. Therefore, the endocannabinoid system (ECS) acts as a retrograde feedback mechanism to regulate and modulate synaptic activity.

1.2.3 Beyond retrograde transmission

Over the past few decades, it has become abundantly clear that the ECS is extremely complex, pleiotropic, and ubiquitous, extending far beyond its classical role in retrograde transmission (see (Castillo et al., 2012; Araque et al., 2017; Busquets-Garcia et al., 2018; Pertwee et al., 2010; Howlett et al., 2002; Howlett, 2005; Di Marzo, 2009; Piomelli, 2003; Ahn et al., 2008; Kano et al., 2009; Katona and Freund, 2012) for reviews on the ECS). A more complete overview of synaptic ECS function is summarised in **Figure 1-9** and aspects are discussed below.

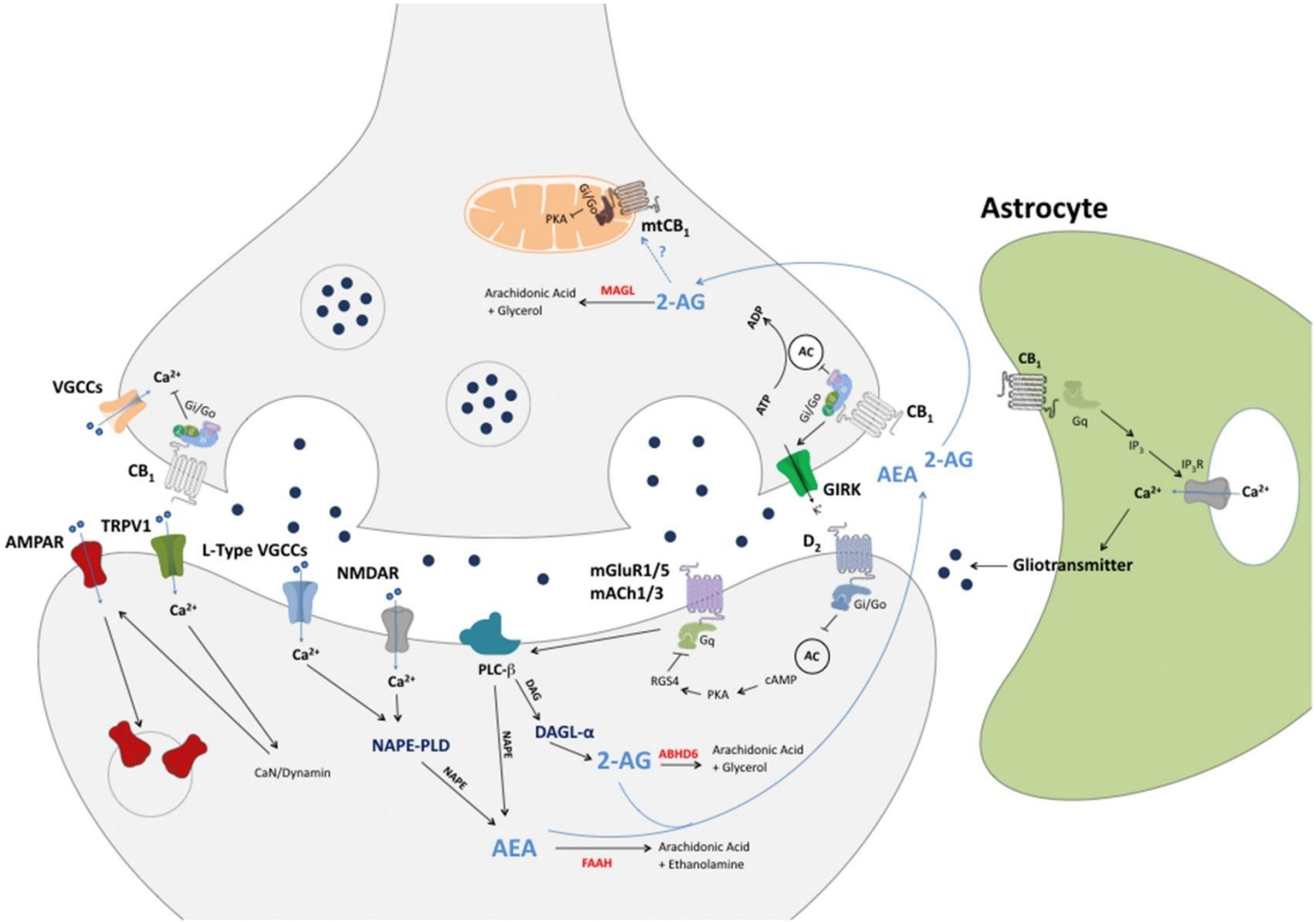

Figure 1-9 Schematic of eCB signalling at the synapse from (Araque et al., 2017)

1.3 CANNABINOID TYPE 1 RECEPTOR (CB1R)

1.3.1 Identification and characterisation

While the effects of cannabis on the brain has been known for thousands of years, CB1R was first cloned and identified in 1990 from rat cortex as the receptor that mediates the effects of Δ^9-THC, the psychoactive component of cannabis (Matsuda et al., 1990). Discovery of the human (Gérard et al., 1991) and mouse (Gérard et al., 1991) homologues soon followed. CB1R is the most abundant GPCR expressed in the brain, with protein levels comparable to that of NMDA and $GABA_A$ receptors (Herkenham et al., 1991; Busquets-Garcia et al., 2018).

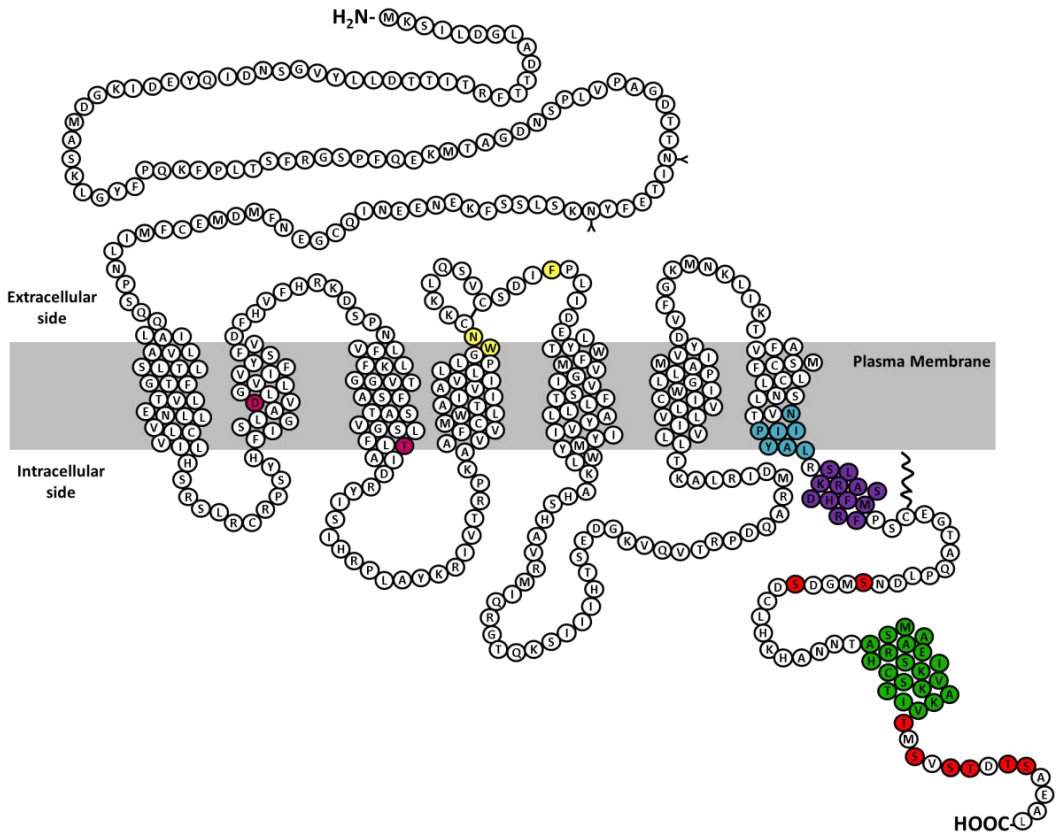

Figure 1-10 Rat CB1R topology.

The predicted topology of CB1Rs based on hydrophobicity plots and analysis from crystal structures of rhodopsin-family GPCRs. Sites of post-translation modification via N-terminal glycosylation (Song and Howlett, 1995) or C-terminal palmitoylation (Oddi et al., 2012, 2017, 2018) are indicated by the (Y) symbol and zigzag line respectively. Putative phosphorylation residues, important for mediating activity-dependent internalization and/or desensitization are shown in red (Daigle et al., 2008b; Hsieh et al., 2002; Jin et al., 1999; Straiker et al., 2012b), whilst two residues located within the 2nd and 3rd transmembrane domains (TM2/TM3), required for constitutive internalization are shown in pink (D'Antona et al., 2006; Roche et al., 1999). Within the second extracellular loop (2EC) a disulphide bridge between to cysteine residues is depicted with a single line, whilst the yellow residues denote putative amino acids involved in ER exit and receptor surface expression (Ahn et al., 2009a). The blue residues indicate the sites of the highly conserved NPXXY motif. Within the C-terminal tail, two helical structural motifs, helix 8 (*H8*) and helix 9 (*H9*) are highlighted in purple and green respectively (Ahn et al., 2009b; Stadel et al., 2011).

Figure is from (Hildick, 2013) and (Stadel et al., 2011). Figure legend is from (Hildick, 2013).

CB1R is a G-protein-coupled receptor (GPCR) of the Rhodopsin (class A) family, subgroup α. It comprises of an extracellular N-terminal tail, 7 transmembrane helical domains (TM1-7), and an intracellular C-terminal tail with two additional helices (helix 8 and helix 9; **Figure 1-10**).

1.3.2 Expression profile of CB1R in the CNS

1.3.2.1 Neurons

CB1R is expressed in a wide variety of cell types in the CNS at varying levels. For review, see (Marsicano and Kuner, 2008; Busquets-Garcia et al., 2018; Mackie, 2005).

However, strangely, the expression level of CB1R does not always correlate with level of activity. For example, while the hypothalamus expresses lower levels of CB1R than the cortex and hippocampus, it displays higher levels of cannabinoid-dependent activity than areas with high levels of CB1R (Breivogel et al., 1997).

Furthermore, deletion of CB1R in cortical glutamatergic neurons reduces total CB1R protein by about 10% while deletion of CB1R in GABAergic interneurons reduces CB1R protein by about 90% (Steindel et al., 2013). However, deletion of CB1R in cortical glutamatergic neurons has a several fold larger effect on cannabinoid-dependent G-protein activation than deletion of CB1R in GABAergic interneurons, suggesting that cannabinoid activation of CB1R in excitatory cells is much more efficacious and requires a lower threshold of activation (Steindel et al., 2013). A higher dose is required to activate CB1R in GABAergic neurons.

Interestingly, this can explain why cannabinoid administration often display a bimodal/biphasic behavioural response with increased dosage. For example, low doses of Δ^9-THC have an anxiolytic effect whereas high dose have an anxiogenic effect (Rey et al., 2012). Similarly, low doses of Δ^9-THC induce hyperphagia (excessive eating) whereas high doses induce hypophagia (Bellocchio et al., 2010). Understanding this dual effect is critical for the development of future cannabinoid-based therapies.

1.3.2.2 Glia: astrocytes

Astrocytes express even lower levels of CB1R (Navarrete et al., 2014; Navarrete and Araque, 2008, 2010). Endocannabinoid activation of astroglial CB1R increases intracellular Ca^{2+} levels, likely via G_q protein coupling rather than $G_{i/o}$

(Navarrete and Araque, 2008). This causes astrocytes to release gliotransmitters, e.g. D-serine (Robin et al., 2018), thus modulating synaptic activity and certain types of memory (see (Araque et al., 2017; Navarrete et al., 2014) for review).

1.3.3 Subcellular localisation of CB1R

1.3.3.1 Plasma membrane localisation

1.3.3.1.1 Presynaptic

Consistent with its role in attenuating presynaptic neurotransmitter release (Katona, 2009), CB1R has a highly polarised axonal surface expression (Irving et al., 2000; Coutts et al., 2001; Leterrier et al., 2006; Thibault et al., 2013; Rozenfeld and Devi, 2008; McDonald et al., 2007a). Within the axonal membrane, CB1R displays a disto-proximal gradient of expression (Simon et al., 2013) and immunocytochemistry in brain sections using immunogold electron microscopy (Katona et al., 1999; Nyíri et al., 2005) or STORM super-resolution imaging (Dudok et al., 2015) detect CB1R predominantly at the presynaptic terminal.

1.3.3.1.2 Plasma membrane microdomains

CB1R contains several cholesterol binding motifs (Wickert et al., 2018; Oddi et al., 2011) and is enriched at cholesterol-rich microdomains of plasma membrane called lipid rafts (Asimaki et al., 2011; Sarnataro et al., 2005). See 1.3.5.2 Internalisation for more details.

1.3.3.2 Intracellular localisation

Due to the lipophilic nature of endocannabinoids, CB1R activation is likely not limited to the plasma membrane but occurs intracellularly as well.

1.3.3.2.1 Endosomal

Around 80% of CB1R is located in endosomes (Leterrier et al., 2006; Rozenfeld and Devi, 2008). This pool is reportedly activatable (Rozenfeld and Devi, 2008; Brailoiu et al., 2011). See 1.3.4.3 Third wave: intracellular signalling for more details.

1.3.3.2.2 Mitochondrial

Recently, the Marsicano group has made the surprising discovery that a small, but significant, proportion of CB1R is associated with the mitochondrial outer membrane and activation of this pool reduces mitochondrial respiration (Bénard et

al., 2012). Despite some initial controversy (Morozov et al., 2013; Hebert-Chatelain et al., 2014), this finding has since been verified independently and in other tissues (Mendizabal-Zubiaga et al., 2016; Koch et al., 2015), and has been shown to be important for certain types of memory (Hebert-Chatelain et al., 2016).

1.3.4 CB1R signalling

CB1R signalling is highly complex and pleiotropic, with a multitude of downstream effectors and signalling pathways that emerge under specific spatiotemporal and contextual constraints (Busquets-Garcia et al., 2018; Araque et al., 2017). In general, CB1R signalling occurs over three spatiotemporal waves: 1) activation of heterotrimeric G proteins (<10 minutes), 2) β-arrestin mediated activation of mitogen kinases (>5 minutes), and 3) intracellular signalling by either G-proteins or β-arrestin (>30 minutes) (Nogueras-Ortiz and Yudowski, 2016). For extensive reviews of CB1R signalling, see (Howlett, 2005; Turu and Hunyady, 2010; Irving et al., 2008; Araque et al., 2017; Hunter et al., 2017; Busquets-Garcia et al., 2018).

1.3.4.1 First wave: G protein-mediated signalling

The classical signalling pathway of GPCRs such as CB1R is mediated through activation of heterotrimeric G proteins (**Figure 1-11**; see (Ritter and Hall, 2009; Jong et al., 2018; Pavlos and Friedman, 2017; Rajagopal and Shenoy, 2018; Dupré et al., 2009; Sánchez-Fernández et al., 2014; Pierce et al., 2002) for reviews on canonical and non-canonical GPCR signalling). Activation of a GPCR by binding of an extracellular ligand causes a conformational change allowing it to interact with a heterotrimeric G protein complex comprised of α, β, and γ subunits. Guanine nucleotide exchange activates the Gα subunit, causing it to dissociate it from the Gβγ subunit. The activated Gα subunit binds downstream effectors and regulates the activity downstream signalling pathways depending on the subtype of Gα.

Four major families of subtypes exist: $G\alpha_s$, $G\alpha_i$, $G\alpha_{q/11}$, and $G\alpha_{12/13}$. These effectors and downstream signalling pathways of each family are summarised in **Figure 1-11** (see also (Ritter and Hall, 2009; Pierce et al., 2002)). Briefly, $G\alpha_s$ and $G\alpha_i$ family subtypes activate and inhibit adenylyl cyclase (AC), respectively. AC catalyses the cyclization of adenosine triphosphate (ATP) to the second messenger Adenosine 3',5'-cyclic monophosphate (cAMP). cAMP signalling is complex and has a multitude of effects but most classically the downstream target of cAMP is protein kinase A (PKA) (Antoni, 2012). Thus $G_{i/o}$ proteins inhibit the

PKA phosphorylation pathway and G_s proteins activate it. $G\alpha_{q/11}$ family subunits activate the downstream effector phospholipase C type β (PLCβ), a Ca^{2+}-dependent enzyme that catalyses the hydrolysis of phosphatidylinositol 4,5 bisphosphate (PI(4,5) P_2) to inositol 1,4,5 trisphosphate ($Ins(1,4,5)P_3$) and diacylglycerol (DAG). $Ins(1,4,5)P_3$ and DAG are second messengers which together increase Ca^{2+} levels by opening intracellular ER Ca^{2+} stores and activate protein kinase C (PKC). The downstream effector for $G\alpha_{12/13}$ are RhoGEFs, thus regulating actin cytoskeleton remodelling by activation of RhoA. Signalling of the Gβγ subunit is less well understood but Gβγ can regulate downstream effectors such as various ion channels and PLCβ.

1.3.4.1.1 CB1R coupling to Gi/o proteins

Characterisation of the signalling of CB1R started even before CB1R was identified with the observation that application of exogenous cannabinoids, including Δ^9-THC, to neuroblastoma cells inhibited adenylyl cyclase (AC), causing a reduction in cAMP levels (Howlett and Fleming, 1984; Howlett, 1987, 1984). The cannabinoid-mediated inhibition of cAMP was blocked in the presence of pertussis toxin (PTX), which specifically blocks $G\alpha_i$-protein signalling by keeping it in the inactive GDP-bound state (Howlett et al., 1986). Thus, the first characterised signalling pathway of CB1R described was through coupling with $G_{i/o}$ proteins, which, when activated by cannabinoid binding, inhibits AC, causing a decrease in cAMP levels, thus inactivating the PKA phosphorylation pathway (**Figure 1-11 A**).

1.3.4.1.2 Other G protein coupling

CB1R has been shown to not only couple to $G_{i/o}$ proteins but also to G_s, G_q, and $G_{12/13}$ depending on the cell type (Busquets-Garcia et al., 2015), agonist type (Diez-Alarcia et al., 2016), or cellular/protein context (Kearn et al., 2005) in which CB1R is expressed (**Figure 1-11 B**; for review, see (Busquets-Garcia et al., 2018)).

1.3.4.1.2.1 Gs

Heterodimerisation of CB1R with dopamine D2 receptors can switch the signalling of CB1R and D2 from $G_{i/o}$ to G_s, generating the opposite effect: an increase in cAMP levels (Kearn et al., 2005; Glass and Felder, 1997; Jarrahian et al., 2004). A limited subpopulation of neurons in the basal ganglia co-express D2 and CB1R (Hermann et al., 2002; Marsicano and Kuner, 2008), suggesting that these cells may have different properties in terms of their CB1R signalling because of the cellular/protein context.

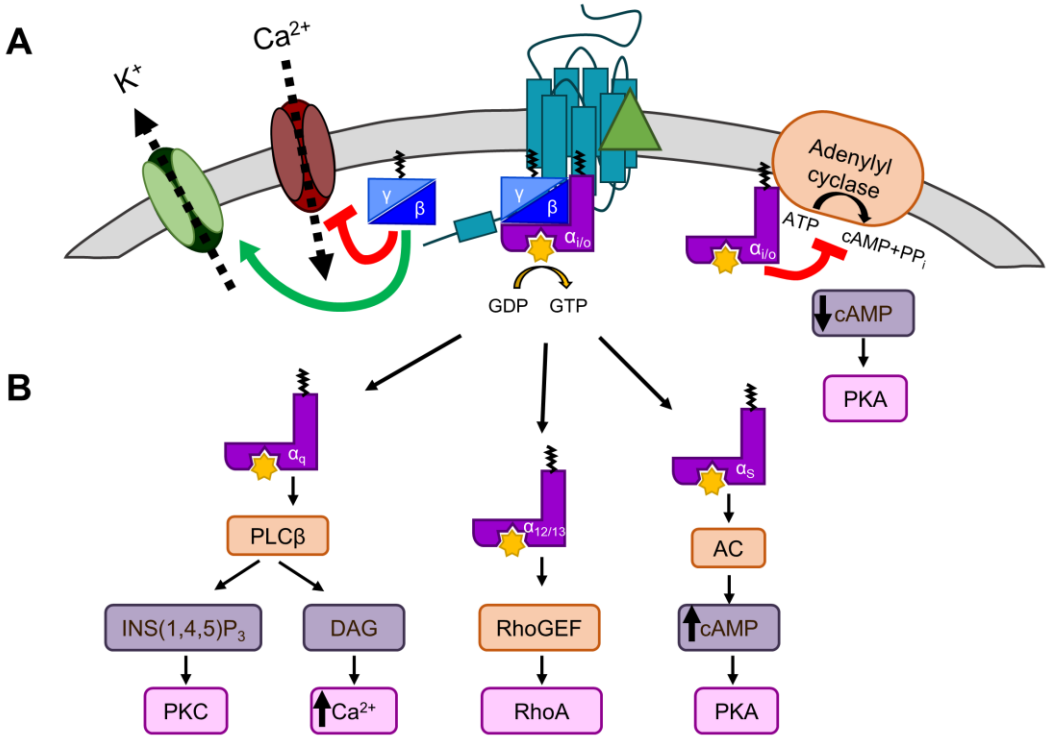

Figure 1-11 G-protein signalling of CB1R.

(**A**) Classically, CB1R signalling is mediated by $G_{i/o}$ signalling. CB1R is activated by ligand (green triangle), generating a conformational change that allows for heterotrimeric G-protein (α, β, and γ subunits) binding. The receptor then acts as a guanine nucleotide exchange factor (GEF), activating Gα by GDP-to-GTP exchange. This triggers the dissociation of Gα from Gβγ. $G\alpha_{i/o}$ inhibits adenylyl cyclase (AC), a membrane protein that catalyses that conversion of ATP to cAMP+PP_i, causing a decrease in cAMP levels and inhibiting the PKA phosphorylation pathway. Gβγ inhibits voltage gated Ca^{2+} channels (VGCCs) and activates G protein-coupled inwardly rectifying K^+ channels (GIRKs).

(**B**) CB1R has also been shown to couple to $G\alpha_q$, $G\alpha_{12/13}$, and $G\alpha_s$ subunits. The classical downstream effectors of these subunits are depicted.

Redrawn and adapted from (Ritter and Hall, 2009).

1.3.4.1.2.2 Gq

Application of endocannabinoids to astrocytes leads to an PLCβ-dependent increase in Ca^{2+} levels from intracellular stores, suggesting that CB1R in astrocytes couples to $G_{q/11}$ rather than $G_{i/o}$ (Navarrete and Araque, 2008; Navarrete et al., 2014) (see also 1.3.2.2 Glia: astrocytes). Cannabinoid-mediated $G_{q/11}$ coupling has also been observed in certain cell lines (Lauckner et al., 2005) and upon activation with certain agonists, specifically WIN55212-2, Δ^9-THC, and ACEA in the mouse cortex (Diez-Alarcia et al., 2016).

1.3.4.1.2.3 G12/13

Anandamide was shown to induce rounding in B103 rat neuroblastoma cells in a PTX-insensitive, but Rho inhibitor-sensitive manner, suggesting the potential to couple to $G_{12/13}$ (Wilson and Nicoll, 2002). Furthermore, WIN55212-2, but not Δ^9-

THC and ACEA, was able to stimulate $G_{12/13}$ subunit in mouse cortex (Diez-Alarcia et al., 2016).This biased agonism of CB1R is an important and emerging concept in the field.

1.3.4.1.3 CB1R ion channel modulation

1.3.4.1.3.1 Ca2+ channels

CB1R activation inhibits N-type (Pan et al., 1996; Mackie and Hille, 1992; Twitchell et al., 1997), L-type (Gebremedhin et al., 1999), and P/Q type (Fisyunov et al., 2006; Twitchell et al., 1997) voltage gated Ca^{2+} channels (VGCCs) in a PTX-dependent manner, likely through Gβγ (**Figure 1-11 A**; (Wilson and Nicoll, 2002)).

1.3.4.1.3.2 K+ channels

Endocannabinoid stimulation of CB1R leads to activation of G protein-coupled inwardly rectifying K^+ channels (GIRKs) (Mackie et al., 1995; Henry and Chavkin, 1995; Ho et al., 1999; McAllister et al., 1999). CB1R activation of GIRKs is blocked by PTX, indicating that it is dependent on $G_{i/o}$ activation, likely through Gβγ (**Figure 1-11 A**; (Ho et al., 1999; Mackie et al., 1995; Yamada et al., 1998)).

1.3.4.2 Second wave: Beta-arrestin mediated signalling

The second wave of CB1R signalling is by β-arrestin binding, a common non-G protein mechanism of GPCR desensitisation and internalisation (**Figure 1-12**; (Zastrow, 2003)). Desensitization and internalisation are important for regulation of GPCR signalling, dampening the signal even in the presence of continued agonist. As with G protein-mediated signalling, CB1R β-arrestin-mediated signalling is highly complex, and depends strongly on the cell-type, agonist bias, and cellular milieu (Nogueras-Ortiz and Yudowski, 2016).

1.3.4.2.1 Desensitisation

Upon activation by extracellular ligands, CB1R is desensitised in a matter of minutes by phosphorylation of two serine residues (S426 and S430) in the C-terminal tail by GPCR kinases 2/3 (GRK2/3) and subsequent recruitment of β-arrestin1/2 recruitment, preventing further G protein coupling (**Figure 1-12 1**) (Jin et al., 1999; Kouznetsova et al., 2002; Daigle et al., 2008a; Morgan et al., 2014). Further phosphorylation of six serines and threonines in the extreme C-terminal tail modulates β-arrestin1/2 recruitment and is necessary for internalisation (Straiker et al., 2012b; Daigle et al., 2008b).

1.3.4.2.2 Activation of kinase signalling cascades

β-arrestin1/2 recruitment to desensitised CB1R facilitates the activation of several kinase signalling cascades (**Figure 1-12 2, 3b**). For example, ORG27569 activation of exogenously expressed CB1R in HEK293 cells strongly elicited ERK1/2, Src, and MEK1/2 phosphorylation (Ahn et al., 2013). This kinase activation was dependent on β-arrestin1 recruitment, but not on β-arrestin2 recruitment (Ahn et al., 2013). Furthermore, 2-AG activated ERK1/2, JNK1/2/3, CREB, and P38α activation via β-arrestin1 in mouse cortex (Delgado-Peraza et al., 2016). Interestingly, β-arrestin2 recruitment was instead required for receptor internalisation, suggesting that the two isoforms of β-arrestins play different roles (Ahn et al., 2013; Delgado-Peraza et al., 2016). However, anandamide activation of CB1R in smooth muscle activated ERK1/2 and Src kinase via both β-arrestin1 and β-arrestin2 (Mahavadi et al., 2014). This suggests that β-arrestin signalling of CB1R is heavily ligand-dependent.

1.3.4.2.3 Internalisation

β-arrestins act as a scaffold for the recruitment of the endocytic machinery, binding the desensitised receptor by its N-terminus and clathrin/adaptor protein 1 (AP-2) by its C-terminus, leading to internalisation of the desensitised receptor by clathrin-mediated endocytosis (Goodman et al., 1996; Laporte et al., 1999). Upon agonist stimulation, CB1R is rapidly internalised (**Figure 1-12 3a**; (Grimsey et al., 2010; Jin et al., 1999; Hsieh et al., 2002)), although rate and amount of internalisation is dependent on agonist type (Wu et al., 2008; Hsieh et al., 2002). Following internalisation into early endosomes, CB1R is mainly sorted for lysosomal degradation by GASP1 (see also 1.3.7.3.1 G-protein coupled receptor associate protein 1 (GASP1); (Grimsey et al., 2010; Tappe-Theodor et al., 2007; Martini et al., 2007, 2010; Blume et al., 2016)), although resensitisation and recycling of the receptor back to the cell surface can occur with short-term agonist treatment (Hsieh et al., 2002).

1.3.4.3 Third wave: intracellular signalling

Interestingly, GPCRs can continue to signal when in endosomes by G protein or β arrestin signalling pathways (Irannejad, 2014). Furthermore, CB1Rs are unique for GPCRs in that their agonists are lipophilic, and thus cell permeable. Therefore, it is likely that prolonged CB1R signalling can endure intracellularly, by either G protein- or β-arrestin-dependent means (Nogueras-Ortiz and Yudowski, 2016).

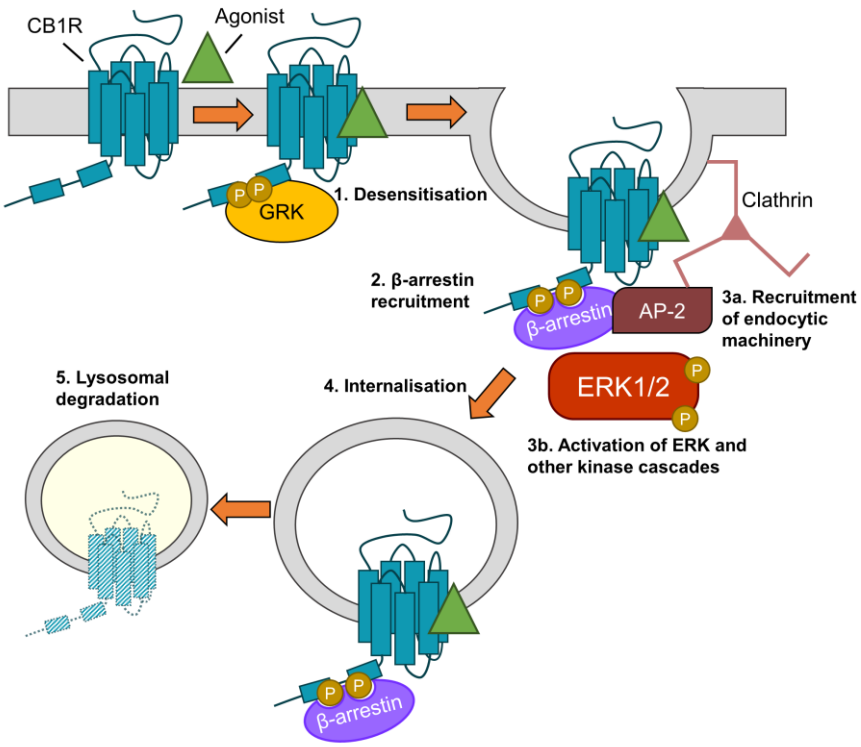

Figure 1-12 β-arrestin signalling of CB1R.

1) Following agonist binding, GPCR kinases (GRKs) phosphorylate the C-terminal tail of CB1R.

2) Phosphorylation of ctCB1R leads to recruitment of β-arrestins.

3) β-arrestin recruitment a) acts as scaffold for recruitment of AP-2 and clathrin and b) elicits the activation of downstream kinase cascades, most classically, the phosphorylation of ERK1/2.

4) The desensitised CB1R is internalised by resulting in clathrin-mediated endocytosis (CME).

5) Endosomal CB1R is sorted for lysosomal degradation.

1.3.4.3.1 Endosomal signalling

CB1R is particularly enriched in endosomes of both Neuro2A (Rozenfeld and Devi, 2008) and hippocampal neurons (Leterrier et al., 2006; McDonald et al., 2007a). Evidence for endosomal signalling came from the observation that treatment with agonist WIN55212-2 induced ERK1/2 phosphorylation even when surface CB1Rs were blocked by hemopressin, a cell impermeable antagonist (Rozenfeld and Devi, 2008). Furthermore, CB1R was found to associate with $G\alpha_i$ in Rab7 positive endosomal fractions (Rozenfeld and Devi, 2008). Lastly, intracellular injection of anandamide into HEK293 cells expressing CB1R induced Ca^{2+} release from intracellular stores (Brailoiu et al., 2011).

1.3.4.3.2 Mitochondrial signalling

CB1R is also localised to mitochondrial membranes where activation leads to decreased mitochondrial respiration (Bénard et al., 2012). CB1R-dependent

decrease in mitochondrial respiration is sensitive to PTX, indicating that it is mediated by $G\alpha_{i/o}$ activation of a soluble form of adenylyl cyclase (sAC) (Hebert-Chatelain et al., 2016).

1.3.5 CB1R trafficking

1.3.5.1 Forward trafficking

GPCRs such as CB1R are trafficked to the plasma membrane via the secretory pathway (**Figure 1-2**). Like many GPCRs, CB1R does not have a canonical, cleavable signal peptide, but rather, the first transmembrane domain is thought to act as a 'reverse anchoring sequence' which is recognized by the signal recognition particle (SRP) and translocated across the ER membrane (Andersson et al., 2003; Nordström and Andersson, 2006). The large size of N-terminal tail of CB1R impedes its reverse translocation across the membrane, meaning that the majority of synthesized CB1R is likely misfolded and sent for proteosomal degradation (Andersson et al., 2003; Nordström and Andersson, 2006). Furthermore, an N-terminally truncated form of CB1R is produced, probably truncated in the cytosol in the small amount of time before translocation can occur (Nordström and Andersson, 2006).

In the ER, CB1R is modified by N-linked glycosylation at two sites (N78, N84) which undergo further processing in the Golgi before it is trafficked to the plasma membrane (Song and Howlett, 1995).

1.3.5.2 Internalisation

Typically agonist-induced internalisation of GPCRs, including of CB1R, occurs by clathrin-mediated endocytosis (**Figure 1-3**; (Jin et al., 1999; Hsieh et al., 2002; Ahn et al., 2013; Blume et al., 2016)). However, blocking CME only partially impairs CB1R internalisation (Keren and Sarne, 2003; Wu et al., 2008).

CB1R is associated with lipid rafts (Asimaki et al., 2011; Sarnataro et al., 2005), specialised microdomains of plasma membranes rich in sphingolipids and cholesterol (**Figure 1-13 A**; (Allen et al., 2007)). Cargo in lipid rafts can be internalised by caveolin-mediated endocytosis (**Figure 1-13 B**; (Razani et al., 2002). Membrane cholesterol depletion by methyl-β-cyclodextrin (MβCD) is an effective way of preventing CB1R endocytosis (Leterrier et al., 2006, 2004; Keren and Sarne, 2003). Conversely, a mutation that increases lipid raft association of CB1R also increased constitutive endocytosis of CB1R (Wickert et al., 2018).

CB1R undergoes both agonist-induced and constitutive internalisation, reportedly by different mechanisms – β-arrestin2 binding is required for agonist-induced internalisation but not constitutive internalisation (Gyombolai et al., 2013; McDonald et al., 2007a)

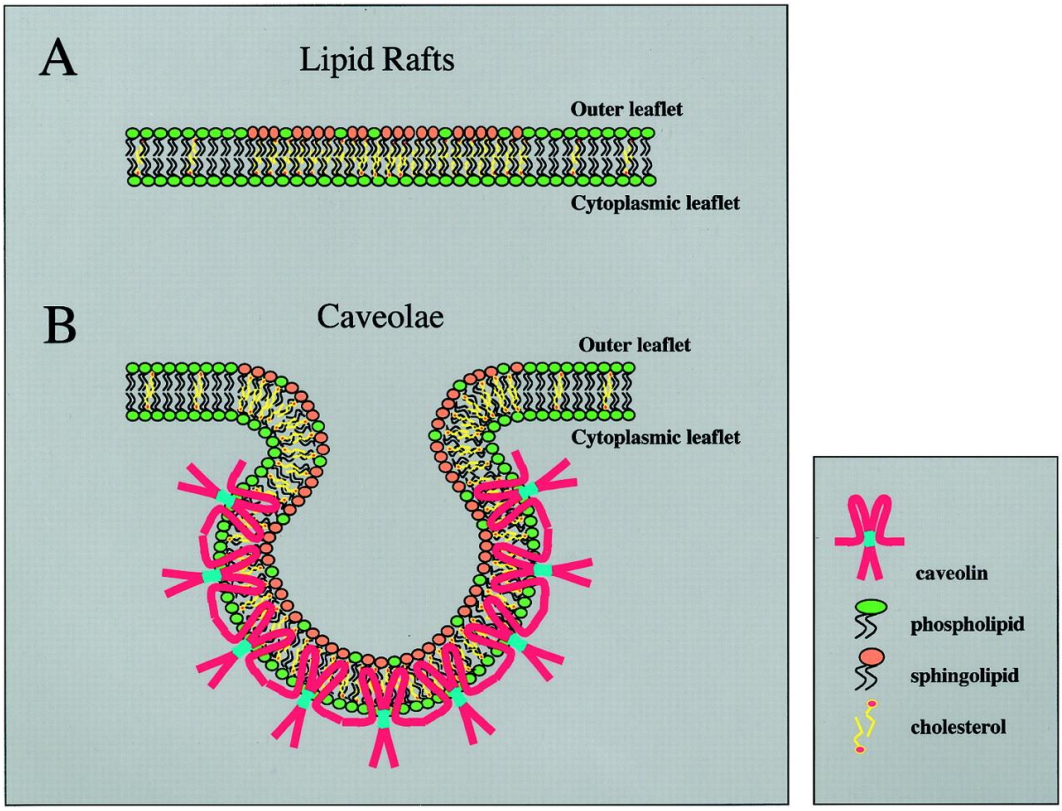

Figure 1-13 Lipid rafts and caveolae mediated endocytosis.

(**A**) Lipid rafts are microdomains in the plasma membrane that are enriched in sphingolipids and cholesterol.

(**B**) Caveolin-1 integrates with lipid rafts to form small invaginations called caveolae to initiate caveolin-mediated endocytosis.

Figure from (Razani et al., 2002).

1.3.6 Three currently proposed models of CB1R polarity

Different research groups have proposed different mechanisms for the polarised surface distribution of CB1R.

1.3.6.1 Model 1: Differential endocytosis rates due to differential 2-AG production in somatodendritic and axonal membranes

1.3.6.1.1 Differential rates of internalisation

The Lenkei group suggest that CB1R is delivered in a non-polarised manner to the plasma membrane but is then selectively endocytosed away from the somatodendritic membrane in an agonist-dependent manner (**Figure 1-7**, pathway

2; (Leterrier et al., 2006)). The Lenkei group propose that any CB1R that reaches the somatodendritic membrane is immediately activated by the tonal presence 2-AG specifically in the somatodendritic membrane and therefore undergoes agonist-induced internalisation (Leterrier et al., 2006; Simon et al., 2013; Thibault et al., 2013; Ladarre et al., 2015; Ladarre and Lenkei, 2017). 2-AG is constitutively present in the somatodendritic membrane because the 2-AG synthetic enzyme DAGLα is specifically located in the somatodendritic compartment, but excluded from the axonal compartment (Ladarre et al., 2015; Zhou et al., 2016). Conversely, the 2-AG degradative enzyme MAGL is exclusively located in axons (Gulyas et al., 2004; Ludányi et al., 2011).

This model is supported by the fact that, in their hands, application of the antagonist/inverse agonist AM281 caused an increase in surface localisation of somatodendritic CB1R (Leterrier et al., 2006) and a constitutively inactive version of CB1R (T210A) displayed a non-polarised surface distribution (Simon et al., 2013). Furthermore, application of AM281 inhibited constitutive cAMP/PKA signalling in dendrites but not in axons, indicating that there is more constitutive activation of CB1R in dendrites than in axons (Ladarre et al., 2015)

1.3.6.1.2 Transcytosis

What happens to somatodendritic CB1R following internalisation from the somatodendritic membrane is unclear. The Lenkei group presented evidence that CB1R may traffic in a transcytotic manner, with endosomal somatodendritic CB1R being sorted and sent to the axonal membrane, particularly to more distal areas (**Figure 1-7**, pathway 3; (Simon et al., 2013)). To investigate this, they grew primary neurons in microfluidic chambers, which allows for the separation of the somatodendritic and axonal domains. Interestingly, a small amount of N-terminal antibody fed into the somatodendritic compartment of the chamber was picked up after 4 hours on the surface of the axonal membrane, especially in the very distal end of the axon (Simon et al., 2013).

Furthermore, the Lenkei group examined the forward trafficking of CB1R using Brefeldin A block and release protocol (Leterrier et al., 2006). Brefeldin A blocks ARF1-dependent *cis*- and *trans*-Golgi transport (**Figure 1-14**) and has been used historically to inhibit canonical secretory pathway trafficking, although it has also been shown to affect endocytosis and recycling (Wood et al., 1991; Hunziker et al., 1991; Damke et al., 1991; Miller et al., 1992; Hunziker et al., 1992; Graham et al.,

1993). By incubating with BFA for 20 hours post transfection followed by a BFA washout, Leterrier et al. were able to pulse chase FCB1R-EGFP (N-terminal FLAG tag, C-terminal EGFP tag), and examine CB1R trafficking either under control conditions or in the presence of the antagonist/inverse agonist AM281. Under control conditions, they found that 4-8 hours after BFA washout, the majority of neurons displayed a non-polarised or somatodendritically polarised surface distribution, indicating that CB1R is non-discriminately sent to the plasma membrane. Axonal polarisation was established 24 hours after washout. Strikingly, under AM281, the majority of neurons exhibited a non-polarised distribution even 24 hours after BFA washout, supporting a role in endosomal somatodendritic CB1R transcytosis to the axonal membrane (Leterrier et al., 2006).

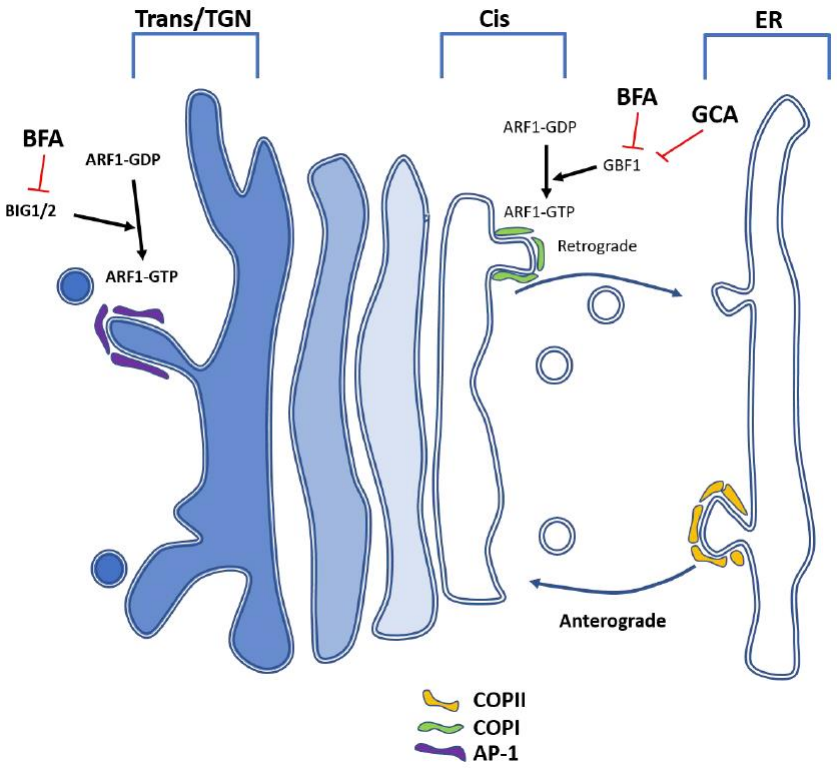

Figure 1-14 Brefeldin A (BFA) and Golgicide A (GCA) inhibit Golgi transport.

BFA reversibly inhibits ARF1-dependent cis- and trans-Golgi transport. GCA is a more specific ARF-1 inhibitor, only inhibiting the cis-Golgi

Figure and caption adapted from (Evans, 2017).

1.3.6.1.3 Lenkei model of polarity: differential endocytosis rates due to differential 2-AG production in somatodendritic and axonal membranes

The Lenkei group thus proposed a model whereby newly synthesized CB1R is delivered non-discriminately to the plasma membrane of either compartment. Because of the higher concentration of 2-AG present in the somatodendritic

membrane than the axonal membrane, CB1R is selectively internalised from the dendritic membrane, but remains in the axonal membrane. Endosomes containing CB1R are then actively sorted, targeted, and recycled to the distal ends of axons (Simon et al., 2013; Ladarre and Lenkei, 2017). This model is summarised in **Figure 1-15**.

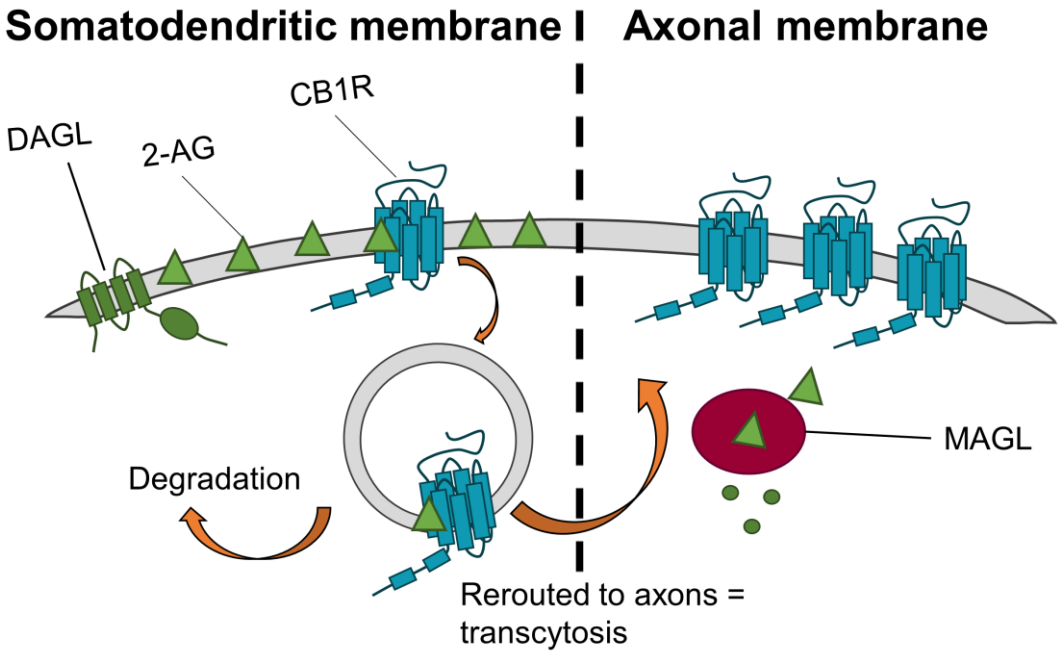

Figure 1-15 Model 1: Differential endocytosis rates due to differential 2-AG production in somatodendritic and axonal membranes.

The presence of DAGLα exclusively on the somatodendritic surface causes a polarised production of 2-AG with high levels in the somatodendritic membrane. Therefore, *de novo* CB1R delivered to the somatodendritic membrane is immediately activated and internalised. Internalised CB1R is either degraded or rerouted to distal end of axons. On the other hand, the absence of DAGLα as well as the presence of the degradative enzyme MAGL in the axonal compartment means that newly delivered CB1R is retained on the axonal surface. This results in the axonally polarised distribution, where it is available to be bound by retrogradely crossing endocannabinoids produced under specific synaptic conditions.

1.3.6.2 Model 2: differential constitutive endocytosis

The Irving group also suggests that CB1R polarity is established by differential rates of endocytosis between the somatodendritic and axonal compartments (McDonald et al., 2007a; Irving et al., 2008). However, the Irving group differs in opinion on what causes CB1R to selectively internalise from the somatodendritic membrane, but not the axonal membrane. This is because they did not observe an increase in dendritic surface CB1R with AM281 incubation (McDonald et al., 2007a). Furthermore, truncated (ctΔ14) and point mutated (D164N) versions of CB1R that should also lack agonist-induced internalisation did not display a different pattern of surface polarity in their hands (McDonald et al., 2007a).

Nevertheless, blocking constitutive internalisation with the expression of a dominant negative dynamin-1 (K44A) did cause the accumulation of CB1R on the somatodendritic membrane, thus still supporting pathway 2 (**Figure 1-7**), but through a constitutive, agonist-independent means (summarised in **Figure 1-16**).

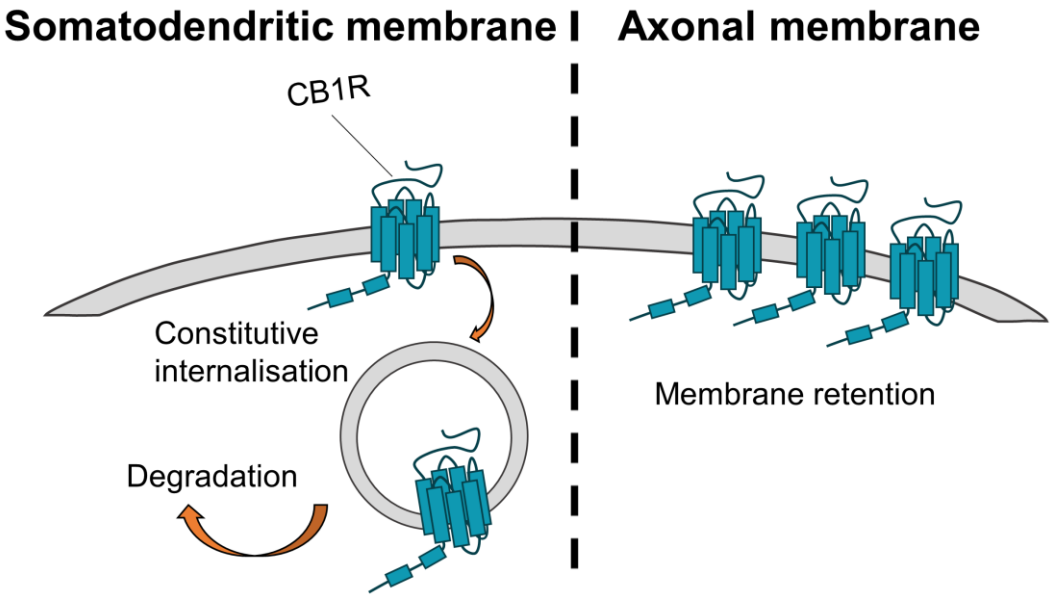

Figure 1-16 Model 2: differential rates of constitutive internalisation.

CB1R is delivered to the surface in a nonpolarised manner, but selectively removed from the somatodendritic surface via an agonist-independent, dynamin-dependent pathway and sent for degradation. This results in the axonally polarised distribution of CB1R.

1.3.6.3 Model 3: Constitutive AP-3-mediated lysosome delivery

An alternative model by Rozenfeld and Devi suggests that CB1R does not, in fact, reach the somatodendritic surface. In work done primarily in Neuro2A cells, they show that an untagged CB1R expressed very poorly at the cell surface, and instead mostly colocalised with Rab7-positive late endosomes/lysosomes (Rozenfeld and Devi, 2008).

In co-immunoprecipitate studies they detected the delta subunit of AP-3 (AP-3δ), but not AP-2, in CB1R immunoprecipitates (Rozenfeld and Devi, 2008), suggesting that CB1R associates with AP-3, an adapter complex that mediates trafficking between the TGN and lysosomes (Odorizzi et al., 1998; Scales et al., 1999; Guardia et al., 2018), but not AP-2 which mediated endocytosis. Furthermore, AP-3δ siRNA knockdown increased the surface expression of CB1R in both Neuro2A cells and in primary hippocampal neurons (Rozenfeld and Devi, 2008). The site of CB1R/AP-3 interaction was determined, although AP-3 generally binds to

dileucine- or tyrosine-based sorting signals (Ohno et al., 1998; Darsow et al., 1998).

They therefore propose that CB1R is constitutively targeted for lysosomal degradation by AP-3 association at the TGN (Rozenfeld and Devi, 2008; Rozenfeld, 2011). However, a small proportion of CB1R rescued from degradation and rerouted to the axon.

AP-3 isoforms have been proposed to play additional specialised roles in neurons including biogenesis of synaptic vesicle and sorting of transmembrane proteins from endosomes to synaptic vesicles (Nakatsu et al., 2004; Salazar et al., 2004; Guardia et al., 2018; Danglot and Galli, 2007). Recently, AP-3 has been suggested to sort polarised proteins from the TGN to axons in *C. elegans* (Li et al., 2016). These data suggest the possibility of additional roles of AP-3 in trafficking of CB1R to axons and further investigation is required determine the role of AP-3/CB1R interaction on CB1R trafficking. **Figure 1-17** summarises this model.

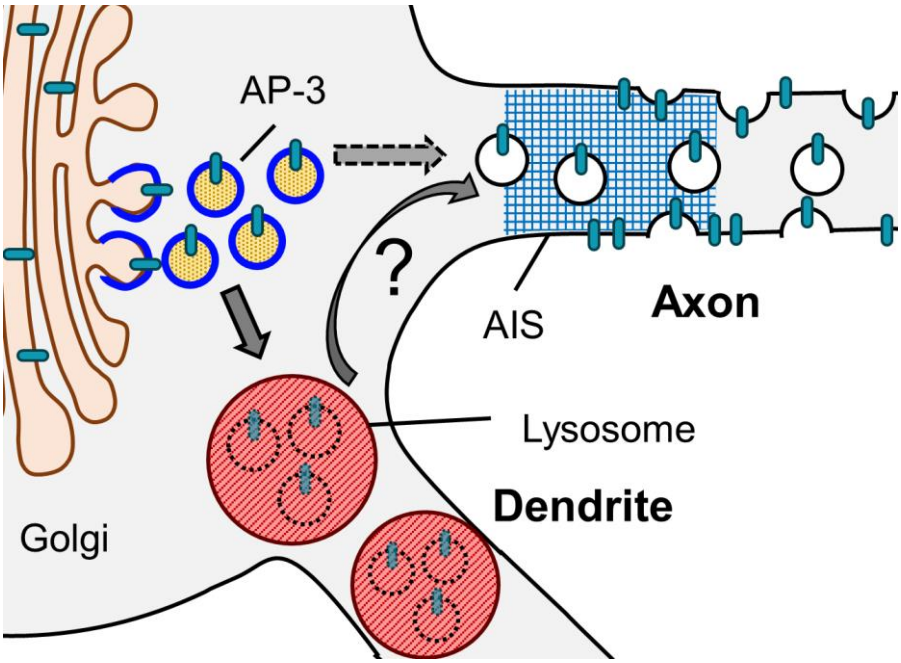

Figure 1-17 Model 3: Constitutive sorting somatodendritic lysosomes.

CB1R is constitutively sorted by AP-3 from the TGN to somatodendritic lysosomes. Under unknown conditions, CB1R is rescued from degradation and rerouted to axons (arrow with question mark). It is possible that this unknown mechanism is also AP-3-dependent since in AP-3 sorts cargo from the TGN to axons in *C. elegans* (dotted arrow). AIS = axon initial segment.

The discrepancies can, in part, be attributed to differences in tagging CB1R (e.g. N-terminal vs. C-terminal; small affinity tags vs. fluorophore tags), as well as differences in methodology and cell type used. Lenkei's group use a CB1R tagged C-terminally with EGFP and N-terminally tagged with FLAG, whereas the Irving and Devi groups use an N-terminally-tagged construct. C-terminally tagged constructs run the risk of interfering with sorting motifs and/or interactions with trafficking proteins. Indeed, comparisons between C- and N-terminally tagged versions of CB1R expressed in HEK293 cells or Neuro2A cells indicate that C-terminal tagging interfered with CB1R trafficking, causing a 2-3-fold increase in surface expression compared to N-terminal tagging, which, while not directly compared, was closer in phenotype to endogenous CB1R (Rozenfeld and Devi, 2008). Importantly, C-terminal interacting proteins have been reported to modulate surface expression and internalisation of CB1R (see 1.3.7.3 Interacting proteins). Therefore, the difference in surface expression of N- and C-terminally tagged constructs is likely due to interfering with binding of these proteins. Further studies are needed to address this issue by comparing the surface distribution of N-, and C-terminally tagged CB1R to untagged or endogenous CB1R in primary hippocampal neurons.

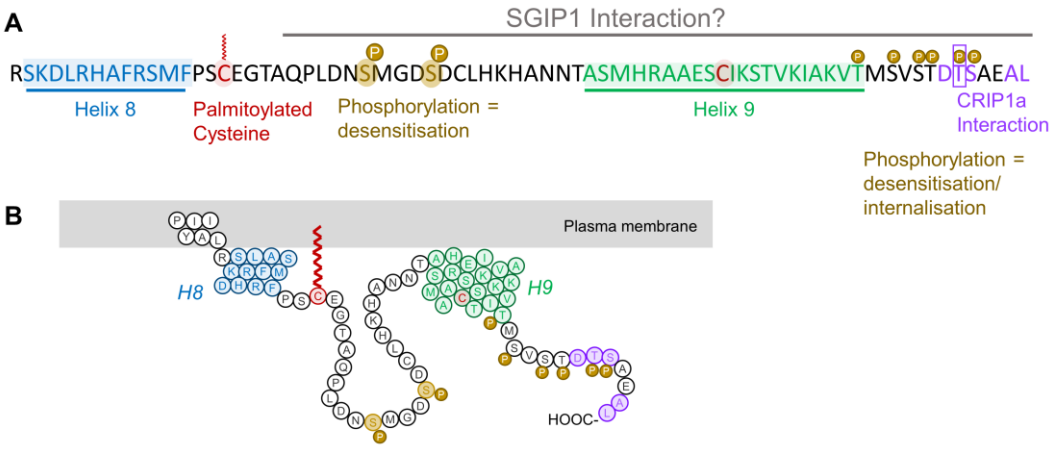

Figure 1-18 Schematic of rat ctCB1R.

Amino acid sequence (**A**) and topology (**B**) of rat CB1R. Two amphipathic helical domains, *H8* and *H9*, are highlighted in blue and green, respectively. A cysteine residue (red) located C-terminally of *H8* is palmitoylated, modulating signalling and internalisation of CB1R. Another cysteine residue located in *H9* has the potential to be modified. In the event of agonist stimulation, phosphorylation of the two serine residues between the helices is required for desensitisation, whereas phosphorylation of 6 serine and threonine residues in the distal C-terminal tail are required for internalisation (yellow). The residues required for CRIP1a binding are highlighted in purple. Phosphorylation of T468 (box) reduces binding efficiency of CRIP1a. The exact binding site of SGIP1 is unknown but occurs within A420-L473 (grey line).

1.3.7 Carboxy-terminus of CB1R (ctCB1R)

The CB1R carboxy-terminal tail has 73 residues (rat CB1R = R401-L473; human CB1R = R400-L472; **Figure 1-18**). It contains two structural motifs, Helix 8 (*H8*) and Helix 9 (*H9*), and several post-translationally modifiable residues.

Like all GPCRs the ctCB2R mediates signalling, by direct interactions with G-proteins and β-arrestins and by interactions with other intracellular loops, and trafficking, especially internalisation, of CB1R (see (Stadel et al., 2011) for review). Here, the focus is mainly on the role of the ctCB1R in its trafficking.

1.3.7.1 Structure

ctCB1R contains two putative amphipathic helices, *H8* and *H9*, that likely associate with the plasma membrane along their non-polar faces (**Figure 1-19**; **Figure 1-18**; (Ahn et al., 2009b; Stadel et al., 2011; Ahn et al., 2010)).

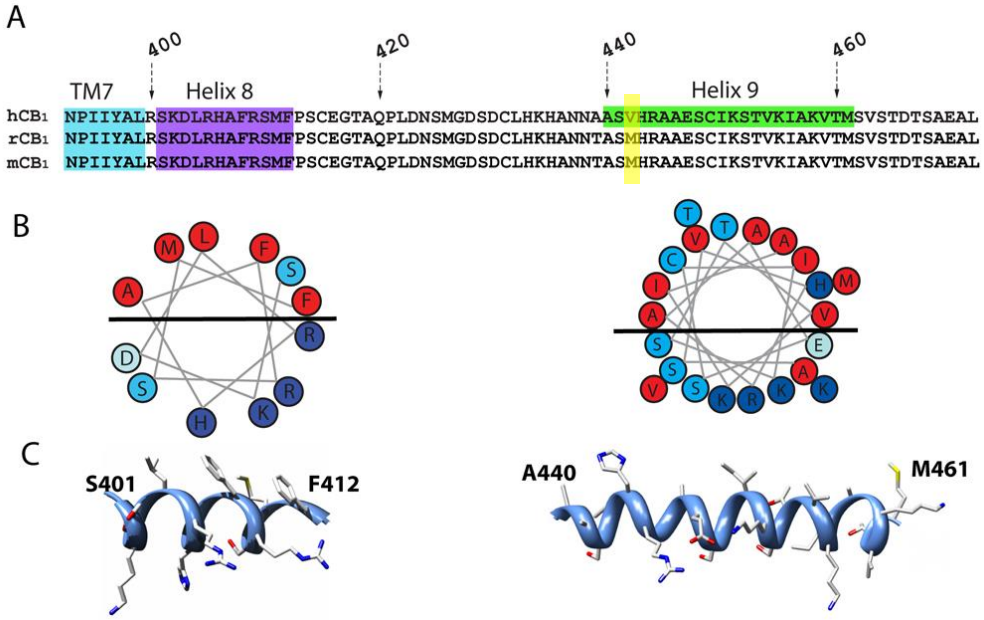

Figure 1-19 Predicted primary and secondary structure ctCB1R *H8* and *H9*.

(**A**) Aligned human, rat, and mouse ctCB1R sequences. TM7 (cyan), helix 8 (purple), and helix 9 (green) are highlighted. While *H9* is only highlighted in the human sequence, the single amino acid difference between human and rodent sequences (Val to Met; highlighted in yellow), is not predicted to perturb the proposed helical nature of conformation of *H9* (personal communications, Dr Drew Thompson, Woolfson Lab).

(**B**) Helical wheel projections of amphipathic helices *H8* (left) and *H9* (right). The black bar in the middle separates the hydrophobic face (red = non-polar residues) from the polar face (dark blue = positively charged residues, light blue = serines/threonines in light blue, turquoise = negatively charged residues).

(**C**) Ribbon illustrations of *H8* (left) and *H9* (right).

This figure is from (Stadel et al., 2011). Legend is modified from (Hildick, 2013).

1.3.7.1.1 Helix 8

The amphipathic *H8* is a common feature of class A GPCRs (Han et al., 2001), and is interchangeable between certain receptors (Spomer et al., 2014). A conserved role of *H8* has yet to be identified, although it has been implicated in ER exit and trafficking, membrane localisation and insertion, and as a site for G-protein coupling and β-arresting binding (Stadel et al., 2011; Pandey et al., 2019). Disruption of *H8* helicity and hydrophobicity impairs the trafficking of CB1R, causing it to accumulate in the ER (Ahn et al., 2010).

Interestingly, *H8* has been reported to undergo a dynamic conformational switch, unravelling during receptor activation to allow for new interactions, potentially controlled by palmitoylation or de-palmitoylation of a conserved cysteine residue usually located close to *H8* (Sensoy and Weinstein, 2015; Gopala Krishna et al., 2002).

1.3.7.1.2 Helix 9

H9 is also proposed to be an amphipathic and likely associates with the plasma membrane along its polar face (Stadel et al., 2011; Ahn et al., 2009b). Analogous domains have only been reported in squid rhodopsin and the bradykinin receptor (Piserchio et al., 2005; Murakami and Kouyama, 2008). Squid rhodopsin *H9* interacts with *H8* and transmembrane domain 6 (TM6) and other intracellular loops, suppressing its rotational freedom (Stadel et al., 2011; Shimamura et al., 2008).

Little is known about the functional relevance of *H9*, although, interestingly, the analogous regions in squid rhodopsin and bradykinin receptor constitute a $G\alpha_q$ binding site (Piserchio et al., 2005; Murakami and Kouyama, 2008).

1.3.7.2 Post-translational modifications

1.3.7.2.1 Phosphorylation

During ligand activation, phosphorylation of S426 and S430 (**Figure 1-18**) is required for desensitisation of CB1R (Jin et al., 1999; Kouznetsova et al., 2002; Daigle et al., 2008a; Morgan et al., 2014), but is not sufficient for internalisation. Further phosphorylation of T461, S463, S465, T466, T468, and S469 is required for internalisation (Straiker et al., 2012b; Daigle et al., 2008b). See 1.3.4.2.1 Desensitisation for more details.

1.3.7.2.2 Palmitoylation

The presence of a palmitoylation site just C-terminally of Helix 8 is conserved amongst class A GPCRs (Sensoy and Weinstein, 2015; Gopala Krishna et al., 2002). Computational modelling of CB1R, as well as the dopamine D2 receptor and the β2-adrenergic receptor, suggests that palmitoylation of this conserved residue enhances the stability and membrane/lipid raft association of the amphipathic *H8* (Sensoy and Weinstein, 2015; Oddi et al., 2017). When this residue is de-palmitoylated, membrane association of *H8* is no longer energetically favourable, so the helix unravels, causing some interaction sites to be lost and exposing other interaction sites to the aqueous domain (Sensoy and Weinstein, 2015).

Palmitoylation of C415 (C416 in rat CB1R) affects the trafficking, localisation, and signalling of CB1R (Oddi et al., 2012, 2017, 2018). Specifically, mutation of this residue to an alanine reduced plasma membrane expression due to a decreased association of CB1R with lipid rafts and caveolin-1(**Figure 1-13**; (Oddi et al., 2012, 2017)). Consistent with its lack of lipid raft association, the mutant displayed higher diffusional mobility and lacked agonist-induced internalisation (Oddi et al., 2017).

CB1R signalling was also diminished in the C416A mutant due to the instability of *H8* which prevented the interaction of CB1R with G-proteins (which themselves are palmitoylated; **Figure 1-11** black zigzag line) and β-arrestins (Oddi et al., 2012, 2017, 2018).

1.3.7.3 Interacting proteins

1.3.7.3.1 G-protein coupled receptor associate protein 1 (GASP1)

GASP1 has been linked to the intracellular sorting of CB1R to lysosomes following chronic exposure of agonist. GASP proteins (GASP1-10) bind the C-termini of several GPCRs, including the D4 dopaminergic receptor, the β2 adrenergic receptor, and the δ opioid receptor, for post-endocytic sorting to lysosomes for degradation (Whistler et al., 2002; Heydorn et al., 2004; Simonin et al., 2004; Moser et al., 2010). GASP1/CB1R interaction was confirmed by co-immunoprecipitations of exogenously expressed GASP1 with full-length CB1R exogenously expressed in HEK293 cells (Tappe-Theodor et al., 2007; Martini et al., 2007). However, the exact binding site of GASP1 is unclear: GASP1 co-immunoprecipitated with the very distal 14 amino acids of ctCB1R (Martini et al.,

2007), but also co-immunoprecipitated with CB1R lacking this section (Tappe-Theodor et al., 2007), suggesting that there may be multiple binding sites for GASP1 (Stadel et al., 2011).

Consistent with its known function, expression of a dominant negative GASP1 attenuates downregulation of surface CB1R induced by chronic (24 hours) WIN55,212-2 treatment in both expressed cells and primary neurons (Tappe-Theodor et al., 2007; Martini et al., 2007). Importantly, this process has been implicated in the development of tolerance to cannabinoids in habitual cannabis users since GASP1 knockout mice do not develop tolerance to repeated administration of WIN55,212-2 unlike wild-type mice (Martini et al., 2010).

1.3.7.3.2 Cannabinoid Receptor Interacting Protein 1a and 1b (CRIP1a/b)

1.3.7.3.2.1 Identification and binding

Cannabinoid receptor interacting protein 1a (CRIP1a), and its primate-specific isoform CRIP1b, were identified as CB1R interacting proteins by yeast-two hybrid screens against a human cDNA library and validated by GST-pulldowns between purified CRIP1a/b protein and ctCB1R (Niehaus et al., 2007). Furthermore, CRIP1a co-localises with CB1R at presynaptic boutons (Guggenhuber et al., 2016).

Five amino acids in the very distal carboxy terminus of CB1R control CRIP1a binding: D467, T468, S469, A472, and L473 (**Figure 1-18**; (Mascia et al., 2017). A similar motif present in $mGlu_{8a}R$ also binds CRIP1a (Mascia et al., 2017). In mice, CRIP1a co-expresses with CB1R in both pyramidal neurons and interneurons of the hippocampus (Guggenhuber et al., 2016). CRIP1a affects CB1R internalisation and modulates its signalling (Mascia et al., 2017; Blume et al., 2017; Guggenhuber et al., 2016; Blume et al., 2016; Smith et al., 2015; Blume et al., 2015; Niehaus et al., 2007)

1.3.7.3.2.2 CRIP1a prevents CB1R internalisation

CRIP1a overexpression supresses agonist-induced downregulation of CB1R but not desensitisation (Smith et al., 2015; Blume et al., 2016) by competing with β-arrestin 2 for binding of ctCB1R (Blume et al., 2017). Phosphorylation of ctCB1R residue T468 reduced binding efficiency of CRIP1a, allowing for β-arrestin2 binding (Blume et al., 2017). This is consistent with the fact that phosphorylation of central ctCB1R residues is necessary for desensitization but not internalisation, which

requires phosphorylation of the distal tail (Jin et al., 1999; Kouznetsova et al., 2002; Daigle et al., 2008a; Morgan et al., 2014; Straiker et al., 2012b).

1.3.7.3.2.3 CRIP1a modulates CB1R signalling

Overexpression of CRIP1a attenuates CB1R G-protein signalling in HEK293 cells, N18TG2 cells, and autaptic neuronal cultures, affecting the inhibition of N-type VGCCs and ERK phosphorylation (Smith et al., 2015; Niehaus et al., 2007; Blume et al., 2015).

1.3.7.3.2.4 CRIP1a and disease

Cannabis use, especially in adolescence, is associated with development of psychosis and schizophrenia in those who already have an underlying genetic predisposition for the disease (Arseneault et al., 2002; Andréasson et al., 1989; Henquet et al., 2005). Furthermore, individuals with schizophrenia display aberrations in CB1R expression and ligand binding (Zavitsanou et al., 2004; Dalton et al., 2011).

Genome-wide methylation analysis of human patients with schizophrenia revealed aberrant methylation of the CRIP1a DNA promoter (Wockner et al., 2014). Moreover, overexpression of CRIP1a in the hippocampus of Sprague Dawley rats induced schizophrenia-like symptoms and changes in dopamine activity (Perez et al., 2019) These data suggest that modulation CRIP1a-mediated regulation of CB1R could be a therapeutic target for treatment of schizophrenia.

1.3.7.3.3 Src homology 3-domain growth factor receptor-bound 2-like (endophilin) interacting protein 1 (SGIP1)

1.3.7.3.3.1 Identification

Src homology 3-domain growth factor receptor-bound 2-like (endophilin) interacting protein 1 (SGIP1) was first identified as a novel transcript in 2005 in a screen of hypothalamic mRNA in the obesity model of *Psammomys obesus*, also called the fat sand rat (Trevaskis et al., 2005). SGIP1 mRNA was upregulated in the hypothalamus in obese fat sand rats compared to lean ones and siRNA-mediated reduction of hypothalamic SGIP1 inhibited food intake, suggesting that SGIP1 in the hypothalamus plays a role in energy expenditure (Trevaskis et al., 2005). In humans, genetics studies indicate that single nucleotide polymorphisms (SNPs) in SGIP1 associate with fat mass (Cummings et al., 2012; Yako et al., 2015).

1.3.7.3.3.2 SGIP1 domains and function

As its name implies, SGIP1 interacts strongly with endophilins, important regulators of clathrin-mediated endocytosis (CME), specifically with endophilin 3 (Trevaskis et al., 2005). SGIP1 is an orthologue of Fer/Cip4 homology domain-only proteins (FCHo1/2), members of the muniscin family of cargo adaptors (**Figure 1-20**) (Hollopeter et al., 2014). It contains an N-terminal membrane phospholipid binding (MP) domain (although not an F-BAR domain like the rest of the muniscin family) capable of binding liposomes containing PS, PI 3-phosphate, PI 4-phosphate, PI 3,4-bisphosphate, PI 3,5-bisphosphate, or PI(4,5)P_2 (Uezu et al., 2007). Next is an AP-2 activator motif (APA) that directly binds to AP-2 (Hollopeter et al., 2014). A proline rich domain (PRD) likely contains several SH3-domain binding sites. SH3-domain containing proteins is binds to include endophilin (Trevaskis et al., 2005), intersectin 1 (ITSN1), a plasma membrane-associated scaffolding protein important for recruitment of components of the endocytic complex, and amphiphysin, an important membrane-deforming protein that regulates dynamin oligomerisation (Dergai et al., 2010). Lastly, the C-terminal µ homology domain (µHD), highly conserved in the muniscin family, mediates the interaction with Eps15, an important adaptor protein of CME (Uezu et al., 2007) and binds to cargo such as synaptotagmin (Lee et al., 2019) and CB1R (Hájková et al., 2016).

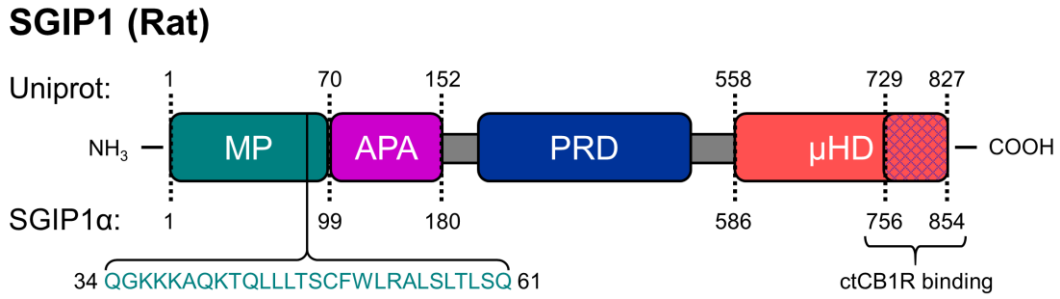

Figure 1-20 Domains of SGIP1 and SGIP1α.

Domains of the 827 aa long SGIP1 (Uniprot sequence) and the 854 aa long SGIP1α. The brain-specific splicing variant SGIP1α contains an extra sequence in the MP domain. The last 99 residues (crosshatching) binds ctCB1R.

Key: MP = membrane phospholipids binding domain; APA = AP-2 Activator motif; PRD = Proline-Rich Domain; µHD = µ Homology Domain.

Apart from its domain structure and interacting partners, SGIP1 is also functionally connected to CME. SGIP1 overexpression in Cos7 cells reduces transferrin (Tfn) and epidermal growth factor (EGF) uptake (Uezu et al., 2007). Knockdown of

SGIP1 in N1E115 cells (mouse neuroblastoma cells) reduces Tfn uptake, but not EGF uptake, potentially due to compensatory pathways (Uezu et al., 2007).

1.3.7.3.3.3 SGIP1 and CB1R

SGIP1, including the brain-specific isoform SGIP1α, is enriched in presynaptic boutons (Wilhelm et al., 2014) and co-localises with CB1R, bassoon, and synaptotagmin (Hájková et al., 2016; Lee et al., 2019). Furthermore, SGIP1 selectively promotes the internalisation of synaptotagmin, but not synaptophysin or VAMP2 at presynaptic boutons (Lee et al., 2019).

A yeast two-hybrid screen using ctCB1R C-terminally of *H8* as bait detected the last 99 amino acids of SGIP1 as prey (Hájková et al., 2016) (**Figure 1-20**). The association between CB1R and SGIP1 was verified using co-immunoprecipitation, bioluminescence resonance energy transfer (BRET) assays (Hájková et al., 2016). Interestingly, co-expression of SGIP1 with CB1R in HEK293 cells interfered with agonist-induced internalisation of CB1R compared to HEK293 cells expressing CB1R alone (Hájková et al., 2016). This reduction in agonist-induced internalisation was almost the same the reduction in internalisation that occurs when blocking CME using expression of a dominant negative dynamin (Dyn K44A). Furthermore, a smaller, but significant, reduction in constitutive internalisation was observed in CB1R/SGIP1 co-expressing cells with exogenous agonised applied compared to HEK293 cells expressing CB1R alone. Furthermore, SGIP1 affected the signalling of activated CB1R: it enhanced β-arrestin2 – but not β-arrestin1 – association with activated CB1R and reduced downstream ERK1/2 activation. However, $G_{i/o}$-protein activation and downstream Ca^{2+} mobilisation were unaffected (Hájková et al., 2016). The reported effects of SGIP1 on CB1R signalling and internalisation is summarised in **Figure 1-21**.

1.4 THERAPEUTIC POTENTIAL OF THE ECS

There has been a lot of interest in recent decades in the use of cannabis, or cannabis constituents (specifically, Δ^9-THC and/or cannabidiol), to treat a wide range of diseases. There has been some success: e.g. Sativex (a combination of THC and CBD) is legal in both the USA and the UK as an effective treatment for chronic pain and multiple sclerosis and treatment of epileptic patients with CBD can reduce seizure frequency by up to 50% (Freeman et al., 2019). However, there have also been a few failures. Rimonabant, a CB1R antagonist, was launched in

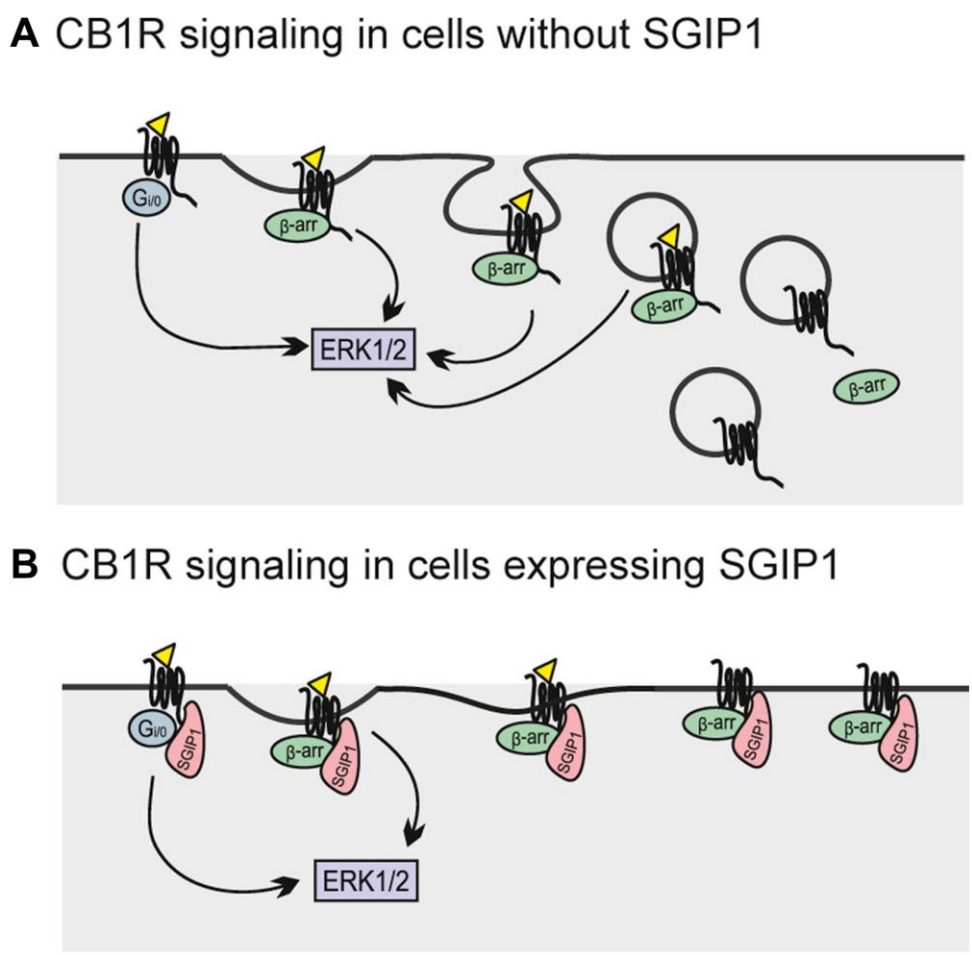

Figure 1-21 Schematic of SGIP1 effect on CB1R signalling and internalisation

A) Without SGIP1, CB1R undergoes β-arrestin mediated agonist-induced internalisation. β-arrestin signalling activates ERK1/2.

B) With SGIP1, CB1R activation still recruits β-arrestin. However, internalisation does not occur, and ERK1/2 activation is attenuated.

Figure from (Hájková et al., 2016).

2006 as a weight-loss treatment. However, it was pulled off the market in 2008 due to adverse side effects, including the development of serious mood disorders including suicidal ideation (Johansson et al., 2009). More recently, a clinical trial of a FAAH inhibitor (degradative enzyme for anandamide) was stopped at phase I as a result of the development of serious side effects, tragically resulting in the death of one subject (Kaur et al., 2016b; a).

It is not entirely surprising that drugs that target the ECS as a whole would have a multitude of unwanted side effects given the ubiquity, complexity, and pleiotropic nature of the CB1R. Therefore, in recent years, studies have focussed on a more targeted approach. One approach is to target drugs to specific tissues and tightly control the dosage (Kaur et al., 2016a). Furthermore, there has been a huge push

to identify new allosteric modulators of CB1R because they have the potential for subtype- and pathway-specificity (Khurana et al., 2017).

This push draws on the amassed wealth of knowledge of CB1R physiology and pharmacology. However, comparatively little is understood about the basic cellular mechanisms underpinning ECS trafficking and distribution. Thus, better understanding of how cannabinoid receptors and eCBs are synthesized, trafficked, and degraded holds massive promise for therapeutic intervention for a wide range of diseases.

1.5 AIMS

The overarching aim of my work was to characterise the mechanisms that establish the stringent axonal polarisation of CB1R and determine the underpinning cell biological mechanisms. This is important because defining the trafficking pathways and protein interactions that mediate axonal CB1R localisation could provide novel targets to enhance or reduce ECS signalling without the need to directly activate or block the receptor.

More specifically, the objective of each series of experiments were:

1.5.1 Chapter 3:

- To examine how the axonally polarised surface distribution of CB1R is both (1) established and (2) maintained.
- To define the contribution of forward trafficking to the polarised surface distribution of CB1R.

1.5.2 Chapter 4:

- To determine whether the C-terminus of CB1R plays a role (1) selective delivery and/or (2) selective retention of axonal CB1R.
- To determine the role of the C-terminal motif Helix 9 (*H9*) in CB1R trafficking and surface polarisation.

1.5.3 Chapter 5:

- To determine the mechanism by which *H9* increases membrane retention.
- To screen for interacting partners of *H9* that may play a role in 1) preferential axonal delivery and/or 2) membrane retention.

Chapter 2 – MATERIALS & METHODS

2.1 MATERIALS

2.1.1 Chemicals

All chemicals were purchased from Sigma-Aldrich (Merck) unless otherwise stated. Non-fat milk powder was own-brand from The Co-operative. Acids and solvents were purchased from Fisher Scientific unless otherwise stated.

2.1.2 Consumables and equipment

2.1.2.1 Glass- and plastic-ware

Gilson-style basic and sterile filter pipette tips (10 µL, 20 µL, 200 µL, 1000 µL, and 1250 µL) were purchased from STARLAB. 0.2 mL and 0.5 mL thin-walled PCR tubes were also purchased from STARLAB, and 1.5 mL microcentrifuge tubes were purchased from Eppendorf. 15 mL and 50 mL Falcon tubes, 5 mL Bijou tubes, and 30 mL Universal tubes were from Greiner. 5 mL, 10 mL, and 25 mL serological pipettes were purchased from Greiner as well. Cell culture plates (12-well and 6-well), dishes (35 mm, 60 mm, 10 cm), and flasks (T25, T75, and T175) were also bought from Greiner. Glass coverslips (24 mm and 25 mm) were from VWR. Syringes and needles were from Terumo. 0.2 µm syringe filters were from Sartorius.

2.1.2.2 Electrical equipment

Laminar flow hoods were from Holten LaminAir. Cell culture incubators were from RS Biotech and were serviced every 6 months. Gel electrophoresis power packs were from Bio-Rad Laboratories. Centrifuges were from Bechman-Coulter and Jouan. Benchtop microcentrifuges were from Eppendorf. The PCR Thermocycler was a MJ Research PTC-2000 Peltier Thermal Cycler. DNA and RNA concentrations were quantified using the NanoDrop™ ND-1000 (LabTech). The X-ray film developer (SRX-101A) was from Konica and the Odyssey Fc detection system was from LI-COR.

2.1.2.3 Confocal microscope specifications

A Leica SPE single channel, a Leica SP8, and a Leica SP5II confocal laser scanning microscope (Wolfson Bioimaging Facility, University of Bristol), or a Zeiss

LSM510 UV META Axiovert 200M laser scanning microscope was used for fixed confocal microscopy. 40x or 63x oil immersion objectives were used.

2.1.3 Cell culture reagents

2.1.3.1 Cell lines and primary cultures

Human Embryonic Kidney (HEK293T) cells, HeLa cells, and Baby Hamster Kidney (BHK-21) cells were obtained from the European Collection of Authenticated Cell Cultures (ECACC). Stocks were aliquoted in 1% DMSO, frozen slowly to −70°C in a Mr. Frosty™ freezing container (Thermo) and stored in liquid nitrogen.

Primary hippocampal and cortical neurons were cultured from E17-E18 Wistar Han rats housed in the University of Bristol Animal Services Unit in accordance with Home Office guidelines.

2.1.3.2 Media reagents

Table 2-1 contains a list of components of different cell culture media.

Table 2-1 Media Reagents

REAGENT	SUPPLIER	CELL TYPE	CAT. NO.
Neurobasal	Thermo Fisher Scientific (Gibco)	Neuronal	21103049
Horse Serum	Merck (Sigma-Aldrich)	Neuronal	H1270
B27	Thermo Fisher Scientific (Gibco)	Neuronal	A3582801
GS21	MTI GlobalStem	Neuronal	3100
GlutaMAX	Thermo Fisher Scientific (Gibco)	Neuronal	35050038
B27 plus	Thermo Fisher Scientific (Gibco)	Neuronal	A3582801
DMEM	Lonza	HEK293T/ HeLa	12-614F
L-Glutamine	Merck (Sigma-Aldrich)	Cell lines	G7513
FBS	Merck (Sigma-Aldrich)	Cell lines	F7524
Alpha MEM medium	Merck (Sigma-Aldrich)	BHK cells	M8042

2.1.4 Molecular biology reagents

2.1.4.1 Kits and enzymes

RNA was extracted from cells with the RNeasy Mini Kit (QIAGEN). cDNA was synthesized with the RevertAid First Strand cDNA Synthesis kit (Thermo). DNA fragments were purified using the GeneJET Gel Extraction kit (Thermo). Amplified plasmid DNA was isolated from *E. coli* using the GeneJET Plasmid Miniprep or Midiprep kits (Thermo).

Restriction enzymes, Calf Intestinal Alkaline Phosphatase (CIP), and 10x CutSmart buffer were from New England BioLabs (NEB) and T4 DNA Ligase was from TaKaRa.

2.1.4.2 E. coli competent cells and bacterial reagents

Home grown and commercially bought DH5α and XL1-blue competent cells were used to amplify plasmid DNA (**Table 2-2**). XL1-blue competent cells were exclusively used for amplification of viral plasmids due to their reduced tendency to recombine long terminal repeats (LTRs) present in viral vectors.

Table 2-2 Competent *E. coli* strains

STRAIN	CHROMOSOMAL GENOTYPE	SUPPLIER
DH5α	F- Φ80*lac*ZΔM15 Δ(*lac*ZYA-*arg*F) U169 *rec*A1 *end*A1 *hsd*R17 (rk^-, mk^+) *pho*A *sup*E44 λ^- *thi*-1 *gyr*A96 *rel*A1	Thermo Fisher
XL1-Blue	*recA1 endA1 gyrA96 thi-1 hsdR17 supE44 relA1 lac* [F´ *proAB* $lacI^qZ\Delta M15$ Tn*10* (Tet^r)*]*	Agilent

2.1.4.3 Plasmid Vectors

Table 2-3 contains a list of plasmid vector backbones used.

Table 2-3 Plasmid vector backbones

BACKBONE	NOTES
pcDNA3.1(+)	CMV promoter
pFLAG	pcDNA3.1(+) with N-terminal FLAG tag; Made by Dr Kevin Wilkinson
pEGFP-C2	To tag protein of interest N-terminally with EGFP
pmCherry	To tag protein of interest N-terminally with mCherry

pSUPER.neo+mCherry	H1 RNA promoter + shRNA cassette; PGK protein promoter + mCherry; Based on pSUPER.neo+GFP (Oligogene); Made by Dr Kevin Wilkinson
pXlg3	Lentiviral vector; Modified to contain a PacI/XhoI restriction sites where H1 promoter + shRNA can be cloned in for knockdown of protein of interest; protein expression driven under an SFFV promoter; contains a WPRE sequence to enhance expression; made by Dr Kevin Wilkinson
pSinRep5	Sindbis viral vector
pIRESneo3	RUSH construct; expression of an ER localised streptavidin-KDEL is driven under a CMV promoter; expression of the receptor of interest is driven under an IRES element

2.1.4.4 Oligonucleotides

All primers were bought as oligonucleotides from Sigma-Aldrich (now Merck).

2.1.4.4.1 Primers for overexpression constructs

A list of primers for overexpression constructs can be found in **Table 2-4**.

Table 2-4 Primers for overexpression constructs

PRIMER	SEQUENCE (5'-3')	RESTRICTION SITE
CB1R For	CACGGCCGGCCA***ATG***ACATTCAGTATGAAGAT	FseI
CB1R FFL For	CACGGCCGGCCAAAGTCGATCCTAGATGGC	FseI
SP^{Il-2} For	CACGGATCCACGCCACC***ATG***TACAGGATGC	BamHI
SP^{Il-2} For	CACACTAGTGCCACC***ATG***TACAGGATGCAA	SpeI
ctCB1R For	CACGAATTCAGGAGCAAGGACCTGAGACAT	EcoRI
EGFP For	CACGCTAGCGCCACC***ATG***GTGAGCAAGG	NheI
CB1R Rev	GTGTTAATTAATCACAGAGCCTCGGCGGACGT	PacI
CB1R Rev	GTGGCGGCCGCATCACAGAGCCTCGGCGGA	NotI
CB1R Rev	CTCGGATCCTCACAGAGCCTCGGCGGACGT	BamHI
CB1R Rev	CTCGGGCCCTCACAGAGCCTCGGCGGACGT	ApaI
SGIP1 For	CACGGTACCGAAGGACTGAAAAAACGTACAAGA	KpnI
SGIP1 Rev	GTGGGATCCTTAGTTATCTGCCAAGTATTTTCCTGCAGC	BamHI

Key: green, underlined – restriction site; blue – complementary to template; blue, bold, italics – start codon; orange – Kozak consensus sequence.

2.1.4.4.2 Primers for site-directed mutagenesis

In order to generate point mutations by site-directed mutagenesis (SDM), primers were designed to incorporate the desired point mutation flanked by 21-30 base pairs on either side that were entirely complementary to the template. In order to delete a part of a construct (in this case, SBP), primers were designed to be complementary to 30 base pairs on either side of the area that needed to be deleted. Sense and antisense primers were ordered from Sigma. A list of SDM primers can be found in **Table 2-5**.

Table 2-5 Primers for site-directed mutagenesis

PROTEIN	MUTATION	PRIMER	SEQUENCE (5'-3')
CB1R	C450A	Sense	CACAGGGCCGCGGAGAGCGCCATCAAGAGCA CCGTTAAG
		Antisense	CTTAACGGTGCTCTTGATGGCGCTCTCCGCGG CCCTGTG
CB1R	2P A447P + V455P	Sense	GCCAGCATGCACAGGGCCCCGGAGAGCTGCAT CAAGAGC AGCTGCATCAAGAGCACCCCTAAGATCGCGAA GGTG
		Antisense	GCTCTTGATGCAGCTCTCCGGGGCCCTGTGCA TGCTGGC CACCTTCGCGATCTTAGGGGTGCTCTTGATGCA GCT
Rab5	S34N (DN)	Sense	GGAGAGTCCGCTGTTGGCAAAAATAGCCTAGT GCTTCGTTTTGTG
		Antisense	CACAAAACGAAGCACTAGGCTATTTTTGCCAAC AGCGGACTCTCC
Rab5	Q79L (DA)	Sense	GAAATATGGGATACAGCTGGTCTAGAACGATAC CATAGCCTAGCA
		Antisense	TGCTAGGCTATGGTATCGTTCTAGACCAGCTGT ATCCCATATTTC
CB1R	Minus SBP	Sense	GCACTAAGTCTTGCACTTGTCACGAATTCCGTG AGCAAAGGCGAGGAGCTGTTCACCGGG
		Antisense	CCCGGTGAACAGCTCCTCGCCTTTGCTCACGG AATTCGTGACAAGTGCAAGACTTAGTGC

Key: Blue – complementary to template; red – point mutation change

2.1.4.4.3 Primers for knockdown constructs

Table 2-6 is a list of oligos for the generation of shRNA knockdown constructs.

Table 2-6 Knock-down oligos

PROTEIN	NAME		PRIMER	SEQUENCE (5'-3')
AP3D1	KD#1	21mer	Sense	GATCCCCAGCTGCTCACCAAGATCATTGTTCAA GAGACAATGATCTTGGTGAGCAGCTTTTTTC
			Antisense	TCGAGAAAAAAGCTGCTCACCAAGATCATTGTC TC TTGAACAATGATCTTGGTGAGCAGCTGGG
	KD#2	20mer	Sense	GATCCCCACCGCATGTTCGACAAGAACTTCAA GAGAGTTCTTGTCGAACATGCGGTTTTTTC
			Antisense	TCGAGAAAAAACCGCATGTTCGACAAGAACTCT C TTGAAGTTCTTGTCGAACATGCGGTGGG
SGIP1	KD#1	25mer	Sense	GATCCCCCCAATACCAAGGAATTCTGGGTAAAT TCAAGAGATTTACCCAGAATTCCTTGGTATTGG TTTTTC
			Antisense	TCGAGAAAAACCAATACCAAGGAATTCTGGGTA AATCTCTTGAATTTACCCAGAATTCCTTGGTATT GGGGG

Key: green – restriction site (BamHI/XhoI); green, underlined – overhang; yellow – target sequence

A list of non-targeting control shRNA oligos is found in **Table 2-7**.

Table 2-7 Non-targeting oligos

NAME	PRIMER	SEQUENCE
19mer	Sense	GATCCCCAATTCTCCGAACGTGTCACTTCAA GAGAGTGACACGTTCGGAGAATTTTTTTC
	Antisense	TCGAGAAAAAAATTCTCCGAACGTGTCACTCTC TTGAAGTGACACGTTCGGAGAATTGGG
21mer	Sense	GATCCCCAACGTACGCGGAATACTTCGATTCAA GAGATCGAAGTATTCCGCGTACGTTTTTTTC
	Antisense	TCGAGAAAAAAACGTACGCGGAATACTTCGATCTC TTGAATCGAAGTATTCCGCGTACGTTGGG
29mer	Sense	GATCCCCGCACTACCAGAGCTAACTCAGATAGTACTTTCA A GAGAAGTACTATCTGAGTTAGCTCTGGTAGTGCTTTTTC
	Antisense	TCGAGAAAAAGCACTACCAGAGCTAACTCAGATAGTACTT CTC TTGAAAGTACTATCTGAGTTAGCTCTGGTAGTGCGGG

Key: green – restriction site (BamHI/XhoI); green, underlined – overhang; yellow – target sequence

2.1.4.5 Mammalian overexpression and shRNA plasmids

A list of overexpression constructs can be found in **Table 2-8**. CB1R, CRIP1a, and SGIP1 correspond to *Rattus norvegicus* sequences. Rab5 is a *Homo sapiens* sequence.

All CB1R constructs lack the first 25 N-terminal amino acids to avoid possible cleavage of the SBP-EGFP tag (McDonald et al., 2007b; Nordström and Andersson, 2006). A full full-length construct (FFL) was also generated. SGIP1 was cloned out of a cDNA library made from RNA extracted from DIV 21 cortical cultures. The SGIP1 transcript variant corresponds to the predicted *Rattus norvegicus* SH3-domain GRB2-like (endophilin) interacting protein 1 (Sgip1), transcript variant X21, mRNA.

A list of shRNA knockdown constructs and their sources can be found in **Table 2-9**. Targeting sequences were designed either according to previously published targeting sequences (Uezu et al., 2007) or from verified sequences found in Sigma's online shRNA tool. 19mer (Choy et al., 2014; Carmichael et al., 2018; Zhu et al., 2018) and 21mer (Haar et al., 2007) non-targeting sequences have been previously published as scrambled controls. The 29mer non-targeting control sequence is from the Origene HuSH-29 kit.

Table 2-8 Overexpression plasmids

VECTOR	INSERT	PCR TEMPLATE	PRIMERS	RESTRICTION SITES	SOURCE
pcDNA1-	SP^{HgH}-SEP-$CB1R^{WT}$	N/A	N/A	N/A	Andrew Irving
pcDNA3.1-	SP^{HgH}-SEP-$CB1R^{WT}$	N/A	N/A	N/A	Keri Hildick
pcDNA3.1-	SP^{HgH}-SEP-$CB1R^{\Delta H9}$	N/A	N/A	N/A	Keri Hildick
pIRESneo3_Str-KDEL_IRES-	$SP^{Il\text{-}2}$-SBP-mCherry-Ecadherin	N/A	N/A	N/A	Perez
pIRESneo3_Str-KDEL_IRES-	$SP^{Il\text{-}2}$-SBP-EGFP-$CB1R^{WT}$	pcDNA3.1-SP^{HgH}-SEP-$CB1R^{WT}$	CB1R For CB1R Rev	FseI PacI	Ash Evans
pIRESneo3_Str-KDEL_IRES-	$SP^{Il\text{-}2}$-SBP-EGFP-$CB1R^{\Delta H9}$	pcDNA3.1-SP^{HgH}-SEP- $CB1R^{\Delta H9}$	CB1R For CB1R Rev	FseI PacI	This thesis
pIRESneo3_Str-KDEL_IRES-	$SP^{Il\text{-}2}$-SBP-mCherry-$CB1R^{WT}$	pcDNA3.1-SP^{HgH}-SEP- $CB1R^{WT}$	CB1R For CB1R Rev	FseI PacI	This thesis
pcDNA3.1-	$SP^{Il\text{-}2}$-SBP-EGFP-$CB1R^{WT}$	pIRESneo3_Str-KDEL_IRES- $SP^{Il\text{-}2}$-SBP-EGFP-$CB1R^{WT}$	$SP^{Il\text{-}2}$ For ctCB1 Rev	BamHI NotI	This thesis
pcDNA3.1-	$SP^{Il\text{-}2}$-SBP-EGFP-$CB1R^{\Delta H9}$	pIRESneo3_Str-KDEL_IRES- $SP^{Il\text{-}2}$-SBP-EGFP-$CB1R^{\Delta H9}$	CB1R For CB1R Rev	BamHI NotI	This thesis
pcDNA3.1-	$SP^{Il\text{-}2}$-SBP-EGFP-CB1R C450A	pcDNA3.1-$SP^{Il\text{-}2}$-SBP-EGFP-$CB1R^{WT}$	C450A	N/A	This thesis
pcDNA3.1-	$SP^{Il\text{-}2}$-SBP-EGFP-CB1R 2P	pcDNA3.1-$SP^{Il\text{-}2}$-SBP-EGFP-$CB1R^{WT}$	2P	N/A	This thesis
pcDNA3.1-	$SP^{Il\text{-}2}$-EGFP-$CB1R^{WT}$	pcDNA3.1-$SP^{Il\text{-}2}$-SBP-EGFP-$CB1R^{WT}$	Minus SBP	N/A	This thesis
pcDNA3.1-	$SP^{Il\text{-}2}$-EGFP-$CB1R^{\Delta H9}$	pcDNA3.1-$SP^{Il\text{-}2}$-SBP-EGFP-$CB1R^{\Delta H9}$	Minus SBP	N/A	This thesis

pXlg3-	$SP^{Il\text{-}2}$-EGFP-$CB1R^{WT}$	pcDNA3.1-$SP^{Il\text{-}2}$-EGFP-$CB1R^{WT}$	$SP^{Il\text{-}2}$ For CB1R Rev	SpeI BamHI	This thesis
pXlg3-	$SP^{Il\text{-}2}$-EGFP-$CB1R^{FFL}$	pcDNA3.1-HA-CB1R (including N-terminus)	CB1R FFL For CB1R Rev	FseI BamHI	This thesis
pEGFP-C2-	ct$CB1R^{WT}$	pcDNA3.1-SP^{HgH}-SEP- $CB1R^{WT}$	ctCB1R For CB1R Rev	EcoRI BamHI	Kevin Wilkinson
pEGFP-C2-	ct$CB1R^{\Delta H9}$	pcDNA3.1-SP^{HgH}-SEP- $CB1R^{\Delta H9}$	ctCB1R For CB1R Rev	EcoRI BamHI	This thesis
pSinRep5-	EGFP	N/A	N/A	N/A	Kevin Wilkinson
pSinRep5-	EGFP- ct$CB1R^{WT}$	pEGFP- ct$CB1R^{WT}$	EGFP For CB1R Rev	NheI ApaI	This thesis
pSinRep5-	EGFP- ct$CB1R^{\Delta H9}$	pEGFP- ct$CB1R^{\Delta H9}$	EGFP For CB1R Rev	NheI ApaI	This thesis
pCB6-	$CD4^{\Delta ct}$	N/A	N/A	N/A	B Dargent
pCB6-	$CD4^{\Delta ct}$-ct$CB1R^{WT}$	N/A	N/A	N/A	Keri Hildick
pCB6-	$CD4^{\Delta ct}$-ct$CB1R^{\Delta H9}$	N/A	N/A	N/A	Keri Hildick
pFLAG-	SGIP1	cDNA (primary cortical cultures)	SGIP1 For SGIP1 Rev	KpnI BamHI	This thesis
pmCherry-	Rab5 WT	N/A	N/A	N/A	Pete Cullen, Chris Danson
pmCherry-	Rab5 S34N (DN)	pmCherry-Rab5 WT	S34N	N/A	This thesis
pmCherry-	Rab5 Q79L (DA)	pmCherry-Rab5 WT	Q79L	N/A	This thesis

Table 2-9 shRNA knockdown plasmids

VECTOR	TARGET PROTEIN	TARGET SEQUENCE	NAME	SOURCE	OVEREXPRESSION
pSUPER.neo	AP3D1	**5'** AGCTGCTCACCAAGATCATTG **3'**	AP3D1 KD#1	Sigma	mCherry
pSUPER.neo	AP3D1	**5'** ACCGCATGTTCGACAAGAAC **3'**	AP3D1 KD#2	Sigma	mCherry
pSUPER.neo	SGIP1	**5'** CCAATACCAAGGAATTCTGGGTAAA **3'**	SGIP1 KD#1	(Uezu et al., 2007)	mCherry
pSUPER.neo	SGIP1	**5'** GCTGAGCAGACCTTCATTAAA **3'**	SGIP1 KD#2	Sigma	mCherry
pSUPER.neo	Non-targeting 19mer	**5'** AATTCTCCGAACGTGTCAC **3'**	Nt19	(Choy et al., 2014)	mCherry
pSUPER.neo	Non-targeting 21mer	**5'** AACGTACGCGGAATACTTCGA **3'**	Nt21	(Haar et al., 2007)	mCherry
pSUPER.neo	Non-targeting 29mer	**5'** GCACTACCAGAGCTAACTCAGATAGTACT **3'**	Nt29	Origene	mCherry
pXlg3	AP3D1	**5'** AGCTGCTCACCAAGATCATTG **3'**	AP3D1 KD#1	Sigma	$SP^{Il\text{-}2}$-EGFP-$CB1R^{WT}$
pXlg3	AP3D1	**5'** ACCGCATGTTCGACAAGAAC **3'**	AP3D1 KD#2	Sigma	$SP^{Il\text{-}2}$-EGFP-$CB1R^{WT}$
pXlg3	SGIP1	**5'** CCAATACCAAGGAATTCTGGGTAAA **3'**	SGIP1 KD#1	(Uezu et al., 2007)	$SP^{Il\text{-}2}$-EGFP-$CB1R^{WT}$
pXlg3	SGIP1	**5'** GCTGAGCAGACCTTCATTAAA **3'**	SGIP1 KD#2	Sigma	$SP^{Il\text{-}2}$-EGFP-$CB1R^{WT}$
pXlg3	Non-targeting 19mer	**5'** AATTCTCCGAACGTGTCAC **3'**	Nt19	(Choy et al., 2014)	$SP^{Il\text{-}2}$-EGFP-$CB1R^{WT}$

pXlg3	Non-targeting 21mer	**5'** AACGTACGCGGAATACTTCGA **3'**	Nt21	(Haar et al., 2007)	$SP^{Il\text{-}2}$-EGFP-$CB1R^{WT}$
pXlg3	Non-targeting 29mer	**5'** GCACTACCAGAGCTAACTCAGATAGTACT **3'**	Nt29	Origene	$SP^{Il\text{-}2}$-EGFP-$CB1R^{WT}$
pXlg3	AP3D1 (KD#1)	**5'** AGCTGCTCACCAAGATCATTG **3'**	AP3D1 KD#1	Sigma	$SP^{Il\text{-}2}$-EGFP-$CB1R^{\Delta H9}$
pXlg3	AP3D1 (KD#2)	**5'** ACCGCATGTTCGACAAGAAC **3'**	AP3D1 KD#2	Sigma	$SP^{Il\text{-}2}$-EGFP-$CB1R^{\Delta H9}$
pXlg3	SGIP1 (KD#1)	**5'** CCAATACCAAGGAATTCTGGGTAAA **3'**	SGIP1 KD#1	(Uezu et al., 2007)	$SP^{Il\text{-}2}$-EGFP-$CB1R^{\Delta H9}$
pXlg3	SGIP1 (KD#2)	**5'** GCTGAGCAGACCTTCATTAAA **3'**	SGIP1 KD#2	Sigma	$SP^{Il\text{-}2}$-EGFP-$CB1R^{\Delta H9}$
pXlg3	Non-targeting 19mer	**5'** AATTCTCCGAACGTGTCAC **3'**	Nt19	(Choy et al., 2014)	$SP^{Il\text{-}2}$-EGFP-$CB1R^{\Delta H9}$
pXlg3	Non-targeting 21mer	**5'** AACGTACGCGGAATACTTCGA **3'**	Nt21	(Haar et al., 2007)	$SP^{Il\text{-}2}$-EGFP-$CB1R^{\Delta H9}$
pXlg3	Non-targeting 29mer	**5'** GCACTACCAGAGCTAACTCAGATAGTACT **3'**	Nt29	Origene	$SP^{Il\text{-}2}$-EGFP-$CB1R^{\Delta H9}$

2.1.5 Antibodies

2.1.5.1 Primary antibodies used for ICC and WB

Table 2-10 lists all primary antibodies used for immunocytochemistry and Western blotting.

Table 2-10 Primary antibodies

ANTIBODY	SPECIES	CLONE	SUPPLIER	CAT. NO.	USE	DILUTION
Ankyrin-G	Mouse	N106/36	NeuroMab	75-146 AB_10673030	ICC	1:500
AP-3 delta subunit	Mouse	SA4	DSHB	AB_2056641	WB	1:5,000
β Actin	Mouse	AC-15	Sigma-Aldrich	A5441 AB_476744	WB	1:10,000-1:40,000
CD4	Mouse	OKT4	BioLegend	317402 AB_571963	ICC	1:400
FLAG	Mouse	M2	Sigma-Aldrich	F1804 AB_262044	WB	1:2,000-1:10,000
GAPDH	Mouse	6C5	Abcam	ab8245 AB_2107448	WB	1:20,000
GFP	Chicken	(Poly)	Abcam	ab13970 AB_300798	ICC	1:1,000
GFP	Rat	3H9	Chromotek	3h9-100 AB_10773374	WB	1:2,000-1:5,000
MAP Kinase, Activated Phosphothreonine	Mouse	ERK-PT115	Sigma-Aldrich	M7802 AB_260658	WB	1:1,000
MAP Kinase, Non-Phosphorylated	Mouse	ERK-NP2	Sigma-Aldrich	M3807 AB_260501	WB	1:250
MAP2	Rabbit	(Poly)	Synaptic Systems	188 003 AB_2281442	ICC	1:500
SBP-tag	Mouse	20	Sigma-Aldrich	MAB10764	ICC	1:500

Key: DSHB – Developmental Studies Hybridoma Bank; ICC –Immunocytochemistry; WB – Western Blotting.

2.1.5.2 Secondary antibodies used for ICC and WB

Table 2-11 lists all secondary antibodies used for immunocytochemistry and Western blotting.

Table 2-11 Secondary antibodies

ANTIBODY	CONJUGATE	SPECIES	SUPPLIER	CAT. NO.	USE	DILUTION
chicken IgY	Alexa Fluor® 647	Donkey	JIR	703-606-155 AB_2340380	ICC	1:400
chicken IgY	Cy2	Donkey	JIR	703-225-155 AB_2340370	ICC	1:400
chicken IgY	Cy3	Donkey	JIR	703-165-155 AB_2340363	ICC	1:400
mouse IgG	Cy3	Donkey	JIR	715-165-150 AB_2340813	ICC	1:400
mouse IgG	Cy5	Donkey	JIR	715-175-150 AB_2340819	ICC	1:400
mouse IgG	DyLight™ 405	Goat	JIR	115-475-003 AB_2338786	ICC	1:400
mouse IgG	HRP	Goat	Sigma-Aldrich	A3682 AB_258100	WB	1:10,000
rabbit IgG	Alexa Fluor® 488	Donkey	JIR	711-545-152 AB_2313584	ICC	1:400
rabbit IgG	DyLight™ 405	Goat	JIR	111-475-003 AB_2338035	ICC	1:400
rat IgG	HRP	Rabbit	Sigma-Aldrich	A5795 AB_258259	WB	1:10,000

Key: JIR – Jackson ImmunoResearch; ICC – Immunocytochemistry;
WB – Western Blotting; NB. JIR secondary antibodies are distributed by Stratech.

2.2 MOLECULAR BIOLOGY METHODS

2.2.1 RNA extraction from cells

RNA extraction was performed using the RNeasy Mini Kit using RNAse free tubes and filter tips. The workspace, pipettes, and gloves were sprayed down with RNAseZap (Thermo Fisher Scientific) prior to RNA extraction.

To generate rat SGIP1, RNA was extracted from a 10 cm dish of DIV 21 cortical neurons according to the manufacturer's instructions.

2.2.2 cDNA synthesis

cDNA was synthesized from 1 µg of RNA using the RevertAid First Strand cDNA synthesis kit according to the manufacturer's instructions. The oligo(dT)$_{18}$ primer, which selectively binds poly(**A**) tails of mRNA, was used reverse transcribe only mRNA and generate a cDNA library. 'No RT' and 'no template' controls were included.

2.2.3 Polymerase Chain Reaction (PCR)

Polymerase Chain Reactions (PCRs) were performed using the KOD Hot Start DNA Polymerase Kit and a PCR Thermocyler as indicated in **Table 2-12** and **Table 2-13** Template DNA consisted of synthesized 2-3 µL of cDNA for SGIP1. For all other constructs, template DNA consisted of 10 ng plasmid DNA as indicated in **Table 2-4**.

Table 2-12 PCR components

COMPONENT	VOLUME	FINAL CONCENTRATION
10x Buffer for KOD Hot Start DNA Polymerase	5 µL	1x
25 mM $MgSO_4$	3 µL	1.5 mM
dNTPs (**2 mM each**)	5 µL	0.2 mM each
Milli-Q water	20.5 µL	
DMSO	2.5 µL	5%
Sense (**5'**) **Primer** (10 µM)	1.5 µL	0.3 µM
Anti-Sense (**3'**) **Primer** (10 µM)	1.5 µL	0.3 µM
Template DNA (plasmid: 1 ng/µL; cDNA: 2-3µL)	10 µL	0.2 ng/µL
KOD Hot Start DNA Polymerase (1 U/µL)	1 µL	0.02 U/µL
TOTAL REACTION VOLUME	**50 µL**	

Table 2-13 Cycling conditions.

STEP	TARGET SIZE			
	< 500 bp	**500-1000 bp**	**1000-3000 bp**	**> 3000 bp**
1. Polymerase activation	95°C for 2 min			
2. Denature	95°C for 20 s			
3. Annealing	55°C for 10 s			
4. Extension	70°C for 10 s/kb	70°C for 15 s/kb	70°C for 20 s/kb	70°C for 25 s/kb
5. Repeat steps 2-4	20-35 cycles			
6. Hold	At 10°C			

2.2.4 Agarose Gel Electrophoresis

PCR products were resolved using 0.8% or 1.5% (w/v) agarose gels containing 0.5 µg/mL of ethidium bromide. 6x gel loading dye (NEB) was added 5 µL of the sample and the sample was loaded into the gel alongside 10 µL of HyperLadder™ 1kb molecular weight marker. The samples were run at 135V in 0.5x TAE buffer (20mM Tris acetate, 0.5mM EDTA) using a Mupid-exU electrophoresis system (Mupid Co. Ltd) for 20 minutes, then visualised on a UV transilluminator (Ultra-Violet Products Ltd.).

2.2.5 DNA fragment purification

Once the presence of a PCR product of the right size was confirmed, the PCR product was purified using the GeneJET gel extraction kit according to the manufacturer's instructions with some slight modifications. 5x volume of binding buffer was added to the PCR product before adding it to the column. The product was eluted in 43 µL of ddH_2O.

2.2.6 Restriction digest

The cleaned PCR product and 2-3 µg of vector plasmid DNA were incubated with 20 U of each restriction enzyme in the appropriate NEB buffer (total volume 50 µL) at 37°C for 2 hours. 10 U of calf intestinal alkaline phosphatase (CIP; NEB) was also added to the vector DNA.

5 µL of each digest was resolved on an agarose gel to check that the vector had linearised, and the DNA was purified with the GeneJET gel extraction kit. The PCR product was eluted in 50 µL of ddH_2O and the vector was eluted in 25 µL of ddH_2O and the concentration of DNA was determined using a nanodrop.

2.2.7 Sticky end ligation

1:1 and 3:1 insert:vector molar ratios were calculated using the online NEBio ligation calculator, and the PCR product was diluted accordingly. 1 µL of insert and 1 µL of vector were then added to 2 µL of TaKaRa T4 DNA ligase solution. The ligation mix was mixed by pipetting and incubated at RT for 30 minutes. A control of 1 µL vector, 1 µL ddH_2O, and 2 µL ligase solution was also included.

2.2.8 Transformation of competent *E. coli*

40 µL of DH5α or XL1-Blue competent cells was added to the ligation mixture on ice and flicked to mix. XL1-Blue competent cells were used for viral vectors (Xlg3 and pSinRep5) to prevent recombination of the long terminal repeats (LTRs). Following a 30-minute incubation on ice, the competent *E. coli* were heat shocked at 42°C for 45-90 seconds and returned to ice for 2 minutes. 100 µL plain LB broth or SOC media was added to the transformed cells. For ampicillin resistant vectors, the transformed cells were immediately plated onto LB-Agar plates containing 100 µg/mL ampicillin. For kanamycin resistant vectors, the transformed cells were incubated at 37°C for 1 hour before plating onto LB-Agar plates containing 25 µg/mL kanamycin. The plates were incubated overnight at 37°C.

2.2.9 DNA miniprep and PCR screen

Single colonies were picked from the plate and added to culture tubes containing 3 µL LB broth with the appropriate selection antibiotic. They were incubated overnight at 37°C in a shaking incubator. Plasmid DNA was isolated using the GeneJET Miniprep kit according to the manufacturer's instructions. The presence of an insert was determined with by a mini PCR (1/5 of PCR mix in **Table 2-12**) amplification and running on a DNA agarose gel.

2.2.10 Plasmid DNA sequencing

1-2 mini preps containing an insert were sent for sequencing by Eurofins Genomics. Sequences were checked for accuracy using the NCBI blast/alignment tools and SnapGene. Mini preps of the correct sequence were either used in experiments or midi prepped, depending on the quantity of plasmid DNA needed.

2.2.11 DNA Midi Preps

1 µL of validated mini preps was used to transform 10 µL of DH5α or XL1-Blue *E. coli* competent cells. The transformed *E. coli* were added to 100 µL of LB broth containing the appropriate selection antibiotic and incubated overnight at 37°C in a shaking incubator. Plasmid DNA was isolated using the GeneJET Midiprep kit according to the manufacturer's instructions (high speed spin).

2.2.12 Site-directed mutagenesis

The protocol above was slightly modified for site-directed mutagenesis. 50 ng of plasmid DNA was used as the PCR template. The number of cycles was kept as low as possible (20-25) in order to minimize errors. The extension time was calculated for the full length of the plasmid.

To remove the template DNA, 20 units of DpnI, which only cleaves methylated DNA, and not the PCR product, was added to the PCR mix, which was then incubated at 37°C for 1-2 hours. The DNA was purified using the GeneJET gel extraction kit and eluted in 10 µL of ddH_2O twice. 5 µL of the purified product used to transform 50 µL of DH5α. Single colonies were picked for screening by sequencing.

2.2.13 shRNA synthesis

shRNA vectors were designed according to the pSUPER.neo RNAi system (Oligoengine). Sense and antisense oligos were designed to target a particular region (19-29 bp) of the gene of interest as well as non-targeting controls. The oligos included sense and antisense target sequences, a hairpin loop, and overhangs corresponding to BamHI/BglII and XhoI sites as shown in **Table 2-14**.

Table 2-14 shRNA oligo design

	BamHI			*Target sequence (Sense)*	**Hairpin**	*Target sequence (Antisense)*		**XhoI**		
5'	GATC	C	CC		TTCAAGAGA		TTTTT	C		**3'**
3'		G	GG		AAGTTCTCT		AAAAA	G	AGCT	**5'**

The oligos were dissolved to 100 µM in TE buffer (1M Tris pH8.0, 100mM). 2 µL each of sense and antisense oligos were mixed, heated to 95°C to denature secondary structures for 5 minutes, then cooled and incubated at RT for 30 minutes to anneal. The annealed primers were diluted in 250 µL of ddH_2O. 1 µg of vector (pSUPER.neo+mCherry) was digested with BglII (which produces an overhang complementary to BamHI overhang in the primers) and XhoI (without CIP) in

NEB3.1 buffer and purified using the GeneJET gel extraction kit. 1 µL of vector and 1 µL of annealed primers were added to 2 µL of TaKara I ligation mix and left at RT for 30 minutes, before being transformed into competent cells as above. Since the HindIII site is located between the BglII and XhoI site, mini preps were screened for the presence of an insert by digestion with HindIII.

In order to make shRNA virus, or to allow for the co-expression of shRNA and an overexpressed protein, the entire H1 promotor and target sequence was inserted Xlg3 using PacI and XhoI sites located upstream of the SFFV protein promoter in Xlg3 using standard primers.

2.3 CELL CULTURE METHODS

All cell culture was carried out using aseptic techniques in a laminar flow hood. Cells were grown in incubators kept at 37°C, 90% humidity, 5% CO_2, and 95% O_2.

2.3.1 Primary Neuronal Cultures

2.3.1.1 Plastic or glass preparation

2.3.1.1.1 Glass coverslips treatment

Glass coverslips (24-25mm) were washed overnight at RT in nitric acid with gentle agitation. They were then washed three times in cell culture grade water and sterilized overnight in 70% ethanol with gentle agitation. After several washes in cell culture grade water, coverslips were stored in cell culture grade water in a 140 mm cell culture dish.

2.3.1.1.2 Coating

Treated glass coverslips were added to 35mm dishes and coated with Poly-D-Lysine (1mg/mL; Sigma) or Poly-L-Lysine (1mg/mL; Sigma) in sterile borate buffer (10mM borax, 50mM boric acid) or cell culture grade water. Plastic 6 well plates, 35mm dishes, or 10 cm dishes were coated in Poly-L-Lysine (0.5mg/mL; Sigma) in borate buffer or cell culture grade water. Following an overnight incubation at 37°C, dishes and coverslips were washed 3 times in cell culture grade water and then incubated in 1.5mL plating medium (Neurobasal, Gibco supplemented with 10% horse serum, Sigma; 2 mM GlutaMAX, Gibco; and either GS21, GlobalStem, or B27, Thermo Fisher) overnight at 37°C or until required.

2.3.1.2 Rat embryonic dissection

All animal care and procedures were carried out in accordance with UK Home Office and University of Bristol guidelines. All dissection tools were sterilised with 70% EtOH, although the dissection occurred outside a laminar flow hood. Pregnant E17-E18 Wister rats were sacrificed under Home Office Schedule 1 regulations by overdose of isoflurane followed by cervical dislocation by a trained individual. The skin of the abdomen was sterilised 70% EtOH and embryos were extracted from womb and placed in RT Hank's Buffered Salt Solution (without Ca^{2+} or Mg^{2+}; HBSS) where they were immediately removed from their amniotic sac and decapitated. Severed heads were placed into fresh RT HBSS and the brains were removed using forceps under a dissection microscope at RT and outside a laminar flow hood. The brains were moved into fresh HBSS and the hemispheres were divided in two. The olfactory bulbs, hind brain, midbrain, and meninges were removed. The hippocampus was dissected from the cortex and hippocampi and cortices were pooled separately in RT HBSS.

2.3.1.3 Cortical and hippocampal dissociation

Cortical and hippocampal dissociation was carried out in a laminar flow hood using aseptic technique. HBSS (without Ca^{2+} or Mg^{2+}) and plating media were used at RT. For hippocampal dissociation, dissected hippocampi were placed in a 15 mL Falcon tube and washed 3x in 10 mL HBSS. Hippocampi were then incubated in 10 mL 0.005% Trypsin-EDTA (Thermo) in HBSS for 9 minutes in a 37°C water bath. Trypsinised hippocampi were then washed 3x in 10 mL HBSS and 1x in 1 mL plating media in order to remove residual trypsin. Hippocampal tissue was then dissociated in 1 mL plating media by trituration using a P1000 pipette and then diluted with an additional 4 mL of plating media. The number of cells in a 1:10 dilution mixed with 0.4% Trypan blue (Thermo) was counted using a haemocytometer and the dissociated cells were diluted to a concentration of 1 million per mL.

Dissected cortices were dissociated similarly, but with a few extra steps due to the size of the tissue and with larger volume of reagents due to the greater number of cells. Specifically, dissected cortices were cut into smaller pieces using a sterile scalpel blade before being added to a 50 mL Falcon. The HBSS washes and trypsinisation occurred as above, but in a volume of 30 mL and a trypsin incubation time of 15 min. After washing in 5mL plating media, cortical tissue was dissociated in 5 mL plating media by trituration with a 5 mL serological pipette. The dissociated

cells were then strained through a sterile 70 µm cell strainer into a fresh 50 mL Falcon tube to remove any debris before being counted and diluted to 5 million per mL.

2.3.1.4 Plating and Feeding

Cells were then plated at various densities according to the experimental design. Generally, between 150,000 and 400,000 hippocampal cells were plated per 25 mm coverslip and 500,000-700,000 hippocampal or cortical cells were plated per 6-well dish. For proteomics, 5 million cortical cells were plated per 10 cm dish. The following day, the plating media was replaced with 3 mL feeding medium (Neurobasal supplemented with 1.2 mM GlutaMAX and either GS21 or B27). Neurons were incubated at 37°C and 5% CO_2 for up to 2 weeks.

2.3.2 Mammalian cell line culture

2.3.2.1 Cell lines used

Human embryonic kidney (HEK293T) cells were used for protein biochemistry experiments. Due to their flatter shape and greater ability to stick to glass, HeLa cells were used for imaging experiments. Baby hamster kidney (BHK-21) cells were used to produce Sindbis virus. All cell lines were obtained from the European Collection of Cell Cultures (ECACC).

2.3.2.2 Cell culture media components

HEK293T cells and HeLa cells were grown in complete DMEM medium supplemented with 10% FBS and 1% L-glutamine. BHK-21 cells were grown in complete Alpha MEM medium supplemented with 5% FBS and 1% Penicillin/Streptomycin (Thermo).

2.3.2.3 Long-term storage and thawing of cell lines

Aliquots of HEK293T, HeLa, and BHK-21 cells mixed with 1% DMSO were stored in liquid nitrogen. An aliquot was removed from storage and quickly thawed in a 37°C water bath and then transferred to a 15 mL Falcon tube with 10 mL complete medium. To remove the DMSO, the cells were pelleted at 1000 g for 2 min at RT and the medium was aspirated and replaced with 1 mL of fresh medium. The cells were then gently resuspended and transferred to a T25 flask containing 5 mL complete medium and incubated overnight. The next day, the cells were dissociated and re-plated into a T75 flask. Cell lines were treated with Ciprofloxacin (10 µg/mL) for several passages after thawing to prevent mycoplasma infection.

2.3.2.4 Passaging of cell lines

HEK293T and HeLa cells were grown in T75 flasks until they were 70-90% confluent and then passaged 1/10 (about 2 times a week) as below. HEK293T cells were not kept beyond P25. BHK-21 cells were more carefully monitored because they are more sensitive to overgrowth – they were passaged about every 2 days and $1x10^6$ cells were added to a new T75 flask in order to prevent overgrowth and to not split them too harshly.

HEK293T, HeLa, and BHK-21 cells were gently washed with 10 mL pre-warmed PBS (no Ca^{2+} or Mg^{2+}) and dissociated with 1 mL 0.05% trypsin-EDTA incubated at 37°C for 2-5 minutes. Cells were then triturated in 4-9 mL of medium with a serological pipette. To remove the trypsin, cells were pelleted by centrifugation at 1700 g for 2 minutes at RT, the supernatant was removed, and the pellet was resuspended in 10 mL of medium. For stock maintenance, 1 mL of cells was added to a T75 flask with 11 mL of fresh medium.

2.3.2.5 Plating HEK293T and HeLa cells

2.3.2.5.1 Plastic or glass preparation

The wells of a 6 well plate were coated in 0.1 mg/mL PLL in cell culture grade water and left to incubate at 37°C for at least 1 hour. The wells were then washed 3x in cell culture grade water. 2 mL of complete DMEM was added to each well.

For imaging experiments, 25 mm coverslips were sterilised and stored in 70% EtOH. A coverslip was added to each well of a 6 well plate and washed 3x in cell culture grade water. The coverslips were then coated in PLL and washed as above.

2.4 IMMUNOCYTOCHEMISTRY METHODS

2.4.1 Lipofectamine transfection

2.4.1.1 Cell line transfection

HeLa cells or HEK293T cells were transfected the day after plating with Lipofectamine2000 (Thermo). Per transfection, 1-2 µg of plasmid DNA and 3-5 µL of Lipofectamine2000 were added to 200 µL plain DMEM. The transfection mix was vortexed, spun down, and incubated at RT for 30 minutes. The transfection mix was then added dropwise to the cells and the cells were returned to the incubator for 20-72 hours.

2.4.1.2 Neuronal transfection

Hippocampal cultures were usually transfected at DIV 12 with Lipofectamine2000. For knockdown constructs, neurons were transfected at DIV 9 to allow extra time for the knockdown to work. Amounts of plasmid DNA and Lipofectamine2000 were optimised for each plasmid, but, generally, 2-5 µL of Lipofectamine per well was added to 200 µL per well of plain neurobasal and vortexed. 1-2.5 µg of DNA per well was added to the lipofectamine/neurobasal mix and the tubes were vortexed, spun down, and incubated at RT for about 30 minutes. Neuronal cultures on coverslips were prepared for transfection during the incubation. Two (of three) mL of media were withdrawn from each well and added to a 50 mL Falcon tube labelled "Conditioned Media." An additional mL per well of fresh feeding medium was added to the tube, and the tube was kept warm in a 37°C water bath during transfection. The neurons were then usually transfected in the remaining mL of conditioned medium. Because B27 reduces the efficiency of transfection, neurons kept in B27 media were sometimes transfected in plain neurobasal media, depending on how well the plasmid expressed. After the 30-minute incubation, the DNA/ Lipofectamine mix was added dropwise to the neurons and the neurons were returned to their incubator for 45 minutes to 1.5 hours. The transfection mixture was then removed, and the neurons were washed in 1 mL of fed conditioned media. The remaining 2 mL of fed conditioned media was added to the neurons, and the neurons were placed back in the incubator and immunostained at DIV 13 or DIV 14.

2.4.2 Live surface staining

To measure surface expression, DIV 13 or DIV 14 hippocampal neurons transfected with the construct of interest were cooled at room temperature for 5-10 min (to reduce further internalisation), then incubated with the appropriate antibody (chicken anti-GFP or mouse anti-CD4) in 100 µL conditioned media for 10-20 min at RT. The antibody mix was dotted onto parafilm, and the coverslip was incubated upside down to ensure even coating.

For agonist and inverse agonist experiments, the neurons were treated with either 5 µM ACEA (in EtOH), 10 µM AM281 (in DMSO), or vehicle control (0.1% EtOH or DMSO) for 3 hours at 37°C and 5% CO_2, and then subsequently surface stained as above.

The neurons were washed multiple times in PBS before fixation.

2.4.3 Staining of endocytosed receptors

To measure endocytosed receptors, DIV 14 hippocampal neurons transfected with the construct of interest were fed with the appropriate antibody (chicken anti-GFP or mouse anti-CD4) for 2 hours in 200 µL of conditioned media at 37°C and 5% CO_2. Neurons were washed several times in PBS and cooled to 4°C to prevent further internalisation. Anti-GFP surface antibody was stripped by two quick washes with ice-cold pH 2.5 PBS. Because two acid washed did not completely remove surface fluorescence, anti-CD4 surface antibody was stripped using a harsher condition – a 4 min incubation with 0.5 M NaCl and 0.2 M acetic acid (pH 3.5). Neurons were washed several times in PBS before fixation.

2.4.4 Fixation

Cultured neurons were fixed in pre-warmed (37°C) 4% formaldehyde in PBS for 12 minutes. Following three washes in PBS, excess formaldehyde was quenched with one wash in 100 mM Glycine in PBS. The cells were then washed three more times in PBS and either blocked immediately or left in PBS at 4°C overnight.

2.4.5 Blocking and permeabilisation

Neurons were blocked and permeabilised in 1 mL 3% BSA + 0.1% Triton-X 100 in 1x PBS for 20 minutes at RT.

2.4.6 Fixed immunostaining

In general, for fixed immunostaining, the antibodies were diluted in 100 µL 3% BSA in PBS per coverslip. 90 µL antibody mix was dotted onto parafilm, and the coverslip was incubated upside down at room temperature for 45 minutes to one hour. The cells were washed at least three times in 1x PBS between incubations. Primary concentrations can be found in (**Table 2-10**). All secondaries were used at 1:400 (**Table 2-11**)

Fixed, blocked, and permeabilised neurons that had been live stained for surface or endocytosed receptors were incubated in secondary antibody at (Alexa Fluor 647 donkey anti-chicken IgY for GFP primary antibody or Cy5-labelled donkey anti-mouse IgG for CD4 primary antibody) to label surface or endocytosed primary. The neurons were then re-stained with primary antibody (chicken anti-GFP or mouse anti-CD4) to label total receptor of interest. At the same time, they were labelled with mouse anti-AnkyrinG antibody and/or rabbit anti-MAP2 antibody in order to

mark the axon initial segment or the dendrites, respectively, and then incubated in the appropriate secondary.

2.4.7 Retention Using Selective Hooks (RUSH)

2.4.7.1 HeLa RUSH

HeLa cells grown on 25mm glass coverslips were transfected with the mCherry RUSH $CB1R^{WT}$ construct for no longer than 24 hours to prevent ER stress resulting from accumulation of retained receptors. Receptors were released with the addition of 40 µM D-biotin (Merck) for different lengths of time. At the end of the timepoint, the cells were washed three times in PBS and fixed in pre-warmed 4% formaldehyde in PBS for 10 minutes. They were then washed three times in PBS, one time in 100 mM glycine, and three times in PBS.

Cells were then blocked in a non-permeabilising buffer (3% BSA in 1x PBS) for 20 minutes at RT and subsequently incubated in mouse anti-SBP antibody (in 3% BSA in 1x PBS) for 45 minutes at RT in order to stain surface receptors. After 3 washes in PBS, the cells were then incubated in Cy5-labelled anti-mouse IgG for 45 minutes at RT. Following 3 washes in PBS, coverslips were mounted in Fluoromount-G with DAPI onto glass slides.

2.4.7.2 Neuronal RUSH

Hippocampal neurons were transfected with RUSH constructs at DIV 12 for no longer than 24 hours to prevent ER stress resulting from accumulation of unreleased receptors. To release the receptor, neurons were incubated in 200 µL conditioned media containing D-biotin (40 µM) for different lengths of time at 37°C and 5% CO_2. Chicken anti-GFP antibody (1:1,000) was also added to the media to label receptors reaching the surface. The 0 min timepoint was only incubated with chicken anti-GFP antibody without biotin for 60 min. For the O/N timepoint, neurons were incubated in 40 µM D-biotin immediately following transfection and then left overnight at 37°C and 5% CO_2 before being incubated with biotin and chicken anti-GFP for 60 min to label surface CB1R. Every independent experiment included a 60 min timepoint to which values were normalised and a 0 min control to make sure that the receptors had been retained prior to release.

Following biotin treatment, neurons were washed several times in PBS and cooled to 4°C to prevent further internalisation. They were then live labelled with 647-labelled anti-chicken IgY (1:400) in conditioned media for 15 min at 4°C before

being fixed and permeabilised and stained with Cy3-labelled anti-chicken IgY. Therefore, in the text, “surface” thus refers to 647 fluorescence acquisition. Because the 647-labelled secondary was unlikely to saturate the primary antibody, especially with a 15 min incubation at 4°C, Cy3 fluorescence acquisition is referred to as “surface+endocytosed”.

The neurons were then re-stained with chicken anti-GFP antibody, followed by Cy2-labelled anti-chicken IgY antibody, to boost the GFP signal and to measure the total amount of receptor present. Concurrently, they were stained with mouse anti-AnkyrinG antibody, followed by DyLight 405 anti-mouse IgG antibody to label the axon initial segment.

2.4.8 Image acquisition and analysis

2.4.8.1 Image acquisition

Images were acquired using either a Leica SPE single channel, a Leica SP8, or a Leica SP5II confocal laser scanning microscope (Wolfson Bioimaging Facility, University of Bristol), or a Zeiss LSM510 UV META Axiovert 200M laser scanning microscope. All settings were kept the same within experiments. To avoid bias, neurons were selected for data acquisition based only on their total staining and surface/endocytosed was stained in far red. Based on previous experiments, 4-10 cells were acquired per experiment per condition, and at least three independent experiments (i.e. on different neuronal cultures from different dams on different days) were performed.

2.4.8.2 Image analysis

2.4.8.2.1 Surface and endocytosed normalisation

All quantification was performed using FIJI (ImageJ) software. Images were max projected, and regions of interest (ROIs) of approximately similar lengths were drawn around axons and 3–4 proximal and secondary dendrites based on the total channel only. Axons were defined either as processes whose initial segment was positive for Ankyrin-G or as processes negative for MAP2. The mean fluorescence was measured for each channel and the dendritic values were averaged. ‘Surface’ or ‘endocytosed’ mean fluorescence values were normalised to the ‘total’ mean fluorescence value for each ROI to account for varying levels of expression of transfected constructs. These values were then normalised to the axon value of the control (WT or CD4). For drug treatments, surface values were normalised to

their respective vehicle treated controls and sampled at the same time-point (i.e. WT + drug was normalised to WT + vehicle and ΔH9 + drug was normalised to ΔH9 + vehicle) to account for possible differences in steady-state surface expression between the constructs and/or constitutive internalisation.

2.4.8.2.2 RUSH

Because of the change in total mean fluorescence in axons throughout the different conditions, the above image analysis was slightly modified for RUSH experiments. In these experiments, neurites were traced using NeuronJ so that only the mean fluorescence of exactly the first 50 µm of the axons and 30–40 µm of 2–4 primary dendrites for each channel was measured. All 'surface' and 'surface + endocytosed' values (of both axons and dendrites) were normalised to the average total dendritic value for each neuron. Axon total mean fluorescence was also normalised to the average total dendritic value within each cell. All values were then normalised to the WT 60 min axon value within each experiment. In a slightly smaller subset of RUSHed neurons, axons were traced for ~100 µm using NeuronJ. Line plots were generated, and the mean fluorescence was averaged in 10 µm segments. The averages for each 10 µm segment from each cell were normalised first to the dendritic total value, then to the axonal 60 min value of the first 50 µm.

2.4.8.2.3 Polarity indices

Polarity indices (A/D ratio) were calculated by dividing the axonal mean fluorescence value by the average dendritic mean fluorescence value.

2.5 SINDBIS METHODS

2.5.1 Preparation of BHK-21 cells for electroporation

BHK-21 cells were cultured and maintained in T75 flasks as described in "2.3.2 Mammalian cell line culture". Two days before electroporation, $1x10^6$ cells were plated into T175 flasks. To ensure that there would be enough cells, two T175 flasks were plated for every virus.

During *in vitro* transcription, the BHK cells were prepared for electroporation. Per T175 flask, the cells were washed twice in 5mL PBS, then dissociated in 3 mL 0.05% trypsin-EDTA for 5 min at 37°C. The cells were then triturated and pooled together in 10 mL growth medium, pelleted by centrifugation at 1700rpm for 4 min

at RT, and resuspended in 10 mL PBS. Following another round of centrifugation and resuspension in PBS to wash the cells, 100 µL of cells were mixed with 100 µL and were counted using a haemocytometer. The cells were then recentrifuged and resuspended in the volume needed to make a suspension of $1x10^7$ cells/mL.

2.5.2 Preparation of viral RNA

Tagged genes of interest (goi) were cloned into the pSinRep5 plasmid which contains the non-structural genes (Replicase) for Sindbis. These constructs, as well as the defective helper plasmid, pDH-BB (tRNA; TE12), which provides the structural proteins for Sindbis, were midiprepped. In this thesis, Sindbis virus was made to overexpress EGFP-tagged c-terminus of CB1R (ctCB1R) – specifically EGFP-ctCB1^{WT} and EGFP-ctCB1$^{\Delta H9}$ – as well as an empty EGFP control.

2.5.2.1 Linearising templates

30-50 µg of pSinRep5 plasmid with gene of interest (goi) and 50 µg of pDH-BB were linearised by restriction enzyme digest overnight at 37°C (**Table 2-15**).

Table 2-15 Template linearisation reactions

GENE OF INTEREST		**DEFECTIVE HELPER**	
pSinRep5-goi	30-50 µg	pDH-BB	50 µg
10xCutSmart buffer	10 µL	10xCutSmart buffer	10 µL
NotI-HF (20 units/µL)	2 µL	XhoI (20 units/µL)	2 µL
dH_2O	**to 100 µL**	dH_2O	**to 100 µL**

1 µL of the digest was run on an agarose gel to check for the presence of a single band. The linearised DNA was then purified using a Gel Extraction Purification Kit on 2 columns so as not to overload the columns.

2.5.2.2 Ethanol precipitation

The purified DNA was then ethanol precipitated in order to obtain a concentration of 0.5 µg/µL. 0.1x (of volume of DNA) 3M sodium acetate was added first. Then 2.5x 100% EtOH (pre-chilled to -20°C) was added and mixed well. To pellet the DNA, the tube was centrifuged for at 13.2K rpm for 15 min at RT. The supernatant was removed, and the pellet was washed in 500 µL 70% EtOH by inverting 3 times. The DNA was re-pelleted by centrifugation at 13.2K rpm for 5 minutes at RT, the

supernatant was removed thoroughly, and the pellet was left to air-dry. The DNA was resuspended in 5 µL DEPC-treated water, the concentration was measured using a nanodrop, and the DNA was diluted to 0.5 µg/µL

2.5.2.3 In vitro transcription of viral RNA

RNA was transcribed from the linearised DNA *in vitro* using the mMessage mMachine SP6 transcription kit (Ambion) and SUPERaseIn (Ambion) RNAse inhibitor in a work area cleaned with RNaseZap and with RNase-free tubes and pipette tips (**Table 2-16**). For the defective helper plasmid, one reaction per virus being made plus one was set up.

Table 2-16 In vitro transcription reaction

FOR ONE REACTION:	
DEPC-treated water	0.55 µL
Linearised DNA (0.5 µg/µL)	0.6 µL
2x ribonucleotide mix (NTP/CAP)	2.5 µL
20mM GTP	0.25 µL
10x Reaction Mix	0.5 µL
SUPERaseIn	0.1 µL
10x SP6 enzyme mix	0.5 µL
TOTAL REACTION VOLUME	**5 µL**

The reaction was incubated at 37°C for 2 hours. Then, 5 µL of defective helper RNA was mixed with 5 µL of goi RNA and the mixture was kept on ice.

2.5.3 Electroporation

0.5 mL of suspended cells were added with the RNA mix a gene pulse cuvette (0.2 cm gap) and quickly pulsed twice at 1.5kV and 20 µF. Cells were allowed to recover on ice for 5-10 minutes and then plated into a T25 flask containing 3.5 mL of growth medium.

2.5.4 Harvesting pseudovirion

24 hours after electroporation, the expression of EGFP was confirmed using a fluorescent microscope. Between 36 and 48 hours after electroporation, the supernatant was collected in a 15 mL centrifuge tube which was centrifuged at 2000rcf for 10 minutes to pellet any cell debris. The supernatant was then

transferred to a fresh 15 mL Falcon tube, aliquoted, and either used right away or stored at -80°C.

2.5.5 Viral transduction of primary neurons with Sindbis virus

Aliquots of Sindbis virus were thawed on ice and added to cultured cortical neurons for no longer than 24 hours to prevent toxicity.

2.6 Protein Biochemistry Methods

2.6.1 Cell lysis

To prevent protein degradation, all steps were carried out on ice or at 4°C. In general, transfected HEK293T cells or virally transduced primary neurons were lysed in the appropriate lysis buffer (as outlined in **Table 2-17**), scraped with a cell scraper, pipetted into an Eppendorf tube, vortexed, and sonicated.

Table 2-17 Types of lysis buffer

Application	Lysis Buffer
GFP Traps	50 mM Tris HCl pH 7.4 150 mM NaCl 0.5% Triton X 1 x protease inhibitors
Mass Spec/GFP Traps	50 mM Tris HCl pH 7.4 0.5% NP40 1 x protease inhibitors 200 µM sodium orthovanadate
Surface biotinylations; **Solubilizing full length CB1**	50 mM Tris HCl pH 7.4 150 mM NaCl 1% CHAPS 1 x protease inhibitors
Phospho-ERK assay	50 mM Tris HCl pH 7.4 150 mM NaCl 1% CHAPS 1 x protease inhibitors 1 x phosphatase inhibitors
Knockdown validation	1 x Laemmli Sample Buffer

Samples lysed in lysis buffers were incubated on ice for 20-30 minutes then centrifuged at 13.2k rpm at 4°C for 20 minutes. The supernatant was pipetted to a new tube. An equal volume of 2x Laemmli sample buffer (4% SDS, 20% glycerol, 0.004% bromophenol blue, 0.125M Tris-HCl pH 6.8, 10% 2-mercaptoethanol) was added to the lysate which and it was boiled at 95°C for 10 minutes. To avoid

aggregation of CB1R, samples that needed to be blotted for CB1R were not boiled, but left overnight at RT.

Samples lysed in 1x sample buffer were heated to 95°C for 10 minutes while shaking, spun down, and kept at room temperature or on the freezer (long term storage).

2.6.2 GFP-Trap

Cortical cells transduced with Sindbis virus were lysed in lysis buffer as above and the around 40 µL of the supernatant was added to an Eppendorf tube to act as a total/input. 500 µL of lysis buffer was added to 13 µL of washed GFP-Trap beads and incubated on a rotating wheel at 4°C for 1 hour. The beads were pelleted for 2 minutes at 6.6k rpm, and the supernatant was removed. The beads were washed in 500 µL of lysis buffer, inverted and flicked gently to mix. This washing was repeated 3 times. 40 µL of 2x Laemmli sample buffer was added to the beads and the inputs and the samples were incubated at 75°C – 95°C for 5-10 minutes.

2.6.2.1 GFP-Trap for proteomics

Sindbis virus was added to cortical neurons 24 hours prior to starting the GFP trap protocol. HEK293T cells were transfected 48 hours prior to starting the GFP trap. The cells were washed twice in ice-cold PBS and lysed in 500 µL of lysis buffer (50 mM Tris HCl pH 7.4, 0.5% NP40, 1xprotease inhibitors, 200 µM sodium orthovanadate), inverted, and left on ice for 20 minutes. Cell debris was spun out at 13.2k rpm for 20 minutes and the supernatant was added to 35 µL of washed GFP-trap (ChromoTek) beads and incubated on a rotating wheel at 4°C for 1 hour. The beads were then washed four times in lysis buffer and brought to the University of Bristol Proteomics facility.

2.6.3 Proteomics

Tandem Mass Tagging (TMT) quantitative mass spectrometry analysis was performed by Dr Kate Heesom at the University of Bristol Proteomics facility. Data was analysed using Perseus with help from Dr Lea Hampton-O'Neil.

2.6.4 Surface biotinylation assay

2.6.4.1 Surface biotinylations

All solutions were pre-chilled to 4°C and steps were carried out on ice. HEK293T cells expressing GFP- (but not SBP-) tagged CB1R constructs were chilled on ice

for a few minutes before being washed 3x in 2 mL PBS. The cells were then incubated in 1.5 mL 0.3 mg/mL of EZ-link Sulfo-NHS-SS-Biotin dissolved in 1xPBS for 10 minutes. Unreacted biotin was washed off with 3 washes in 2 mL PBS and quenched in 1.5 mL of 50 mM NH_4Cl in PBS for 2 minutes. The cells were washed 3 more times in PBS and lysed in 200 µL lysis buffer (**Table 2-17**). Cells were scraped into a labelled Eppendorf tube, vortexed, sonicated, and left on ice for 30 minutes. The lysate was centrifuged at 13.2k rpm for 20 minutes. 40 µL of lysate was removed to a new tube to act as the total.

2.6.4.2 Streptavidin pulldown

Biotinylated surface proteins were isolated using streptavidin-coated agarose beads. The beads were washed 2 times in lysis buffer by centrifugation at low speed (<3k rpm). 100 µL of centrifuged lysate was added to 30 µL of beads along with 250 µL of lysis buffer. The beads were incubated on a rotating wheel at 4°C for 1.5 hours, then washed in wash buffer (lysis buffer without protease inhibitors) 3 times, pelleting the beads for 2 minutes at 6.6k rpm between washes. 40 µL of 2x Laemmli sample buffer was added to both the surface and total fractions. The samples were vortexed, spun down, and incubated overnight at RT.

2.6.5 SDS-PAGE

2.6.5.1 Gel preparation

Separation of proteins by molecular weight was performed by sodium dodecyl sulphate-polyacrylamide gel electrophoresis (SDS-PAGE) using the Bio-Rad Mini-PROTEAN system. 8-12% acrylamide gels were cast in 1.5 mm glass plates using a Bio-Rad gel stand. Resolving gel (375 mM Tris-HCl pH 8.8, 8-12% acrylamide, 0.1% SDS, 0.1% APS, and 0.01 % TEMED) was added to the glass plates and overlayed with ethanol to ensure an even surface. Once the resolving gel polymerised, the ethanol was washed off with ddH_2O. A 5% stacking gel (125 mM Tris-HCl pH 6.8, 5% acrylamide, 0.1% SDS, 0.1% APS, 0.01% TEMED) was added on top of the resolving gel, and a 15-well comb was inserted. Once polymerised, the gel was either used straight away or stored at 4°C in paper towel soaked in 1 x SDS-PAGE running buffer.

2.6.5.2 SDS-PAGE

Acrylamide gels were mounted into electrophoresis tanks and which were filled with running buffer (25 mM Tris base, 250 mM glycine, 0.1% (w/v) SDS). Samples

were loaded into the wells along with 5 µL of molecular weight marker (PageRuler Prestained Protein Ladder, Thermo). The gel was run at 80V until the samples cleared the stacking gel, then at 120-180V until the dye front ran off the bottom of the gel.

2.6.6 Wet transfer

Following SDS-PAGE, resolved proteins were transferred onto methanol-activated PVDF (0.45 µm, Millipore). The gel was removed from the glass plates and the PVDF membrane was activated in methanol then equilibrated in transfer buffer (50 mM Tris base, 40 mM glycine, 20% methanol). The PVDF was then layered on top of the gel, and both were sandwiched in a cassette with three pieces of filter paper and one sponge on either side. The cassette was added to an electrophoresis tank with the membrane facing the cathode (red) and the gel facing the anode (black). An ice pack and a magnetic flea were added to the tank and the tank was filled with transfer buffer. The proteins were transferred at 400mA for 70-90 minutes with constant stirring.

2.6.7 Immunoblotting

Following transfer, membranes were removed from the cassette and blocked in 6% (w/v) non-fat milk (the Cooperative) or 4% (w/v) bovine serum albumin (BSA) dissolved in PBST (1x PBS + 0.1% Tween-20) for 1 hour with gentle shaking. Primary antibody was then added at an appropriate concentration (**Table 2-10**) diluted in either 6% milk or 4% BSA according to the manufacturer's recommendation. Full blots or cut parts of blots were incubated in primary antibody either overnight at 4°C or for 1.5 hours at RT with gentle shaking. Primary antibody was removed from the blot (and kept in order to be re-used, with sodium azide) and the blot was washed 3x quickly in PBST and 3x 5 minutes in PBST. The blot was then incubated with the appropriate secondary antibody conjugated to horseradish peroxidase (HRP) and diluted 1:10,000 in 6% milk or 4% BSA for 1 hour at RT. The blot was washed 3x quickly in PBST and 3x 5 minutes in PBST.

2.6.8 Chemiluminescence detection

Protein bands were visualised by incubation of an enhanced chemiluminescence (ECL) HRP substrate of different sensitivity depending on the antibody used (

Table 2-18). Excess PBST was blotted off on tissue paper, and membranes were incubated for 1-2 minutes in the appropriate substrate (**Table 2-18**).

Table 2-18 ECL HRP Substrates

SUBSTRATE	SUPPLIER	SENSITIVITY
Pierce™ ECL Western Blotting Substrate	Thermo	Low
Immobilon Classico Western HRP substrate	Merck	
Immobilon Crescendo Western HRP substrate	Merck	
Immobilon Forte Western HRP substrate	Merck	
SuperSignal™ West Femto Maximum Sensitivity Substrate	Thermo	High

Excess ECL was blotted off on tissue paper, and the membrane was transferred to either a film cassette or tray and covered with a thin sheet of overhead projector plastic smoothed to remove any bubbles so that the membrane did not dry out.

Protein bands were visualised either by X-ray film exposure or by image acquisition. CL-Xposure X-ray film (Thermo) was exposed to the bands in a light-tight cassette for varying lengths of time. The film was developed using an automated X-ray film developer (Konica SRX-101A). Images of the bands were acquired using an Odyssey Fc imaging system (LI-COR).

2.6.9 Stripping and re-probing

To re-probe the blot with another antibody, the blots were stripped of bound antibody with Restore PLUS Western Blot Stripping Buffer (Thermo) at 60°C for 15 minutes. The blots were washed 5 x in PBST and re-blocked in milk or BSA for 1 hour before being incubated with the relevant antibody.

2.6.10 Quantification of chemiluminescence

Blots on film were scanned and the density of the bands was analysed using the ImageJ Gel Analysis Tool. Rectangles of equal size were drawn around each band and profile plots were drawn for each band. The background was removed by drawing a straight line under the peak, and the area under the peak was calculated for each band. The values were copied over to an Excel spreadsheet for further analysis.

Blots acquired on the LI-COR were analysed using Image Studio. Rectangles were drawn around each band. A border 3 pixels wide around each rectangle was used

to calculate the background. If the bands were too close together, the background was calculated only from the top/bottom borders. The “signal” (“total” – “background”) was copied over into an Excel spreadsheet for further analysis.

2.6.11 Normalisation

Values for proteins of interest were normalised to the values of the sample’s loading control – usually beta Actin. For surface biotinylations, surface values were normalised to total values instead.

To control for variations in exposure/acquisition, values for each condition within an experiment were normalised to the average value for the experiment. Each value in the whole data set were then normalised to the average control value so that the control value was set to 1 and each condition represented a proportion of the control.

2.7 STATISTICAL METHODS

All statistics were performed using GraphPad Prism.

For imaging experiments, the ROUT method was used to identify outliers for all parameters measured before normalising to control. Neurons were removed from analysis if any one parameter was found to be an outlier. As is the convention in the field (Leterrier et al., 2006; Coutts et al., 2001; Simon et al., 2013; Evans et al., 2017; McDonald et al., 2007a; Leterrier et al., 2004, 2017), ‘N’ denotes the number of separate neuronal cultures prepared from litters of pups from separate dams and ‘n’ denotes the total number of neurons across the separate cultures assessed.

To determine statistical significance between two groups, a D’Agostino and Pearson normality test was performed. Unpaired t-tests were performed on data that passed the normality test whereas the Mann-Whitney test was used if it did not. One- or Two-way ANOVAs with Tukey’s or Sidak’s *post hoc* test were used to determine statistical significance between more than two groups depending on the comparisons required. *$p \leq 0.05$, **$p \leq 0.01$, ***$p \leq 0.001$, ****$p \leq 0.0001$. All data are presented as mean ± SEM.

Chapter 3 – NEWLY SYNTHESISED CB1R IS PREFERENTIALLY TRAFFICKED TO THE AXON

3.1 AIMS

- To examine how the axonally polarised surface distribution of CB1R is both (1) established and (2) maintained.
- To apply retention using selective hooks (RUSH) to examine the contribution of forward trafficking to the polarised surface distribution of CB1R.

3.2 INTRODUCTION

3.2.1 Surface polarity of CB1R

CB1R has a highly polarised axonal surface expression (Irving et al., 2000; Coutts et al., 2001; Leterrier et al., 2006; Thibault et al., 2013; Rozenfeld and Devi, 2008; McDonald et al., 2007a), where it acts to attenuate neurotransmitter release (Katona, 2009) and modulate synaptic plasticity (Lu and Mackie, 2016). Although CB1R is not stably surface expressed on somatodendritic plasma membrane, ~80% of total CB1R is present in intracellular vesicular clusters in the soma and dendrites (Leterrier et al., 2006).

How this near exclusive axonal surface expression of CB1R is established remains the subject of debate (see 1.3.6 Three currently proposed models of CB1R polarity). One suggestion is that high rates of endocytosis due to constitutive activity selectively remove CB1Rs from the somatodendritic plasma membrane, resulting in an accumulation at the axonal surface; (Leterrier et al., 2006). These internalised somatodendritic CB1Rs may then be either sorted for degradation or recycled to axons via a transcytotic sorting pathway (Simon et al., 2013). Alternatively, newly synthesized CB1Rs may be constitutively targeted to lysosomes, but under appropriate circumstances the CB1Rs destined for degradation are retrieved and rerouted to axons (Rozenfeld, 2011; Rozenfeld and Devi, 2008).

3.2.1.1 The role of the secretory pathway

Surprisingly little is known about the contribution of the secretory pathway to CB1R surface polarisation. Since siRNA knockdown of adaptor protein 3 subunit δ (AP-3δ) increases surface expression of CB1R in Neuro2A cells and primary hippocampal neurons, (Rozenfeld and Devi, 2008) suggest that at the TGN, CB1R is constitutively sorted by AP-3 for lysosomal degradation. By an unknown mechanism, a small proportion may be rescued and rerouted to axons.

(Leterrier et al., 2006) examined the forward trafficking of CB1R using a Brefeldin A (BFA) block and release protocol (**Figure 1-14**). Blocking the secretory pathway with BFA caused newly synthesized cargo to accumulate. By washing out the BFA, they were able to pulse-chase exogenously expressed CB1R. They found that CB1R is non-discriminately delivered to the membrane, and then retrieved in the somatodendritic compartment and rerouted to axons.

However, both of these experiments are limited by the fact that they block the secretory pathway as a whole – BFA blocks any cargo from trafficking, and furthermore has been shown to also affect endocytosis and recycling (Wood et al., 1991; Hunziker et al., 1991; Damke et al., 1991; Miller et al., 1992; Hunziker et al., 1992; Graham et al., 1993), and AP-3δ knockdown affects any cargo sorted by AP3.

In this chapter, I present a more targeted, genetic approach to examine CB1R forward trafficking by applying retention using selective hooks (RUSH) and show that CB1R is preferentially delivered to the axonal membrane by the secretory pathway.

3.2.2 Non-canonical secretory pathway trafficking in neurons

3.2.2.1 Local synthesis

Because of the unique architecture of neurons, cargo must often travel long distances. In order to accommodate for this, neurons have a local secretory pathway system in place. mRNA can be sent to dendrites for local synthesis and the machinery required for translation, assembly, and trafficking – the rough endoplasmic reticulum (rER), ER Exit Sites (ERES), and Golgi outposts are all present in dendrites (Horton and Ehlers, 2003, 2004; Holt and Schuman, 2013; Valenzuela and Perez, 2015; Quassollo et al., 2015; Evans et al., 2017).

It is conventionally thought that local synthesis of transmembrane proteins is impossible in axons because axons contain neither rER nor a traditional stacked Golgi. However, recent, somewhat controversial, evidence, especially from the Couve lab, suggests that local synthesis may indeed occur, through local smooth ER (sER) and a Golgi-independent pathway (see (González et al., 2018) for review).

3.2.2.2 Golgi bypass

Another recent, and also somewhat controversial, study reported that cargo can reach the surface with immature glycosylation profiles (Hanus et al., 2016). This suggests that certain cargo may bypass the Golgi and go straight from the ER to the plasma membrane. Furthermore, it has been reported that Kv2.1, a voltage-gated K^+ channel present in both the somatodendritic compartment and the axon initial segment (AIS) traffics to the two compartments by different mechanisms – Kv2.1 reaches the somatodendritic membrane through the conventional secretory pathway, but appears to bypass the Golgi in order to go to the AIS (Jensen et al., 2017).

I present below some preliminary data suggesting that CB1R traffics through the conventional secretory pathway.

3.2.3 Axonal morphology

In the canonical representation of a neuron, excitatory and inhibitory inputs received throughout the dendritic arbour are summed up and integrated in the soma. Under the right conditions, depolarisation of the soma may then initiate an all-or-nothing action potential, which travels down the axon and passes the signal on. This action potential is triggered by the axon initial segment (AIS), a dense cluster of voltage-gated Na^+ channels and anchoring proteins that emanates directly from the soma.

However, a body of evidence collected over the past couple of decades suggests that axons can emanate from dendrites rather than the soma in a variety of cell types (**Figure 3-1**), including neuroendocrine cells (Herde et al., 2013), dopaminergic neurons (Häusser et al., 1995), interneurons (Martina et al., 2000), cortical neurons (Sloper and Powell, 1979; Peters et al., 1968), and hippocampal neurons (Lorincz and Nusser, 2010; Thome et al., 2014). In the hippocampus, as many as 50% of CA1 pyramidal neurons and 25% of CA3 pyramidal neurons have

axons of dendritic origin (DO) rather than axons of somatic origin (SO; (Thome et al., 2014)). The majority of these DO axons emanate from a basal dendrite (Thome et al., 2014), although ones originating from apical dendrites have also been observed (Lorincz and Nusser, 2010). In these neurons, the axon carrying dendrite (AcD) holds a privileged position – it is more likely to generate dendritic spikes and input into the AcD elicits an action potential at a lower threshold compared to normal basal dendrites.

Apart from the privileged electrical properties of the dendrite carrying them, little else is known about the properties of the DO axons themselves. Trafficking of axonally polarised cargo to the DO axons is conceivably even more complex since cargo must travel along a portion of dendrite before entering the axon rather than traveling directly from the soma.

In preliminary data outlined below, I show that less CB1R traffics to DO axons than SO axons.

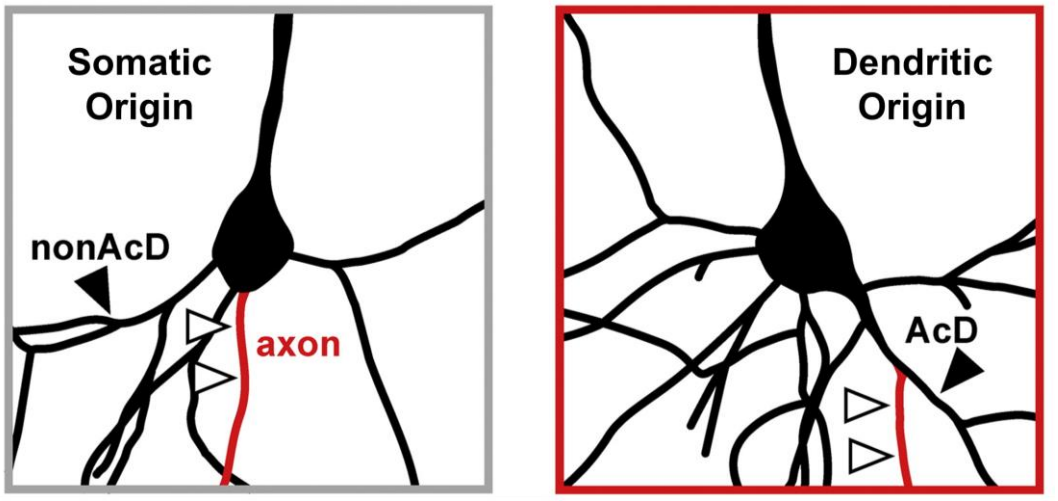

Figure 3-1 Somatic origin and dendritic origin axons in CA1 pyramidal neurons.

Schematic of example morphologies of CA1 pyramidal neurons of transgenic mice. Axons (red, white arrows) can emanate either from the soma (left) or an axon-carrying dendrite (AcD; right). In this example, the authors determined the whole cell morphology by DsRed expression whereas axon origin was identified by ankyrin-G labelling indicating the AIS.

Figure adapted from (Thome et al., 2014)

3.3 RESULTS

3.3.1 Exogenous expression of an N-terminally tagged CB1R construct in primary hippocampal neurons

In order to examine the trafficking of CB1R, it was necessary to exogenously express a tagged construct of CB1R that faithfully recapitulates the properties of endogenous CB1R as closely as possible. Therefore, several aspects needed to be considered. Since we are particularly interested in the role that the C-terminus plays in the trafficking of CB1R, we used an N-terminally tagged construct rather than a C-terminally tagged one to prevent the C-terminal tag from occluding potential localisatiosn motifs and/or interfering with potential protein-protein interactions important for CB1R trafficking. Indeed, comparisons between C- and N-terminally tagged versions of CB1R expressed in HEK293 cells or Neuro2A cells indicate that C-terminal tagging interfered with CB1R trafficking, causing a 2-3-fold increase in surface expression (Rozenfeld and Devi, 2008).

However, the N-terminal tail of CB1R is exceptionally long, and its large size, even without a tag, impedes its ability to translocate across the ER membrane (Nordström and Andersson, 2006; Andersson et al., 2003). Therefore, the addition of a 27kDa fluorescent protein might further impede its translocation. For these reasons, it is necessary to add an exogenous signal peptide before the fluorescent tag in order to achieve stable surface expression (Nordström and Andersson, 2006; McDonald et al., 2007b; Andersson et al., 2003).

Moreover, the N-terminal tail of CB1R, like those of other GPCRs, does not contain a canonical, cleavable signal peptide. However, CB1R has been reported to undergo N-terminal truncation, removing the N-terminal tag (Nordström and Andersson, 2006). Therefore, the first 25 amino acids of the N-terminus have previously been removed in order to prevent cleavage of the N-terminal tag (McDonald et al., 2007b). Interestingly, the first 22 amino acids of the N-terminus have subsequently been reported to constitute a mitochondrial targeting motif (Hebert-Chatelain et al., 2016). Importantly, while constructs with this type of N-terminal truncation display impaired trafficking to mitochondria, the trafficking to plasma membrane is unaffected (McDonald et al., 2007b; Hebert-Chatelain et al., 2016). Since this thesis focuses on the plasma membrane trafficking and localisation of CB1R, the N-terminal truncation adds the advantage that it

circumvents potential complications due to mitochondrial targeting which, although of interest, are not the focus of our study.

A SP^{HgH}-SEP-CB1R (rat) construct, containing a human growth hormone signal peptide (SP^{HgH}), a 25 amino acid N-terminal truncation, and an N-terminal superecliptic pHluorin (SEP) tag was kindly donated by Dr Andrew Irving (Dundee) (McDonald et al., 2007b; a). This construct was subcloned by a previous PhD student (Dr Keri Hildick) in the Henley lab into pcDNA3.1 or pSinRep5 for either transfection or Sindbis viral transduction of hippocampal neurons, respectively (**Figure 3-2 A-B**). Transfected cells displayed a polarised surface distribution analogous to that of endogenous CB1R which was stained using the N-terminal rabbit FP1A antibody kindly provided by Professor Ken Mackie (Indiana University; **Figure 3-2 A upper and middle panels, B**). However, the method of transduction has an effect on surface localisation – the vast majority of the surface expression of Sindbis virally transduced CB1R was non-polarised, presumably due to excessive CB1R expression, which might saturate the polarising mechanisms (**Figure 3-2 A lower panel, B**). Therefore, throughout this thesis, primary hippocampal neurons were transfected with tagged CB1R, not virally transduced.

To confirm that the N-terminal truncation does not affect surface localisation, the surface expression of a construct lacking the first 25 amino acids ($CB1R^{WT}$) was compared to that of a full, full length CB1R construct ($CB1R^{FFL}$; **Figure 3-3 A**). No significant difference in surface polarity (axon/dendrite ratio) between EGFP-$CB1R^{WT}$ and EGFP-$CB1R^{FFL}$ was found (**Figure 3-3 B**). Indeed, there was no significant difference in the surface-to-total expression of axons and dendrites between EGFP-$CB1R^{WT}$ and EGFP-$CB1R^{FFL}$ (**Figure 3-3 C**). Nevertheless, there was a non-significant trend towards decreased surface expression of EGFP-$CB1R^{FFL}$, especially in axons. However, it cannot be ruled out that this might have been due to N-terminal cleavage removing the tag.

Thus, because it showed a highly similar surface distribution, to avoid loss of the tag, and to avoid complications with potential mitochondrial targeting, the N-terminally truncated form of CB1R was used (named as $CB1R^{WT}$) to examine the trafficking of CB1R throughout this thesis. Any additional deletions/mutations used $CB1R^{WT}$ as a template meaning that the changes in trafficking observed were due to the additional deletions/mutations, not due to the N-terminal tagging, presence of an exogenous signal peptide, or deletion of the first 25 amino acids.

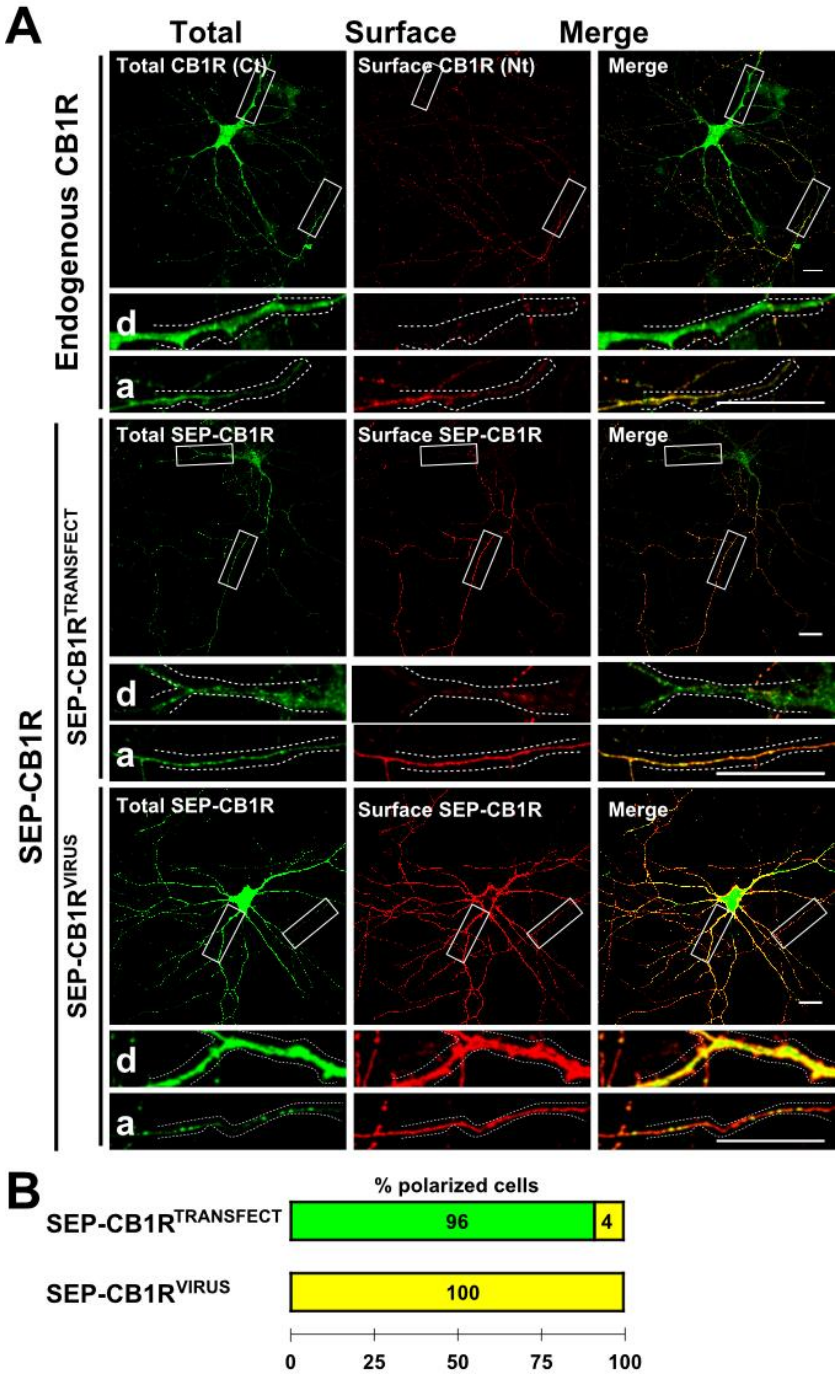

Figure 3-2 Comparison of endogenous CB1R surface distribution with transfected (SEP-CB1R^{TRANSFECT}) or virally overexpressed (SEP-CB1R^{VIRUS}) SEP-CB1R in primary hippocampal neurons.

(**A**) Representative DIV 15 hippocampal neurons analysed by immunocytochemistry to compare surface and total receptor distributions for neurons endogenously expressing CB1Rs (top panels; FP1A) with neurons expressing SEP-CB1R either by transfection (middle panels) or viral transduction (lower panels). SEP-CB1R expressing neurons were either transfected on DIV 12 or virally transduced 15 h prior to surface immunostaining with anti-GFP antibody (Roche). Acquisition parameters were maintained constant across SEP-CB1R^{TRANSFECT} and SEP-CB1R^{VIRUS}, for direct comparison of total expression levels.

(**B**) Quantification of relative percentage of polarize (green) to non-polarized (yellow) SEP-CB1R surface distributions observed across experiments (SEP-CB1R^{TRANSFECT} n = 25 neurons; SEP-CB1R^{VIRUS} n = 30 neurons; n = 4 independent experiments).

Experiments, figure, and figure legend by Dr Keri Hildick (Hildick, 2013).

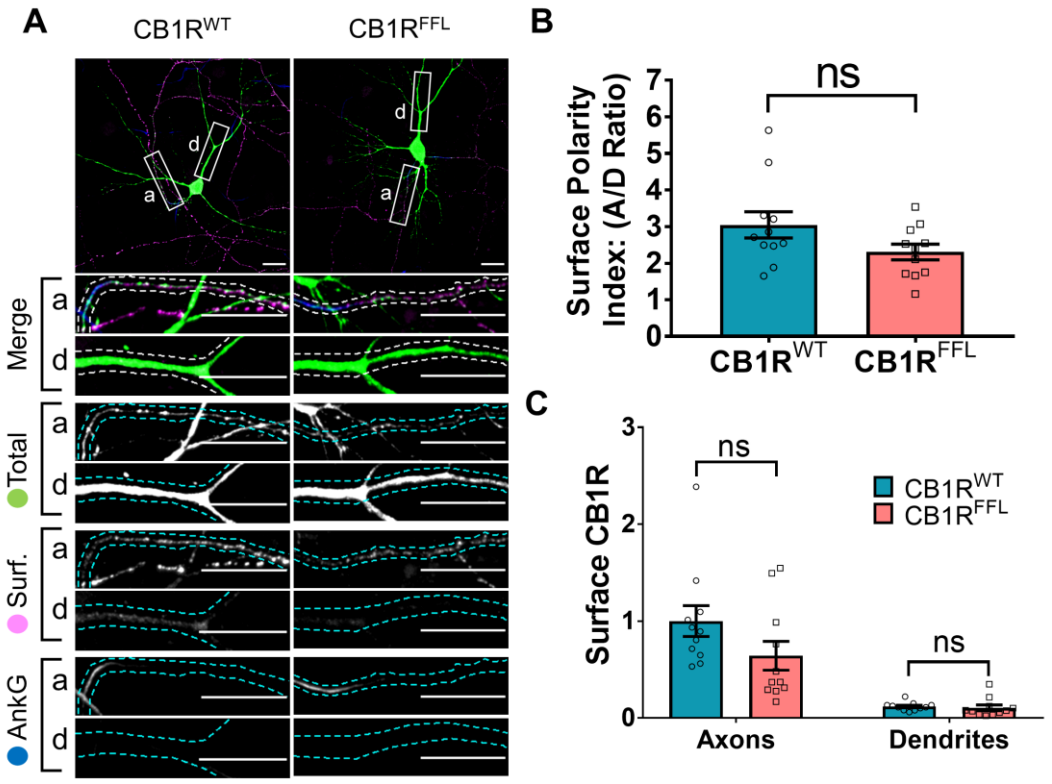

Figure 3-3 Indistinguishable axonal surface polarisation of EGFP-tagged full-length CB1R (CB1R^{FFL}) and CB1R lacking the first 25 N-terminal residues (CB1R^{WT}).

(**A**) Representative confocal images of surface stained DIV 14 hippocampal neurons expressing EGFP-CB1R^{WT} or EGFP-CB1R^{FFL}. Merge: surface to total seen as white. Scale bar = 20 µm.

(**B**) Quantification of data shown in (**A**) presented as surface polarity index (A/D). There was no significant difference in surface polarity between EGFP-CB1R^{WT} and EGFP-CB1R^{FFL}. Unpaired t test. N = three independent experiments; n = 11 neurons per condition. $^{ns}p < 0.05$.

(**C**) Quantification of data shown in (**A**). Surface expression of CB1R^{WT} in both axons and dendrites was not significantly different to that of CB1R^{FFL}. Two-way ANOVA with Tukey's *post hoc* test. N = three independent experiments; n = 11 neurons per condition. $^{ns}p < 0.05$.

3.3.2 Synchronous forward trafficking of plasma membrane receptors using the retention using selective hooks (RUSH) system

3.3.2.1 Retention using selective hooks (RUSH)

To investigate how CB1R surface polarity is established we used the retention using selective hooks (RUSH) system (**Figure 3-4**; **Figure 3-5**) and antibody feeding (**Figure 3-9**) techniques to examine its examine its secretory pathway trafficking and surface expression (Boncompain et al., 2012; Evans et al., 2017). The layout of the RUSH cloning cassette is shown in (**Figure 3-4**). Streptavidin is expressed and translocated to the endoplasmic reticulum (ER) due to the presence of a stromal interaction molecule 1 (STIM-1) signal peptide (SP^{STIM-1}). It is prevented from being secreted due to the addition of a KDEL ER retention peptide sequence at the C-terminal end of the protein (Munro and Pelham, 1987; Stornaiuolo et al., 2003). The expression of this ER 'hook' is driven under a CMV

promoter. An IRES insert allows for the expression of the reporter, in this case CB1R. The membrane topology of CB1R means that the N-terminus is in the lumen of ER. Thus, the reporter is translocated to the ER due to the presence of an exogenous interleukin-2 signal peptide (SP^{Il-2}) and an N-terminally located streptavidin binding peptide (SBP) tag binds to the ER-located streptavidin, thus anchoring it to the ER. Because translation under an IRES sequence is about a tenth as efficient as under a CMV promoter (Kaufman et al., 1991; Bouabe et al., 2008), this ensures a saturating amount of hook and prevents leakage of the reporter. The receptor of interest is also N-terminally tagged with a fluorescent protein (EGFP or mCherry) to allow for the monitoring of the progress of the reporter.

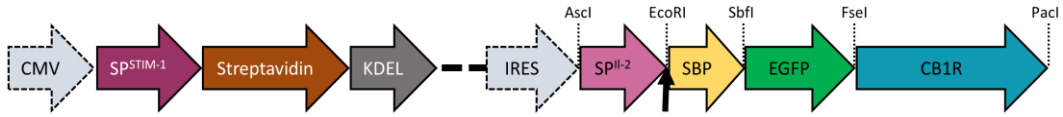

Figure 3-4 Schematic of the RUSH cloning cassette structure.

The expression of an ER localised streptavidin-KDEL hook is driven under a CMV promoter. An IRES sequence drives expression of the receptor of interest, in this case CB1R, N-terminally tagged with SBP, which binds to the streptavidin, thus causing it to be retained in the ER. A fluorescent protein tag (here EGFP) allows for detection of the localisation of the reporter. Each section of the reporter is flanked by restriction sites, thus allowing flexibility in changes of signal peptides, fluorescent proteins, and reporters. Arrows indicate signal peptide cleavage sites.

Thus, in biotin-free media, the SBP-tagged reporter is anchored in the ER by the streptavidin-KDEL hook (**Figure 3-5 left**). The addition of biotin, which has a greater affinity for streptavidin than SBP (Keefe et al., 2001), outcompetes the hook-reporter interaction and the reporter is synchronously released and trafficked by bulk flow through the secretory system to the plasma membrane (**Figure 3-5 right**). The progress of the reporter can be monitored by live imaging of the fluorescent protein or by fixed immunostaining for SBP and/or EGFP (Evans et al., 2017).

3.3.2.2 Validation of RUSH SBP-EGFP-CB1R in HeLa cells

The N-terminally truncated rat CB1R was cloned into the RUSH cassette by Dr Ash Evans (**Figure 3-4**). Versions with two different fluorescent reporters were generated (EGFP or mCherry), depending on the specifications of the confocal microscopes used.

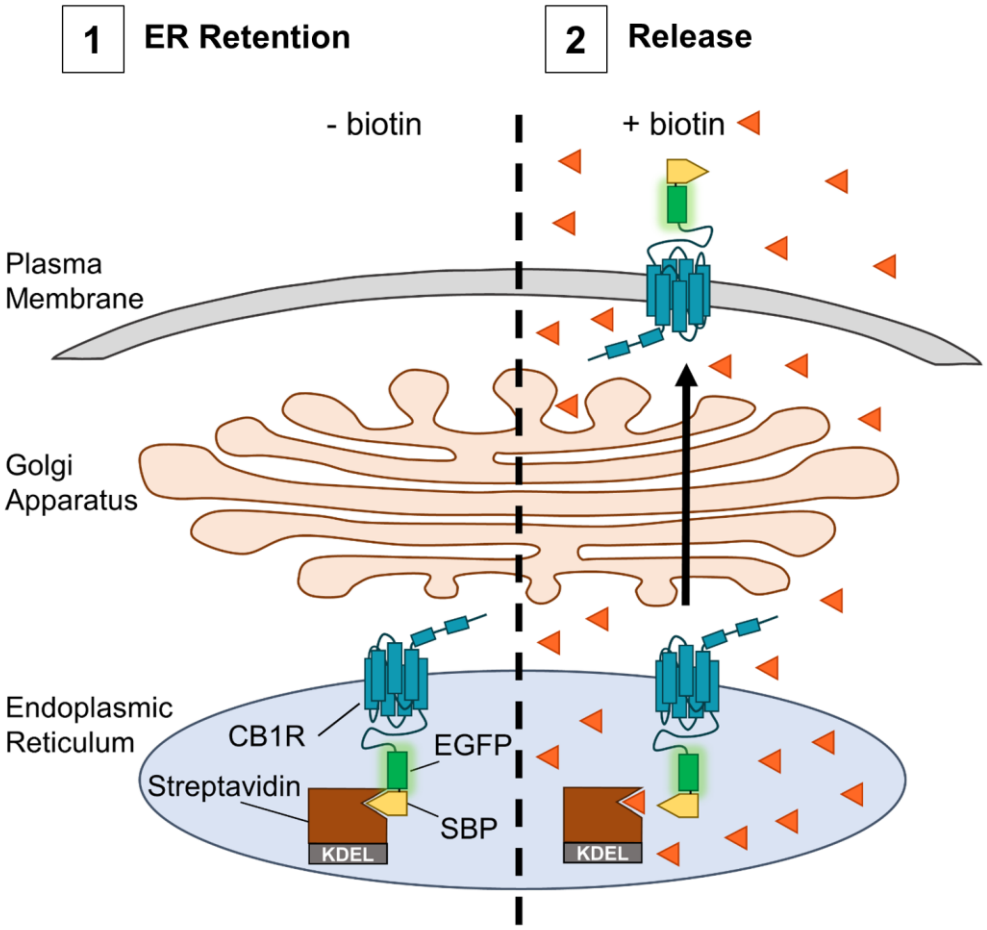

Figure 3-5 Schematic of RUSH protocol.

(1) Before the addition of biotin, SBP-EGFP-CB1R is retained in the ER by a streptavidin-KDEL hook (0 min).

(2) Addition of biotin (orange triangles), which has a higher affinity for streptavidin than SBP, releases the receptor from the ER, causing it to traffic through the Golgi Apparatus and accumulate at the plasma membrane.

To validate that the RUSH assay was working as expected, RUSH SBP-mCherry-CB1R was transfected into HeLa cells (**Figure 3-6**). Biotin was added for incrementally longer times before the cells were fixed in 4% formaldehyde in non-permeabilising conditions and immunostained for SBP present at the surface.

In the no-biotin condition (0 min), there was generally no SBP detected on the surface, indicating that the SBP-mCherry-CB1R was successfully retained in the ER. Rarely, the occasional cell that expressed the construct very highly did show SBP staining – therefore moderately-expressing cells were chosen for analysis for all timepoints. After 25 minutes of biotin-mediated release, SBP staining began to be detectable at the surface. Surface SBP-mCherry-CB1R continued to accumulate at the surface until 60 minutes, when the accumulation began to plateau (**Figure 3-6 B**).

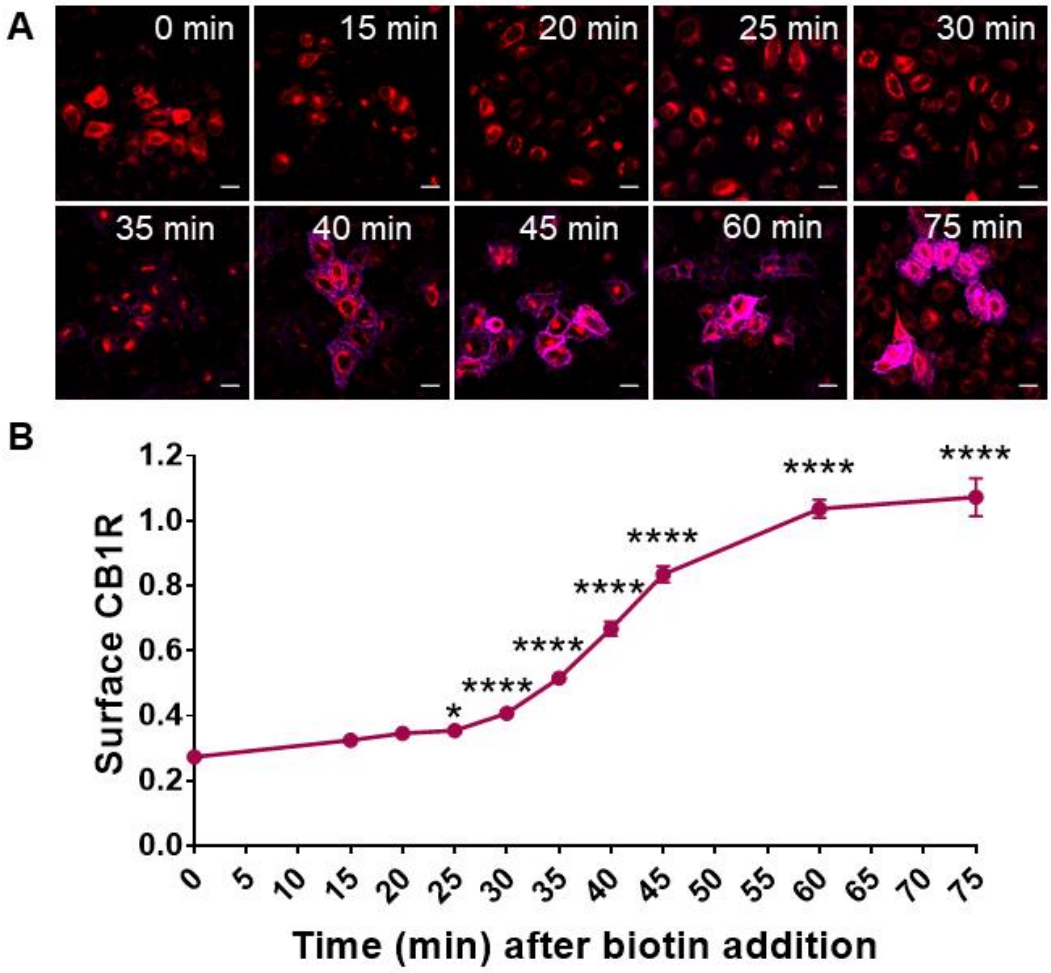

Figure 3-6 Validation of RUSH CB1R in HeLa cells.

(**A**) Representative confocal images of RUSH SBP-mCherry-CB1R total (red) and surface (magenta) localisation in HeLa cells following the addition of biotin for 0 (no biotin), 15, 20, 25, 30, 35, 40, 45, 60, and 75 minutes. HeLa cells were fixed in non-permeabilizing conditions then surface stained with anti-SBP antibody (magenta). At 0 minutes (no biotin), SBP-mCherry-CB1R was retained in the ER. Surface labelling began to appear 25 minutes following biotin-mediated release and continued to accumulate until it plateaus after about 60 minutes. Scale bar = 20 µm.

(**B**) Quantification of data represented in (**A**). Surface CB1R was normalised to total CB1R. N = 1-4 independent experiments; n = 40-120 cells per timepoint. One-way ANOVA with Tukey's post hoc test. *p ≤ 0.05, ****p ≤ 0.0001 compared to no biotin control (0 min).

These data indicate that RUSH CB1R is successfully hooked in the ER by the streptavidin-KDEL, and that the addition of biotin successfully releases it, allowing it to go through the secretory pathway and be delivered to the surface.

3.3.2.3 CB1R is directly trafficked to the axon by the secretory pathway

Next, I transfected primary hippocampal neurons with RUSH SBP-EGFP-CB1R and added biotin incrementally longer times. At 0 minutes, SBP-EGFP-CB1R was retained in the ER and displayed a diffuse somatic localisation. After addition of biotin, SBP-EGFP-CB1R trafficked through the secretory pathway and by 15

minutes, it was located in bright clusters in the soma, indicating that it was most likely located in the somatic Golgi, although co-staining with a Golgi marker would be needed to definitively confirm this (**Figure 3-7**). These bright clusters were still present after 25 minutes but were gone by 45 minutes (**Figure 3-7**).

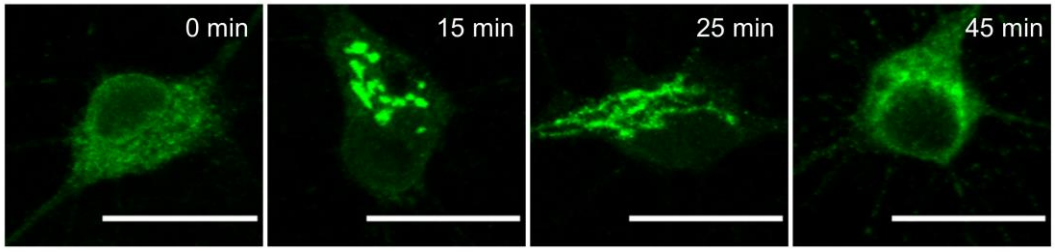

Figure 3-7 Once released, SBP-EGFR-CB1R progresses through the secretory pathway.

Representative confocal images of the somatic localisation of SBP-EGFP-CB1R as it goes through the secretory pathway. Images are lower exposures of representative neurons and are enlarged post acquisition to examine the soma. At 0 min, SBP-EGFP-CB1R was retained in the somatodendritic ER. After 15 min, bright clustering of SBP-EGFP-CB1R suggestive of cargo progression to the Golgi. This clustering was gone by 45 min. However, co-staining with a Golgi marker such as Giantin would be needed to fully confirm that these clusters do, indeed, represent Golgi-based cargo. Scale bar = 20 µm.

Next, I examined the synchronous trafficking of total SBP-EGFP-CB1R in the somatodendritic and axonal compartments of primary hippocampal neurons (**Figure 3-8**). Since the secretory pathway components are only present in the soma and proximal dendrites, and axons contain very little, if any, rough ER (rER), I first examined the total distribution of CB1R during retention and biotin-mediated release between the somatodendritic and axonal compartments. Prior to biotin-mediated release, SBP-EGFP-CB1R was retained in the ER in the soma and proximal dendrites but was absent from the axonal compartment (0 min; **Figure 3-7**, **Figure 3-8 A, left**). Between the different the retention and release timepoints, the expression levels of SBP-EGFP-CB1R was identical, as indicated by mean total dendritic fluorescence (**Figure 3-8 B**). In the unretained control (O/N), SBP-EGFP-CB1R expressed at slightly lower levels, most likely due to the normal turnover of the protein when not retained in the ER (**Figure 3-8 B**).

After 25 minutes, SBP-EGFP-CB1R began to enter the proximal segment of the axonal compartment, where it continued to accumulate until 45 minutes when it reached its peak. By 30 minutes, the level of SBP-EGFP-CB1R was not significantly different from and unretained control (O/N) (**Figure 3-8 C**) and exceeded the average amount of total CB1R present in an average dendrite,

indicating a polarised total distribution towards the axons. These data suggest that once released from the ER, CB1R was immediately trafficked towards the axonal compartment, and passed through the axon initial segment (AIS), which constitutes an exclusion and diffusion barrier to separate the axonal from the somatodendritic compartments (Leterrier and Dargent, 2014), via the intracellular secretory pathway.

3.3.2.4 De novo CB1R is more rapidly surface expressed in axons than in dendrites

Having established that SBP-EGFP-CB1R released from the ER trafficked directly to axons, I next investigated where and when the newly synthesised SBP-EGFP-CB1R first reaches the plasma membrane. I determined how much SBP-EGFP-CB1R was surface expressed during a given time period using an antibody feeding assay (**Figure 3-9**). Antibody feeding was performed concurrent with the addition of biotin to release ER-retained SBP-EGFP-CB1R. This protocol labels both surface expressed CB1Rs and those that have been surface expressed and subsequently endocytosed (surface+endocytosed), giving a measure of total amount of surface expression irrespective of internalisation. SBP-EGFP-CB1R was surface expressed in the proximal segment of axons 40 min after release from the ER, whereas in dendrites, CB1R was not surface expressed until 60 min after release (**Figure 3-10 B; hash signs**). Moreover, significantly more SBP-EGFP-CB1R reached the surface of axons than the surface of dendrites 45, 60, and 90 min after release from the ER (**Figure 3-10 B; asterisks**). These data demonstrate that the secretory pathway delivers a greater amount of CB1R more rapidly to the axonal membrane than to the dendritic membrane.

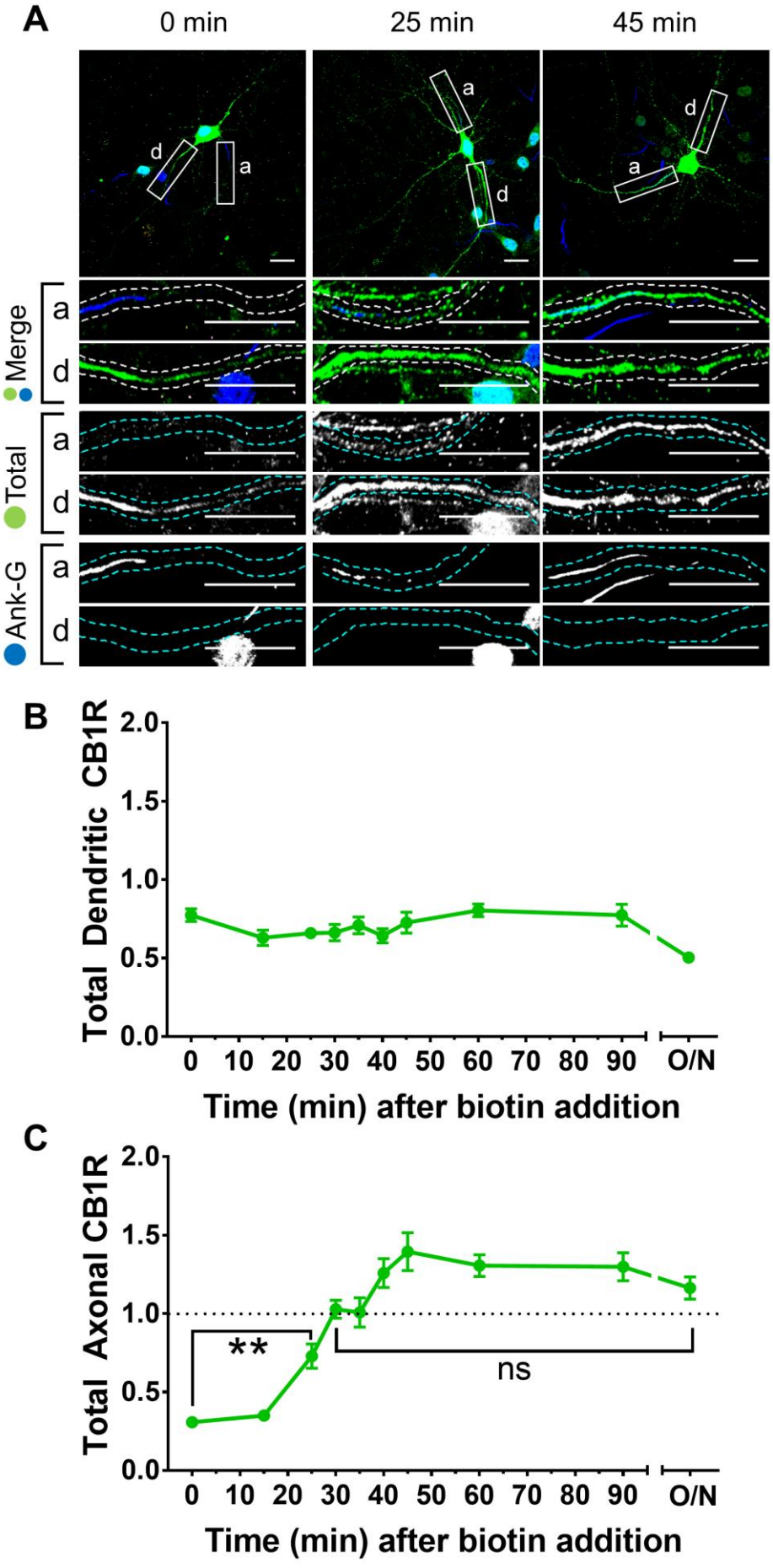
A
0 min
25 min
45 min
d
a
Merge
Total
Ank-G
B
Total Dendritic CB1R
2.0
1.5
1.0
0.5
0.0
0 10 20 30 40 50 60 70 80 90 O/N
Time (min) after biotin addition
C
Total Axonal CB1R
**
ns
Time (min) after biotin addition

Figure 3-8 Rapid trafficking of newly synthesized CB1R to the axon.

The trafficking of SBP-EGFP-CB1R following release with biotin was monitored after 0 (no biotin), 15, 25, 30, 35, 40, 45, 60, 90 min, and overnight (O/N; non-retained control) in DIV 13 hippocampal neurons.

(**A**) Representative images of hippocampal neurons expressing the RUSH SBP-EGFP-CB1R construct without biotin (0 min), 25 min, and 45 min after biotin-mediated release. Without biotin, SBP-EGFP-CB1R is anchored in the ER of the somatodendritic compartment and is not detected in the proximal 50 µm of axons. 25 min after biotin-mediated release, SBP-EGFP-CB1R entered the axon. Upper panels for each condition show whole cell field of view and lower panels are enlargements of axonal (a) and dendritic (d) ROIs. Merge: green = total; blue = Ankyrin G. In all images the scale bar = 20 µm.

(**B**) Quantification of data represented in (**A**). Analysis of the normalised total dendritic fluorescence (average of 2-3 dendrites) indicates that SBP-EGFP-CB1R was expressed equally amongst the retained and released timepoints. There is a trend to a decrease in the unretained O/N control that is significantly different only from the 0, 60, and 90 timepoints, but not the other timepoints. This is most likely due to normal turnover in the unretained control that would not be possible in the retained and released timepoints. One-way ANOVA with Tukey's *post hoc* test. N = three to six independent experiments, n = 19–45 neurons per condition.

(**C**) Quantification of data represented in (**A**). SBP-EGFP-CB1R was initially absent from the axon but entered after 25 min and by 30 min, the amount of SBP-EGFP-CB1R in the axon was not significantly different from the unretained control (O/N) and had surpassed the amount present in dendrites (>1; dotted line). The amount of SBP-EGFP-CB1R in the axon peaked after 45 minutes. To measure axonal entry of SBP-EGFP-CB1R, the average fluorescence of the first 50 µm of the axon was normalised to the average fluorescence of 2-3 dendrites (so that a value of 1 is equal amounts in both). One-way ANOVA with Tukey's post hoc test. N = three to six independent experiments, n = 19–45 neurons per condition. **p ≤ 0.01 compared to 0 min; ^{ns}p > 0.05 compared to O/N.

3.3.2.5 De novo CB1R is retained longer at the surface of axons than of dendrites

It has been suggested CB1R polarity is maintained by differential rates of endocytosis in the somatodendritic and axonal compartments (Leterrier et al., 2006; McDonald et al., 2007a). To test this, we also stained for retained surface SBP-EGFP-CB1R at the end of the timepoint by live incubation with Alexa 647-conjugated chicken anti-GFP (**Figure 3-9**) and compared the amount of surface expressed SBP-EGFP-CB1R to the amount of surface+endocytosed SBP-EGFP-CB1R in axons (**Figure 3-11 A, B**) and in dendrites (**Figure 3-11 A, C**). In the proximal segment of axons, the normalised surface and surface+endocytosed curves were identical, suggesting that most surface expressed SBP-EGFP-CB1R is stable and retained at the axonal membrane (**Figure 3-11 B**). This may be due either to minimal endocytosis or to the efficient recycling of endocytosed receptors. In stark contrast, however, in dendrites there is significantly less surface than surface+endocytosed SBP-EGFP-CB1R 90 min after addition of biotin, indicating that surface expressed CB1R is more rapidly endocytosed from and/or not recycled back to the dendritic membrane (**Figure 3-11 C**).

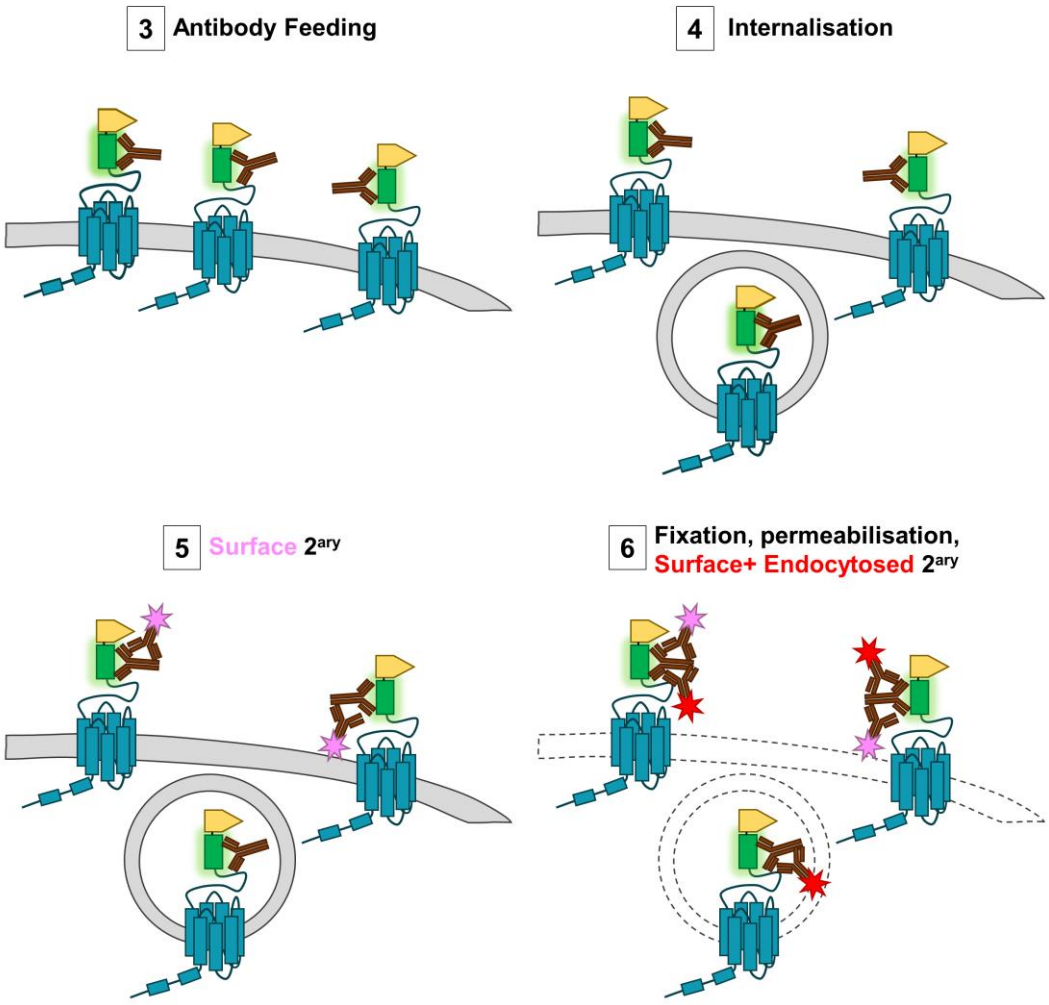

Figure 3-9 Antibody feeding protocol.

Numbering is continued from Figure 3-5.

(3) Antibody feeding with anti-GFP antibodies during biotin-mediated release labels newly delivered, surface expressed SBP-EGFP-CB1R.

(4) A proportion of receptors internalise, still bound to primary antibody.

(5) Cells are cooled to 4°C to prevent further internalisation. Live secondary antibody incubation labels retained surface receptors (indicated by magenta star).

(6) Cells are then fixed and permeabilised (dotted lines). Incubation with a different secondary antibody labels all receptors delivered to the surface during the time course of the experiment (red star = surface+endocytosed).

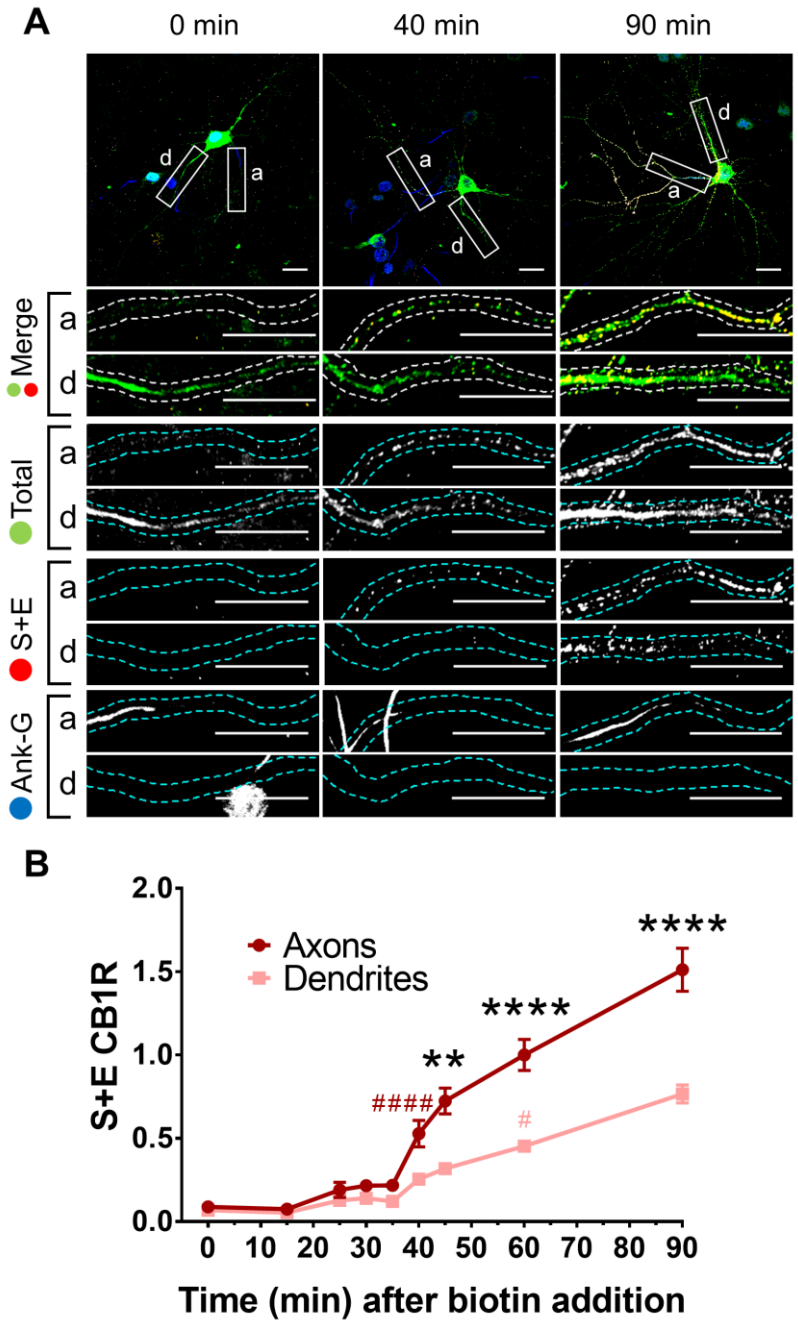

Figure 3-10 Newly synthesized CB1R is preferentially delivered to the axonal surface.

The trafficking of SBP-EGFP-CB1R following release with biotin was monitored after 0 (no biotin), 15, 25, 30, 35, 40, 45, 60, 90 min, and overnight (O/N; non-retained control) in DIV 13 hippocampal neurons.

(**A**) Representative confocal images of total and surface expressed SBP-EGFP-CB1R in DIV 13 hippocampal neurons 0 min, 40 min, and 90 min after biotin-mediated release showing that SBP-EGFP-CB1R is preferentially delivered to the axonal surface. Merge: surface+endocytosed to total seen as yellow.

(**B**) Quantification of data represented in (**A**). SBP-EGFP-CB1R reached the proximal surface of the axon 40 min after release and the surface of dendrites 60 min after release. Furthermore, significantly more SBP-EGFP-CB1R reached the axonal versus dendritic surface at 45, 60, and 90 min. Asterisks represent **p ≤ 0.01, ****p ≤ 0.0001 comparing axons vs. dendrites. Coloured hash signs represent $^{\#}$p ≤ 0.05, $^{\#\#\#\#}$p ≤ 0.0001 compared to respective 0 min.

Statistical analyses in (**B** and **Figure 3-11 B-C**); Two-way ANOVA with Tukey's post hoc test (all analysed and corrected for multiple comparisons together). N = three to six independent experiments, n = 19–45 neurons per condition.

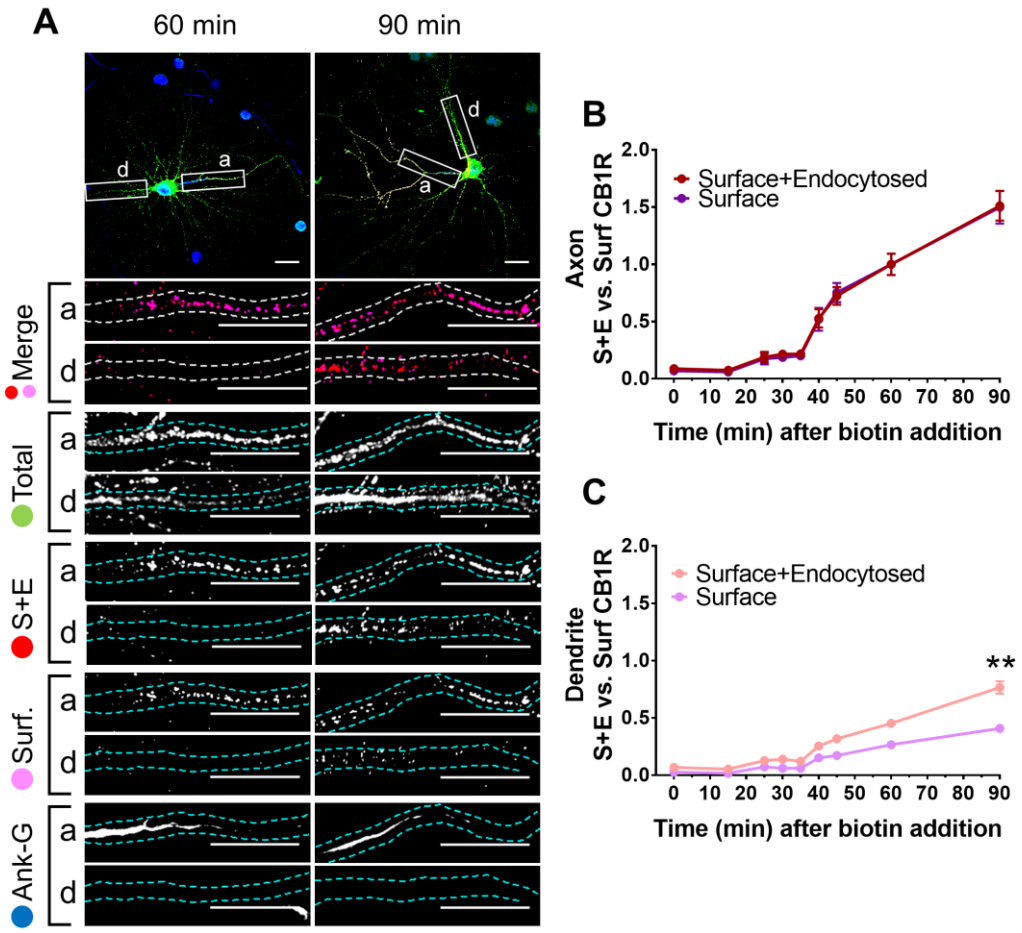

Figure 3-11 Newly delivered CB1R is preferentially retained at the surface of axons.

The trafficking of SBP-EGFP-CB1R following release with biotin was monitored after 0 (no biotin), 15, 25, 30, 35, 40, 45, 60, 90 min, and overnight (O/N; non-retained control) in DIV 13 hippocampal neurons.

(**A**) Representative confocal images of total and surface expressed SBP-EGFP-CB1R in DIV 13 hippocampal neurons 60 min and 90 min after biotin-mediated release showing that SBP-EGFP-CB1R is preferentially retained at the axonal surface, but not at the dendritic surface. Merge: retained surface (overlap between surface and surface+endocytosed) is seen as magenta; endocytosed only is seen as red.

(**B**) Quantification of data represented in (**A**). Comparison between surface+endocytosed (red; see **Figure 3-10 B**) and surface (magenta) curves show that SBP-EGFP-CB1R was retained on the surface of axons. For all $p > 0.9999$.

(**C**) Quantification of data represented in (**A**). Comparison between surface+endocytosed (pale red; see **Figure 3-10**) and surface (pale magenta) curves show that SBP-EGFP-CB1R was internalised from the surface of dendrites. **$p \leq 0.01$ comparing 90 min surface+endocytosed and surface.

Statistical analyses in (**Figure 3-10 B** and **B-C**); Two-way ANOVA with Tukey's post hoc test (all analysed and corrected for multiple comparisons together). N = three to six independent experiments, n = 19–45 neurons per condition.

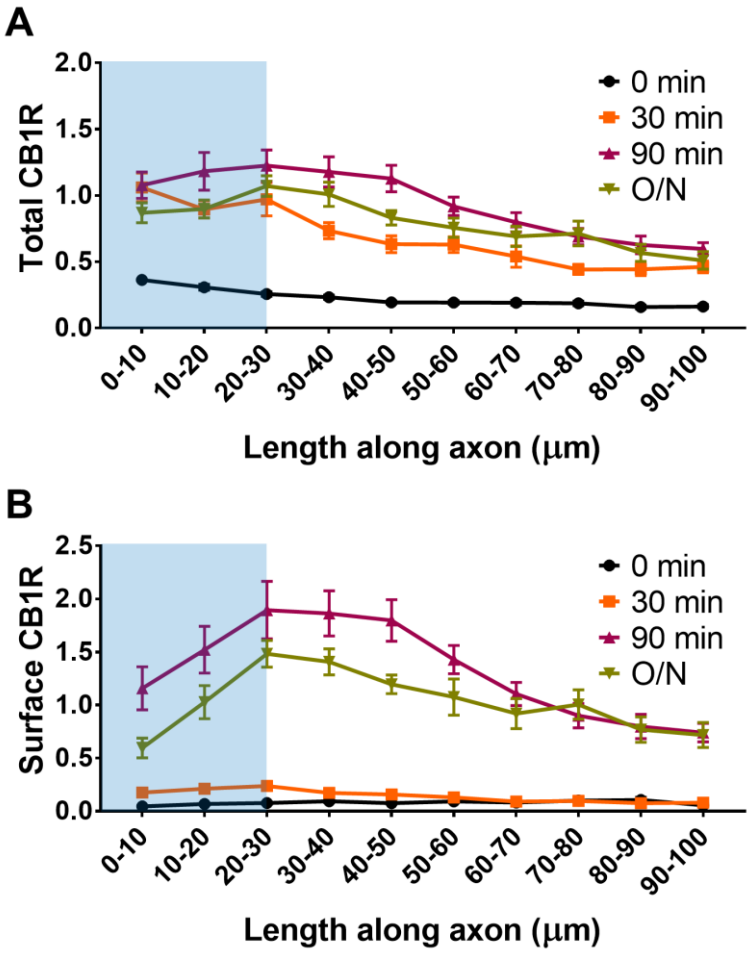

Figure 3-12 Intracellular trafficking and lateral diffusion to more distal parts of the axon.

(**A**) Distribution of total CB1R along the first 100 µm of the axon indicates that CB1R is trafficked within the axon. By 30 min after release from the ER, and before CB1R reaches the surface, CB1R is present at least 100 µm away from the soma at levels comparable to an unretained control (O/N). The blue shaded portion indicates the location of the AIS (defined by Ankyrin-G immunostaining). Two-way ANOVA with Sidak's post hoc test. N = four to six independent experiments, n = 12–18 neurons per condition. 90–100 µm: *p ≤ 0.05. 90–100 µm comparing 30 min to 0 min, $^{ns}p > 0.05$ comparing 30 min to O/N.

(**B**) Distribution of surface expressed CB1R along the first 100 µm of the axon shows an accumulation of CB1R at the distal region of the AIS 90 min after release from the ER. This accumulation in the AIS is reduced in the O/N unretained control consistent with lateral diffusion within the membrane. Two-way ANOVA with Sidak's post hoc test. N = four to six independent experiments, n = 12–18 neurons per condition. 0–50 µm, 90 min vs. O/N: All points p ≤ 0.05. 50–100 µm, 90 min vs. O/N: All points $^{ns}p \geq 0.05$.

3.3.2.6 CB1R may be trafficked to more distal parts of the axon via both intracellular mechanisms and lateral diffusion.

Analysis of CB1R total fluorescence along the axon indicates that by 30 min after release from the ER, and before CB1R appears on the surface, intracellular CB1R has progressed through the AIS and is already present at least 100 µm along the axon at levels similar to the unretained control (O/N; **Figure 3-12 A**). These data indicate that CB1R-containing secretory vesicles can rapidly travel to more distal areas of the axon. Furthermore, surface CB1Rs delivered from the secretory

pathway accumulate at the final portion of the AIS, before then progressing further along the axon (**Figure 3-12 B**). Interestingly, 100 µm along the axon CB1R levels reach a steady state 90 min after release, at levels similar to when receptors are released overnight. However, following overnight release, fewer receptors remain in the most proximal region of the axon. These results suggest that additional mechanisms contribute to the delivery of CB1R receptors the distal axon and presynaptic boutons. This process occurs over a time-course of several hours and could involve lateral surface diffusion and trapping analogous to the accumulation of AMPARs at the postsynaptic membrane (Borgdorff and Choquet, 2002). More studies would need to be done to elucidate the mechanisms by which CB1R is delivered to distal areas of the axon and the presynapse.

3.3.2.7 SBP-EGFP-CB1R traffics through the canonical secretory pathway

Since SBP-CB1R-EGFP trafficked very rapidly to the axon, extending to at least 100 µm down the axon and appearing at the axonal surface long before appearing at the dendritic surface (**Figure 3-12**), I wondered whether the faster trafficking to the axon was due to axonal CB1R bypassing the Golgi, such as it has been reported for Kv2.1 (Jensen et al., 2017). I tested this by adding 10 µM Golgicide A (**Figure 1-14**) concurrent to biotin release for 60 minutes (**Figure 3-10 B**; **Figure 3-13**). However, inhibition of the Golgi prevented visible axonal entry of CB1R and prevented accumulation of CB1R at the surface of any compartment (**Figure 3-13;** unquantified observation), suggesting that CB1R traffics through the canonical secretory pathway to both the somatodendritic and axonal compartments.

3.3.2.8 Less SBP-EGFP-CB1R is delivered to axons of dendritic origin than axons of somatic origin

Previously, Dr Ash Evans in the lab noticed that when RUSHing SBP-EGFP-GluK2 significantly less cargo would enter axons of dendritic origin (DO) than those of somatic origin (SO). In order to determine whether this might be a generic trend or something specific to GluK2, I also compared CB1R axonal delivery between SO and DO axons (**Figure 3-14**).

Less SBP-EGFP-CB1R entered DO axons than SO axons after both 30 minutes and 60 minutes of trafficking (**Figure 3-14 A-B**). This could, perhaps, be simply due to the fact that in order to enter DO axons, cargo has farther to go – along an additional section of dendrite – before it reaches the axon and thus simply takes more time to get there. However, intriguingly, this difference in axonal entry/polarity

is also present in the unretained control (O/N; **Figure 3-14 B**). This may indicate that DO axons have different properties to SO axons.

Importantly, in all the above and subsequent RUSH experiments, only SO axons were analysed to prevent false positive differences due to the number of SO or DO axons analysed.

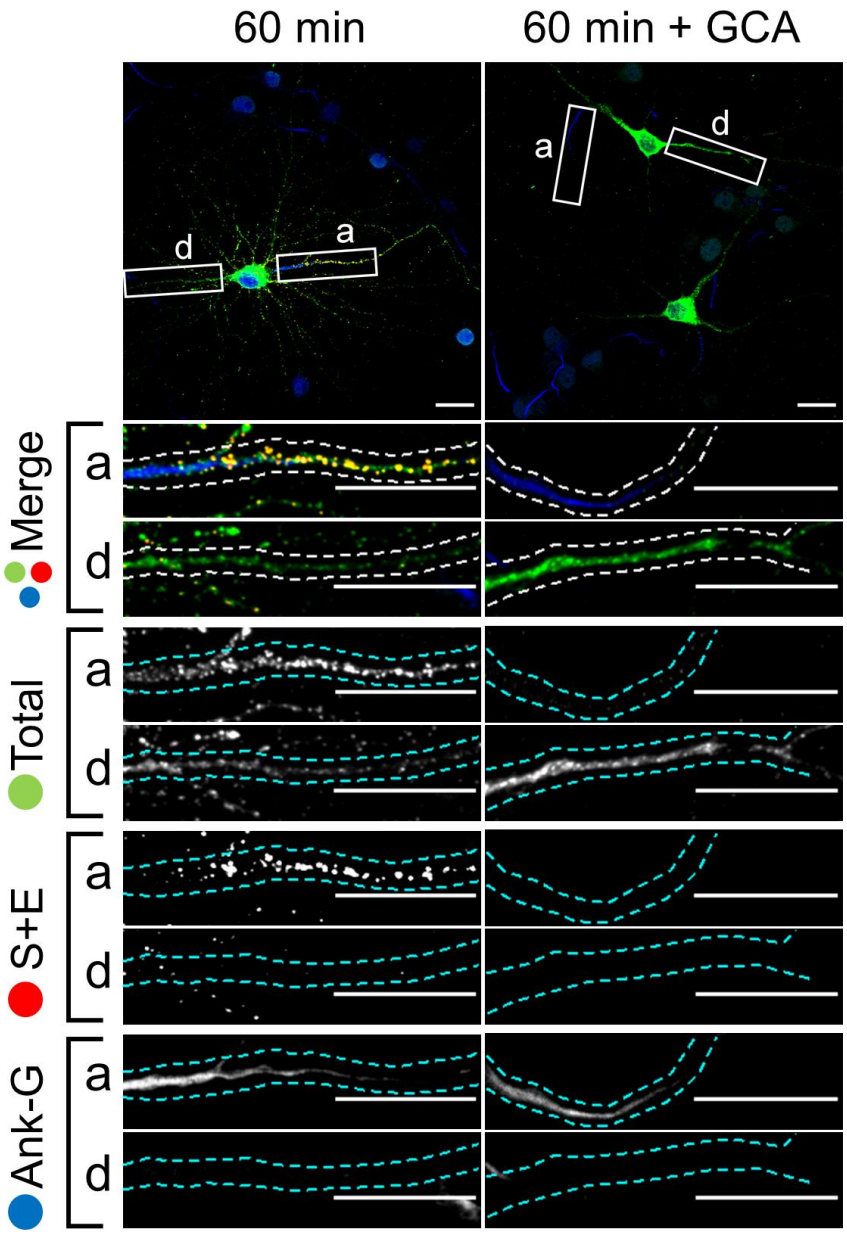

Figure 3-13 SBP-EGFP-CB1R traffics through the canonical secretory pathway.

Representative images of DIV 13 hippocampal neurons expressing SBP-EGFP-CB1R released for 60 minutes. Golgicide A was added concurrent to biotin (right-hand panels). In the presence of Golgicide A, SBP-EGFP-CB1R does not enter the axon, nor does it reach the surface in any compartment. Merge: surface+endocytosed to total seen as yellow.

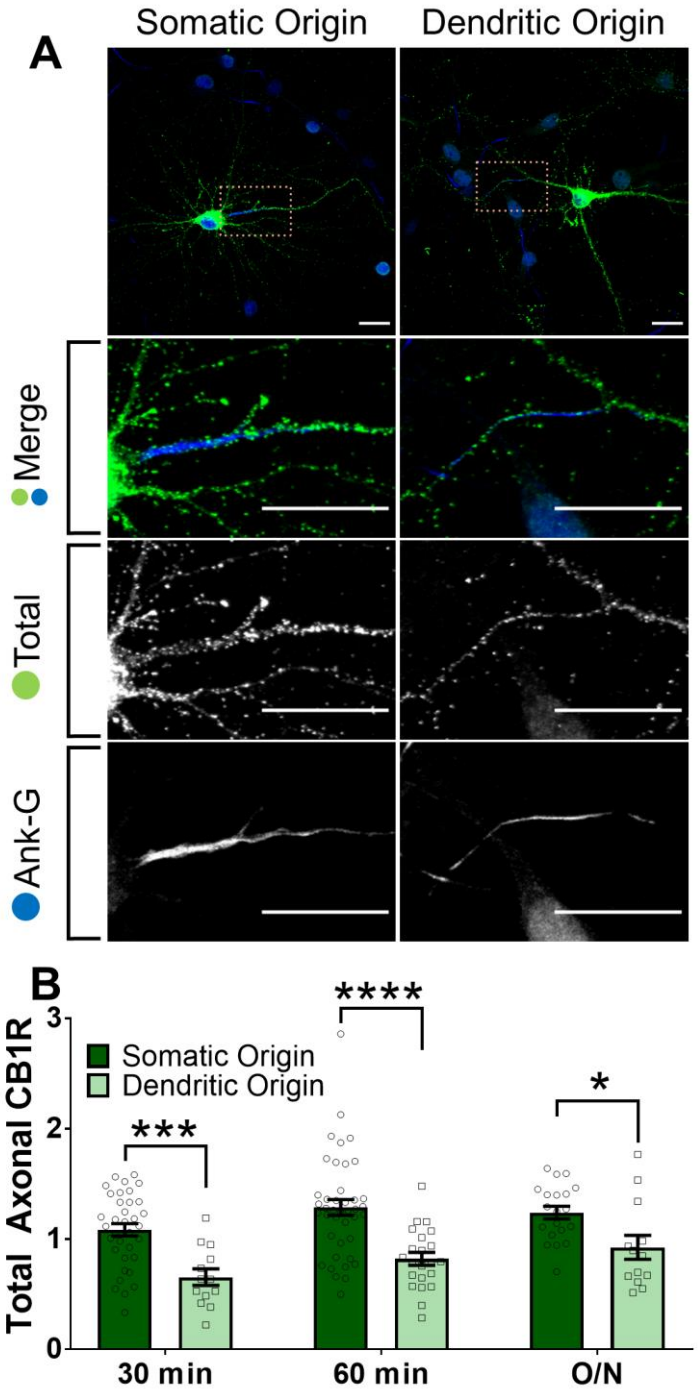

Figure 3-14 Less SBP-EGFP-CB1R is delivered to axons of dendritic origin than axons of somatic origin.

The trafficking of SBP-EGFP-CB1R following release with biotin was monitored after 0 (no biotin), 15, 25, 30, 35, 40, 45, 60, 90 min, and overnight (O/N; non-retained control) in DIV 13 hippocampal neurons.

(**A**) Representative images hippocampal neurons expressing RUSH SBP-EGFP-CB1R after 60 min of biotin-mediated release. Left panels show an axon of somatic origin and right panels show an axon of dendritic origin Upper panels for each condition show whole cell field of view and lower panels are enlargements of the axon initial segment (AIS) and from where it originates. Merge: green = total; blue = Ankyrin G. In all images the scale bar = 20 µm.

(**B**) Quantification of data shown in (**A**). Significantly less SBP-EGFP-CB1R entered the axon 30 and 60 min after biotin-mediated release. This difference was maintained in the unretained overnight control. Two-way ANOVA with Sidak's *post hoc* test. N = four to nine independent experiments, n = 13-41 neurons per condition. *p ≤ 0.05, ***p ≤ 0.001, ****p ≤ 0.0001.

3.4 DISCUSSION

3.4.1 A two-part model of CB1R polarity

Our results using RUSH time-resolved analysis show that CB1R surface polarity is initially established and maintained by two distinct but complementary mechanisms (see **Figure 3-15** for summary schematic). Firstly, I show the novel finding that the secretory pathway preferentially delivers CB1R to the axonal surface, with significantly less going to the dendritic surface. Secondly, by distinguishing between surface and surface+endocytosed receptors, the antibody feeding experiments show that newly delivered CB1R is preferentially retained/stabilised at the axonal membrane and internalised from the dendritic membrane. Previous literature proposes that this differential internalisation is due to the presence of agonist in the dendritic membrane and absence of agonist on axonal membrane (Leterrier et al., 2006; Ladarre and Lenkei, 2017), although a potential role for constitutive internalisation distinct to agonist-induced internalisation has also been proposed (McDonald et al., 2007a). Taken together, I propose that preferential delivery to the proximal segment of the axon and less rapid internalisation of axonally surface expressed CB1Rs are major contributors to the axonal surface polarisation of CB1R in hippocampal neurons.

3.4.2 Preferential axonal trafficking

The Lenkei group has previously reported that CB1R is delivered in a non-polarised manner to plasma membrane and is then transcytosed from somatodendritic endosomes to distal axon to generate a polarised surface distribution. In particular, they presented data from a BFA block showing that 2-4 hours after release from the BFA block, the majority of cells examine display either a non-polarised or even somatodendritically polarised CB1R surface distribution, with the axonal polarity only arising 24 hours post release once transcytosis has occurred (Leterrier et al., 2006).

While the data presented above do not exclude the possibility of transcytosis as a secondary mechanism to boost axonal polarisation, our results strongly suggest that axonal polarisation occurs much earlier than previously described by the Lenkei group due to preferential delivery of CB1R by the secretory pathway to axons. The discrepancy between my data and data from the Lenkei group may be the result of several differences in methods. The genetically targeted RUSH approach is a much more precise method than the BFA block which targets the

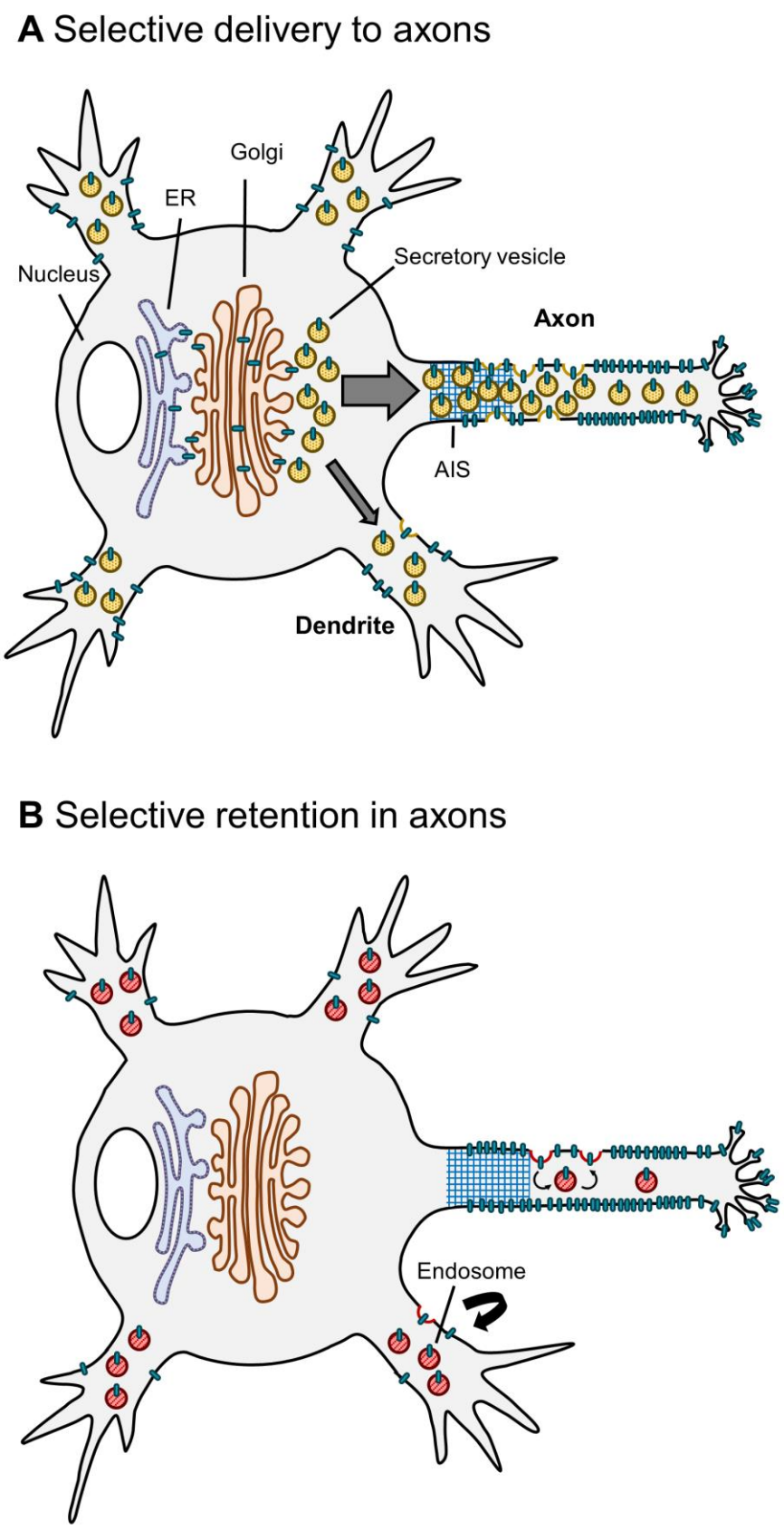

Figure 3-15 Schematic summarising the two-part model of CB1R polarity.

Polarised surface distribution of CB1R is established and maintained by two complementary mechanisms: (**A**) selective delivery of newly synthesized CB1R to the axon (or restricted delivery to dendrites) and (**B**) selective retention in axons and/or selective retrieval from dendrites.

secretory system as a whole. The difference in results from the targeted and whole block methods may hint at the possibility that the axonal preference of CB1R surface expression may require some kind of “chaperone” that needs to have passed the secretory pathway already, so that blocking the secretory pathway as a whole also interferes with this process, while the more specific CB1R retention does not. Furthermore, BFA has been found to affect several other trafficking pathways including endocytosis and recycling (Wood et al., 1991; Hunziker et al., 1991; Damke et al., 1991; Miller et al., 1992; Hunziker et al., 1992; Graham et al., 1993), which may present other confounding issues. Moreover, the Lenkei group used a C-terminally tagged CB1R, thus potentially occluding C-terminal motifs required for axonal sorting.

The microfluidic chamber experiments from the Lenkei group suggests that transcytosis is more important for getting CB1R to distal parts of axons (Simon et al., 2013). Since I have only examined the initiation of polarisation as measured by fluorescence at the first 50 μm, it would be intriguing to repeat the microfluidics transcytosis experiments in combination with my RUSH experiments in order to examine whether transcytosis or direct secretory pathway delivery accounts for the majority or the minority of distal axonal CB1R.

3.4.3 Possible mechanisms behind preferential delivery

The mechanism behind polarised membrane trafficking in neurons is a fundamental question and our data suggest a sorting mechanism at the level of the secretory pathway that preferentially targets CB1R to the axon. Since dendritic and axonal cargo are synthesized in the somatodendritic compartment, selective sorting to the correct domain is crucial. While several sorting signals and adaptors have been described for dendritic cargo, the mechanisms behind selective sorting to axons are less well known (Lasiecka and Winckler, 2011; Bentley and Banker, 2016). However, a recent study in *C. elegans* has suggested that sorting of cargos to axons or dendrites depends on binding to different types of clathrin-associated adaptor proteins (AP); axonal cargo bind to AP-3 whereas dendritic cargo bind to AP-1 (Li et al., 2016). Interestingly, AP-3 has been shown to bind CB1R and an siRNA knockdown of AP-3 caused the accumulation of CB1R at the dendritic surface of primary hippocampal neurons (Rozenfeld and Devi, 2008). The authors attribute this to the canonical role of AP-3 of trafficking from the TGN to the lysosome in the dendritic compartment, but also note that neuronal isoforms of AP-3 are associated with axonal cargo (Rozenfeld and Devi, 2008).

One possibility is that CB1R may be sorted by AP-3 to produce the preferential delivery to axons. Further studies using RUSH to examine the trafficking of CB1R in AP-3 KD hippocampal neurons may shed light on the exact role AP-3 plays in CB1R trafficking.

3.4.4 Trafficking and surface localisation within the axon

My RUSH experiments measured the transit through the secretory pathway and incorporation into, and passage through, the highly organised axon initial segment (AIS) that acts as a 'gate-keeper' for proteins entering the axonal compartment. Our data show that CB1R polarisation was initiated in the first 90 min since they were directly targeted to, and surface expressed within, proximal axonal regions.

Immunocytochemistry in brain sections using immunogold electron microscopy (Katona et al., 1999; Nyíri et al., 2005), or STORM super-resolution imaging (Dudok et al., 2015) detect CB1R predominantly at the presynaptic terminal, consistent with a disto-proximal gradient of expression at the axonal plasma membrane (Simon et al., 2013). Therefore, given the highly branched morphology of typical CB1R expressing neurons, correct axonal polarisation likely requires specific distal targeting mechanisms in addition to the processes we describe using time-resolved RUSH experiments.

CB1Rs are highly mobile and diffuse rapidly in the plasma membrane (Mikasova et al., 2008; Oddi et al., 2012), so the accumulation of surface CB1R I observe may be followed by lateral diffusion and 'capture' of surface CB1R at presynaptic sites, analogous to the diffusion and retention models proposed for AMPARs and $GABA_A$Rs at the postsynaptic membrane (Hastings and Man, 2018; Kneussel and Hausrat, 2016).

On the other hand, the observation that intracellular CB1R is present at least 100 µm along the axon before it appears at the surface (**Figure 3-12**) supports the concept of a rapid and direct trafficking of CB1R-containing secretory vesicles to more distal areas of the axon, although more detailed tracking of these secretory vesicles to presynaptic boutons would be required to confirm this. It would be interesting to RUSH SBP-EGFP-CB1R in hippocampal neurons grown in a microfluidic chamber, since the distance travelled along the axon would be slightly better controlled, to determine whether SBP-EGFP-CB1R reaches distal axonal areas internally in secretory vesicles or through surface diffusion.

Overall, we interpret our data to suggest that arrival at, and progression through, the AIS constitutes the initial phase of CB1R axonal polarisation. Once within the axonal compartment trafficking to more distal locations and to presynaptic sites is then mediated by additional mechanisms that probably include both intracellular transport and lateral diffusion and trapping.

3.4.5 Local synthesis and Golgi bypass

Recent reports suggest that synthesis and trafficking of transmembrane receptors can occur through other ways than the canonical somatic rER-to-Golgi stack pathway. Transmembrane proteins can be locally synthesized in dendrites (Valenzuela and Perez, 2015) and even perhaps in axons (González et al., 2016). A proportion of receptors can also bypass the Golgi as revealed by the fact that surface receptors can have immature glycosylation profiles (González et al., 2018; Hanus et al., 2016). Furthermore, it has been reported that Kv2.1 bypasses the Golgi only when proceeding to the axon – blocking the Golgi only prevented Kv2.1 from accumulating at the somatodendritic membrane, but not at the axonal membrane (Jensen et al., 2017). The RUSH assay allowed me to make some preliminary observations as to whether CB1R traffics via these non-canonical methods.

Firstly, in the ER retained condition (0 minutes), SBP-EGFP-CB1R was only located in the soma and some of the proximal dendrites, but not in the proximal segment of the axons (**Figure 3-8 A, C**). This suggests that CB1R is not locally translated in axons. However, it is possible that local translation occurs at more distal areas of the axon or at such low levels that it could not be detected. Distal areas of the axons were not examined here since, due to the way the experiment was set up, it was impossible to trace axons much further than the axon initial segment (usually around 50 μm) when there was no marker in them.

Secondly, in some very preliminary and unquantified experiments, I added the Golgi transport blocker GCA concurrent to biotin addition for 60 minutes. Unlike the 60 minute control, SBP-EGFP-CB1R did not enter the axon or go to the surface of the dendrites in the presence of GCA (**Figure 3-13**), strongly suggesting that CB1R does not bypass the Golgi.

3.4.6 Dendritic and somatic origin axons

Previous experiments in the lab suggested that significantly less SBP-EGFP-GluK2 entered axons of dendritic origin (DO) than those of somatic origin (SO). Whether this observation was specific to GluK2 or a generic trend in trafficking was unclear. My observation that SBP-EGFP-CB1R also traffics less to DO axons than SO axons suggests that this may be a generic property of DO axons.

This observation makes intuitive sense – CB1R released from the somatic Golgi presumably has to travel farther to reach DO axons since it must traverse a section of the Golgi. Therefore, it might not be that less cargo enters DO axons, but it just enters it more slowly. However, I also found less SBP-EGFP-CB1R in DO axons compared to SO axons in the unretained control (O/N).

Little is known about the properties of DO axons or how/why there are generated, apart from the fact that the dendrite carrying the DO axon has preferential effect on whether the axon generates an action potential or not. Our data, suggest that DO axons may also have different intrinsic properties than SO axons.

3.5 CONCLUSION

Overall, this chapter shows provides novel molecular insights into the pattern of forward trafficking of CB1R, an axonally polarised cargo, using RUSH.

Chapter 4 – Helix 9 (*H9*) regulates trafficking of CB1R

4.1 Aims

- To determine whether the C-terminus of CB1R plays a role (1) selective delivery and/or (2) selective retention of axonal CB1R.
- To determine the role of the C-terminal motif Helix 9 (*H9*) in CB1R trafficking and surface polarisation.

4.2 Introduction

Having determined that CB1R surface polarisation is established and generated by (1) selective delivery of newly synthesized CB1R to the axon and (2) selective retention of CB1R at the axonal membrane and selective retrieval from the dendritic membrane, I next sought to determine by what mechanisms these two pathways might occur.

4.2.1 The C-terminus of CB1R (ctCB1R)

Surprisingly, a direct role for the 73-residue intracellular C-terminal domain of CB1R (ctCB1R) in axonal/somatodendritic trafficking and/or polarised surface expression has not been identified (**Figure 4-1**). It has, however, been reported that two serine residues (S426, S430) within ctCB1R are required for receptor desensitization and β-arrestin-mediated agonist-induced internalization (Daigle et al., 2008a; Mackie, 2008; Hsieh et al., 2002; Jin et al., 1999). Furthermore, two ctCB1R interacting proteins, SGIP1 and CRIP1a have been implicated in CB1R surface stability (Hájková et al., 2016; Smith et al., 2015; Blume et al., 2017; Mascia et al., 2017). Moreover, CB1R palmitoylation at C416 is required for agonist-induced internalisation (Oddi et al., 2012, 2017, 2018).

ctCB1 contains two amphipathic putative helical domains: Helix 8 (*H8*) and Helix 9 (*H9*; (Ahn et al., 2009b)). *H8* is common to many GPCRs and has been proposed to play a role in ER assembly and/or exit during biosynthesis (Stadel et al., 2011; Ahn et al., 2010). The role of the 21-residue *H9* motif is unknown, although analogous regions have been reported to act as a $G_{\alpha q}$-binding site in both squid rhodopsin (Murakami and Kouyama, 2008) and bradykinin receptors (Piserchio et al., 2005).

In this chapter, I examine the role of ctCB1R in general, and *H9* in particular, on the trafficking and surface expression of CB1R.

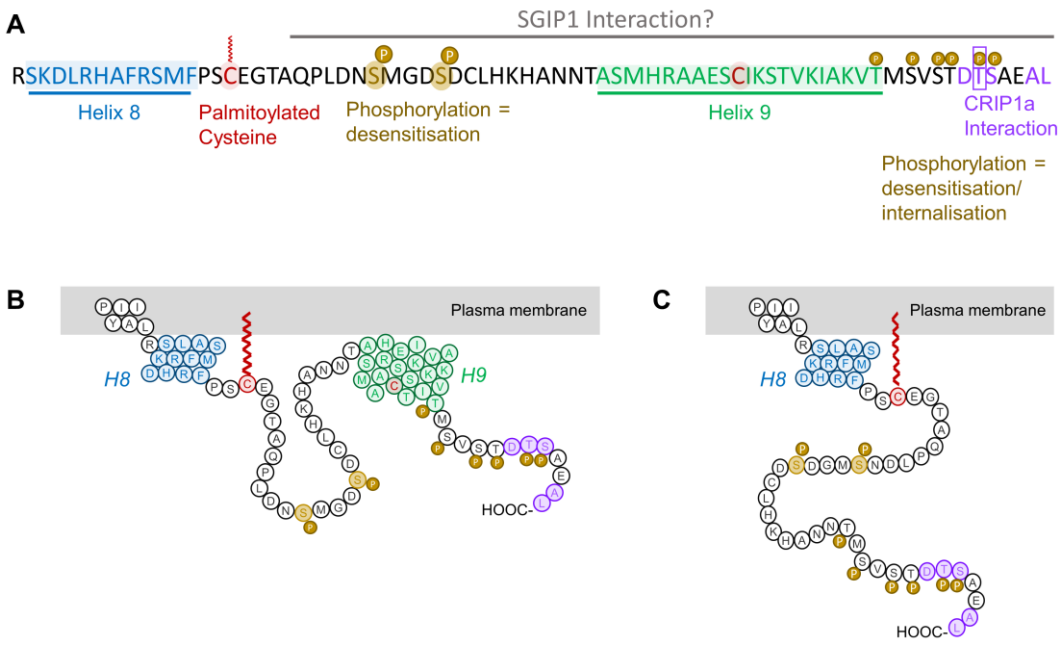

Figure 4-1 The C-terminus of rat CB1R.

(**A**) Amino acid sequence of the C-terminus of rat CB1R highlighting helical motifs (Helix 8 and Helix 9) predicted from NMR spectroscopy and computational modelling. The proposed interaction domains of CRIP1a, SGIP1, and β-arrestin1/2, the palmitoylated cysteine residue involved in membrane association and agonist-induced internalisation, and the two serine residues which are phosphorylated during desensitisation, are also indicated. A potentially post-translationally modified cysteine in *H9* is highlighted.

(**B**) Schematic diagram of ctCB1R^{WT} and (**C**) ctCB1R$^{\Delta H9}$.

4.2.2 Using CD4 chimeras to identify polarising localisation motifs

CD4 and CD8 are simple single transmembrane glycoproteins found on the surface of T cells. Because of their simplicity, the abundance of N-terminal antibodies against them, and the fact that they lack of any intrinsic localisation signals in neurons and are therefore surface expressed in a non-polarised manner, they have been used in several studies to investigate localisation motifs of polarised transmembrane proteins (see (Gu et al., 2003; Fache et al., 2004; Yap et al., 2008a; Biermann et al., 2010; Johnson et al., 2018; Frazier et al., 1998; Garrido et al., 2001; Bel et al., 2009; Sampo et al., 2003) for examples). In these studies, the putative localisation motif of interest is fused to the C-terminus of CD4/8 and the localisation of this chimera is compared to CD4/8 alone. This allows the putative localisation motif to be examined in isolation from any other localisation motifs mechanisms located in the transmembrane protein of interest.

I therefore used this strategy to examine the role that ctCB1R and *H9* play in determining the polarised distribution of CB1R using CD4-ctCB1R chimeras.

4.2.3 Agonist-induced internalisation and CB1R polarity

The Lenkei group propose that CB1R surface polarity is due to differences in endocannabinoid levels between the somatodendritic and axonal compartments (**Figure 1-15**; (Ladarre and Lenkei, 2017)). This difference is generated because the 2-AG synthetic enzyme, DAGLα, is located in the somatondendritic compartment, whereas the degradative enzyme, MAGL, is located in the axonal compartment (Ladarre et al., 2015). Therefore, they suggest that any CB1R that reaches the somatodendritic membrane is immediately activated by the tonal presence 2-AG specifically in the somatodendritic membrane and therefore undergoes agonist-induced internalisation (Leterrier et al., 2006; Simon et al., 2013). This model is supported by the fact that, in their hands, application of the antagonist/inverse agonist AM281 causes an increase in surface localisation of somatodendritic CB1R (Leterrier et al., 2006).

4.3 RESULTS

4.3.1 The C-terminus of CB1R, particularly Helix 9 (H9), contributes to CB1R surface polarisation.

To test the role of the C-terminal domain of CB1R (ctCB1R) in CB1R polarisation I initially used CD4, a single-pass membrane protein that has no intrinsic localisation signals and is normally surface expressed in a non-polarised manner (Garrido et al., 2001; Fache et al., 2004). I expressed CD4 alone or chimeras of CD4 fused to either ctCB1R^{WT} (**Figure 4-1 B**; **Figure 4-2 A**) or a ctCB1R lacking the *H9* domain (ctCB1R$^{\Delta H9}$; **Figure 4-1 C**; **Figure 4-2 A**). I expressed these in hippocampal neurons and examined surface and total expression distributions by immunostaining with an N-terminal CD4 antibody (clone OKT4; **Figure 4-2 B-E**). In this way, I could examine the contribution of the C-terminus as a whole, and *H9* in particular, to the polarised distribution of CB1R in the absence of any other potential localisation signals on intracellular loops and, importantly, without the effect that agonist activation may have on trafficking.

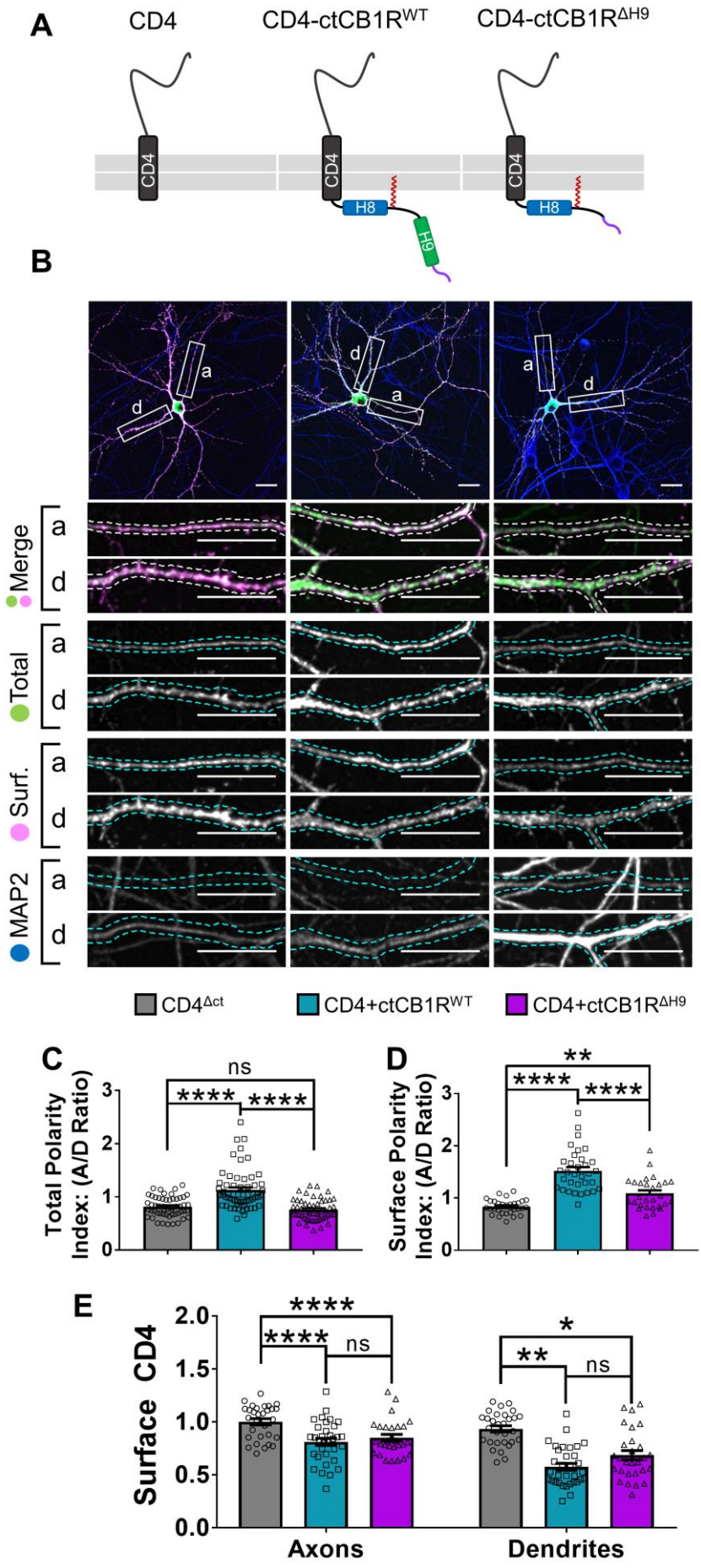
A
CD4
CD4-ctCB1R^WT
CD4-ctCB1R^ΔH9
CD4
H8
H9
B
a
d
Merge
Total
Surf.
MAP2
CD4^Δct
CD4+ctCB1R^WT
CD4+ctCB1R^ΔH9
C
Total Polarity Index: (A/D Ratio)
ns
****
****
D
Surface Polarity Index: (A/D Ratio)
**
****
****
E
Surface CD4
****
****
ns
*
**
ns
Axons
Dendrites

Figure 4-2 The C-terminal domain of CB1R, especially the Helix 9 motif, plays a role in axonal polarisation.

(**A**) Schematic of the CD4-ctCB1R chimeric proteins used.

(**B**) Representative confocal images of hippocampal neurons showing the distribution of expressed CD4 (left), CD4-ctCB1R^{WT} (middle), or CD4-ctCB1R$^{\Delta H9}$ (right). Upper panels for each condition show a whole cell field of view and lower panels are enlargements of axonal (a) and dendritic (d) ROIs. Green = total; magenta = surface; blue = dendrite marker (MAP2). Merge: surface to total seen as white. Scale bar = 20 µm.

(**C**) Quantification of data represented in (**B**) presented as the total polarity index (A/D ratio). Total CD4-ctCB1R^{WT} strongly favoured the axonal compartment compared to CD4 alone. CD4-ctCB1R$^{\Delta H9}$ showed no bias towards the axonal compartment and was identical to CD4 alone. Kruskal-Wallis test with Dunn's *post hoc* test (WT was strongly non-parametric). N = six independent experiments; n = 52–59 neurons per condition. Pooled with data from **Figure 4-3**.

(**D**) Quantification of data represented in (**B**) presented as the surface polarity index (A/D ratio). CD4-ctCB1R^{WT} strongly favoured the axonal compartment compared to CD4 alone. CD4-ctCB1R$^{\Delta H9}$ favoured the axonal compartment significantly less than CD4-ctCB1R^{WT}. One-way ANOVA with Tukey's *post hoc* test. N = three independent experiments; n = 28–33 neurons per condition.

(**E**) Quantification of data represented in (**B**) presented normalised surface-to-total ratios (CD4 Axons = 1) for axons and dendrites. CD4-ctCB1R^{WT} and CD4-ctCB1R$^{\Delta H9}$ displayed a significantly more internal distribution compared to CD4 alone. This may be due to either increased internalisation or decreased forward trafficking. Two-way ANOVA with Tukey's *post hoc* test. N = three independent experiments; n = 28–33 neurons per condition.

Firstly, I examined the total distribution of the CD4 chimeras (the total polarity index = (mean fluorescence of axon)/(average mean fluorescence of 3-4 dendrites)). Intriguingly, CD4-ctCB1R^{WT} was markedly more axonally polarised than CD4 alone (**Figure 4-2 B**), suggesting that ctCB1R, despite its lack of defined canonical localisation signals, contains some motif(s) that direct axonal sorting. Indeed, the CD4-ctCB1R$^{\Delta H9}$ chimera did not show a polarised total distribution (**Figure 4-2 B**), suggesting that *H9* constitutes that sorting motif.

Analysis of the surface polarity index (A/D ratio) revealed that CD4-ctCB1R^{WT} was also markedly more axonally surface polarised than CD4 alone (**Figure 4-2 C**), further indicating that ctCB1R may play a role in polarisation. Nevertheless, this polarisation was not complete and there was still CD4-ctCB1R^{WT} detectable on the dendritic membrane. This suggests that either other localisation motifs or agonist-induced internalisation (Leterrier et al., 2006) is required for full polarisation.

However, in agreement with the total polarisation results, the degree of surface polarisation was significantly lower for CD4-ctCB1R$^{\Delta H9}$ than CD4-ctCB1R^{WT}. Intriguingly, however, CD4-ctCB1R$^{\Delta H9}$ was still significantly more axonally surface polarised than CD4 alone (**Figure 4-2 C**).

Compared to CD4, both CD4-ctCB1R^{WT} and CD4-ctCB1R$^{\Delta H9}$ were less surface expressed (surface-to-total ratio) to equal degrees (**Figure 4-2 D**). Whether this

more internal distribution could be due to increased internalisation or less forward trafficking (the CD4 control does not have a C-terminus at all, meaning that it is possible it traffics very rapidly to the surface) cannot be distinguished in this experiment.

Therefore, I next analysed constitutive endocytosis of CD4-ctCB1R^{WT} and CD4-ctCB1R$^{\Delta H9}$ by 'feeding' with anti-CD4 antibody for 2 hours, followed by a harsh stripping of surface antibody using two washes in 0.5 M NaCl and 0.2 M acetic acid at pH 3.5 (**Figure 4-3 A-B**). My data indicate that *H9* does not determine surface polarity by driving differential constitutive endocytosis from either the dendritic or axonal membrane since there was no difference between the internalisation of CD4-ctCB1R^{WT} or CD4-ctCB1R$^{\Delta H9}$. However, both CD4-ctCB1R^{WT} and CD4-ctCB1R$^{\Delta H9}$ were significantly more internalised than CD4 alone in dendrites, but not in axons (**Figure 4-3**).

These results suggest that a C-terminal domain other than *H9* promotes constitutive, but reportedly not activity-dependent (McDonald et al., 2007a) internalisation in dendrites but not in axons. Moreover, it provides an explanation for why CD4-ctCB1R$^{\Delta H9}$ surface polarity index does not return to the same level of CD4 like the total polarity index – the increased internalisation in dendrites increases the surface polarity index.

Importantly, however, because this increase in internalisation in identical between CD4-ctCB1R^{WT} and ctCB1R$^{\Delta H9}$, this endocytic mechanism does not account for the failure of CD4-ctCB1R$^{\Delta H9}$ to surface polarise to the level of CD4-ctCB1R^{WT}.

Since CD4-ctCB1R^{WT} and CD4-ctCB1R$^{\Delta H9}$ chimeras cannot bind agonist, these results are consistent with ctCB1R contributing to constitutive polarisation via a mechanism distinct from the proposed continuous activation of CB1R by the presence of the endogenous agonist 2-AG in the dendritic membrane (Ladarre and Lenkei, 2017). Thus, our data demonstrate that ctCB1R, particularly *H9*, contributes to the constitutive preferential delivery of CB1R to the axonal membrane.

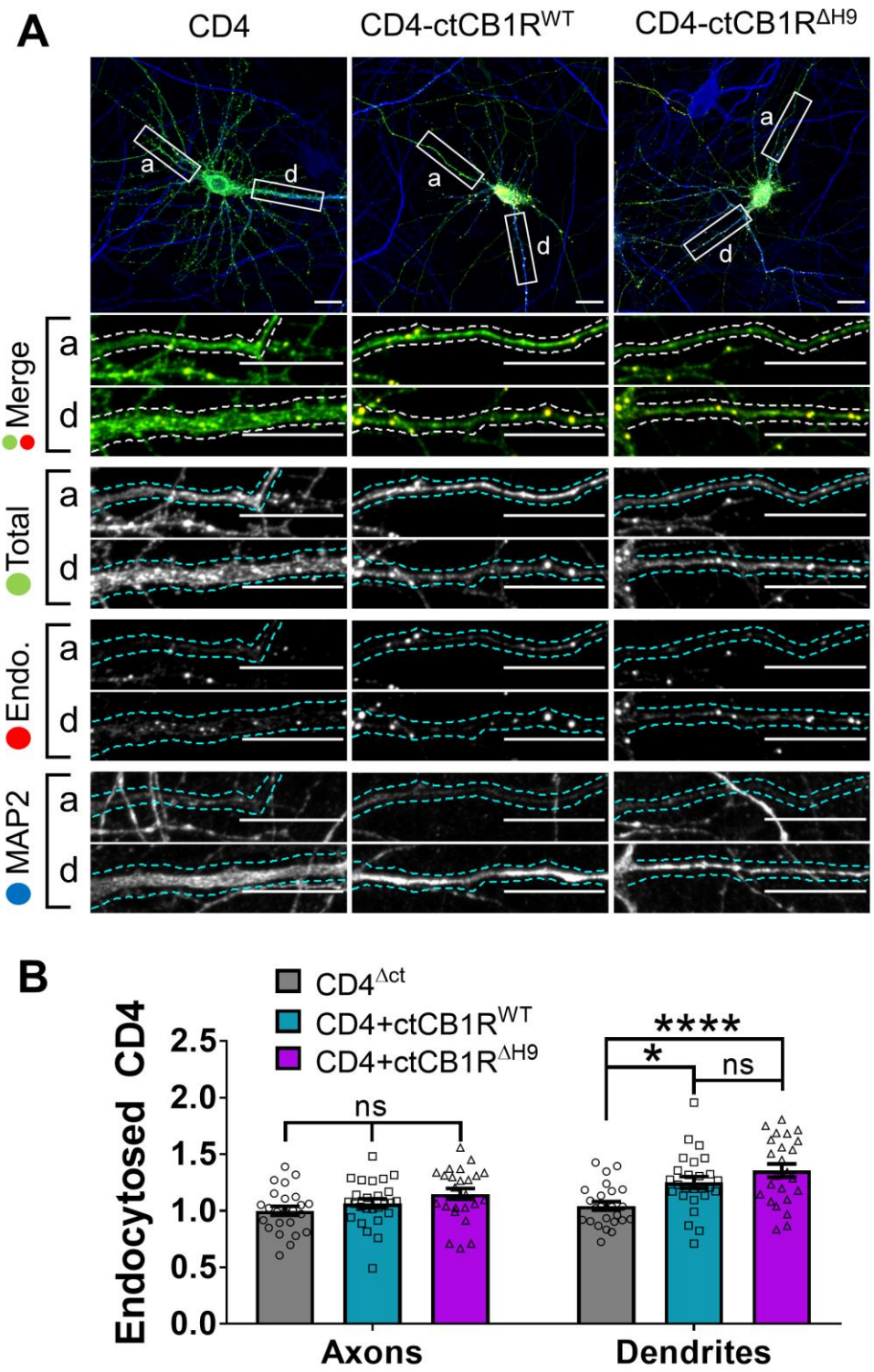

Figure 4-3 the C-terminal domain of CB1R plays a role in constitutive internalisation in dendrites independent of *H9.*

(**A**) Representative confocal images of DIV 14 primary hippocampal neurons expressing CD4$^{\Delta CT}$ (left), CD4-ctCB1R^{WT} (middle), or CD4-ctCB1R$^{\Delta H9}$ (right). Neurons were subjected to 2 hr of antibody feeding followed by stripping of surface antibody to reveal the endocytosed pool of receptors. Upper panels for each condition show a whole cell field of view and lower panels are enlargements of axonal (a) and dendritic (d) ROIs. Green = total; red = endocytosed; blue = dendritic marker (MAP2). Merge: endocytosed to total seen as yellow. Scale bar = 20 µm.

(**B**) Quantification of data presented in (**A**). Both CD4-ctCB1R^{WT} and -ctCB1R$^{\Delta H9}$ were significantly more internalised in dendrites, but not in axons, than CD4 alone. N = three independent experiments; n = 24–26 neurons per condition. Two-way ANOVA with Sidak's *post hoc* test.

4.3.2 *H9* plays a role in the forward trafficking of CB1R

The CD4 chimera experiments indicate that the *H9* motif is involved in CB1R trafficking and axonal polarity. Therefore, I next used the RUSH assay to compare the dynamics of forward trafficking of SBP-EGFP-CB1R^{WT} and SBP-EGFP-CB1R$^{\Delta H9}$ in a time-resolved manner (**Figure 4-4**).

4.3.2.1 H9 plays contributes to, but is not essential for, axonal entry of CB1R

Since CD4-ctCB1R$^{\Delta H9}$ displayed a dramatic loss of total polarity compared to CD4-ctCB1R^{WT} (**Figure 4-2**), I examined the dynamics of total SBP-EGFP-CB1R$^{\Delta H9}$ in to axons (**Figure 4-5 A**). SBP-EGFP-CB1R$^{\Delta H9}$ entered axons at a slower rate than SBP-EGFP-CB1R^{WT} – there was significantly less axonal expression after 30 minutes and 60 minutes of biotin-mediated release (**Figure 4-5 A**). However, by 90 minutes, the level of axonal CB1R was the same between the WT and mutant CB1R. These data suggest that while *H9* may be involved in total delivery to axons, there other mechanisms outside of ctCB1R that can compensate when *H9* is removed.

It is important to note that there was no difference in total dendritic expression between WT and ΔH9 or between the four timepoints (**Figure 4-5 B**). This control indicates that the expression of the RUSH construct was the same for all conditions. Because total dendritic expression did not vary over time or mutation, every measure (including total axonal expression) was normalised to the dendritic total to control for variation in expression between neurons within conditions.

4.3.2.2 H9 restricts delivery of CB1R to the dendritic membrane

I next compared the delivery of SBP-EGFP-CB1R^{WT} to that of SBP-EGFP-CB1R$^{\Delta H9}$ to the surface of axons and dendrites 0, 30, 60, and 90 min after biotin-mediated release from the ER. As explained in Chapter 3, this surface+endocytosed parameter measures all the CB1R that had been surface expressed, regardless of whether it has subsequently been internalised.

There was no difference in the amount of CB1R delivered to the surface of axons between SBP-EGFP-CB1R$^{\Delta H9}$ and SBP-EGFP-CB1R^{WT} (**Figure 4-5 C**).

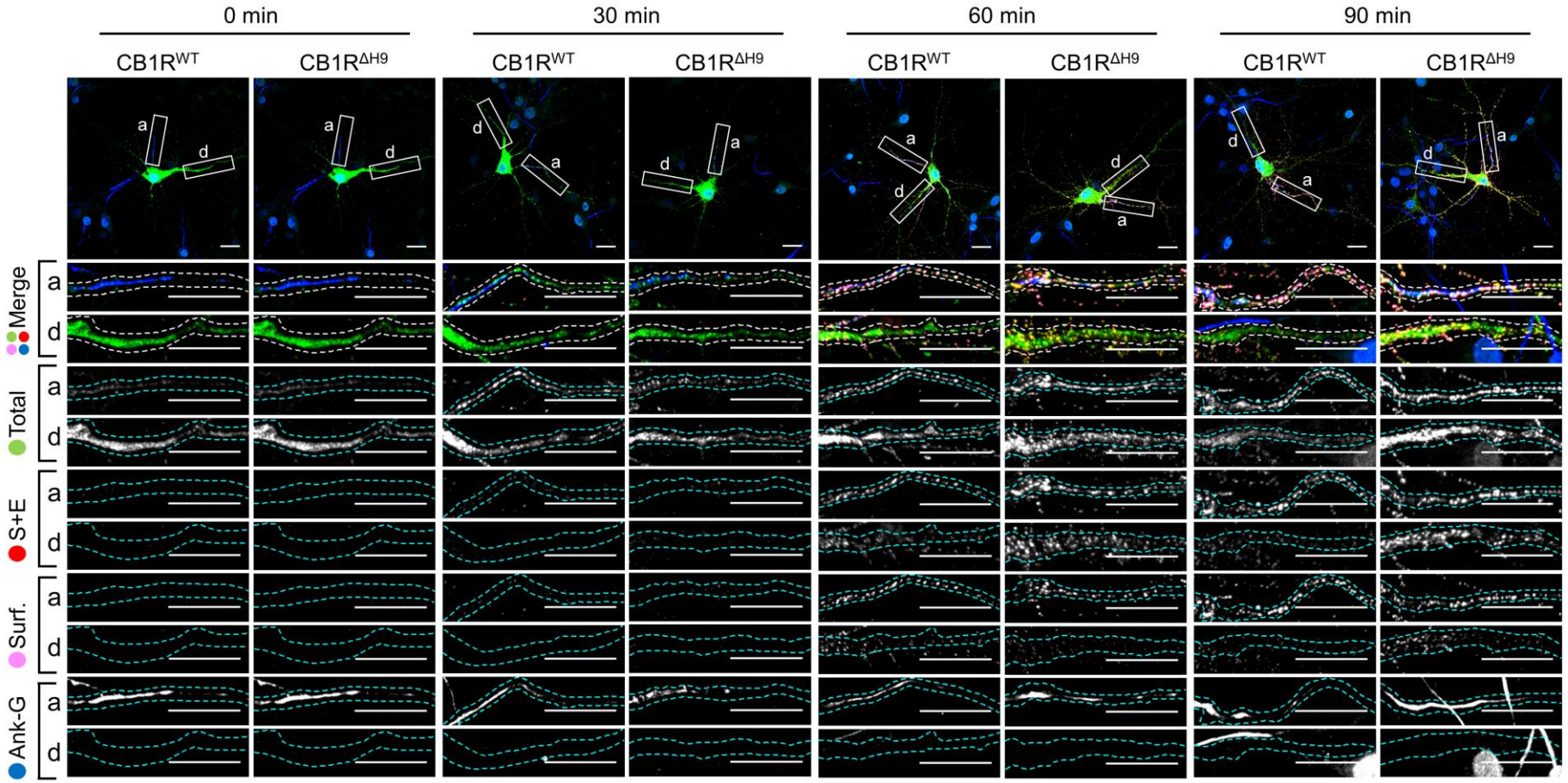

Figure 4-4 The trafficking of SBP-EGFP-CB1R^{WT} was compared to that of SBP-EGFP-CB1R$^{\Delta H9}$ in a time resolved manner using RUSH.

Representative confocal images of hippocampal neurons expressing SBP-EGFP-CB1R^{WT} or SBP-EGFP-CB1R$^{\Delta H9}$ 0 (no biotin), 30, 60, and 90 min after release with biotin. Upper panels for each condition show whole cell field of view and lower panels are enlargements of axonal (a) and dendritic (d) ROIs. Green = total; red = surface + endocytosed; magenta = surface; blue = axon marker (Ankyrin-G). Merge: surface to total seen as white; endocytosed to total seen as yellow. Scale bar = 20 µm.

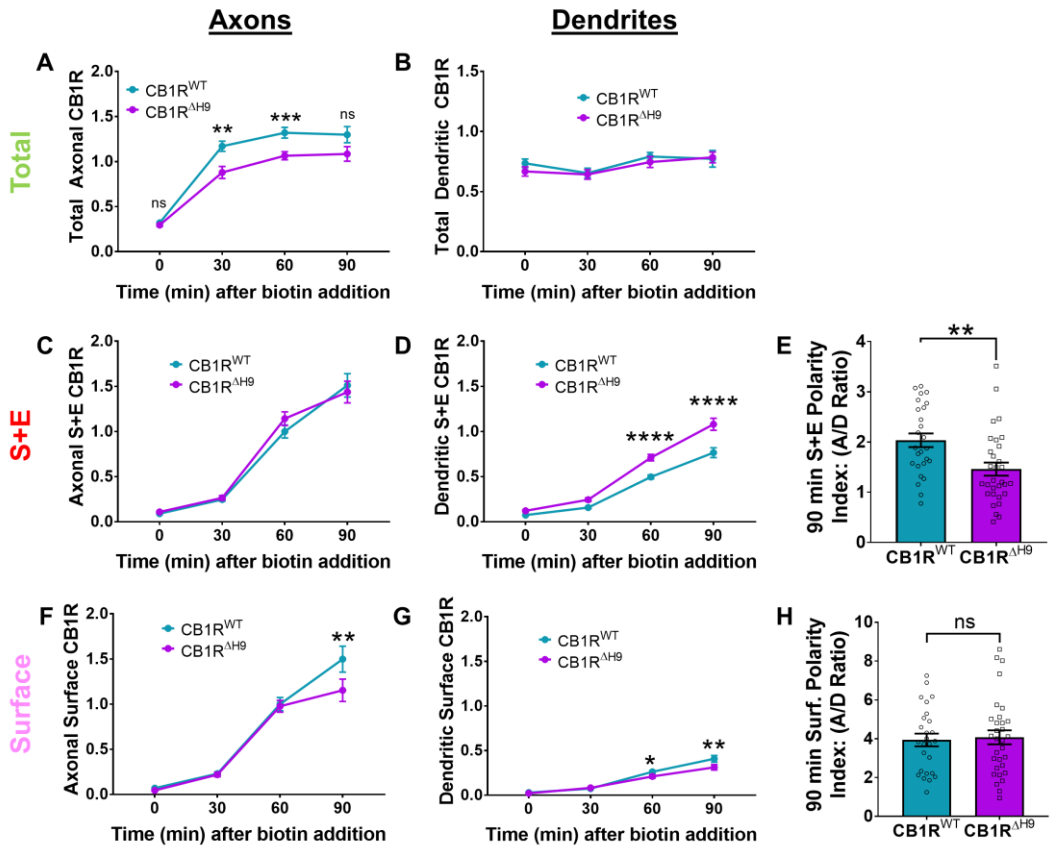

Figure 4-5 *H9* both restricts delivery of CB1R to the dendritic membrane and plays a role in surface retention of CB1R.

Quantification of data shown in **Figure 4-4**. **A-D, F-G**: Two-way ANOVA with Sidak's *post hoc* test. N = three to seven independent experiments, n = 26–63 neurons per condition. **E, H**: N = four independent experiments, n = 26–31 neurons per condition. Unpaired t-test.

(**A**) Time-resolved analysis of total axonal CB1R fluorescence (normalised to total dendrite fluorescence) indicates that SBP-EGFP-CB1R$^{\Delta H9}$ entered the axon at a slower rate than SBP-EGFP-CB1R^{WT}. However, by 90 min there was no significant difference in axonal total fluorescence between WT and ΔH9.

(**B**) Quantification of the total dendritic fluorescence confirms equal expression levels of SBP-EGFP-CB1R between timepoints and between WT vs. ΔH9.

(**C**) Time-resolved analysis of surface+endocytosed receptors shows no difference between SBP-EGFP-CB1R^{WT} and SBP-EGFP-CB1R$^{\Delta H9}$ in reaching the surface of the axon.

(**D**) Time-resolved analysis of surface+endocytosed receptors shows significantly more SBP-EGFP-CB1R$^{\Delta H9}$ reached the surface of dendrites than SBP-EGFP-CB1R^{WT}, indicating that *H9* may play a role in restricting delivery to the dendritic surface.

(**E**) Analysis of surface+endocytosed polarity index (A/D) demonstrates a defect in polarised delivery of SBP-EGFP-CB1R$^{\Delta H9}$ compared to SBP-EGFP-CB1R^{WT}.

(**F**) Time-resolved analysis of surface receptors shows significantly less SBP-EGFP-CB1R$^{\Delta H9}$ than SBP-EGFP-CB1RWT on the surface of axons 90 min after release, most likely due to increased endocytosis of the ΔH9 mutant.

(**G**) Time-resolved analysis of surface receptors shows significantly less SBP-EGFP-CB1R$^{\Delta H9}$ than SBP-EGFP-CB1R^{WT} on the surface of dendrites 60 and 90 min after release, most likely due to increased endocytosis of the ΔH9 mutant.

(**H**) Analysis of surface polarity index (A/D) revealed no difference between SBP-EGFP-CB1R^{WT} and SBP-EGFP-CB1R$^{\Delta H9}$.

Interestingly, however, significantly more SBP-EGFP-CB1R$^{\Delta H9}$ than SBP-EGFP-CB1R^{WT} reached the surface of dendrites after 60 and 90 minutes of ER release (**Figure 4-5 D**). This altered profile of delivery resulted in a significant difference in the surface+endocytosed polarity index after 90 min (the latest timepoint measured; **Figure 4-5 E**) similar to the difference in surface polarity observed in the CD4 chimera experiment (**Figure 4-2**). These data indicate that *H9* plays a role in restricting secretory pathway delivery of CB1R to the dendritic membrane.

4.3.2.3 H9 plays a role in the surface retention of CB1R

Surprisingly, in contrast to the total amount of CB1R that had been surface expressed during the time course (surface+endocytosed; **Figure 4-5 E**), the polarity of the amount of CB1R on that remained on the cell surface 90 min after biotin-mediated release was identical for SBP-EGFP-CB1R^{WT} and SBP-EGFP-CB1R$^{\Delta H9}$ (surface; **Figure 4-5 H**). Closer analysis dissecting what occurs at axons vs. dendrites revealed identical levels of axonal surface expression of both SBP-EGFP-CB1R^{WT} and SBP-EGFP-CB1R$^{\Delta H9}$ 60 min after release from the ER. However, at 90 min there is significantly less surface expression of Δ*H9* mutant (**Figure 4-5 F**) suggesting that, although similar amounts of SBP-EGFP-CB1R^{WT} and SBP-EGFP-CB1R$^{\Delta H9}$ reach the surface, surface expression of SBP-EGFP-CB1R$^{\Delta H9}$ is less stable than that of the wild-type. Furthermore, in dendrites, the increased delivery and surface trafficking of the Δ*H9* mutant is counteracted by the fact that less is retained at the surface 60 min and 90 min after ER release (**Figure 4-5 G**).

Taken together these results suggest that, separate from its role in restricting delivery to the dendritic membrane, *H9* also plays a role in membrane stability and retention at both axons and dendrites.

The lack of effect of deleting *H9* on surface CB1R polarity is inconsistent with the CD4 chimera data. This may indicate that other regions of CB1R may play a role in its localisation. It also suggests the possibility that agonist-induced activation may be affected by *H9* deletion.

4.3.3 *H9* stabilises CB1R at the surface

To investigate the role of *H9* in membrane stability and surface polarity, I next compared surface expression of EGFP-CB1R^{WT} and EGFP-CB1R$^{\Delta H9}$ in axons and dendrites at steady-state. To do this, I cloned the entire SP^{II-2}-SBP-EGFP-

CB1R$^{WT/\Delta H9}$ cassette out of the RUSH construct (**Figure 3-4**) and into pcDNA3.1, transfected the constructs into primary hippocampal neurons, and surface stained with anti-GFP antibody after 48 hours (**Figure 4-6 A**).

EGFP-CB1R$^{\Delta H9}$ displayed lower levels of surface expression in both axons and dendrites (**Figure 4-6 B**) resulting in no difference in either surface polarity (**Figure 4-6 C**) or total polarity (**Figure 4-6 D**) compared to EGFP-CB1R^{WT}.

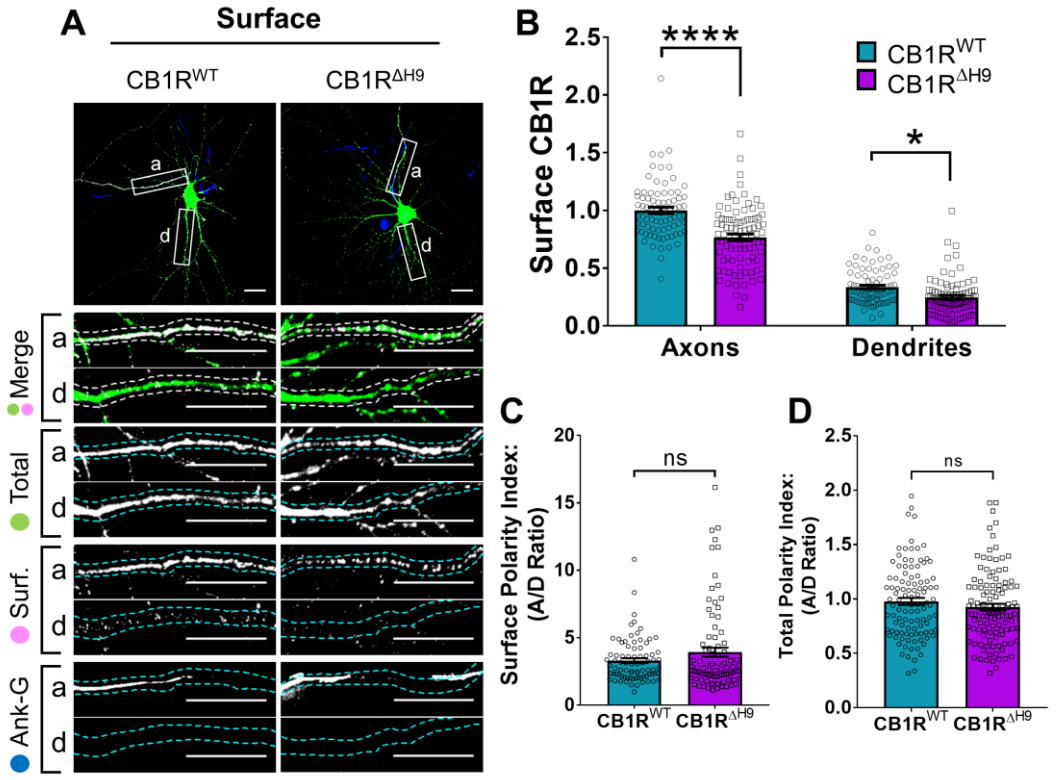

Figure 4-6 *H9* stabilises CB1R at the surface.

(**A**) Representative confocal images of surface stained DIV 14 hippocampal neurons expressing EGFP-CB1R^{WT} or EGFP-CB1R$^{\Delta H9}$. Green = total; magenta = surface; blue = axon marker (Ankyrin-G). Merge: surface to total seen as white.

(**B**) Quantification of data shown in (**A**). Surface expression of EGFP-CB1R$^{\Delta H9}$ in both axons and dendrites was significantly reduced compared to EGFP-CB1R^{WT}. Two-way ANOVA with Tukey's *post hoc* test. N = ten independent experiments; n = 80–88 neurons per condition. Experiments include pooled results from Vehicle controls of **Figure 4-9** and **Figure 4-10**.

(**C**) Quantification of data shown in (**A**) presented as the surface polarity index. There was no difference in surface polarity between EGFP-CB1R^{WT} or EGFP-CB1R$^{\Delta H9}$. Mann-Whitney test. N = ten independent experiments; n = 80–88 neurons per condition. Experiments include pooled results from Vehicle controls of **Figure 4-9** and **Figure 4-10**.

(**D**) Quantification of data shown in (**A**) presented as the total polarity index. There was no difference in total polarity between EGFP-CB1R^{WT} or EGFP-CB1R$^{\Delta H9}$. Mann-Whitney test. N = fourteen independent experiments; n = 107-117 neurons per condition. Experiments include pooled data from Vehicle controls of **Figure 4-7**, **Figure 4-9**, and **Figure 4-10**.

4.3.4 *H9* prevents CB1R internalisation

To investigate the role of *H9* in membrane stability, I next compared internalisation of EGFP-CB1R^{WT} and EGFP-CB1R$^{\Delta H9}$ in axons and dendrites at steady-state (i.e. non-RUSH; **Figure 4-7**). To do this, I fed with anti-GFP antibody for 2 hours, then stripped off surface antibody to only label the endocytosed pools.

EGFP-CB1R$^{\Delta H9}$ displayed increased endocytosis in both axons and dendrites compared to EGFP-CB1R^{WT} (**Figure 4-7 A-B**), consistent with the decrease of surface expression observed in both axons and dendrites (**Figure 4-6**). These data suggest *H9* plays a role in stabilising CB1R at the surface of both axons and dendrites.

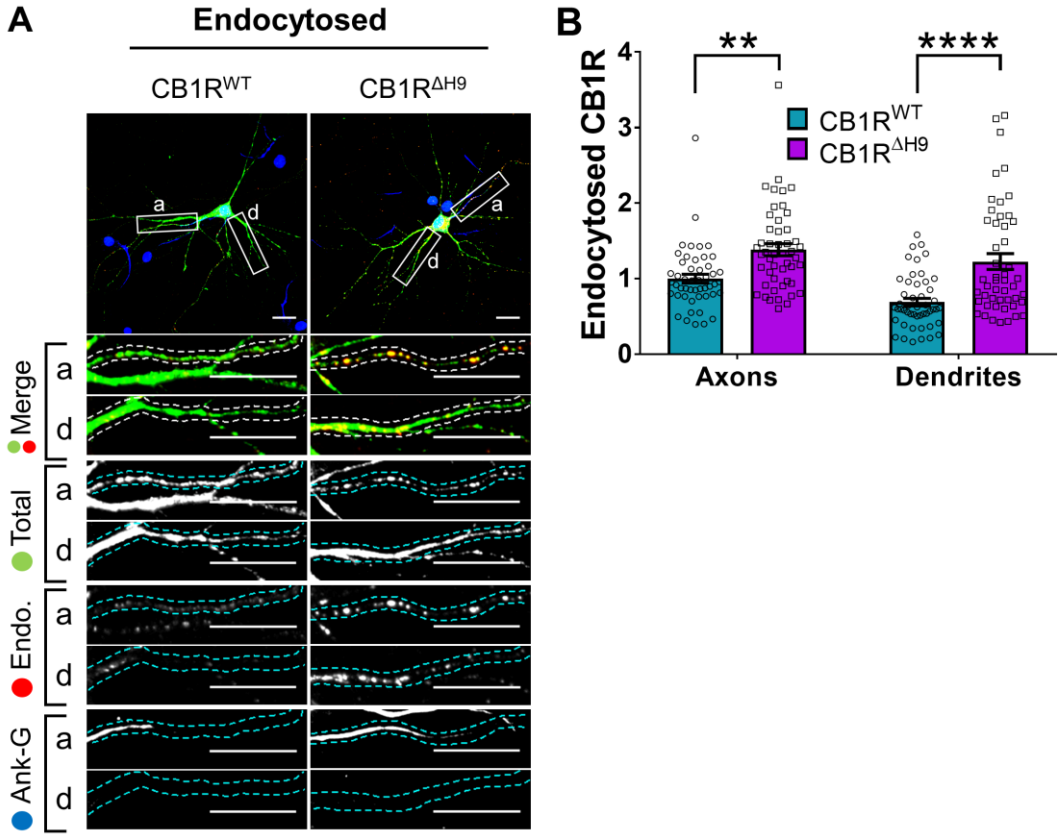

Figure 4-7 *H9* prevents internalisation in both axons and dendrites.

(**A**) Representative confocal images of DIV 14 primary hippocampal neurons expressing EGFP-CB1R^{WT} or EGFP-CB1R$^{\Delta H9}$. Neurons were subjected to 2 hr of antibody feeding with anti-GFP antibody followed by stripping off of surface antibody to reveal the endocytosed pool of receptors. Green = total; red = endocytosed; blue = axon marker (Ankyrin-G). Merge: endocytosed to total seen as yellow.

(**B**) Quantification of data shown in (**A**). Endocytosis of EGFP-CB1R$^{\Delta H9}$ is significantly increased compared to EGFP-CB1R^{WT} in both axons and dendrites. Two-way ANOVA with Tukey's *post hoc* test. N = seven independent experiments; n = 49 neurons per condition.

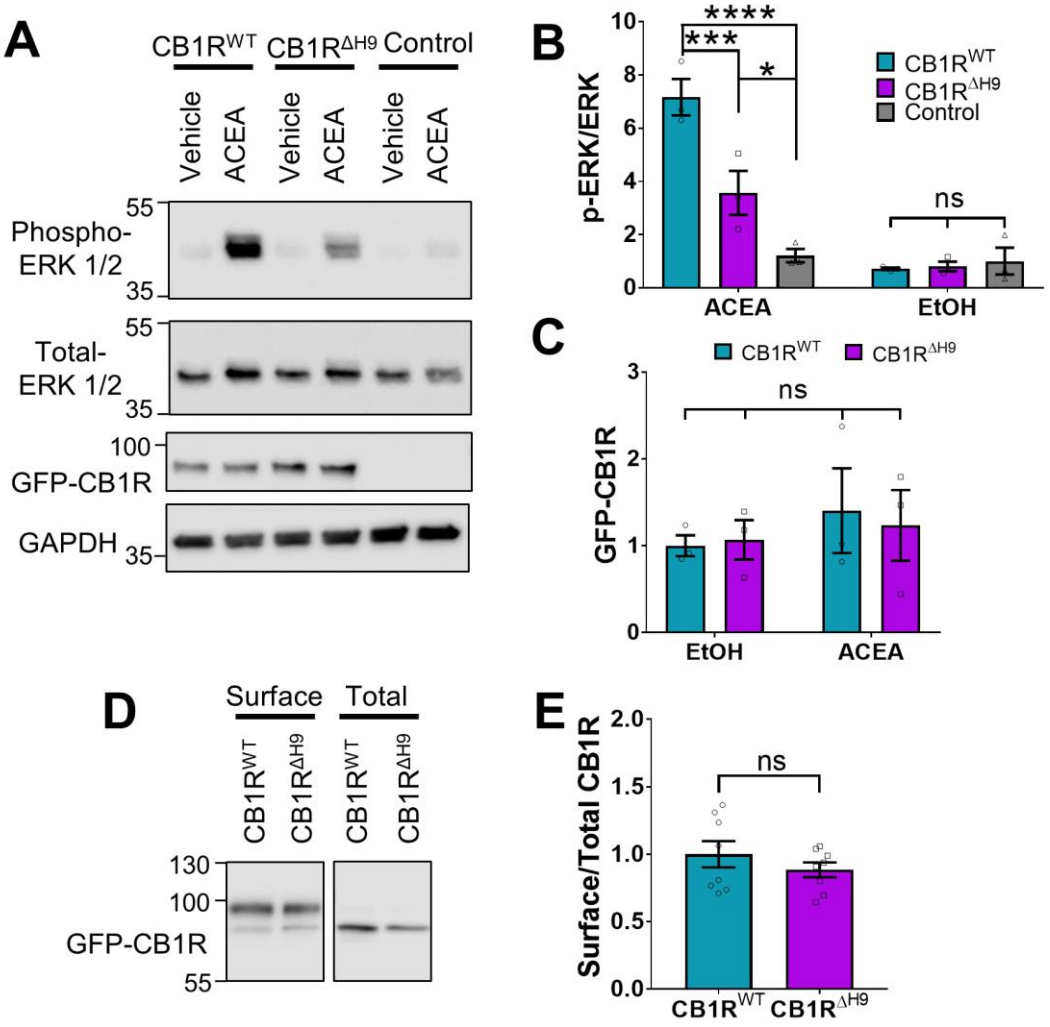

Figure 4-8 CB1R$^{\Delta H9}$ is less efficient at activating the downstream signalling pathways.

(**A**) Representative blots showing ERK1/2 phosphorylation in HEK293T cells expressing EGFP-CB1R^{WT} or EGFP-CB1R$^{\Delta H9}$ following vehicle (0.1% EtOH) or ACEA (1 μM) treatment for 5 min after overnight serum starvation.

(**B**) Quantification of data shown in (**A**). Following treatment with ACEA, ERK1/2 was significantly more phosphorylated in EGFP-CB1R^{WT}- and EGFP-CB1R$^{\Delta H9}$-transfected cells compared to untransfected cells. However, ERK1/2 activation was significantly reduced in EGFP-CB1R$^{\Delta H9}$-expressing cells compared to EGFP-CB1R^{WT}-expressing cells. There was no significant difference in ERK1/2 phosphorylation in vehicle-treated cells. Two-way ANOVA with Tukey's *post hoc* test. N = three independent experiments.

(**C**) Quantification of data shown in (**A**). EGFP-CB1R^{WT} and EGFP-CB1R$^{\Delta H9}$ expressed equally in HEK293T cells. Two-way ANOVA with Sidak's *post hoc* test. Three independent experiments.

(**D**) Representative immunoblots from surface biotinylation experiments showing surface and total fractions of EGFP-CB1R^{WT} and EGFP-CB1R$^{\Delta H9}$ in HEK293T cells.

(**E**) Quantification of data shown in (**D**). EGFP-CB1R^{WT} and EGFP-CB1R$^{\Delta H9}$ were surface expressed at equivalent levels in HEK293T cells. Unpaired t-test. Eight independent experiments.

4.3.5 CB1R$^{\Delta H9}$ is less efficient at activating downstream signalling pathways

Because CB1R surface expression and polarisation has been linked to its activity (Leterrier et al., 2006; Ladarre et al., 2015), I investigated if deleting *H9* affects CB1R downstream signalling pathways. Measuring the signalling efficiency of EGFP-CB1R$^{\Delta H9}$ in neurons would require the complete removal of endogenous CB1R. However, HEK293T do not express endogenous CB1R (Atwood et al., 2011) and are routinely used to measure activation of the ERK pathway. I expressed EGFP-CB1R^{WT}, EGFP-CB1R$^{\Delta H9}$, or empty vector in HEK293T cells and treated with vehicle (EtOH) or stimulated with the selective CB1R agonist ACEA (arachidonyl-2'-chloroethylamide) (Hillard et al., 1999) and blotted for ERK1/2 phosphorylation as a measure of downstream signalling of CB1R (Daigle et al., 2008a).

There was no significant difference in ERK1/2 phosphorylation in cells expressing EGFP-CB1R^{WT}, EGFP-CB1R$^{\Delta H9}$, or empty vector under basal conditions in the absence of ACEA. Upon ACEA stimulation, ERK1/2 phosphorylation increased significantly in both EGFP-CB1R^{WT} and -CB1R$^{\Delta H9}$ transfected cells (**Figure 4-8 A-C**). However, the level of ERK1/2 activation were significantly less in EGFP-CB1R$^{\Delta H9}$-transfected cells compared to EGFP-CB1R^{WT}-transfected cells expressing equivalent amounts of receptor (**Figure 4-8 A-C**).

Because the Δ*H9* mutant is more internalised than the wild-type in neurons, I examined whether the deficiency in ERK1/2 phosphorylation was due to a similarly reduced surface expression in HEK283T cells. However, EGFP-CB1R^{WT} and EGFP-CB1R$^{\Delta H9}$ were surface expressed at equivalent levels in HEK293T cells, as determined by surface biotinylation experiments (**Figure 4-8 D-E**), suggesting the Δ*H9* mutant is deficient in its ability to activate this downstream signalling pathway.

4.3.6 CB1R$^{\Delta H9}$ is more susceptible to agonist-induced internalisation

I next monitored ACEA-induced internalisation of EGFP-CB1R^{WT} and EGFP-CB1R$^{\Delta H9}$ in axons of hippocampal neurons (**Figure 4-9 A**). ACEA-induced internalisation of EGFP-CB1R$^{\Delta H9}$ was significantly greater than that observed for EGFP-CB1R^{WT} in axons (**Figure 4-9 B**). Taken together, these data indicate that CB1R$^{\Delta H9}$ is less stable at the axonal surface under basal conditions and that it is more susceptible to agonist-induced internalisation.

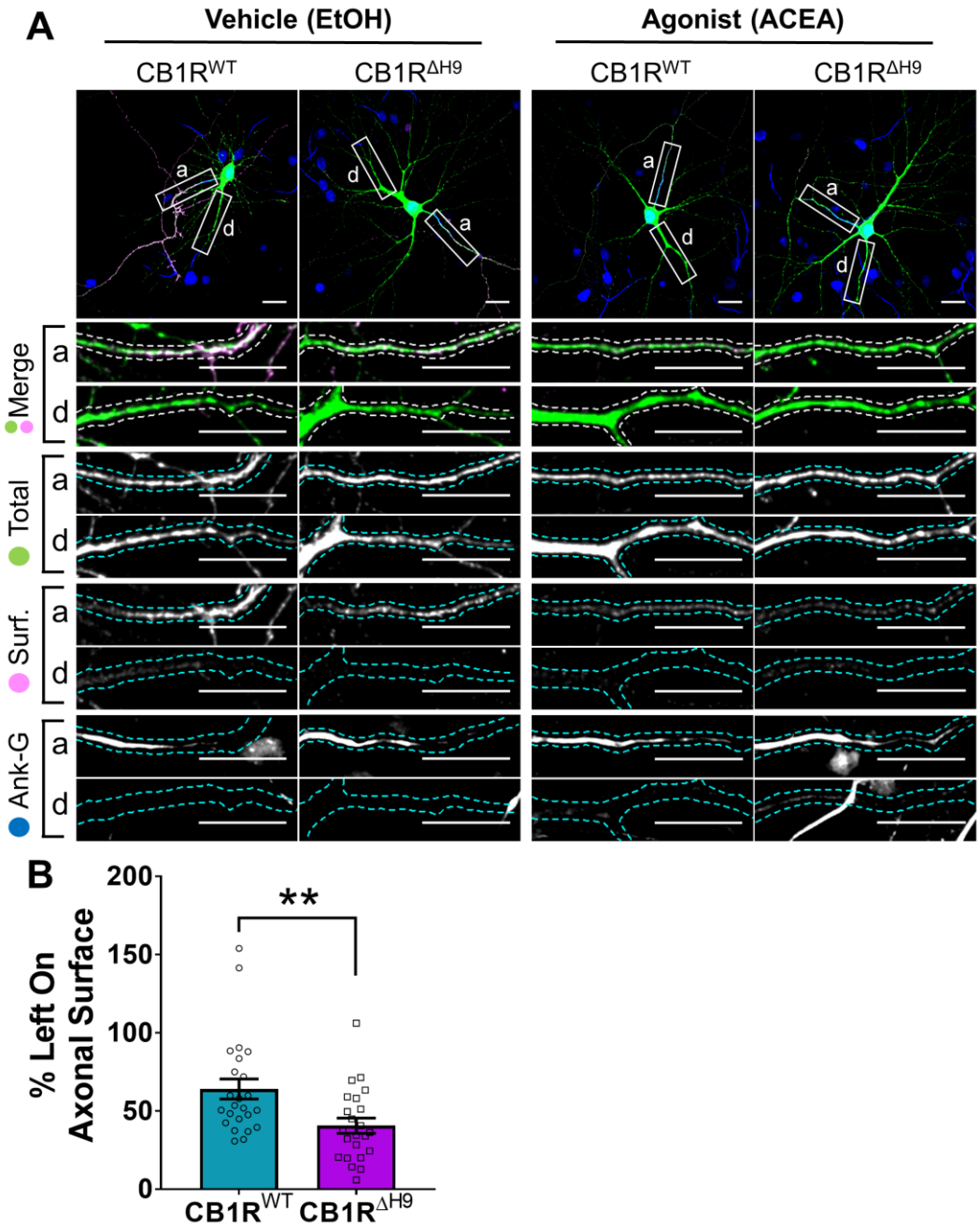

Figure 4-9 Role of *H9* in resisting agonist-induced endocytosis.

(**A**) Representative confocal images of DIV 14 hippocampal neurons expressing EGFP-CB1R^{WT} or EGFP-CB1R$^{\Delta H9}$ and treated with vehicle (0.1% EtOH) or CB1R agonist (5 μM ACEA) for 3 hrs. Upper panels for each condition show whole cell field of view and lower panels are enlargements of axonal (a) and dendritic (d) ROIs. Green = total; magenta = surface; blue = axon marker (Ankyrin-G). Merge: surface to total seen as white.

(**B**) Quantification of data represented in (**A**). Significantly less EGFP-CB1R$^{\Delta H9}$ than EGFP-CB1R^{WT} remained on the surface of axons after agonist application, indicating greater sensitivity to agonist-induced internalisation. The surface mean fluorescence was first normalised to the total mean fluorescence for each ROI, then to the average axonal EtOH value within a condition (set to 100%). Unpaired t-test. N = three independent experiments; n = 23–24 neurons per condition.

4.3.7 The role of *H9* in polarity is revealed in the presence of inverse agonist

My data indicate that ctCB1R, and the *H9* domain in particular, can determine the surface and total polarity of a CD4 chimera (**Figure 4-2**), and promote polarised surface delivery of CB1R (**Figure 4-5**). In contrast, deletion of *H9* has no effect on CB1R surface polarity at steady state (**Figure 4-6**). However, deletion of *H9* does have a striking effect on the surface stability of CB1R with CB1R$^{\Delta H9}$ being less surface expressed in both axons and dendrites and displaying increased endocytosis (**Figure 4-6**, **Figure 4-7**). Furthermore, CB1R $^{\Delta H9}$ is more responsive to agonist-induced internalisation (**Figure 4-9**).

I therefore wondered whether the difference between the CD4 chimeras and the full-length receptor and between surface+endocytosed and surface polarity may be attributable to the agonist binding capability of the full-length receptor. To test this, I used the CB1R-specific inverse agonist AM281 to prevent the receptor entering an active conformation and which has previously been shown to increase somatodendritic surface expression similar to treatment with an endocytosis inhibitor (Leterrier et al., 2006). I reasoned that AM281 might reveal a difference in surface polarity between EGFP-CB1R^{WT} and EGFP-CB1R$^{\Delta H9}$, like that observed with the CD4 chimeras and in surface+endocytosed polarity.

In hippocampal neurons treated with the DMSO control both EGFP-CB1R^{WT} and EGFP-CB1R$^{\Delta H9}$ displayed similar levels of surface polarity (**Figure 4-10 A-B**). In the presence of AM281, however, EGFP-CB1R$^{\Delta H9}$ had significantly reduced surface polarity compared EGFP-CB1R^{WT} (**Figure 4-10 B**). This was due to a significantly increased dendritic surface expression (**Figure 4-10 C**). These data indicate that the increased dendritic delivery that occurs in EGFP-CB1R$^{\Delta H9}$ is offset and 'masked' by the increase in agonist-induced endocytosis.

Next, I examined more closely what happens in axons and dendrites during AM281 application. **Axons**: Consistent with the above results, with Vehicle treatment (DMSO), the ΔH9 mutant was less surface expressed than WT in axons (**Figure 4-10 D black asterisks**). This difference was reversed upon AM281 incubation, where there was no significant difference in axonal surface expression between WT and ΔH9 after AM281 incubation (**Figure 4-10 D black asterisks**). This increase was due to significantly enhanced surface expression during AM281 treatment for ΔH9 that did not occur in WT (**Figure 4-10 D coloured asterisks**).

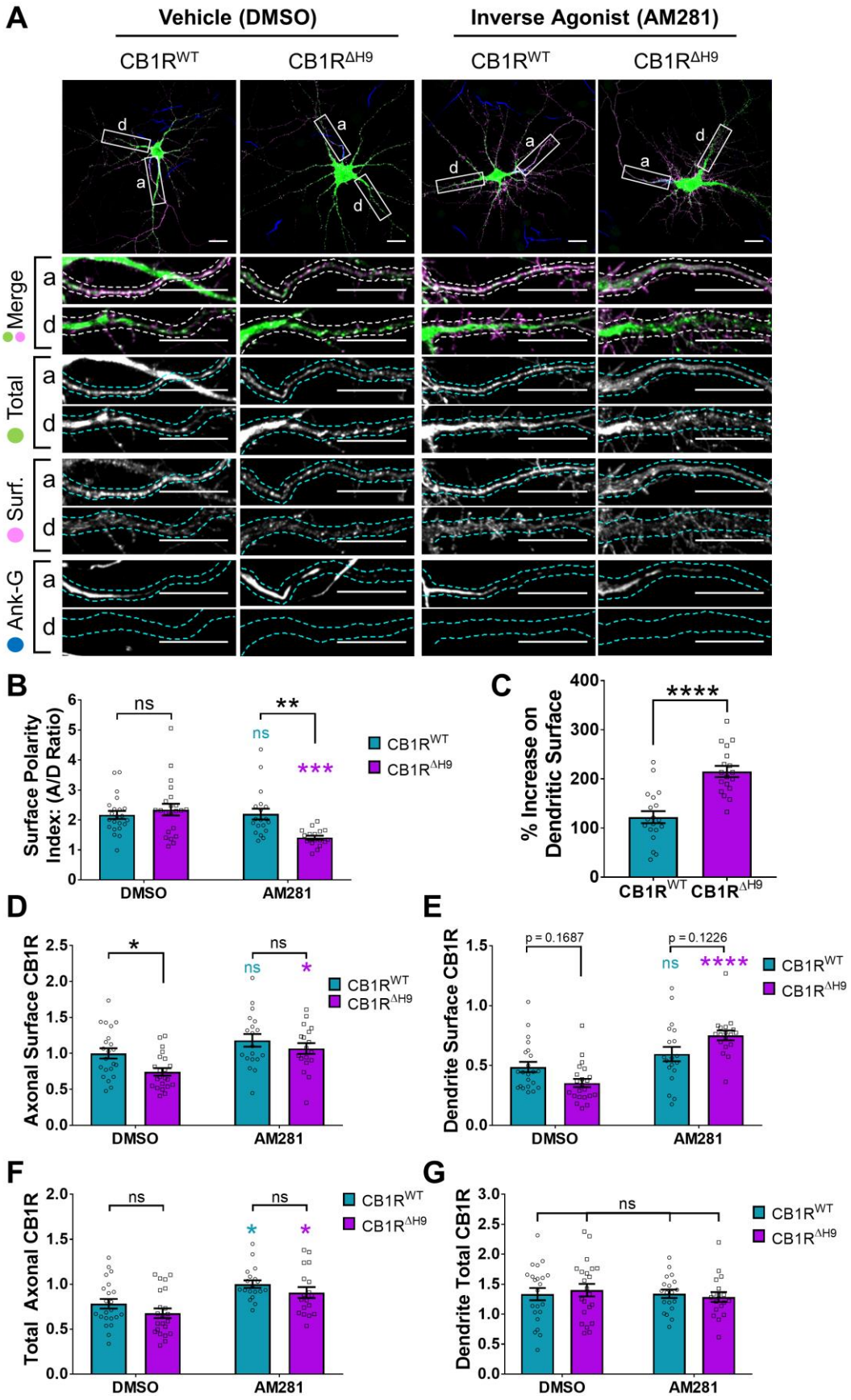
A
Vehicle (DMSO)
Inverse Agonist (AM281)
CB1R^WT
CB1R^ΔH9
CB1R^WT
CB1R^ΔH9
Merge
Total
Surf.
Ank-G
a
d
B
Surface Polarity Index: (A/D Ratio)
ns
**
ns
***
DMSO
AM281
CB1R^WT
CB1R^ΔH9
C
% Increase on Dendritic Surface
****
CB1R^WT
CB1R^ΔH9
D
Axonal Surface CB1R
*
ns
ns
*
DMSO
AM281
CB1R^WT
CB1R^ΔH9
E
Dendrite Surface CB1R
p = 0.1687
p = 0.1226
ns
****
DMSO
AM281
CB1R^WT
CB1R^ΔH9
F
Total Axonal CB1R
ns
ns
*
*
DMSO
AM281
CB1R^WT
CB1R^ΔH9
G
Dendrite Total CB1R
ns
DMSO
AM281
CB1R^WT
CB1R^ΔH9

Figure 4-10 The role of H9 in polarity is revealed in the presence of inverse agonist.

(**A**) Representative confocal images of DIV 14 hippocampal neurons expressing EGFP-CB1R^{WT} or EGFP-CB1R$^{\Delta H9}$ and treated with vehicle (0.2% DMSO) or CB1R inverse agonist (10 µM AM281) for 3 hr. Upper panels for each condition show whole cell field of view and lower panels are enlargements of axonal (a) and dendritic (d) ROIs. Green = total; magenta = surface; blue = axon marker (Ankyrin-G). Merge: surface to total seen as white.

(**B**) Quantification of data shown in (**A**) presented as the surface polarity index (A/D ratio). In the presence of inverse agonist, but not vehicle, EGFP-CB1R$^{\Delta H9}$ was significantly less axonally polarised than EGFP-CB1R^{WT}. Two-way ANOVA with Sidak's *post hoc* test.

(**C**) Quantification of data represented in (**A**). Significantly more EGFP-CB1R$^{\Delta H9}$ than EGFP-CB1R^{WT} relocated to the surface of dendrites after inverse agonist application. The surface mean fluorescence was first normalised to the total mean fluorescence for each ROI, then to the average DMSO value within a condition (set to 100%). Unpaired t-test. N = three independent experiments; n = 18–19 neurons per condition.

(**D**) Quantification of data represented in (**A**). In axons, inverse agonist application reversed the reduced surface expression phenotype of EGFP-CB1R$^{\Delta H9}$ compared to EGFP-CB1R^{WT}. There is no significant increase in surface expression with inverse agonist application in to EGFP-CB1R^{WT}. The surface mean fluorescence was normalised to the total *dendritic* mean fluorescence for each neuron. Two-way ANOVA with Sidak's *post hoc* test. Coloured asterisks = DMSO vs. AM281; black asterisks = WT vs. ΔH9.

(**E**) Quantification of data represented in (**A**). In dendrites, inverse agonist application reversed the reduced surface expression phenotype of EGFP-CB1R$^{\Delta H9}$ compared to EGFP-CB1R^{WT} (non-significant trend). There is a non-significant trend to increased surface expression in dendrites for ΔH9 compared to WT after inverse agonist treatment. There is no significant increase in surface expression with inverse agonist application in to EGFP-CB1R^{WT}. The surface mean fluorescence was normalised to the total dendritic mean fluorescence for each neuron. Two-way ANOVA with Sidak's *post hoc* test. Coloured asterisks = DMSO vs. AM281; black asterisks = WT vs. ΔH9.

(**F**) Quantification of data represented in (**A**). In axons, inverse agonist application increased the total amount of receptor for both EGFP-CB1R^{WT} and EGFP-CB1R$^{\Delta H9}$. The total mean fluorescence was normalised to the total dendritic mean fluorescence for each neuron. Two-way ANOVA with Sidak's *post hoc* test. Coloured asterisks = DMSO vs. AM281; black asterisks = WT vs. ΔH9.

(**G**) Quantification of data represented in (**A**). No difference in total dendritic fluorescence confirms equal expression levels of SBP-EGFP-CB1R between WT vs. ΔH9 and DMSO vs. AM281. Because it was the only measure that stayed constant, all the above parameters were normalised to total dendritic fluorescence. Two-way ANOVA with Sidak's *post hoc* test.

These data indicate that the phenotype of reduced surface expression (**Figure 4-6**) and increased internalisation (**Figure 4-7**) in axons in the ΔH9 mutant is due to an increased sensitivity to, and thus increased levels of, agonist-induced endocytosis (**Figure 4-9**).

Dendrites: Interestingly, a similar profile also occurs in the dendrites. In this case, with vehicle treatment, the reduced surface expression of ΔH9 was a non-significant trend (**Figure 4-10 E**). AM281 treatment significantly increased dendritic surface expression of ΔH9, but not of WT (**Figure 4-10 E coloured asterisks**) so that under AM281 treatment, the non-significant trend went the other way – there was a trend to more dendritic surface CB1R for ΔH9 than for WT.

These data indicate that the phenotype of reduced surface expression (**Figure 4-6**) and increased internalisation (**Figure 4-7**) in dendrites of the ΔH9 mutant is due to

an increased amount of agonist-induced endocytosis. Furthermore, the trend towards an increased dendritic surface expression after AM281 treatment reveals the increased delivery of EGFP-CB1R$^{\Delta H9}$ to the dendritic surface as seen in (**Figure 4-5**).

Lastly, AM281 treatment increased the amount of total CB1R in axons in both WT and ΔH9 conditions (normalised to dendrite total; **Figure 4-10 F coloured asterisks**).

Importantly, total levels of CB1R in dendrites remained the same over all conditions (**Figure 4-10 G**). Because this was the only parameter that remained constant throughout all of the conditions, the data in **C-F** were all normalised to dendrite total for each cell to control for within-condition variation in expression (rather than surface expression being normalised to total expression for each ROI).

These results indicate that in the absence of constitutive activity of the receptor, *H9* plays a role in mediating CB1R surface polarity, because *H9* restricts delivery of CB1R to the dendritic surface. Furthermore, these data suggest that the increased internalisation observed both dendrites and in axons with *H9* deletion may be mediated by the presence of endogenous agonist and reaffirm the importance of the neuronal milieu on CB1R trafficking.

4.4 Discussion

4.4.1 Summary of results

The data presented in this chapter demonstrate that ctCB1R in general, and especially the *H9* motif, is important for generating and maintaining axonal surface polarity (summarised in **Figure 4-11**). In Chapter 3, I identified a two-part model of CB1R polarisation (**Figure 3-15**). In the present chapter, I show that *H9* plays a role in both the 1) preferential delivery and 2) selective retention of CB1R at the axonal membrane. I show that deleting *H9* (CB1R$^{\Delta H9}$) causes 1) an increase in secretory pathway delivery to dendrites, and 2) a reduction surface retention in both the dendrites and axons (**Figure 4-4**; **Figure 4-5**), resulting, at steady-state, in decreased surface expression (**Figure 4-6**) and increased internalisation (**Figure 4-7**) of the mutant compared to WT. In both dendrites and axons, the reduced surface retention is due to increased susceptibility to agonist-induced internalisation (**Figure 4-9**) as revealed by the fact that incubation with AM281, an

inverse agonist, reverses the reduced surface retention phenotype of EGFP-CB1R$^{\Delta H9}$ compared to EGFP-CB1R^{WT} (**Figure 4-10**).

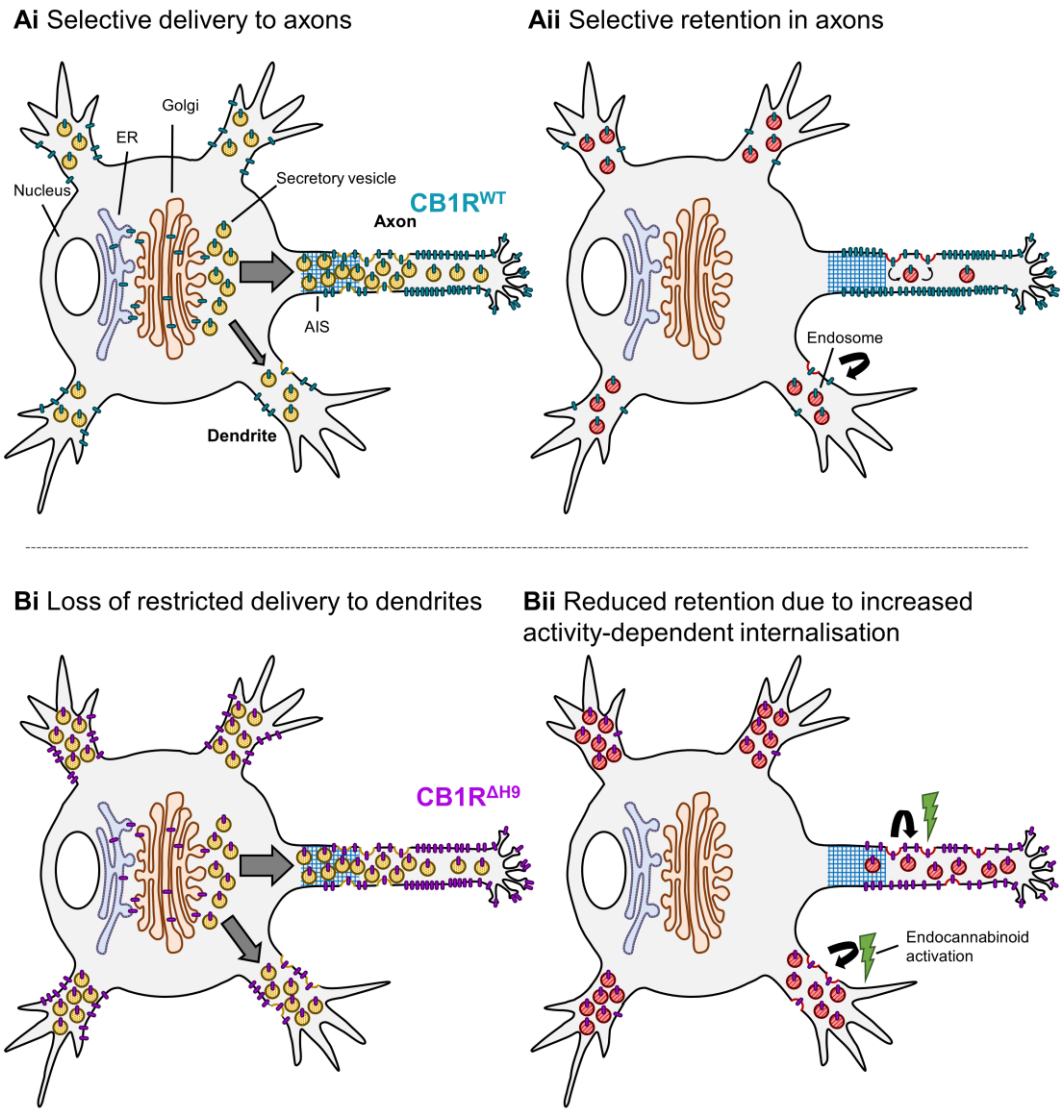

Figure 4-11 Schematic summarising main findings.

Polarised surface distribution of CB1R is established and maintained by two complementary mechanisms: (Ai) selective delivery of newly synthesized CB1R to the axon (or restricted delivery to dendrites) and (Aii) selective retention in axons and retrieval from dendrites. The C-terminal motif Helix 9 plays a role in both of these mechanisms because deletion of *H9* leads to: (Bi) a loss of axon-selective delivery and (Bii) reduced retention in both axons and dendrites that can be reversed in dendrites by inverse agonist application, suggesting that CB1R$^{\Delta H9}$ is more susceptible to activity-driven internalisation.

4.4.2 Total CB1R preference

Although intracellular CB1R is apparently non-polarised and present throughout the neuron surface expressed CB1R displays a characteristic highly polarised surface distribution. However, in this chapter I show that total CB1R does, in fact, display a slight axonal polarisation. The total polarity index (A/D ratio) of the

completely non-polarised CD4 transmembrane protein was around 0.8 (**Figure 4-2 C**). This value is less than 1 most likely due to the larger volume of dendrites compared to axons.

Therefore, if we define a total polarity index of 0.8 as being "non-polarised," the total distribution of CB1R, which is ~1 (**Figure 4-6 D**) indicates an axonal polarisation compared to completely non-polarised CD4. This axonal preference is mediated by ctCB1R, since addition of ctCB1R to CD4 was sufficient to shift CD4 from a non-polarised distribution of ~0.8 to ~1.2 (**Figure 4-2 C**).

Our initial hypothesis was that this polarity shift is mediated by *H9* because the distribution of CD4-CB1R$^{\Delta H9}$ chimera was non-polarised (0.76; **Figure 4-2 C**). However, while the full length SBP-EGFP-CB1R$^{\Delta H9}$ mutant was impaired in its ability to enter the axon when newly synthesised (**Figure 4-5 A**), at steady state, SBP-EGFP-CB1R$^{\Delta H9}$ total polarity is identical to that of SBP-EGFP-CB1R^{WT} (**Figure 4-6 D**). These data indicate that, in addition to *H9*, other as yet undefined motifs are present outside the ct (e.g. in the intracellular loops) that contribute to the polarity of CB1R.

4.4.3 Surface CB1R polarity

The surface polarity index (A/D ratio) of the completely non-polarised CD4 transmembrane protein was also around 0.8 (defined as "non-polarised"; **Figure 4-2 D**). Addition of ctCB1R^{WT} (CD4-ctCB1R^{WT}) shifted the surface polarity index to around 1.5 (**Figure 4-2 D**). This shift in surface polarity index is slightly larger than the shift in total polarity (0.8 to 1.2) indicating that the difference in surface polarity is not solely attributable directed axonal targeting of intracellular CB1R (total polarity).

Indeed, analysis of internalisation reveals a small, but significant, increase in internalisation of CD4-ctCB1R^{WT} in dendrites but not in axons compared to CD4 (**Figure 4-3 B**) which accounts for the greater level of surface polarity than total polarity. This internalisation is, however, *H9*-independent since it occurs in both CD4-ctCB1R$^{\Delta H9}$ and CD4-ctCB1R^{WT} chimeras (**Figure 4-3 B**). Furthermore, since CD4-ctCB1R^{WT} and CD4-ctCB1R$^{\Delta H9}$ chimeras cannot bind CB1R agonist, this internalisation must be constitutive, not agonist-induced.

Nevertheless, CD4-ctCB1R^{WT} surface polarity is not complete – the surface polarity of full length CB1R^{WT} is around 3.3 (**Figure 4-6 C**), indicating that other motifs in CB1R and/or agonist-induced internalisation due to the tonal level of 2-AG in the dendritic membrane are required for complete CB1R surface polarity (Ladarre and Lenkei, 2017).

4.4.4 *H9* plays a role in preferential delivery of *de novo* CB1R to axons

In Chapter 3, I found that *de novo* CB1R is preferentially trafficked to the axonal membrane compared to the dendritic membrane. In this chapter, I found that deletion *H9* results in increased delivery to dendrites (**Figure 4-5 D**), suggesting that *H9* plays a role in restricting delivery to dendrites.

One possibility is that *H9* may modulate CB1R binding to AP-3, allowing for preferential delivery to axons and sorting to dendritic lysosomes, causing a decrease in dendritic membrane CB1R. More studies are needed to examine the possibility of *H9* influencing AP-3 and CB1R interaction.

It would be interesting to co-RUSH SBP-EGFP-CB1R^{WT} and -CB1R$^{\Delta H9}$ to determine at what point in the secretory pathway the diversion occurs. For example, are WT and ΔH9 receptors sorted into different Golgi compartments? Would some secretory vesicles only contain ΔH9 because they are destined to the dendritic membrane? These experiments would provide more insight not only into CB1R polarised secretory pathway trafficking, but into polarised trafficking in general.

4.4.5 *H9* resists agonist-induced endocytosis

The most consistent phenotype that I observed for CB1R$^{\Delta H9}$ was a reduced membrane retention – less surface expression (**Figure 4-6 B**) and more internalisation (**Figure 4-7**) in both axons and dendrites. The lack of an effect of deleting *H9* on CD4-CB1R chimera internalisation (**Figure 4-3**), the increased rate of agonist-induced internalisation of CB1R$^{\Delta H9}$ in axons (**Figure 4-9**), and the reversal of reduced surface expression upon AM281 treatment (**Figure 4-10**), suggest that this phenotype is due to increased agonist-induced endocytosis in the ΔH9 mutant. These data strongly suggest that *H9* functions to resist agonist-induced internalisation.

4.4.5.1 CB1R agonist-induced endocytosis

4.4.5.1.1 β-arrestin recruitment

GPCRs such as CB1R are subject to dynamic regulation by ligand stimulation. Following activation by extracellular cannabinoids, CB1R is desensitised by phosphorylation of two serine residues (S426 and S430) by GCR kinase 3 (GRK3) and β-arrestin recruitment (Jin et al., 1999; Daigle et al., 2008a; Delgado-Peraza et al., 2016). How CB1R is then internalised is not entirely clear, but reports indicate that internalisation may be a result of binding of β-arrestin2 over β-arrestin1 (Ahn et al., 2013; Delgado-Peraza et al., 2016) and that further phosphorylation of six serines and threonines in the distal C-terminal tail is required (Straiker et al., 2012b). *H9* sits right between these two major sites of phosphorylation. Therefore, it is possible that deletion of *H9* favours β-arrestin2 recruitment rather than β-arrestin1 recruitment. Standard assays measuring β-arrestin recruitment to GPCR such as the Pathhunter and Tango assays would shed light on the role of *H9* on β-arrestin recruitment and subsequent internalisation.

4.4.5.1.2 ctCB1R interacting proteins

Other ctCB1R interacting proteins affect agonist-induced internalisation of CB1R. Cannabinoid receptor interacting protein (CRIP1a) binds to the distal C-terminal tail of CB1R (Niehaus et al., 2007; Mascia et al., 2017). CRIP1a prevents agonist-induced internalisation of CB1R by competing with β-arrestin1/2 for binding of ctCB1R (Blume et al., 2016; Mascia et al., 2017; Blume et al., 2017). *H9* sits right between the serine residues important for desensitisation and CRIP1a binding site (**Figure 4-1**). Therefore, *H9* may mediate the interactions between β-arrestin1/2 and CRIP1a binding, and its loss favours β-arrestin2 recruitment over β-arrestin1 or CRIP1a binding, causing an increased amount of agonist-induced internalisation.

Src homology 3-domain growth factor receptor-bound 2-like (endophilin) interacting protein 1 (SGIP1) binds ctCB1R C-terminally of *H8* and prevents agonist-induced internalisation of CB1R (Hájková et al., 2016). SGIP1 is discussed in detail in the next chapter.

4.4.5.2 H9 and AM281

There have previously been conflicting reports on the effect of inverse agonist incubation on CB1R surface expression. In (Leterrier et al., 2006), incubation with AM281 for 3 hours significantly increased the surface expression of both endogenous and exogenously expressed CB1R in dendrites – although the increase was less dramatic in endogenous CB1R compared to exogenously expressed CB1R, requiring EM. This increase was equivalent to the increased surface expression observed with treatment with an endocytosis blocker methyl-β-cyclodextrin (MβCD; (Leterrier et al., 2006)). This result led them to believe that the dendritic internalisation of CB1R in dendrites is dependent on agonist. However, (McDonald et al., 2007a) found no such dendritic increase in surface expression with AM281 in both endogenous and exogenously expressed CB1R. However, co-expression with a dominant-negative dynamin to prevent endocytosis did result in translocation to the dendritic plasma membrane.

One main methodological difference between these two experiments was the tagging of CB1R – in (Leterrier et al., 2006), the CB1R construct was Myc tagged N-terminally (with the full N-terminus) and tagged with EGFP C-terminally. In (McDonald et al., 2007a), a SEP tag was added to the truncated N-terminus. My construct is derived from (McDonald et al., 2007a) – it is N-terminally tagged with SBP and EGFP and the N-terminus is truncated.

In this chapter, I found that EGFP-CB1R$^{\Delta H9}$ strongly translocated to the dendritic membrane with AM281 incubation (**Figure 4-10**). While there was a small increase in dendritic surface expression for EGFP-CB1R^{WT} (around 122%), it is not quite significant ($p = 0.086$; one-sample t-test, and no multiple comparisons corrections). This leads me to wonder whether, while there is some effect of AM281, the exaggerated effect seen by (Leterrier et al., 2006) is due to the C-terminal tagging of CB1R preventing an unknown protein-protein interaction and having a similar effect as deleting *H9*.

It is unlikely that the N-terminal truncation could be the cause of the discrepancy since there was no difference in surface expression of the N-terminally tagged full, full length CB1R compared to the truncated version (**Figure 3-3**) and this truncation does not affect signalling (McDonald et al., 2007a; b). Further studies repeating this experiment with comparing different versions of exogenously expressed,

tagged, and truncated CB1R vs. an untagged CB1R, or preferentially further studies with endogenous CB1R, are needed to fully resolve this discrepancy.

4.4.5.3 What happens next?

While I have shown that CB1R$^{\Delta H9}$ displays increased internalisation compared to WT, further studies are also needed to determine the fate of the internalised WT and ΔH9 receptors in both dendrites and axons. Are they sent for degradation via GASP1 or re-sensitised and recycled back to the surface? Is the fate the same in axons vs. dendrites? Are dendritic endosomal CB1Rs rerouted to the axonal surface (transcytosis)?

The degradation of internalised CB1R can be examined by adding lysosomal inhibitors such as bafilomycin or leupeptin to constitutive or agonist-induced endocytosis experiments, staining for a lysosomal marker such as LAMP1, and screening for colocalization with LAMP1 in axons vs. dendrites.

4.4.6 ctCB1R and constitutive internalisation

While the data presented in this chapter mainly focused on the role of *H9* in agonist-induced internalisation, the CD4 internalisation experiment also provided evidence for the presence of dendrite-specific internalisation controlled by ctCB1R independently of *H9* (**Figure 4-3**). This internalisation may be due to a motif that either interacts either with a dendritically polarised pro-endocytic factor or with an axonally polarised surface stabilising factor.

The ΔH9 mutant retains the final 13 residues. Within this section, 5 amino acids have been shown to be important for binding of cannabinoid receptor interacting protein (CRIP1a; **Figure 4-1**) (Mascia et al., 2017). Because CRIP1a co-localises with CB1R at presynaptic boutons (Guggenhuber et al., 2016) and binding of CRIP1a negatively regulates constitutive endocytosis of CB1R (Mascia et al., 2017), it is possible that CRIP1a binding to the CD4-ctCB1R chimeras in axons but not in dendrites is the source of the differential endocytosis patterns seen in this experiment. Repeating the experiment with a CD4-ctCB1R chimera lacking these 5 residues and/or knocking down CRIP1a would be needed to confirm this possibility.

4.4.7 *H9* affects downstream signalling

4.4.7.1 Kinetics of ERK1/2 activation

My data indicate that deletion of *H9* decreases downstream signalling (**Figure 4-8**) and increases agonist-induced internalisation (**Figure 4-9**). However, more experiments are needed to fully characterise the effect of *H9* deletion on downstream signalling in terms of kinetics and signalling pathways.

A time course of agonist application would provide information regarding the kinetics of ERK1/2 activation. I chose 5 minutes because of a report that the maximum ERK1/2 signal occurs at 5 minutes of 100 nM CP 55,940 treatment in HEK293 cells expressing $CB1R^{WT}$ (Daigle et al., 2008a). This peak is then followed by a rapid decrease which stabilises after around 15 minutes of agonist treatment. This is due to desensitization by phosphorylation of two serine residues (S426, S430) since a mutant where these two serine residues are replaced by alanine residues (phospho-null) does not show the rapid peak and decrease, but rather a stable activation for at least 45 minutes (Daigle et al., 2008a). Since the peak of for ERK1/2 activation occurs so rapidly and so transiently, if the kinetics for ERK1/2 activation are different for the ΔH9 mutant, it is possible that I missed the peak because it did not occur at 5 minutes, but before or afterwards.

4.4.7.2 Desensitisation

This single snapshot approach also provides no insight into the ability of the ΔH9 mutant to desensitise. Therefore, a time course would provide more information both on the role of *H9* in ERK1/2 activation as well as the role of *H9* in desensitization. The two serine residues that are phosphorylated during desensitization (S426 and S430) are located in the stretch of amino acids between *H8* and *H9*, so it is possible that *H9* might play a role in desensitisation by providing or blocking access to the kinases, GRK2/3 (**Figure 4-1**). *H9* may also mediate β-arrestin1/2 recruitment and binding, preventing or promoting desensitisation. The shape of ERK1/2 activation kinetics of the mutant alone or with the additional phospho-null mutations would provide information on the role of *H9* in desensitization.

4.4.7.3 Alternative G protein coupling

While CB1R is traditionally thought to act via $G_{i/o}$ protein coupling, several reports indicate that CB1R also couples with G_S, $G\alpha_z$, $G\alpha_{q/11}$, and $G\alpha_{12/13}$ depending on the

cell type and/or agonist used (Diez-Alarcia et al., 2016; Busquets-Garcia et al., 2018). Indeed, ACEA, the agonist that I used, is capable of activating CB1R-$G\alpha_{q/11}$ (Diez-Alarcia et al., 2016). $G\alpha_{q/11}$ signalling classically activates phospholipase C β isoforms (PLCβ) but can also activate PKC which leads to ERK1/2 activation (Sánchez-Fernández et al., 2014). Since regions analogous to *H9* in the bradykinin receptor and squid rhodopsin acts as the binding site for $G\alpha_{q/11}$ (Piserchio et al., 2005; Murakami and Kouyama, 2008), the defect in ERK1/2 activation observed in this chapter could possibly provide evidence that CB1R *H9* mediates the coupling of $G\alpha_{q/11}$ as well. G-protein coupling assays such as those described in (Diez-Alarcia et al., 2016) would be needed to test this possibility.

4.4.7.4 H9 and other signalling pathways

Lastly, ERK1/2 activation is but one of the many pathways that CB1R activates. The most 'classical' effect of CB1R activation via $G_{i/o}$ proteins is a decrease in cyclic AMP (cAMP) levels through inactivation of adenylyl cyclase (Howlett, 2005). The role of *H9* in activation of this pathway can be tested using standard cAMP assays to detect CB1R-mediated reduction of cAMP under forskolin stimulation (e.g. (Blume et al., 2015; McDonald et al., 2007a)).

4.5 CONCLUSION

Taken together, these results reveal that the C-terminal domain, and *H9* in particular, play important roles in trafficking of CB1R. These findings provide important insight into the mechanisms of CB1R polarity and highlight *H9* as an important regulator of CB1R trafficking, endocytosis, and surface expression.

Chapter 5 – SCREENING FOR *H9* INTERACTING PROTEINS

5.1 AIMS

- To determine the mechanism by which *H9* increases membrane retention.
- To screen for interacting partners of *H9* that may play a role in 1) preferential axonal delivery and/or 2) membrane retention.

5.2 INTRODUCTION

5.2.1 Role of *H9* in CB1R trafficking

In Chapter 3, I showed so far that CB1R is preferentially trafficked to the axon by the secretory pathway and preferentially retained at the axonal membrane, resulting in its the characteristic axonal polarisation. In Chapter 4, I showed that both preferential delivery of CB1R and membrane retention of CB1R during agonist activation are moderated by the Helix 9 (*H9*) motif of the C-terminus of CB1R (ctCB1R).

Building on these data I next investigated the how perturbation of H9 might mediate these effects. NMR and circular dichroism studies suggest that *H9*, like *H8*, is an amphipathic α-helix, associating with the lipid bilayer via a cluster of hydrophobic residues on the non-polar face of the helix (Ahn et al., 2009b). As outlined below, I tested the effects of addition of 'forbidden' prolines to perturb the predicted alpha helical motif due to steric hindrance and the loss of a backbone hydrogen bond (Bright et al., 2002). I mutated two residues of *H9* into prolines (A447P and V455P) to perturb the motif and determine whether that its helicity is required for the decreased surface expression phenotype.

H9 also contains a cysteine residue (C450), raising the possibility that post-translational modifications such as palmitoylation, prenylation, or farnesylation at this site could modulate membrane association. Indeed, CB1R has been shown to be palmitoylated just C-terminally of *H8* at C416, which affects its membrane association, G-protein coupling, and is required for agonist-induced internalisation in HEK293 cells (Oddi et al., 2012, 2017, 2018). I therefore mutated the cysteine

to an alanine (C450A) to determine whether deletion this residue is necessary to produce the reduced surface expression phenotype of $CB1R^{\Delta H9}$.

Because little is known CB1R C-terminal interactors in general, and none have been identified specifically for the *H9* domain, I searched for novel interacting proteins with *H9* by mass spectrometry as well as literature searches.

5.2.2 Possible mechanisms underpinning preferential axonal delivery

5.2.2.1 AP-3 sorting

While several sorting signals and adaptors have been described for dendritic cargo, the mechanisms behind selective sorting to axons are less well known (Lasiecka and Winckler, 2011; Bentley and Banker, 2016). A recent study in *C. elegans* has suggested that sorting of cargos to axons or dendrites depends on binding to different types of clathrin-associated adaptor proteins (AP); axonal cargo bind to AP-3 whereas dendritic cargo bind to AP-1 (Li et al., 2016) Interestingly, AP-3 binding has been associated with CB1R trafficking to the lysosome in the dendritic compartment (Rozenfeld and Devi, 2008). In this paper, they found that knocking down AP-3 with an siRNA resulted in increased surface expression of somatodendritic CB1R (Rozenfeld and Devi, 2008). One possibility is that *H9* may modulate CB1R binding to AP-3, allowing for preferential delivery to axons and sorting to dendritic lysosomes. More studies are needed to examine the possibility of *H9* influencing AP-3 and CB1R interaction.

5.2.3 Mechanisms of endocytosis

5.2.3.1 Rab5 and Rab4 GTPases

It has been reported that transfected CB1R colocalises significantly with Rab5- and Rab4-positive endosomes, but not Rab11-positive endosomes, in HEK293 cells (Leterrier et al., 2004). Rab5 is a small GTPase involved in the delivery of plasma membrane proteins to early endosomes, whereas Rab4 is involved in both fast and slow recycling back to the plasma membrane (see **Figure 1-4**). The co-expression of untagged CB1R with dominantly negative (DN; GDP-bound) or dominantly active (DA; GTP-bound) Rab5 or Rab4 changed the surface-to-total ratio of CB1R in HEK293 cells. DN Rab5 induces an accumulation of the proportion CB1R at the plasma membrane, whereas DA Rab5 induces increased endocytosis of CB1R. On the other hand, DN Rab4 impairs CB1R recycling, causing a decreased surface

to total ratio, and DA Rab4 enhances CB1R recycling, causing an accumulation of CB1R at the plasma membrane.

In neurons, expression of a DN Rab5 decreases the surface polarity index (A/D) of expressed FLAG-CB1R-YFP due to the accumulation of the receptor at the somatodendritic surface (Leterrier et al., 2006).

Together, these data suggest that under steady-state conditions, CB1R is constitutively endocytosed and recycled back to the membrane by Rab5- and Rab-4 dependent means, respectively. However, I could not replicate these results below.

5.2.3.2 SGIP1

SH3-containing GRB2-like protein 3-interacting protein 1 (SGIP1) is an adaptor protein linked to clathrin-mediated endocytosis (Uezu et al., 2007)). SGIP1 binds to ctCB1R at an unknown location C-terminally of *H8* where it interferes with agonist-induced internalisation and modulates β-arrestin association and downstream ERK1/2 signalling in HEK293 cells (Hájková et al., 2016). Specifically, (Hájková et al., 2016) co-expressed CB1R and SGIP1 in HEK293 cells and measured internalisation with agonist (2-AG or WIN 55,212-2) application. They found that co-expression with SGIP1 significantly reduced CB1R internalisation induced by agonist binding compared to HEK293 cells just expressing CB1R to a similar level as blocking internalisation with a dominant negative dynamin (DynK44A). They also observed a significant reduction in constitutive internalisation with SGIP1 co-expression in CB1R-expressing HEK293 cells without exogenous agonist application. An intriguing possibility is that I tested is that SGIP1 might interact via H9.

5.3 RESULTS

5.3.1 H9 perturbation: cysteine mutant, 'forbidden proline',

Having found that deletion of *H9* results in reduced surface expression in axons and in dendrites compared to $CB1R^{WT}$, I next sought to parse what characteristics of *H9* are necessary. Firstly, since *H9* is an amphipathic helix, it is likely that its hydrophobic face is associated with the plasma membrane (Stadel et al., 2011). Furthermore, *H9* contains a cysteine residue (C450), meaning that association with the plasma membrane may be further modulated by posttranslational modification

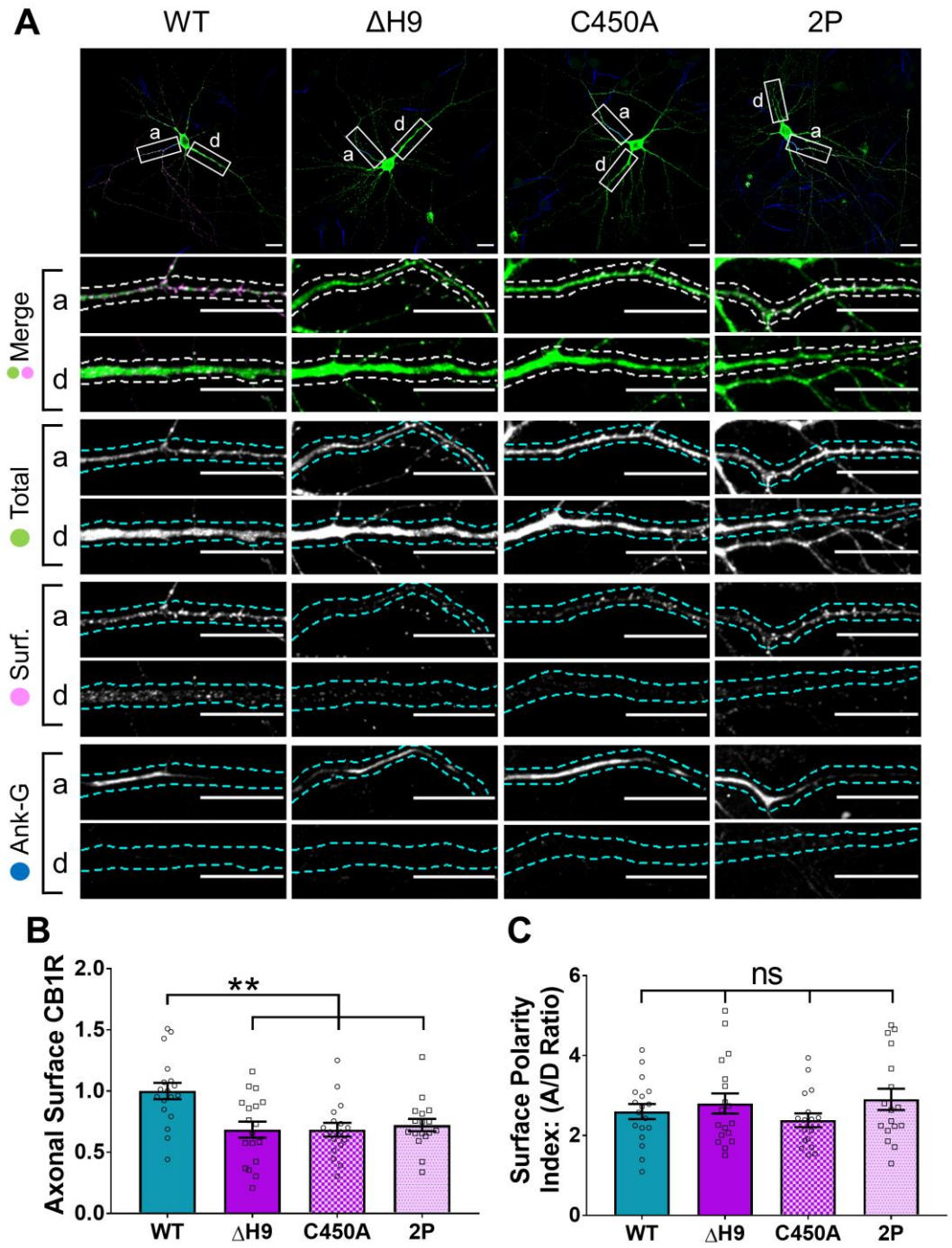

Figure 5-1 Perturbation of H9 by mutation of C450 or incorporation of 2 proline residues result in a similar phenotype of reduced axonal surface expression as EGFP-CB1RΔH9.

(**A**) Representative confocal images of DIV 14 hippocampal neurons expressing EGFP-CB1R^{WT}, EGFP-CB1R$^{\Delta H9}$, EGFP-CB1R^{C450A}, or EGFP-CB1R^{2P}. Upper panels for each condition show whole cell field of view and lower panels are enlargements of axonal (a) and dendritic (d) ROIs. Green = total; magenta = surface; blue = axon marker (Ankyrin-G). Merge: surface to total seen as white.

(**B**) Quantification of data represented in (**A**). Perturbation of *H9* either by substitution of C450 to an alanine residue, or by incorporation of two 'forbidden' prolines resulted in a similar phenotype as removing *H9* completely – CB1R surface fluorescence was significantly reduced in axons compared to WT. One-way ANOVA with Tukey's *post hoc* test. N = three independent experiments; n = 17-18 neurons per condition.

(**C**) Quantification of data represented in (**A**). No significant difference in surface polarity was observed between WT and the three *H9* mutants. One-way ANOVA with Tukey's *post hoc* test. N = three independent experiments; n = 17-18 neurons per condition.

of this residue by palmitoylation, prenylation, or farnesylation. Indeed, palmitoylation of a different cysteine residue located just C-terminally of *H8* (C416) has previously been shown to alter surface stability of CB1R (Oddi et al., 2017). Therefore, I transformed C450 into an alanine residue (EGFP-CB1R^{C450A}) by site directed mutagenesis to determine whether this cysteine residue is necessary for *H9*-mediated surface stabilisation. I also generated another mutant where I converted two residues into 'forbidden' proline residues (A447P + V455P; EGFP-CB1R^{2P}). Because proline is a bulky residue, steric hindrance should prevent the formation of an alpha helix. Analysis of this mutant would determine whether the helicity of *H9*, rather than simply its sequence, is important for its function. I then transfected these *H9* mutants into DIV12 hippocampal neurons and compared their surface expression to EGFP-CB1R^{WT} and EGFP-CB1R$^{\Delta H9}$ (**Figure 5-1 A**). I found that perturbing *H9* in these ways resulted in a reduction of CB1R surface expression in axons identical to that of deleting *H9* compared to WT (**Figure 5-1 B**). Furthermore, consistent with previous results, no mutation influenced surface polarity (**Figure 5-1**). These data indicate that both the C450 residue and the helicity of *H9* are important for its function.

5.3.2 Mechanisms of preferential axonal delivery: Role of AP-3?

Having found that *H9* restricts delivery of CB1R to the somatodendritic membrane, I next sought to determine by what mechanism this occurs. Since AP-3 binds CB1R (Rozenfeld and Devi, 2008) and has also been implicated in TGN-to-axon sorting (Li et al., 2016), I wondered whether *H9* might modulate the binding of CB1R to AP-3. Previously, (Rozenfeld and Devi, 2008) showed that knocking down the delta subunit of AP-3 (AP3D1) by siRNA increased somatodendritic surface CB1R. I generated shRNA constructs targeting AP3D1 which knocked down AP3D1 in HEK293T cells compared to scrambled and untransfected controls (**Figure 5-2 A**). I then transfected DIV12 hippocampal neurons with EGFP-CB1R^{WT} and either AP3D1 shRNA or a SCR21 and examined surface expression at DIV19 (**Figure 5-2 B**). Consistent with (Rozenfeld and Devi, 2008), knockdown of AP3D1 resulted in a non-polarised distribution of surface CB1R. However, the cells did not look very healthy (the somas were blebbing) and lacked Ank-G staining so could not be absolutely identified as being neurons. A more targeted approach would probably be needed in order to examine the role of AP-3 and *H9* in trafficking of CB1R.

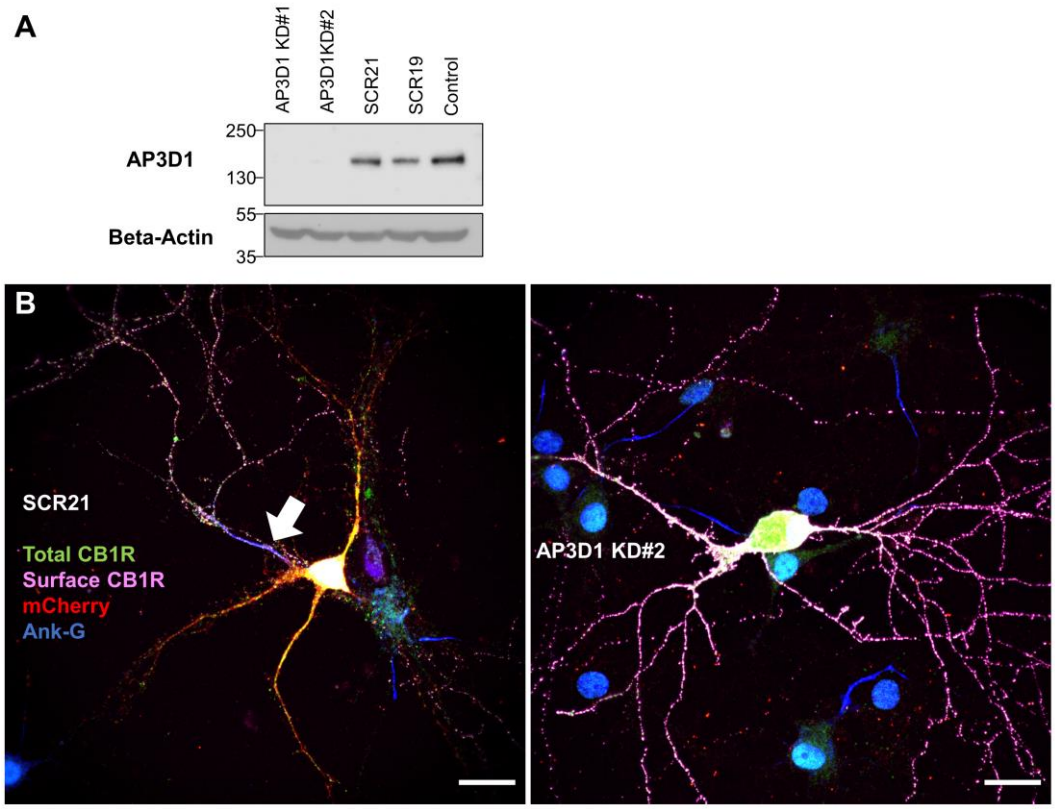

Figure 5-2 Knockdown of AP3D1.

(**A**) Two shRNAs targeting AP3D1 knocked down AP3D1 in HEK293T cells compared to two scrambled controls (SCR21, SCR19). An untransfected control (Control) was also included.

(**B**) Representative confocal images of DIV 19 hippocampal neurons expressing EGFP-CB1R^{WT} and either SCR21 or an shRNA targeting AP3D1 (KD#2; co-expressing mCherry). Green = total EGFP-CB1R^{WT}; magenta = surface EGFP-CB1R^{WT}; red = mCherry, indicating co-transfection of shRNA; blue = axon marker (Ankyrin-G) indicated by white arrow. Merge: surface to total seen as white.

5.3.3 Mechanisms of endocytosis: Rab5

Because it has been previously reported that CB1R internalisation is Rab5-dependent in both HEK293 cells (Leterrier et al., 2004) and the somatodendritic compartment (Leterrier et al., 2006), I sought to determine whether the increased endocytosis phenotype of the ΔH9 mutant is Rab5-dependent as well.

I therefore generated mCherry-tagged Rab5 dominant negative (GDP-bound; S34N; mCherry-Rab5^{DN}) and dominant active (GTP-bound; Q79L; mCherry-Rab5^{DA}) from mCherry-Rab5^{WT}. I co-expressed these constructs with either EGFP-CB1R^{WT} or CB1R$^{\Delta H9}$ in HeLa cells and surface stained using anti-GFP antibody.

I could not replicate the previous reports and found no difference in surface expression of EGFP-CB1R^{WT} between mCherry-Rab5^{WT}, mCherry-Rab5^{DN}, mCherry-Rab5^{DA} (**Figure 5-3 B**), indicating that EGFP-CB1R^{WT} was not

constitutively internalised in a Rab5-dependent manner in HeLa cells. There was also no difference in surface expression of EGFP-CB1R$^{\Delta H9}$ (**Figure 5-3 B**).

5.3.4 Interacting partners screen

To directly compare the interactomes between EGFP-tagged WT or ΔH9 ctCB1R, I generated Sindbis viruses that expressed an EGFP-tagged WT or ΔH9 ctCB1R (EGFP-ctCB1R^{WT} and EGFP-ctCB1R$^{\Delta H9}$) as well as one that expressed a control EGFP. I transduced primary cortical neurons, lysed the cells, and isolated the EGFP-tagged proteins and interacting partners with a GFP-Trap immunoprecipitation. The samples were then sent to the Bristol proteomics facility for analysis by Tandem Mass Tagging (TMT) quantitative proteomics by Dr Kate Heesom. The advantage of the TMT approach is that it not only identifies proteins but also allows for the relative levels of proteins to be compared between samples. By comparing the identities and quantities of hits between the EGFP control, EGFP-ctCB1R^{WT}, and EGFP-ctCB1R$^{\Delta H9}$ potential *H9* interacting partners could be identified. Analysis was completed with the help of Dr Lea Hampton-O'Neil.

Firstly, as a control, a small sample of the lysate was blotted for GFP to ensure that EGFP, EGFP-ctCB1R^{WT}, and EGFP-CB1R$^{\Delta H9}$ were expressed at similar levels (**Figure 5-4 A-B**), so that any difference observed in the mass spectrometry was due to differences in binding, not differences in expression.

In the proteomics data, CB1R was enriched in both WT and ΔH9 compared to GFP (**Table 5-1**), indicating that the GFP-CB1R was successfully immunoprecipitated.

Unfortunately, little else was enriched above GFP levels – most likely because the co-immunoprecipitations were not clean enough. For example, CRIP1a can be used as a positive control, since it binds CB1R at the last 9 residues of ctCB1R, which is included in the ΔH9 mutant. As expected, the level of CRIP1a was similar between ctCB1R^{WT} and ctCB1R$^{\Delta H9}$ (**Table 5-1**). However, there was also a similar level in the GFP sample. For a more extensive and definitive proteomics screen the co-immunoprecipitations will need to be more stringent and optimised with increased washes and salt concentrations. Nonetheless, to gain some information from the proteomics already carried out, compared just ctCB1R$^{\Delta H9}$ and ctCB1R^{WT} data sets, putting aside the GFP values, and screened for proteins that were reduced or enriched in the mutant compared to the WT that are involved in polarity (or preferential delivery) and/or endocytosis.

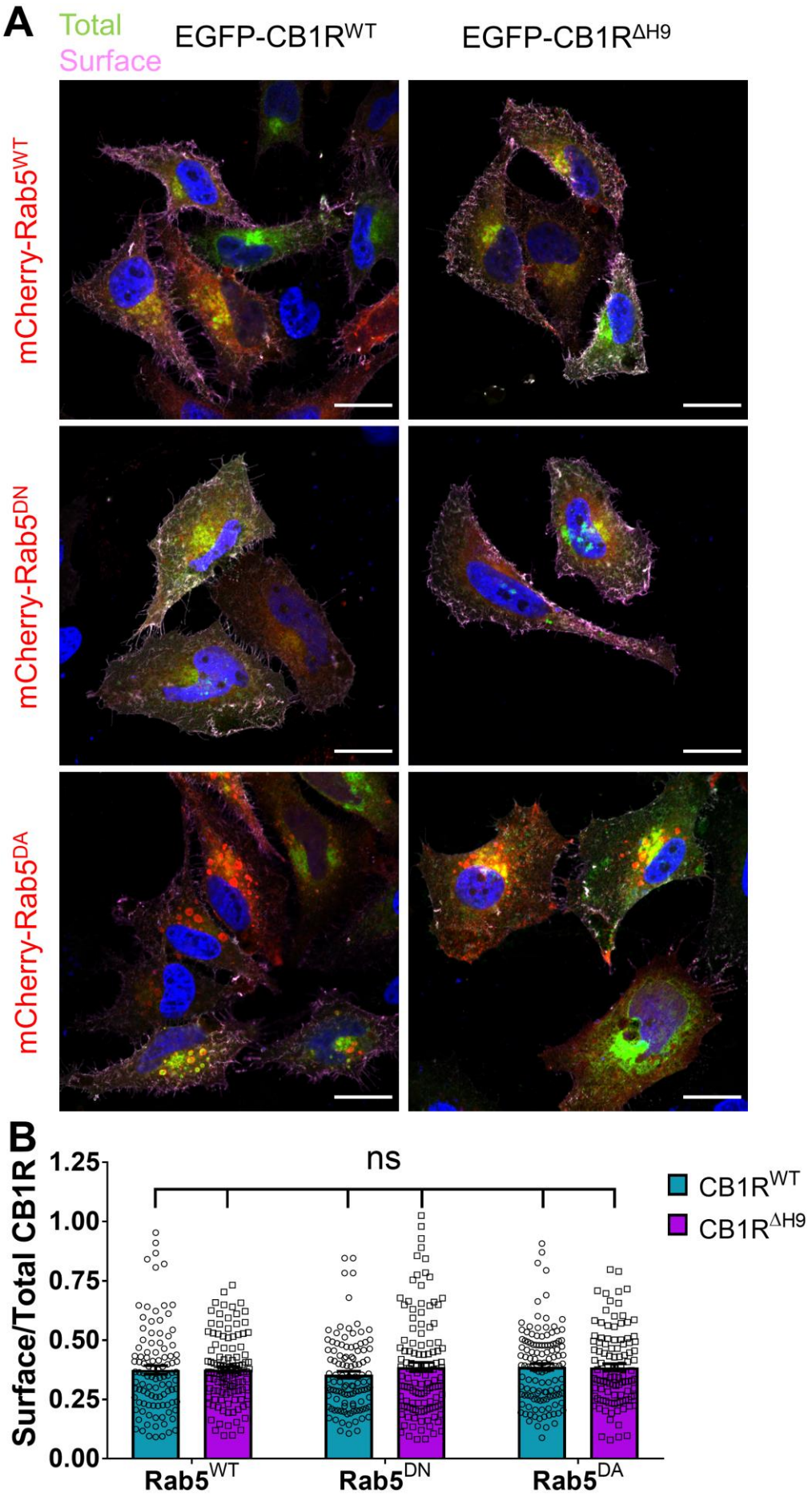
A
Total
Surface
EGFP-CB1R^WT
EGFP-CB1R^ΔH9
mCherry-Rab5^WT
mCherry-Rab5^DN
mCherry-Rab5^DA
B
Surface/Total CB1R
1.25
1.00
0.75
0.50
0.25
0.00
ns
CB1R^WT
CB1R^ΔH9
Rab5^WT
Rab5^DN
Rab5^DA

Figure 5-3 Constitutive endocytosis of EGFP-CB1RWT and EGFP-CB1RΔH9 not regulated by the Rab5 GTPase in HeLa cells.

(**A**) Representative merged confocal images of HeLa cells expressing EGFP-CB1R^{WT} (left panels) or EGFP-CB1R$^{\Delta H9}$ (right panels) and co-expressing either WT Rab5 (mCherry-Rab5; top panels), a dominant-negative (GDP-bound) Rab5 (mCherry-Rab5^{DN}; middle panels), or a dominant-active (GTP-bound) Rab5 (mCherry-Rab5^{DA}; bottom panels). Green = total EGFP-CB1R; magenta = surface EGFP-CB1R; red = mCherry-Rab5; blue = DAPI.

(**B**) Quantification of data presented in (**A**). Analysis of the surface-to-total ratio shows no significant difference between any of the conditions, indicating that EGFP-CB1R endocytosis is not dependent on Rab5 in HeLa cells. Two-way ANOVA with Tukey's *post hoc* test. N = two independent experiments; n = 104-123 cells per condition.

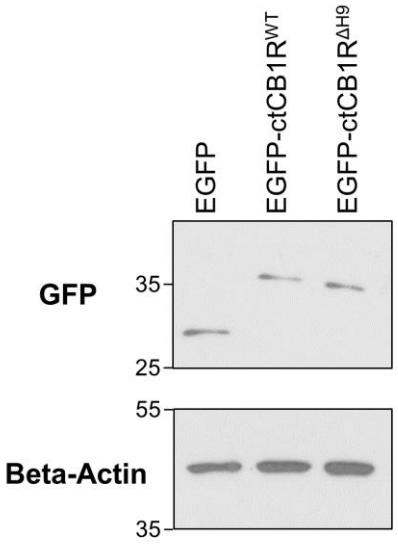

Figure 5-4 The samples sent for proteomics expressed Immunoblots of proteomics lysates.

Immunoblots of lysate used for proteomics blotted for GFP and beta-actin (housekeeping gene). EGFP, EGFP-ctCB1R^{WT} and EGFP-ctCB1R$^{\Delta H9}$ expressed at equivalent levels and contained similar levels of protein.

Table 5-1 Raw proteomics data.

PROTEIN	CTCB1R^{WT}/GFP	CTCB1R$^{\Delta H9}$/GFP	CTCB1R$^{\Delta H9}$/CTCB1R^{WT}
CB1R	13.003	6.618	0.975
CRIP1a	0.927	0.957	1.063

Table 5-2 is a summary of the potential hits. Two hits that were decreased in the ΔH9 samples are potentially involved in polarity. Protein lin-7 homolog A (Lin-7A; aka velis/MALS) belongs to a family of PDZ domain-containing CASK adaptor proteins that are key regulators of cell polarity (van de Pavert et al., 2004). While mostly studied in epithelial cells, Lin-7a has been shown to be enriched in neuronal cell-cell junctions, as well as synapses, both postsynaptically and presynaptically (Perego et al., 2000; Jo et al., 1999; Matsumoto et al., 2014). MAPT (tau) is most famous as a hallmark aggregated protein in several types of dementias, including Alzheimer's disease and frontotemporal dementia. However, physiological tau is an axonally localised microtubule stabiliser (Drechsel et al., 1992; Weingarten et

al., 1975) and plays a role in axonal transport (Vershinin et al., 2007; Butzlaff et al., 2015). Further studies are needed to examine what role these proteins play in CB1R polarity.

A few potential hits are involved in endocytosis. Firstly, as mentioned above, CRIP1a, which regulates constitutive endocytosis of CB1R, was equally present in both WT and ΔH9 samples, presumably because it binds to the last 9 amino acids. Interestingly, all the subunits of AP-2 (μ, α2, β, σ), the adaptor complex that controls clathrin-mediated endocytosis (Rappoport, 2008), were moderately enriched in the ΔH9 sample compared to the WT sample. Lastly, Src homology 3-domain growth factor receptor-bound 2-like (endophilin) interacting protein 1 (SGIP1) was moderately decreased in the ΔH9 sample compared to WT sample.

5.3.5 Mechanisms of endocytosis: SGIP1

I followed up on SGIP1 for several reasons:

1. SGIP1 has previously been shown to bind to ctCB1R. The exact site is not known, but it binds C-terminally of *H8* (Hájková et al., 2016).
2. SGIP1 is primarily located presynaptically, colocalising with bassoon and synaptotagmin (Hájková et al., 2016; Lee et al., 2019).
3. Co-expression of SGIP1 and CB1R increases CB1R surface expression.
4. SGIP1 bound ctCB1R$^{\Delta H9}$ less than ctCB1R^{WT} in my proteomics screen.

5.3.5.1 Cloning an SGIP1 overexpression construct

To obtain an SGIP1 overexpression construct, I designed primers for the start and end of the mRNA sequence for Rat SGIP1 available on Uniprot. I then extracted the SGIP1 sequence from a cDNA library derived from mRNA extracted from DIV 21 primary cortical neurons by PCR amplification. I cloned this sequence into pFLAG in order to add an N-terminal FLAG tag. The sequence of the construct I extracted corresponded to predicted SGIP1 transcript variant X21 (NCBI; **Figure 5-5**). This 660-amino acid variant differs from the full-length Uniprot version by two deletions: a single residue deletion in the membrane phospholipids binding domain (MP; Q34) and a 165-residue deletion in the proline-rich domain (PRD). Given that this variant was directly extracted from our primary neuronal cultures it is likely to be the dominant form expressed in our system. Throughout this chapter, I will refer to this this variant as SGIP1β.

Table 5-2 Summary of proteomics: list of potential ctCB1R interactors

PROTEIN	REFERENCE	$ctCB1R^{\Delta H9}$/ $ctCB1R^{WT}$	KNOWN FUNCTION(S)	BINDING SITE ON CB1R
Protein lin-7 homolog A	N/A	↓ 0.784	Polarity complex involved in asymmetric distribution of channels and receptors at the cell membrane.	Not known
MAPT (Tau)	N/A	↓ 0.866	Axonally localised microtubule stabiliser. Implicated in neurodegenerative disease.	Not known
CRIP1a	(Niehaus et al., 2007; Mascia et al., 2017)	- 1.063	Inhibits constitutive endocytosis of CB1R. Selectively blocks agonist induced signalling.	Last 9 aa
AP-2 μ subunit	N/A	↑ 1.321	Endocytosis - interacts with accessory proteins required for clathrin assembly.	Not known
AP-2 α2 subunit		↑ 1.370		
AP-2 β subunit		↑ 1.168		
AP-2 σ subunit		↑ 1.120		
SGIP1	(Hájková et al., 2016; Lee et al., 2019)	↓ 0.790	Endocytic adaptor – widely distributed but enriched in axon terminals. Interferes with CB1R internalization and signalling.	Not known; C-terminally of *H8*

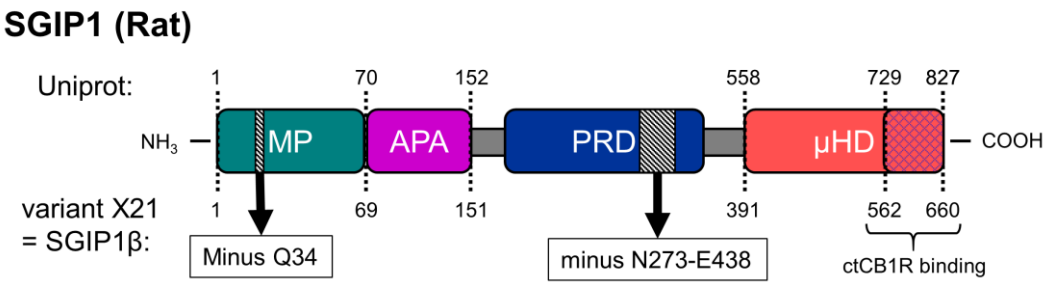

Figure 5-5 Schematic of SGIP1 isoform, designated as SGIP1β.

Predicted SGIP1 transcript variant X21 was cloned out of a cDNA library extracted from rat primary cortical cultures. This variant of SGIP1, named SGIP1β, is 660 amino acids long. This variant differs from the "full-length" variant on Uniprot (which corresponds to predicted transcript variant X10) by two deletions – a single residue deletion (Q34) in the MP domain and a 165-residue deletion in the PRD (black hatched regions). The blue cross-hatched region in the μHD indicates the area where that binds ctCB1R (Hájková et al., 2016). MP = membrane phospholipids binding domain; APA = AP-2 Activator motif; PRD = Proline-Rich Domain; μHD = μ Homology Domain.

5.3.5.2 SGIP1β increases CB1R surface expression independently of H9 in HEK293T cells.

Firstly, I attempted to replicate the results from (Hájková et al., 2016). I co-expressed EGFP-CB1R^{WT} (without the SBP tag) and either FLAG-SGIP1β or empty FLAG vector in HEK293T cells. I then used surface biotinylation to separate surface and total fractions to determine the effect of FLAG-SGIP1β co-expression on surface levels of CB1R^{WT} (**Figure 5-6**). At the same time, also co-expressed EGFP-CB1R$^{\Delta H9}$ with FLAG or FLAG-SGIP1β. If *H9* is the binding site of SGIP1β, then co-expression of FLAG-SGIP1β should have no effect on the surface expression of the mutant.

However, I found that co-expression of FLAG-SGIP1β increased both EGFR-CB1R^{WT} and EGFP-CB1R$^{\Delta H9}$ surface expression at steady state (**Figure 5-6 B**), indicating that SGIP1 increases CB1R surface expression independently of *H9*.

As a control, I also blotted for EGFR, which has been previously shown to be more surface expressed with SGIP1 overexpression (Uezu et al., 2007). However, for EGFP there was only a non-significant trend to increased surface-to-total ratio with FLAG-SGIP1β overexpression (**Figure 5-6 C**).

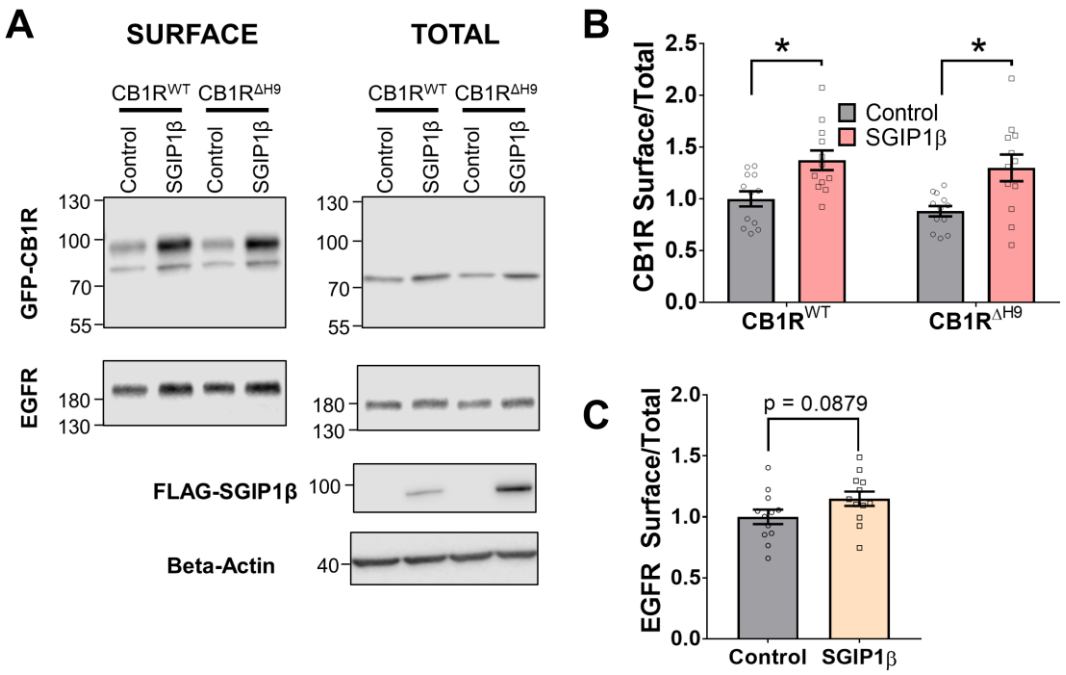

Figure 5-6 SGIP1β increases CB1R surface expression independently of *H9* in HEK293T cells.

(**A**) Representative immunoblots from surface biotinylation experiments showing surface and total fractions of EGFP-CB1R^{WT} or EGFP-CB1R$^{\Delta H9}$ and EGFR in HEK293T cells. EGFP-CB1R was co-expressed with either an empty FLAG control or FLAG-SGIP1β.

(**B**) Quantification of data shown in (**A**). Co-expression with FLAG-SGIP1β increased the surface expression of both EGFP-CB1R^{WT} and EGFP-CB1R$^{\Delta H9}$. Two-way ANOVA with Sidak's *post hoc* test. N = twelve independent experiments.

(**C**) Quantification of data shown in (**A**). Expression of FLAG-SGIP1β non-significantly increased EGFR surface expression. Each experiment is the average value between WT vs. ΔH9 samples. Unpaired t-test. N = twelve independent experiments.

5.3.5.3 SGIP1 knockdown reduces surface expression of CB1R^{WT}, but not CB1R$^{\Delta H9}$ in primary hippocampal neurons.

Although HEK293T cells are a useful model they lack the complexity and polarity of neurons. I therefore next determined the role of SGIP1 in CB1R surface expression in hippocampal neurons. I generated an shRNA knockdown construct targeting SGIP1 using the 25mer sequence from (Uezu et al., 2007) that targets all known isoforms of SGIP1. This shRNA sequence knocked down overexpressed FLAG-SGIP1β by 88% compared to a non-targeting 29mer scrambled control (SCR29) when co-transfected into HEK293T cells (**Figure 5-7 A-B**).

I next added the SGIP1-targeting shRNA or SCR29 to pXlg3-EGFP-CB1R^{WT} and -CB1R$^{\Delta H9}$ and transfected DIV 9 hippocampal neurons with the constructs, left them for 5 days to ensure efficient knockdown, then surface stained using anti-GFP

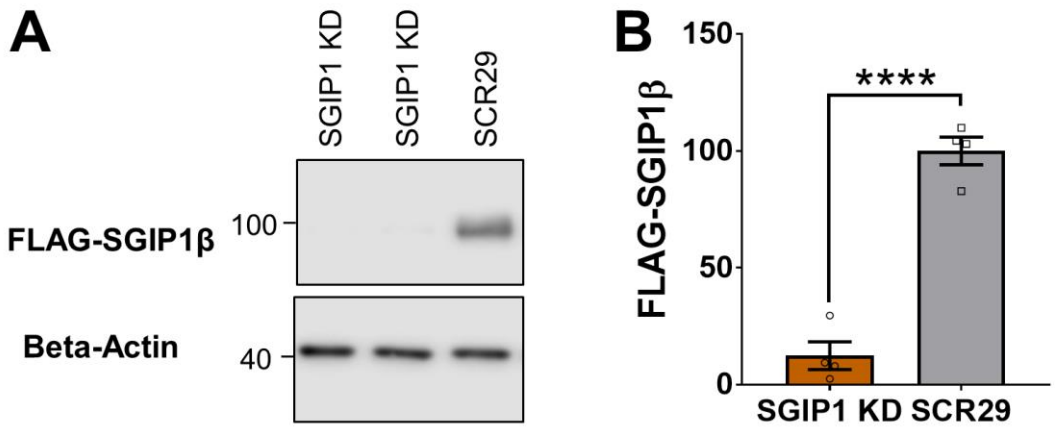

Figure 5-7 Validation of SGIP1 shRNA knockdown.

(**A**) Representative immunoblots showing shRNA knockdown (KD) of overexpressed FLAG-SGIP1β and a beta-actin housekeeping control in HEK293T cells. The first two lanes are duplicate SGIP1 KD conditions. FLAG-SGIP1β and SGIP1-targeting shRNA or SCR29 control shRNA were co-transfected into HEK293T cells and left for 3 days.

(**B**) Quantification of data represented in (**A**). A 25mer shRNA targeting SGIP1 knocked down overexpressed FLAG-SGIP1β by about 88% compared to a scrambled (non-targeting) 29mer control (SCR29).

antibody (**Figure 5-8 A**). Because the shRNA and overexpression cassettes are on the same plasmid, any neuron expressing EGFP-CB1R must also be expressing SCR29 or SGIP1 KD. However, I was not able to unequivocally confirm SGIP1 knockdown because commercial SGIP1 antibodies have only recently been developed and marketed (Lee et al., 2019) and were not available and validated when I was performing these experiments.

Intriguingly, SGIP1 KD reduced the surface expression of EGFP-CB1R^{WT} to levels similar to that of the mutant EGFP-CB1R$^{\Delta H9}$ in both axons (**Figure 5-8 B**) and dendrites (**Figure 5-8 C**) compared to the SCR29 control. Importantly, this reduction of surface expression was occluded for EGFP-CB1R$^{\Delta H9}$ where there was no significant further reduction by SGIP1 KD on surface expression in either axons (**Figure 5-8 B**) and dendrites (**Figure 5-8 C**) compared to the SCR29 control.

These data strongly suggest that the reduced surface expression phenotype of the ΔH9 mutant is due to an inability of SGIP1 to bind in neurons, even though it can bind in HEK293T cells. Although more work is needed, my current interpretation of these results is that the binding may not be direct, or SGIP1 competes for binding with a third-party present in primary hippocampal neurons but not HEK293T cells.

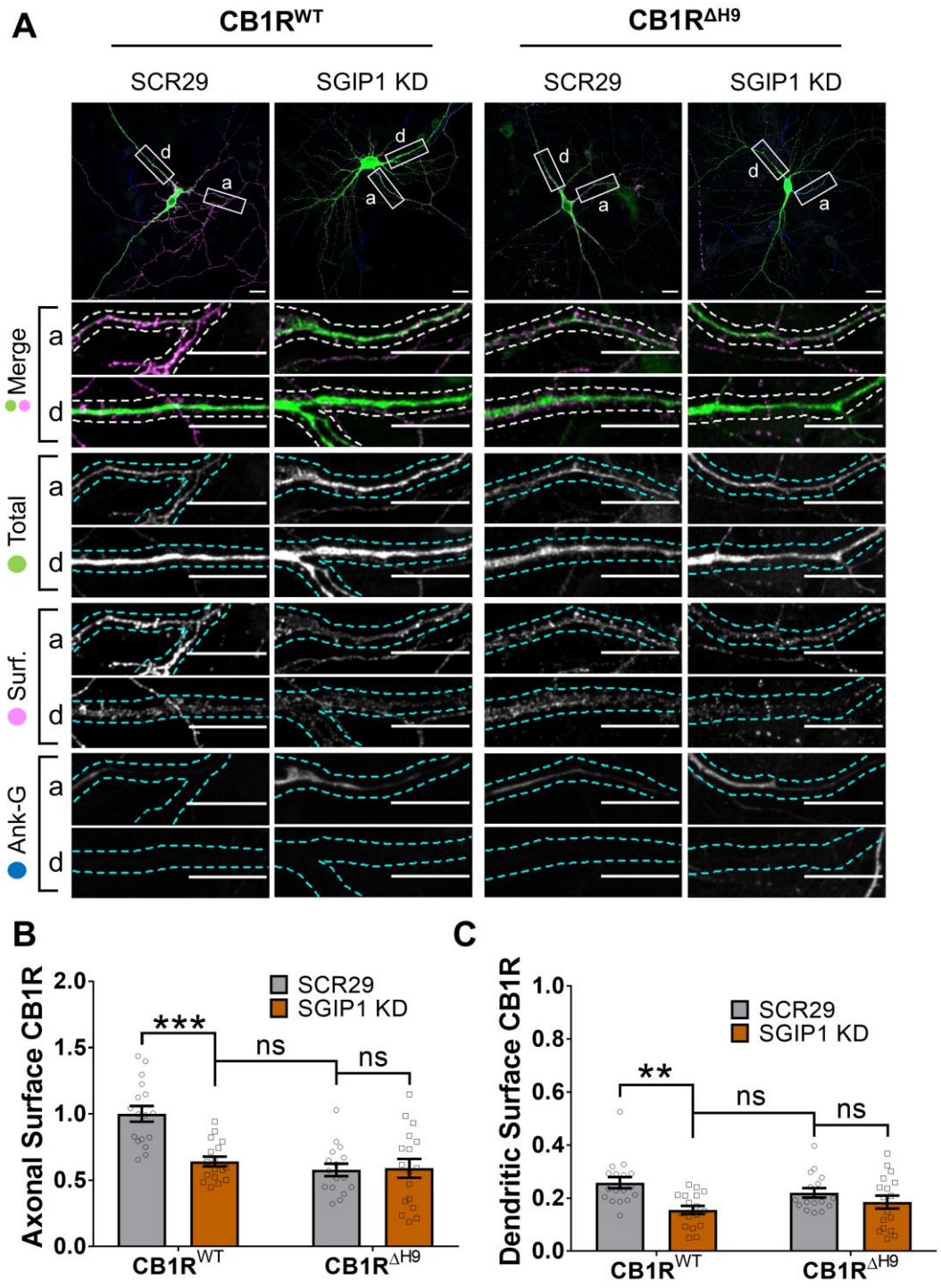

Figure 5-8 SGIP1 KD reduces surface expression of CB1R^{WT}, but not CB1R$^{\Delta H9}$.

(**A**) Representative confocal images of DIV 14 hippocampal neurons expressing EGFP-CB1R^{WT} or EGFP-CB1R$^{\Delta H9}$ and either a 25mer shRNA targeting SGIP1 (SGIP1 KD) or a non-targeting scrambled 29mer control (SCR29). Cells were transfected at DIV 9 and left for 5 days to ensure knockdown then surface stained with anti-GFP antibody. Upper panels for each condition show whole cell field of view and lower panels are enlargements of axonal (a) and dendritic (d) ROIs. Green = total; magenta = surface; blue = axon marker (Ankyrin-G). Merge: surface to total seen as white.

(B and C) Quantification of data represented in (**A**). In axons (**B**) and in dendrites (**C**), knockdown of SGIP1 causes a significant reduction in surface expression of EGFP-CB1R^{WT} identical to the reduced surface expression phenotype of EGFP-CB1R$^{\Delta H9}$. The effect of SGIP1 KD is occluded for EGFP-CB1R$^{\Delta H9}$. Two-way ANOVA with Sidak's *post hoc* test. N = three independent experiments; n = 18-19 neurons per condition.

5.4 DISCUSSION

5.4.1 Summary of results

In this chapter, I attempted to determine by what mechanism *H9* stabilises CB1R at the membrane. Firstly, I attempted to narrow down the characteristics necessary of *H9* to mediate its effect. I inserted two bulky proline residues into *H9* in order to prevent it from forming an α-helix. I also mutated a potentially modifiable cysteine residue to alanine. I found that both modifications caused a reduction in surface expression of CB1R identical to the phenotype of deleting *H9* (**Figure 5-1**). These data indicate that the C450 residue and the α-helical nature of *H9* is necessary for its function.

Next, I searched for interacting proteins of *H9* that may mediate surface expression. I found that knocking down SGIP1 resulted in a phenotype identical to deletion of *H9* – reduced surface expression of $CB1R^{WT}$ in both axons and in dendrites (**Figure 5-8**). Furthermore, this effect was occluded for $CB1R^{\Delta H9}$ (**Figure 5-8**), signifying that *H9* interacts with SGIP1 to stabilise CB1R at the surface of hippocampal neurons.

5.4.2 CB1R and Rab5

CB1R has previously been reported to be internalised in a Rab5-dependent manner in both HEK293T cells and primary hippocampal neurons (Leterrier et al., 2004, 2006). I was unable to replicate this result (**Figure 5-3**). However, I used HeLa cells rather than HEK293T cells because they are more conducive to confocal imaging. Furthermore, closer examination of the $CB1R^{WT}$/$Rab5^{DA}$ condition does reveal visible co-localisation (**Figure 5-9**), even though it did not translate into reduced surface expression (**Figure 5-3**).

Reproducibility in the CB1R trafficking field has been plagued by the problem that different cell lines produce different results. This may be in part due to a misinterpretation of the difference between CB1R intrinsic constitutive activity and constitutive agonist-induced activation (Turu and Hunyady, 2010; Ladarre and Lenkei, 2017). CB1R is thought to be an intrinsically constitutively active receptor due to instability in its 'ionic lock' holding it in the inactive conformation (D'Antona et al., 2006). This seems to be confirmed by the fact that in cell lines and in native tissues, CB1R shows a high degree of activity that can be blocked by application of inverse agonists (Pertwee, 2005). However, because 2-AG is produced by a

common lipid metabolism pathway it is present in most tissues (Sugiura et al., 2004), indicating that what is thought to be intrinsic constitutive activation of the receptor may actually be due to tonic levels of eCBs (Turu and Hunyady, 2010; Ladarre and Lenkei, 2017). Therefore, different cell lines may contain different levels of eCBs, affecting CB1R signalling and trafficking. It is possible that HeLa cells contain lower levels of eCBs, resulting in lower levels of Rab5 mediated internalisation that were undetectable in my experimental setup. More experiments will be needed, preferentially in primary hippocampal neurons, to examine the role of Rab5 in CB1R internalisation.

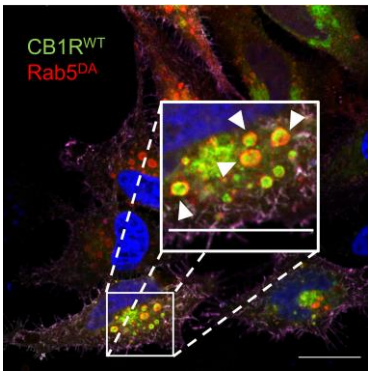

Figure 5-9 CB1R^{WT} visibly colocalises with Rab5^{DA}.

Enlargement of HeLa cell co-expressing EGFP-CB1R^{WT} and mCherry-Rab5^{DA} (dominant active) reveals visible colocalization (white arrows heads).

Green = total EGFP-CB1R; magenta = surface EGFP-CB1R; red = mCherry-Rab5; blue = DAPI.

Scale bar = 20 µm.

5.4.3 SGIP1: role in endocytosis

I show that knockdown of SGIP1 recapitulates the phenotype of CB1R$^{\Delta H9}$ and that this effect is occluded in neurons expressing the mutant (**Figure 5-8**). However, co-expression of FLAG-SGIP1β and EGFP-CB1R^{WT} or -CB1R$^{\Delta H9}$ in HEK293T cells resulted in an identical increase in surface expression of CB1R (**Figure 5-6**), indicating that SGIP1β can bind CB1R$^{\Delta H9}$. These data suggest that the effect of SGIP1 knockdown may be neuron-specific, potentially involving an additional interacting protein.

If SGIP1 is a member of the clathrin-mediated endocytosis complex, why does SGIP1 overexpression *prevent* CB1R internalisation (**Figure 5-6**) whereas knockdown *increases* CB1R internalisation (**Figure 5-8**)? (Hájková et al., 2016) suggest that SGIP1 competes for binding with FCHo1/2 proteins. SGIP1 and FCHo1/2 members of the muniscin family of cargo adapters, containing an N-terminal membrane biding domain, an AP-2 activator domain, a proline rich domain, and a C-terminal µ homology domain (Hollopeter et al., 2014; Dergai et al., 2010). However, the membrane binding domain of FCHo1/2 is an F-BAR domain capable of plasma membrane shaping during pit formation, while the MP

domain of SGIP1 has no sequence similarity suggesting that due to differential membrane binding, it may act as a kind of 'dominant negative' to the rest of the muniscin family. Alternatively, SGIP1 interacts with endophilin 3, which has been suggested to actually inhibit endocytosis (Zhang et al., 2015; Sugiura et al., 2004).

On the other hand, knockdown of SGIP1 has been reported to selectively *impair* internalisation of the pre-synaptic protein synaptotagmin during synaptic vesicle recycling (Lee et al., 2019). Other synaptic vesicle proteins including synaptophysin and VAMP2 were not affected by SGIP1 knockdown (Lee et al., 2019). SGIP1 also reportedly activates AP-2 (Hollopeter et al., 2014) and is actually capable of membrane tubulation (Uezu et al., 2007). More experiments are required to resolve this issue.

5.4.4 Mechanism of preferential delivery

While most data in this chapter has focused on the mechanism behind *H9*-mediated membrane retention, I also found that *H9* plays a role in the preferential delivery of CB1R from the secretory pathway to the axonal membrane. While I show very preliminary evidence confirming previous results that knocking down AP-3 results in a nonpolarized distribution of CB1R (**Figure 5-2**; (Rozenfeld and Devi, 2008)), more targeted approaches are needed to examine the role of H9 and AP-3 in CB1R trafficking. For example, co-immunoprecipitation experiments could determine whether $CB1R^{WT}$ and/or $CB1R^{\Delta H9}$ binds to AP-3. RUSH could also be used to determine whether co-localisation of CB1R and AP-3 at the TGN, indicating a role for AP-3 in sorting CB1R to the axonal membrane (Li et al., 2016).

Furthermore, my proteomics screen highlighted Lin-7A as a potential *H9* interactor. Interestingly, Lin7a belongs to a family of PDZ domain-containing CASK adaptor proteins that are key regulators of cell polarity (van de Pavert et al., 2004). This hit would first need to be validated by co-immunoprecipitation experiments with $ctCB1R^{WT}$ and $ctCB1R^{\Delta H9}$. Next, CB1R surface distribution could be examined in the presence of Lin-7a knockdown or overexpression.

5.5 Conclusion

Taken together, these data reaffirm the importance of *H9* in membrane stability of CB1R and indicate that the mechanism is likely due to 1) the presence of a cysteine residue and 2) interaction with SGIP1.

Chapter 6 – General Discussion

6.1 Summary

In this thesis, I have examined the trafficking of CB1R using the time-resolved RUSH assay. I have presented several advances in our understanding of CB1R trafficking, which are listed below.

1. **Newly synthesised CB1R is preferentially delivered to the axonal membrane by the secretory pathway.**
    - Following release from the secretory pathway, SBP-EGFP-CB1R^{WT} rapidly entered the axon (**Figure 3-8**).
    - SBP-EGFP-CB1R^{WT} was delivered to the axonal membrane quicker and at higher levels than to the dendritic membrane (**Figure 3-10**).
2. **Newly synthesized CB1R is preferentially retained at the surface of axons and removed from the surface of dendrites.**
    - SBP-EGFP-CB1R^{WT} that was delivered to the dendritic surface was not retained at the dendritic surface (**Figure 3-11**).
3. **CB1R is trafficked by the canonical, somatodendritic secretory pathway.**
    - During ER retention, no SBP-EGFP-CB1R^{WT} was detected in axons (**Figure 3-8**).
    - Blocking the Golgi prevented CB1R from entering the axon or going to the plasma membrane (**Figure 3-13**).
4. **The carboxy terminal domain of CB1R (ctCB1R) plays a role in axonal polarisation.**
    - A chimera of non-polarised transmembrane protein CD4 fused to ctCB1R (CD4-ctCB1R^{WT}) was more axonally polarised in both total and surface distribution than CD4 alone (**Figure 4-2**).
5. **ctCB1R triggers constitutive (i.e. activity-independent) internalisation specifically in dendrites but not axons, independently of *H9*.**
    - CD4-ctCB1R^{WT} and CD4-ctCB1R$^{\Delta H9}$ chimeras internalised more than CD4 in dendrites than in axons (**Figure 4-3**).

6. ***H9* plays a role in trafficking of total CB1R to the axon. However, *H9* is not necessary for full-length CB1R total polarisation, indicating the presence of compensatory motifs/pathways of CB1R axonal entry.**
    - The CD4-ctCB1R$^{\Delta H9}$ chimera did not display axonal polarisation of total protein; CD4-ctCB1R^{WT} did (**Figure 4-2**).
    - Newly synthesised SBP-EGFP-CB1R$^{\Delta H9}$ entered the axon slower than SBP-EGFP-CB1R^{WT} (**Figure 4-5 A**).
    - However, there was no difference in total polarisation between EGFP-CB1R^{WT} and EGFP-CB1R$^{\Delta H9}$ at steady state (**Figure 4-6 D**).
7. ***H9* mediates polarised delivery of newly synthesised CB1R.**
    - More newly synthesised SBP-EGFP-CB1R$^{\Delta H9}$ than -CB1R^{WT} was delivered to the dendritic membrane. There was no difference in delivery to the axonal membrane. (**Figure 4-5 C-E**)
    - EGFP-CB1R$^{\Delta H9}$ displayed a reduced axonal surface polarity when agonist-induced internalisation was blocked with inverse agonist treatment (**Figure 4-10**).
8. ***H9* stabilises CB1R at the surface in both axons and dendrites, preventing agonist-induced endocytosis.**
    - EGFP-CB1R$^{\Delta H9}$ was less surface expressed and more internalised than EGFP-CB1R^{WT} in both axons and dendrites (**Figure 4-10 B**). However, there was no difference in surface expression in HEK293T cells (**Figure 4-8 D-E**).
    - EGFP-CB1R$^{\Delta H9}$ showed a higher level of agonist-induced endocytosis than EGFP-CB1R^{WT} in axons (**Figure 4-9**).
    - Treatment with inverse agonist increased EGFP-CB1R$^{\Delta H9}$ surface expression in both axons and dendrites. There was no difference in EGFP-CB1R^{WT} surface expression with inverse agonist treatment. (**Figure 4-10**).
9. ***H9* modulates downstream signalling of CB1R.**
    - EGFP-CB1R$^{\Delta H9}$ activated ERK1/2 to a lesser degree with ACEA treatment than EGFP-CB1R^{WT} (**Figure 4-8**).
10. **The helicity of *H9* is important for its function.**
    - Perturbing *H9* by the addition of ‘forbidden’ prolines resulted in a similar phenotype of reduced surface expression as deleting *H9* (**Figure 5-1**).

11. **Residue C450 of *H9* is important for its function.**
    - Perturbing *H9* by mutating C450 to an alanine residue resulted in a similar phenotype of reduced surface expression as deleting *H9* (**Figure 5-1**).

12. **In neurons, interaction between SGIP1 and *H9* (likely) stabilises CB1R at the surface and prevents agonist-induced endocytosis.**
    - Knocking down SGIP1 resulted in the same phenotype of reduced surface expression as deletion of *H9*. The effect of knocking down SGIP1 on surface expression was occluded in the ΔH9 mutant (**Figure 5-8**).
    - However, in HEK293T cells, overexpression of SGIP1β increased surface expression of both EGFP-CB1R^{WT} and EGFP-CB1R$^{\Delta H9}$ (**Figure 5-6**).

6.2 Model of CB1R polarity

6.2.1 Proposed models of CB1R polarity

Three groups have proposed three different models for how CB1R axonal surface polarity is established and maintained (for details see 1.3.6 Three currently proposed models of CB1R polarity):

1. **Lenkei group:** non-polarised delivery to surface followed by differential endocytosis from dendritic vs. axonal compartments driven by the constitutive presence of 2-AG in the dendritic membrane. Internalised dendritic receptors are then trafficked to distal axons via transcytosis (Thibault et al., 2013; Simon et al., 2013; Ladarre et al., 2015; Ladarre and Lenkei, 2017; Leterrier et al., 2004, 2006).
2. **Irving group:** polarity is driven by constitutive (i.e. activity-independent) internalisation of dendritic CB1R and retention of axonal CB1R (McDonald et al., 2007a).
3. **Devi group:** dendritic CB1R is not targeted to the surface, but rather sent immediately for degradation. Under unknown conditions, CB1R can be rerouted to axons (Rozenfeld and Devi, 2008; Rozenfeld, 2011).

6.2.2 Updated model of CB1R polarity

Using a genetically-targeted and time-resolved approach, I found that newly synthesised CB1R is preferentially delivered to the axonal membrane by the secretory pathway. Nevertheless, a small proportion of CB1R is delivered to the

dendritic membrane, from which it is immediately removed. Internalised somatodendritic CB1R may then be rerouted to the axon, as proposed by the Lenkei group, or degraded.

I show that ctCB1R mediates polarisation independently of CB1R activation, since the CD4-ctCB1R chimera was both polarised to the axonal compartment and differentially internalised in dendrites vs. axons. However, surface polarisation of this chimera was not complete, there was still CB1R present on the dendritic surfaced, indicating that agonist-induced internalisation may play a role in furthering CB1R polarity following the establishment of polarity by decreased delivery to the dendritic membrane and constitutive endocytosis.

6.2.2.1 The role of tonic agonist-driven internalisation in CB1R trafficking

The disagreement between the Lenkei group and the Irving group about whether internalisation of dendritic CB1R is agonist-induced or constitutive, respectively, comes from the observation that incubation with AM281, an inverse agonist of CB1R, results in increased dendritic surface expression of CB1R for the Lenkei group (Leterrier et al., 2006) and no difference in CB1R surface expression for the Irving group (McDonald et al., 2007a).

Here, I found that incubation with AM281 resulted in an ultimately non-significant trend to increased dendritic surface expression of EGFP-CB1R^{WT} (**Figure 4-10**). However, there was a significant increase in dendritic surface expression of EGFP-CB1R$^{\Delta H9}$ with AM281 incubation.

Importantly, the Lenkei group use a C-terminally tagged CB1R construct whereas the Irving group and I use an N-terminally tagged CB1R construct. C-terminally tagged constructs can interfere with C-terminal binding proteins. Indeed, two ctCB1R binding proteins that prevent agonist-induced internalisation have been described: CRIP1a (Blume et al., 2016) and SGIP1 (Hájková et al., 2016). Furthermore, direct comparison between an N-terminally tagged CB1R construct and a C-terminally tagged construct revealed that the C-terminally tagged construct showed 2-3-fold increase in surface expression compared to N-terminally tagged construct in HEK293 cells and N2A cells (Rozenfeld and Devi, 2008). The fact that Lenkei's C-terminally construct act more like my mutant ΔH9 construct than the WT construct suggests that the C-terminal tag is, perhaps, disrupting the same interaction that is disrupted by deleting *H9*.

To examine this further, I searched the literature for examples where surface localisation was examined after incubation with inverse agonist. **Table 6-1** consists of a table of the results, including an rough estimate of the effect size observed (updated from table presented in (Rozenfeld, 2011)). Firstly, there was a huge range of effect sizes, due to a large range of cell types, inverse agonist type and concentration, and time scales used. However, focussing firstly on experiment in primary neurons, it is clear that there is a difference in effect size depending on the tag used: C-terminally tagged CB1R shows effect sizes of around 170-200%, whereas N-terminally tagged CB1R either shows no increase or smaller effect sized (no more than 133%). Indeed, even within the Lenkei group, the effect size seen for endogenous CB1R is far smaller than the effect size for C-terminally tagged exogenously expressed protein. A similar pattern is seen in HEK293 cells – the is an exaggerated phenotype with C-terminally tagged construct compared to the N-terminally tagged construct. Furthermore, in N18TG2 cells, which endogenously express both CB1R and CRIP1a, the inverse-agonist-induced increase in surface expression was small and transient, returning to basal levels after 60 minutes (Blume et al., 2016). These data indicate that the role of agonist-induced internalisation in CB1R polarity has been exaggerated due to the C-terminal tag perturbing the role of the C-terminus in trafficking.

Consistent with their observations, the Lenkei group also reported a high amount of internalisation in dendrites compared to axons as well as non-polarised delivery after BFA retention and release assay (Leterrier et al., 2006). This phenotype is more consistent with my ΔH9 mutant, which is trafficked more to the surface of dendrites than WT CB1R and is then is subsequently more internalised in my more targeted RUSH approach. Furthermore, they observed Rab5 dependent constitutive internalisation of CB1R-GFP in HEK293 cells (Leterrier et al., 2004), a finding that I could not replicate with my EGFP-CB1R in HeLa cells (**Figure 5-3**). I therefore suggest that the C-terminal tag interferes with both TGN sorting and internalisation, causing increased delivery to dendrites and increased internalisation analogous to perturbation of ctCB1R by *H9* deletion.

Therefore, polarity is established from the outset due to preferential delivery to the axonal compartment and decreased delivery to the dendritic compartment. Dendritic CB1R is removed from the surface by a combination of constitutive internalisation and a small amount of agonist-induced internalisation.

Table 6-1 Summary of experiments examining the effect of inverse agonist on CB1R trafficking.

INVERSE AGONIST AFFECT SURFACE EXPRESSION?	TAG	CELL TYPE	INVERSE AGONIST	TIME	REFERENCE
Trend 122%	N-tagged GFP	Primary neurons	10 µM AM281	3 hr	This thesis
No	N tagged GFP, endogenous	Primary neurons	10 µM AM281 SR-141716A	3 hr, 24 hr 18hr	(McDonald et al., 2007a)
No	Endogenous	Primary neurons, F-11 cells	SR-141716A	16 hr	(Coutts et al., 2001)
Yes ~ 132%	Endogenous	Primary neurons	10 µM AM281	3 hr	(Leterrier et al., 2006)
Yes ~ 171%	C-tagged GFP N-tagged FLAG	Primary neurons	10 µM AM281	3 hr	(Leterrier et al., 2006)
Yes ~200	C-tagged GFP N-tagged FLAG	Primary neurons	WT vs. inactive mutant	N/A	(Simon et al., 2013)
ΔH9 mutant: Yes 215%	N-tagged GFP	Primary neurons	10 µM AM281	3 hr	This thesis
Yes: transient peak 133%, returns to basal after 60 min	Endogenous	N18TG2	10 nM SR-141716A	5 min – 114% 15 min – 133% 60 min – 106%	(Blume et al., 2016)
Yes: 220% (also increase in total)	Endogenous	Neuro-2a	1 µM SR-141716A	5 hr	(Grimsey et al., 2010)
Yes: 175% (also increase in total)	N-tagged HA	AtT-20	1 µM SR-141716A	5 hr	(Grimsey et al., 2010)

No	N-tagged HA	HEK293	100 nM SR141716	45 min	(Wickert et al., 2018)
Yes: 150% (also increase in total)	N-tagged HA	HEK293	1 µM SR-141716A	5 hr	(Grimsey et al., 2010)
Yes ~ 600%	C-tagged CFP	HEK293	SR-141716A	3 hr	(Ellis et al., 2006)
Yes ~200%	C-tagged GFP	HEK293	7 µM AM281	3 hr	(Leterrier et al., 2004)
Yes (not quantified, described as "substantial difference")	C-tagged GFP	HEK293	WT vs. inactive mutant	N/A	(D'Antona et al., 2006)
Yes (not quantified, described as "slight but significant")	N-tagged C-myc	CHO cells	50nM SR 141716	30 min, 1 hr, 4 hr, 20 hr	(Rinaldi-Carmona et al., 1998)
Yes: 140% (also increase in total)	N-tagged HA	CHO cells	1 µM SR-141716A	5 hr	(Grimsey et al., 2010)

6.3 *H9* IN CB1R TRAFFICKING AND SIGNALLING

Previously, very little was known about the role of the putative amphipathic helix 9 (Stadel et al., 2011; Ahn et al., 2009b). Here, I show that *H9* plays a role in both the trafficking and signalling of CB1R. *H9* plays a role in forward trafficking of CB1R, restricting delivery of CB1R to the dendritic membrane (**Figure 4-5**). *H9* also prevents agonist-induced internalisation (**Figure 4-6**; **Figure 4-7**; **Figure 4-9**; **Figure 4-10**), potentially by interaction with SGIP1 (**Figure 5-8**).

Deletion of *H9* also causes a reduction of ACEA-induced ERK1/2 activation (**Figure 4-8**). *H9* sits right between the two sets of phosphorylatable sites that regulate desensitisation (central sites) and internalisation (distal sites), suggesting that *H9* may regulate β-arrestin1/2 mediated desensitisation, internalisation, and signalling via ERK1/2 activation (Jin et al., 1999; Kouznetsova et al., 2002; Daigle et al., 2008a; Morgan et al., 2014; Straiker et al., 2012a; Daigle et al., 2008b). Furthermore, analogous *H9* motifs in the bradykinin receptor and squid rhodopsin constitute a $G\alpha_q$ binding site (Piserchio et al., 2005; Murakami and Kouyama, 2008). $G\alpha_q$ activation potentially triggers ERK1/2 phosphorylation as well (Sánchez-Fernández et al., 2014). It would be interesting to determine whether CB1R *H9* also forms a $G\alpha_q$ binding site, especially since CB1R has been shown to signal via $G\alpha_q$ in astrocytes (Navarrete and Araque, 2008). Indeed, I have entirely focussed on trafficking in neurons, but it would be interesting to determine whether the ΔH9 mutant displays a similar reduced surface expression phenotype in astrocytes, especially since it does not in HEK293 cells of HeLa cells (**Figure 4-8**; **Figure 5-3**).

The helicity of *H9* and the presence of residue C450 are important for *H9* function (**Figure 5-1**). Interestingly, this is similar to reported *H8* function: *H8* helicity is dynamic, and it can unravel due to the de-palmitoylation of a nearby cysteine residue (C416), potentially removing some interaction sites, and revealing others (Sensoy and Weinstein, 2015; Gopala Krishna et al., 2002). Therefore, it is possible that the palmitoylation state of C450 is important for *H9* helicity and function. Since H8 is highly conserved in class A GPCRs, but H9 is not, this would add another layer of complexity for CB1R signalling and function. However, firstly it would be necessary to confirm that C450 is palmitoylated as it has been suggested that C416 is the only site of CB1R palmitoylation (Oddi et al., 2012).

6.4 FUTURE DIRECTIONS

6.4.1 Sorting mechanism

While I have shown that CB1R is sorted by the secretory pathway for preferential delivery to the axonal compartment, the sorting mechanism remains unknown. Indeed, comparatively little is known about sorting mechanisms to axons compared to sorting mechanisms to dendrites (Lasiecka and Winckler, 2011; Bentley and Banker, 2016; Bonifacino, 2014). However, relatively recent evidence suggests that AP-3 may mediate axonal secretory vesicle budding from the TGN, analogous to the better understood role of AP-1 and AP-4 in budding of dendritic secretory vesicles (Li et al., 2016; Guardia et al., 2018).

It has been reported that CB1R binds to AP-3 and that knockdown of AP-3 results in a non-polarised surface distribution (Rozenfeld and Devi, 2008), a result that I corroborated in a very preliminary experiment (**Figure 5-2**). However, I found that these neurons also appeared to lack Ankyrin-G staining. While this, in itself, may be interesting, pointing towards a potential role of AP-3 in generating and maintaining the AIS, the disruption of a clearly defined axon does not answer whether CB1R is specifically sorted by AP-3. Therefore, more targeted approaches are needed to examine AP-3/CB1R binding.

One way to do this would be to RUSH $CB1R^{WT}$ and see if it co-localises with AP-3, but not AP-1/4 in the TGN. Indeed, it would be very interesting to co-RUSH $CB1R^{WT}$ and a transmembrane protein that is exclusively somatodendritically polarised to determine at what point they are sorted and diverge in their trafficking.

Another way would be to determine the binding site of AP-3 to CB1R. It is possible that *H9* mediates this interaction seeing as SBP-EGFP-$CB1R^{\Delta H9}$ was missorted to dendritic membrane as well as the axonal membrane, although it does not contain any of the di-leucine or tyrosine-like motifs that usually bind AP-3. Deletion of the AP-3 binding site and RUSHing the mutant would provide insight into the role of AP-3 in the forward trafficking of CB1R.

Lastly, my proteomics screen highlighted Lin-7A as a potential *H9* interactor. Interestingly, Lin7a belongs to a family of PDZ domain-containing CASK adaptor proteins that are key regulators of cell polarity (van de Pavert et al., 2004). This hit would first need to be validated by co-immunoprecipitation experiments with

ctCB1R^{WT} and ctCB1R$^{\Delta H9}$. Next, CB1R surface distribution could be examined in the presence of Lin-7a knockdown or overexpression.

6.4.2 Fate of internalised receptors?

While I have shown that CB1R$^{\Delta H9}$ displays increased internalisation compared to WT, further studies are also needed to determine the fate of the internalised WT and ΔH9 receptors in both dendrites and axons. Studies in cell lines and primary culture suggest that after agonist induced internalisation, CB1R is sent for degradation via GASP1 (Tappe-Theodor et al., 2007; Grimsey et al., 2010; Martini et al., 2007). However, several questions remain: Is the fate of internalised receptors the same in axons vs. dendrites? Are dendritic endosomal CB1Rs rerouted to the axonal surface (transcytosis; (Simon et al., 2013))? Are dendritic endosomal CB1Rs preserved as a discrete signalling pool (Rozenfeld, 2011; Grimsey et al., 2010)?

The degradation of internalised CB1R can be examined by adding lysosomal inhibitors such as bafilomycin or leupeptin to constitutive or agonist-induced endocytosis experiments, staining for a lysosomal marker such as LAMP1, and screening for colocalization with LAMP1 in axons vs. dendrites.

6.4.3 Trafficking to the presynapse

I show that CB1R is preferentially delivered to the axonal compartment. However, once in the axonal compartment it is not known how CB1R is recruited to, and retained at, the presynaptic terminal.

My data showed that SBP-EGFP-CB1R^{WT} was trafficked internally at least 100 µm down the axon 10 minutes before it was delivered to the surface (**Figure 3-12**), indicating that CB1R may traffic to distal areas of the axon intracellularly via secretory vesicles. secretory vesicles traffic to distal areas of the axon.

Alternatively, my data also indicate that CB1R is rapidly surface expressed in the axonal membrane immediately distal to the AIS, a pattern that is not present at steady state, indicative that CB1R preferentially reaches the surface immediately distal to the AIS and then moves along the axon by lateral diffusion (**Figure 3-11**). Therefore, it is possible that, analogous to AMPARs at the postsynapse, CB1Rs in the axonal membrane laterally diffuse until ‘trapped’ at the presynapse (Penn et al., 2017).

One way that CB1R trafficking to distal areas can be tested by live imaging of axons in microfluidic chambers during RUSH release to determine whether SBP-EGFP-CB1R^{WT} fluorescence enters distal areas, including the presynapse, in punctate vesicles (indicative of intracellular secretory vesicular transport mechanism) or as diffuse fluorescence (indicative of lateral diffusion), as has been done recently in a similar experiment with AMPA receptors (Hangen et al., 2018).

6.4.4 The role of ECS and synaptic activity on CB1R forward trafficking

The Henley lab has shown previously using RUSH that activation of receptors at the cell surface can impact the forward trafficking of receptors of the same type (Evans et al., 2017). Interestingly, (Grimsey et al., 2010) reported that in a variety of cells, inverse agonist treatment resulted not only in increased surface expression of CB1R but also increased total expression (**Table 6-1**). Furthermore, blocking synthesis by cycloheximide treatment blocked the inverse-agonist mediated increase of both surface and total expression, indicating that the increase in surface expression is not due to blocking agonist-induced endocytosis, but rather due to the delivery of newly synthesised CB1R (Grimsey et al., 2010). Although I did not observe an increase in axonal surface expression with AM281 incubation, I did observe an increase in total CB1R in axons for both WT and ΔH9 (**Figure 4-10**). It is possible that this increase was made up of newly synthesised receptors being delivered to the axon to repopulate blocked receptors, which would have occurred at a later timepoint. This hypothesis can be tested by concurrently adding cycloheximide to AM281 incubation as well as by extending the timepoints to determine whether axonal surface CB1R increases. If this hypothesis is correct, it would indicate that activation or inactivation of CB1R at the surface affects the forward trafficking of newly synthesised receptors.

The influence of activity on trafficking of CB1R can be tested by treatment with cell permeable and cell impermeable agonists and antagonists of CB1R either during or directly prior to RUSH biotin-mediated release. This is important because is would provide basic molecular understanding of the dynamic regulation of the ECS as well as provide insight of the effect of that cannabinoid intake may have on this system.

Since CB1R acts as a synaptic feedback mechanism and eCBs are produced “on demand” in response to synaptic activity (Kano et al., 2009), it would also be interesting to examine the role of synaptic activity on CB1R forward trafficking.

Treatment with tetrodotoxin (TTX), a potent Na^+ channel blocker, or bicuculine, a $GABA_A$ receptor antagonist, downregulate or upregulates inherent synaptic activity, respectively. Furthermore, synaptic plasticity, both long term potentiation (LTP) and long-term depression (LTD), can be chemically induced in cultured primary neurons. Examining the trafficking of CB1R under these conditions would provide insight into how physiological and pathological synaptic activity impacts CB1R trafficking and surface expression, and therefore function.

6.4.5 SGIP1 and *H9*

I have shown that knockdown of SGIP1 in primary hippocampal neurons reduced the surface expression of CB1R, recapitulating the phenotype of the ΔH9 mutant (**Figure 5-8**). Furthermore, the effect of knocking down SGIP1 on surface expression was occluded in the ΔH9 mutant, strongly suggesting that SGIP1 binds *H9* to prevent agonist-induced internalisation of CB1R. However, in HEK293 cells, co-expression of FLAG-SGIP1β increased surface expression of CB1R independently of *H9* (**Figure 5-6**). Therefore, the next step would be to overexpress FLAG-SGIP1β in primary neuros with either EGFP-$CB1R^{WT}$ or EGFP-$CB1R^{\Delta H9}$. If SGIP1 binding is mediated by *H9* in neurons, then overexpression of FLAG-SGIP1β would increase EGFP-$CB1R^{WT}$, but not EGFP-$CB1R^{\Delta H9}$ surface expression.

Co-immunoprecipitation of EGFP-$CB1R^{WT/\Delta H9}$ and SGIP1 in primary neuronal cultures and GST pulldowns of purified proteins would determine whether SGIP1/H9 binding is direct or indirect. Importantly, SGIP1 has been shown to bind CB1R directly (Hájková et al., 2016).

6.4.6 Functional effects

While I have shown that deletion of *H9* affects trafficking of CB1R in neurons and ERK1/2 signalling in HEK293T cells, I did not have the chance to examine the functional effects of *H9* deletion in primary hippocampal neurons. To do this, I could have measured presynaptic $CB1R^{WT}$ vs $CB1R^{\Delta H9}$ signalling by live cell imaging of eCB-mediated suppression of electrically-evoked presynaptic Ca^{2+} responses (SyGCaMP3) and vesicular neurotransmitter release (SypHy; (Girach et al., 2013; Tang et al., 2015)). Comparing the function of WT and the ΔH9 mutant with application of cell permeable and cell impermeable agonists and antagonists could also potentially provide insight into the role of the endocytic pool in CB1R signalling

since the mutant is more internalised and less surface expressed. Furthermore, the results could be compared to conditions where SGIP1 has been knocked down.

We could also examine the effect of *H9* deletion and SGIP1 knockdown on depolarisation-induced suppression of excitation or inhibition (DSE and DSI), the classical electrophysiological measures of presynaptic CB1R function in neurons (Straiker and Mackie, 2005). These experiments would provide insight into the role of *H9* and SGIP1 on CB1R function.

6.4.7 Therapeutic potential

There has been a lot of interest recently in the possibility of using cannabinoid compounds to treat a range of diseases including epilepsy, chronic pain and inflammation, and multiple sclerosis (Kogan and Mechoulam, 2007). This has led to the legalisation of medical cannabis in 33 US states and the legalisation of a specific cannabinoid-based medication for MS, Sativex, in the UK, as well as the emergence of cannabidiol availability in cafés, vapes, and corner shops. Additionally, there is a substantial academic and commercial interest in the development of new strains of cannabis and synthetic agonists and antagonists. A major focus of research into the endocannabinoid system (ECS) has been understanding its complex pharmacology (Pertwee, 2015). However, cannabinoid-based treatments and clinical trials have been plagued by off target side effects, which does not necessarily come as a surprise given the wide-ranging roles and effects of the ECS in brain function and behaviour (Khurana et al., 2017; Freeman et al., 2019; Johansson et al., 2009; Kaur et al., 2016b; a).

In contrast, relatively little work has been published on CB1R trafficking and the mechanisms and importance of axonal polarisation of the various components of the ECS. However, understanding the molecular mechanisms and protein interactions underpinning CB1R trafficking and surface expression could provide novel targets to enhance or reduce ECS signalling without the need to directly activate or block the receptor.

For example, both SGIP1 and CB1R are strongly associated with diet-induced obesity (DIO; (Trevaskis et al., 2005; Bellocchio et al., 2010; Cardinal et al., 2015). SGIP1 was first discovered because it was upregulated in the hypothalamus of two rodent models of obesity (Trevaskis et al., 2005). Mice lacking CB1R in Sim1-positive glutamatergic paraventricular nucleus (PVN; Sim1-CB1R-KO mice)

neurons are resistant to DIO (Cardinal et al., 2015). Given that overexpression of SGIP1 increases CB1R surface expression (**Figure 5-6**; (Hájková et al., 2016)) and SGIP1 knockdown decreases CB1R surface expression, likely via interaction with *H9* (**Figure 5-8**), I hypothesize that disrupting CB1R/SGIP1 binding in the Sim1-postive PVN neurons would prevent diet induced obesity (DIO).

Therefore, it would be interesting rescue the Sim1-CB1R-KO mice with either $CB1R^{WT}$ or $CB1R^{\Delta H9}$ and/or specifically knock down SGIP1 in Sim1 positive cells compare the phenotype and examine the effect on obesity.

6.5 CONCLUSIONS AND SIGNIFICANCE

In conclusion, the data presented in this thesis has met the original aims of the project, providing novel insight into how CB1R polarised surface distribution is established and maintained. Analysis of ctCB1R has reaffirmed the importance of this region in the forward trafficking and internalisation of the receptor and has uncovered the crucial contribution of the Helix 9 motif to these processes.

Understanding the basic molecular mechanisms and protein interactions that underpin CB1R trafficking has far-reaching therapeutic potential, providing novel targets to enhance or reduce ECS signalling without the need to interfere with its complex pharmacology.

Chapter 7 – REFERENCES

Ahn, K., M.K. McKinney, and B.F. Cravatt. 2008. Enzymatic Pathways That Regulate Endocannabinoid Signaling in the Nervous System. *Chem. Rev.* 108:1687–1707. doi:10.1021/cr0782067.

Ahn, K.H., A.C. Bertalovitz, D.F. Mierke, and D.A. Kendall. 2009a. Dual role of the second extracellular loop of the cannabinoid receptor 1: ligand binding and receptor localization. *Mol. Pharmacol.* 76:833–42. doi:10.1124/mol.109.057356.

Ahn, K.H., M.M. Mahmoud, J.-Y. Shim, and D.A. Kendall. 2013. Distinct roles of β-arrestin 1 and β-arrestin 2 in ORG27569-induced biased signaling and internalization of the cannabinoid receptor 1 (CB1). *J. Biol. Chem.* 288:9790–800. doi:10.1074/jbc.M112.438804.

Ahn, K.H., A. Nishiyama, D.F. Mierke, and D.A. Kendall. 2010. Hydrophobic residues in helix 8 of cannabinoid receptor 1 are critical for structural and functional properties. *Biochemistry*. 49:502–11. doi:10.1021/bi901619r.

Ahn, K.H., M. Pellegrini, N. Tsomaia, A.K. Yatawara, D.A. Kendall, and D.F. Mierke. 2009b. Structural Analysis of the Human Cannabinoid Receptor One Carboxyl-Terminus Identifies Two Amphipathic Helices. *Biopolymers*. 91:565–573. doi:10.1002/bip.21179.

Allen, J.A., R.A. Halverson-Tamboli, and M.M. Rasenick. 2007. Lipid raft microdomains and neurotransmitter signalling. *Nat. Rev. Neurosci.* 8:128–140. doi:10.1038/nrn2059.

Andersson, H., A.M. D'Antona, D.A. Kendall, G. Von Heijne, and C.-N. Chin. 2003. Membrane assembly of the cannabinoid receptor 1: impact of a long N-terminal tail. *Mol. Pharmacol.* 64:570–7. doi:10.1124/mol.64.3.570.

Andréasson, S., P. Allebeck, and U. Rydberg. 1989. Schizophrenia in users and nonusers of cannabis. *Acta Psychiatr. Scand.* 79:505–510. doi:10.1111/j.1600-0447.1989.tb10296.x.

Antoni, F.A. 2012. New paradigms in cAMP signalling. *Mol. Cell. Endocrinol.* 353:3–9. doi:10.1016/J.MCE.2011.10.034.

Araque, A., P.E. Castillo, O.J. Manzoni, and R. Tonini. 2017. Synaptic functions of endocannabinoid signaling in health and disease. *Neuropharmacology*. 124:13–24. doi:10.1016/J.NEUROPHARM.2017.06.017.

Arseneault, L., M. Cannon, R. Poulton, R. Murray, A. Caspi, and T.E. Moffitt. 2002. Cannabis use in adolescence and risk for adult psychosis: longitudinal prospective study. *BMJ*. 325:1212–1213. doi:10.1136/BMJ.325.7374.1212.

Asimaki, O., G. Leondaritis, G. Lois, N. Sakellaridis, and D. Mangoura. 2011. Cannabinoid 1 receptor-dependent transactivation of fibroblast growth factor receptor 1 emanates from lipid rafts and amplifies extracellular signal-regulated kinase 1/2 activation in embryonic cortical neurons. *J. Neurochem.* 116:866–873. doi:10.1111/j.1471-4159.2010.07030.x.

Atwood, B.K., J. Lopez, J. Wager-Miller, K. Mackie, and A. Straiker. 2011. Expression of G protein-coupled receptors and related proteins in HEK293, AtT20, BV2, and N18 cell lines as revealed by microarray analysis. *BMC Genomics*. 12:14. doi:10.1186/1471-2164-12-14.

Auclair, S.M., M.K. Bhanu, and D.A. Kendall. 2012. Signal peptidase I: Cleaving the way to mature proteins. *Protein Sci.* 21:13–25. doi:10.1002/pro.757.

Bel, C., K. Oguievetskaia, C. Pitaval, L. Goutebroze, and C. Faivre-Sarrailh. 2009. Axonal targeting of Caspr2 in hippocampal neurons via selective somatodendritic endocytosis. *J. Cell Sci.* 122:3403–13. doi:10.1242/jcs.050526.

Bellocchio, L., P. Lafenêtre, A. Cannich, D. Cota, N. Puente, P. Grandes, F. Chaouloff, P.V. Piazza, and G. Marsicano. 2010. Bimodal control of stimulated food intake by the endocannabinoid system. *Nat. Neurosci.* 13:281–283. doi:10.1038/nn.2494.

Bénard, G., F. Massa, N. Puente, J. Lourenço, L. Bellocchio, E. Soria-Gómez, I. Matias, A. Delamarre, M. Metna-Laurent, A. Cannich, E. Hebert-Chatelain, C. Mulle, S. Ortega-Gutiérrez, M. Martín-Fontecha, M. Klugmann, S. Guggenhuber, B. Lutz, J. Gertsch, F. Chaouloff, M.L. López-Rodríguez, P. Grandes, R. Rossignol, and G. Marsicano. 2012. Mitochondrial CB1 receptors regulate neuronal energy metabolism. *Nat. Neurosci.* 15:558–564. doi:10.1038/nn.3053.

Bentley, M., and G. Banker. 2016. The cellular mechanisms that maintain neuronal polarity. *Nat. Rev. Neurosci.* 17:611–622. doi:10.1038/nrn.2016.100.

Biermann, B., K. Ivankova-Susankova, A. Bradaia, S.A. Aziz, V. Besseyrias, J.P. Kapfhammer, M. Missler, M. Gassmann, and B. Bettler. 2010. The Sushi Domains of GABAB Receptors Function as Axonal Targeting Signals. *J. Neurosci.* 30:1385–1394. doi:10.1523/JNEUROSCI.3172-09.2010.

Blume, L.C., K. Eldeeb, C.E. Bass, D.E. Selley, and A.C. Howlett. 2015. Cannabinoid receptor interacting protein (CRIP1a) attenuates CB1R signaling in neuronal cells. *Cell. Signal.* 27. doi:10.1016/j.cellsig.2014.11.006.

Blume, L.C., S. Leone-Kabler, D.J. Luessen, G.S. Marrs, E. Lyons, C.E. Bass, R. Chen, D.E. Selley, and A.C. Howlett. 2016. Cannabinoid receptor interacting protein suppresses agonist-driven CB_1 receptor internalization and regulates receptor replenishment in an agonist-biased manner. *J. Neurochem.* 139:396–407. doi:10.1111/jnc.13767.

Blume, L.C., T. Patten, K. Eldeeb, S. Leone-Kabler, A.A. Ilyasov, B.M. Keegan, J.E. O'Neal, C.E. Bass, R.R. Hantgan, W.T. Lowther, D.E. Selley, and A.L.C. Howlett. 2017. Cannabinoid Receptor Interacting Protein 1a Competition with β-Arrestin for CB1 Receptor Binding Sites. *Mol. Pharmacol.* 91:75–86. doi:10.1124/mol.116.104638.

Boncompain, G., S. Divoux, N. Gareil, H. de Forges, A. Lescure, L. Latreche, V. Mercanti, F. Jollivet, G. Raposo, and F. Perez. 2012. Synchronization of secretory protein traffic in populations of cells. *Nat. Methods*. 9:493-U120. doi:10.1038/nmeth.1928.

Bonifacino, J.S. 2014. Adaptor proteins involved in polarized sorting. *J. Cell Biol.* 204:7–17. doi:10.1083/jcb.201310021.

Borgdorff, A.J., and D. Choquet. 2002. Regulation of AMPA receptor lateral movements. *Nature*. 417:649–653. doi:10.1038/nature00780.

Bouabe, H., R. Fassler, and J. Heesemann. 2008. Improvement of reporter activity by IRES-mediated polycistronic reporter system. *Nucleic Acids Res.* 36:e28–e28. doi:10.1093/nar/gkm1119.

Brailoiu, G.C., T.I. Oprea, P. Zhao, M.E. Abood, and E. Brailoiu. 2011. Intracellular cannabinoid type 1 (CB1) receptors are activated by anandamide. *J. Biol. Chem.* 286:29166–74. doi:10.1074/jbc.M110.217463.

Breivogel, C.S., L.J. Sim, and S.R. Childers. 1997. Regional differences in cannabinoid receptor/G-protein coupling in rat brain. *J. Pharmacol. Exp. Ther.* 282:1632–42.

Bright, J.N., I.H. Shrivastava, F.S. Cordes, and M.S.P. Sansom. 2002. Conformational dynamics of helix S6 from Shaker potassium channel: Simulation studies. *Biopolymers*. 64:303–313. doi:10.1002/bip.10197.

Busquets-Garcia, A., J. Bains, and G. Marsicano. 2018. CB1 Receptor Signaling in the Brain: Extracting Specificity from Ubiquity. *Neuropsychopharmacology*. 43:4–20. doi:10.1038/npp.2017.206.

Busquets-Garcia, A., T. Desprez, M. Metna-Laurent, L. Bellocchio, G. Marsicano, and E. Soria-Gomez. 2015. Dissecting the cannabinergic control of behavior: The *where* matters. *BioEssays*. 37:1215–1225. doi:10.1002/bies.201500046.

Butzlaff, M., S.B. Hannan, P. Karsten, S. Lenz, J. Ng, H. Voßfeldt, K. Prüßing, R. Pflanz, J.B. Schulz, T. Rasse, and A. Voigt. 2015. Impaired retrograde transport by the Dynein/Dynactin complex contributes to Tau-induced toxicity. *Hum. Mol. Genet.* 24:3623–3637. doi:10.1093/hmg/ddv107.

Cardinal, P., L. Bellocchio, O. Guzmán-Quevedo, C. André, S. Clark, M. Elie, T. Leste-Lasserre, D. Gonzales, A. Cannich, G. Marsicano, and D. Cota. 2015. Cannabinoid Type 1 (CB_1) Receptors on Sim1-Expressing Neurons Regulate Energy Expenditure in Male Mice. *Endocrinology*. 156:411–418. doi:10.1210/en.2014-1437.

Carmichael, R.E., K.A. Wilkinson, T.J. Craig, M.C. Ashby, and J.M. Henley. 2018. MEF2A regulates mGluR-dependent AMPA receptor trafficking independently of Arc/Arg3.1. *Sci. Rep.* 8:5263. doi:10.1038/s41598-018-23440-0.

Castillo, P.E., T.J. Younts, A.E. Chavez, and Y. Hashimotodani. 2012. Endocannabinoid Signaling and Synaptic Function. *Neuron*. 76:70–81. doi:10.1016/j.neuron.2012.09.020.

Choy, R.W.-Y., M. Park, P. Temkin, B.E. Herring, A. Marley, R.A. Nicoll, and M. von Zastrow. 2014. Retromer Mediates a Discrete Route of Local Membrane Delivery to Dendrites. *Neuron*. 82:55–62. doi:10.1016/J.NEURON.2014.02.018.

Coutts, A.A., S. Anavi-Goffer, R.A. Ross, D.J. MacEwan, K. Mackie, R.G. Pertwee, and A.J. Irving. 2001. Agonist-induced internalization and trafficking of cannabinoid CB1 receptors in hippocampal neurons. *J. Neurosci.* 21:2425–2433.

Cullen, P.J. 2008. Endosomal sorting and signalling: an emerging role for sorting nexins. *Nat. Rev. Mol. Cell Biol.* 9:574–582. doi:10.1038/nrm2427.

Cullen, P.J., and F. Steinberg. 2018. To degrade or not to degrade: mechanisms and significance of endocytic recycling. *Nat. Rev. Mol. Cell Biol.* 19:679–696. doi:10.1038/s41580-018-0053-7.

Cummings, N., K.A. Shields, J.E. Curran, K. Bozaoglu, J. Trevaskis, K. Gluschenko, G. Cai, A.G. Comuzzie, T.D. Dyer, K.R. Walder, P. Zimmet, G.R. Collier, J. Blangero, and J.B.M. Jowett. 2012. Genetic variation in SH3-domain GRB2-like (endophilin)-interacting protein 1 has a major impact on fat mass. *Int. J. Obes.* 36:201–206. doi:10.1038/ijo.2011.67.

D'Antona, A.M., K.H. Ahn, and D.A. Kendall*. 2006. Mutations of CB1 T210 Produce Active and Inactive Receptor Forms: Correlations with Ligand Affinity, Receptor Stability, and Cellular Localization†. doi:10.1021/BI060067K.

Daigle, T.L., C.S. Kearn, and K. Mackie. 2008a. Rapid CB1 cannabinoid receptor desensitization defines the time course of ERK1/2 MAP kinase signaling. *Neuropharmacology*. 54:36–44. doi:10.1016/J.NEUROPHARM.2007.06.005.

Daigle, T.L., M.L. Kwok, and K. Mackie. 2008b. Regulation of CB_1 cannabinoid receptor internalization by a promiscuous phosphorylation-dependent mechanism. *J. Neurochem.* 106:70–82. doi:10.1111/j.1471-4159.2008.05336.x.

Dalton, V.S., L.E. Long, C.S. Weickert, and K. Zavitsanou. 2011. Paranoid Schizophrenia is Characterized by Increased CB1 Receptor Binding in the Dorsolateral Prefrontal Cortex. *Neuropsychopharmacology*. 36:1620–1630. doi:10.1038/npp.2011.43.

Damke, H., J. Klumperman, K. von Figura, and T. Braulke. 1991. Effects of brefeldin A on the endocytic route. Redistribution of mannose 6-phosphate/insulin-like growth factor II receptors to the cell surface. *J. Biol. Chem.* 266:24829–33.

Danglot, L., and T. Galli. 2007. What is the function of neuronal AP-3? *Biol. Cell*. 99:349–361. doi:10.1042/BC20070029.

Darsow, T., C.G. Burd, and S.D. Emr. 1998. Acidic di-leucine motif essential for AP-3-dependent sorting and restriction of the functional specificity of the Vam3p vacuolar t-SNARE. *J. Cell Biol.* 142:913–22. doi:10.1083/jcb.142.4.913.

Delgado-Peraza, F., K.H. Ahn, C. Nogueras-Ortiz, I.N. Mungrue, K. Mackie, D.A. Kendall, and G.A. Yudowski. 2016. Mechanisms of Biased β-Arrestin-Mediated Signaling Downstream from the Cannabinoid 1 Receptor. *Mol. Pharmacol.* 89:618–629. doi:10.1124/MOL.115.103176.

Dergai, O., O. Novokhatska, M. Dergai, I. Skrypkina, L. Tsyba, J. Moreau, and A. Rynditch. 2010. Intersectin 1 forms complexes with SGIP1 and Reps1 in clathrin-coated pits. *Biochem. Biophys. Res. Commun.* 402:408–413. doi:10.1016/J.BBRC.2010.10.045.

Devane, W.A., L. Hanus, A. Breuer, R.G. Pertwee, L.A. Stevenson, G. Griffin, D. Gibson, A. Mandelbaum, A. Etinger, and R. Mechoulam. 1992. Isolation and structure of a brain constituent that binds to the cannabinoid receptor. *Science*. 258:1946–9. doi:10.1126/science.1470919.

Diez-Alarcia, R., I. Ibarra-Lecue, Á.P. Lopez-Cardona, J. Meana, A. Gutierrez-Adán, L.F. Callado, E. Agirregoitia, and L. Urigüen. 2016. Biased Agonism of Three Different Cannabinoid Receptor Agonists in Mouse Brain Cortex. *Front. Pharmacol.* 7:415. doi:10.3389/fphar.2016.00415.

Doherty, G.J., and H.T. McMahon. 2009. Mechanisms of Endocytosis. *Annu. Rev. Biochem.* 78:857–902. doi:10.1146/annurev.biochem.78.081307.110540.

Drechsel, D.N., A.A. Hyman, M.H. Cobb, and M.W. Kirschner. 1992. Modulation of the dynamic instability of tubulin assembly by the microtubule-associated protein tau. *Mol. Biol. Cell*. 3:1141–1154. doi:10.1091/mbc.3.10.1141.

Dudok, B., L. Barna, M. Ledri, S.I. Szabo, E. Szabadits, B. Pinter, S.G. Woodhams, C.M. Henstridge, G.Y. Balla, R. Nyilas, C. Varga, S.H. Lee, M. Matolcsi, J. Cervenak, I. Kacskovics, M. Watanabe, C. Sagheddu, M. Melis, M. Pistis, I. Soltesz, and I. Katona. 2015. Cell-specific STORM super-resolution imaging reveals nanoscale organization of cannabinoid signaling. *Nat. Neurosci.* 18:75-+. doi:10.1038/nn.3892.

Dupré, D.J., M. Robitaille, R.V. Rebois, and T.E. Hébert. 2009. The Role of Gβγ Subunits in the Organization, Assembly, and Function of GPCR Signaling Complexes. *Annu. Rev. Pharmacol. Toxicol.* 49:31–56. doi:10.1146/annurev-pharmtox-061008-103038.

Dwyer, N.D., C.E. Adler, J.G. Crump, N.D. L'Etoile, and C.I. Bargmann. 2001. Polarized Dendritic Transport and the AP-1 μ1 Clathrin Adaptor UNC-101 Localize Odorant Receptors to Olfactory Cilia. *Neuron*. 31:277–287. doi:10.1016/S0896-6273(01)00361-0.

Ellis, J., J.D. Pediani, M. Canals, S. Milasta, and G. Milligan. 2006. Orexin-1 receptor-cannabinoid CB1 receptor heterodimerization results in both ligand-dependent and -independent coordinated alterations of receptor localization and function. *J. Biol. Chem.* 281:38812–24. doi:10.1074/jbc.M602494200.

Evans, A.J. 2017. 'RUSHing' to investigate the secretory pathway trafficking of ionotropic glutamate receptors in primary neurons. University of Bristol.

Evans, A.J., S. Gurung, K.A. Wilkinson, D.J. Stephens, and J.M. Henley. 2017. Assembly, secretory pathway trafficking, and surface delivery of kainate receptors is regulated by neuronal activity. *Cell Rep.* 19:2613–2626.

Fache, M.P., A. Moussif, F. Fernandes, P. Giraud, J.J. Garrido, and B. Dargent. 2004. Endocytotic elimination and domain-selective tethering constitute a potential mechanism of protein segregation at the axonal initial segment. *J. Cell Biol.* 166:571–578. doi:10.1083/jcb.200312155.

Farías, G.G., L. Cuitino, X. Guo, X. Ren, M. Jarnik, R. Mattera, and J.S. Bonifacino. 2012. Signal-Mediated, AP-1/Clathrin-Dependent Sorting of Transmembrane Receptors to the Somatodendritic Domain of Hippocampal Neurons. *Neuron*. 75:810–823. doi:10.1016/J.NEURON.2012.07.007.

Farias, G.G., C.M. Guardia, D.J. Britt, X.L. Guo, and J.S. Bonifacino. 2015. Sorting of Dendritic and Axonal Vesicles at the Pre-axonal Exclusion Zone. *Cell Rep.* 13:1221–1232. doi:10.1016/j.celrep.2015.09.074.

Fath, S., J.D. Mancias, X. Bi, and J. Goldberg. 2007. Structure and Organization of Coat Proteins in the COPII Cage. *Cell*. 129:1325–1336. doi:10.1016/J.CELL.2007.05.036.

Fisyunov, A., V. Tsintsadze, R. Min, N. Burnashev, and N. Lozovaya. 2006. Cannabinoids Modulate the P-Type High-Voltage-Activated Calcium Currents in Purkinje Neurons. *J. Neurophysiol.* 96:1267–1277. doi:10.1152/jn.01227.2005.

Frazier, C.J., A. V Buhler, J.L. Weiner, T. V Dunwiddie, R. Freedman, T. Dunwiddie, A. Fine, M. Moretti, F. Rossi, N. Le Novere, J. McIntosh, A. Gardier, and J. Changeux. 1998. Synaptic potentials mediated via alpha-bungarotoxin-sensitive nicotinic acetylcholine receptors in rat hippocampal interneurons. *J. Neurosci.* 18:8228–35. doi:3282038.

Freeman, T.P., C. Hindocha, S.F. Green, and M.A.P. Bloomfield. 2019. Medicinal use of cannabis based products and cannabinoids. *BMJ*. 365:l1141. doi:10.1136/bmj.l1141.

Gaoni, Y., and R. Mechoulam. 1964. Isolation, Structure, and Partial Synthesis of an Active Constituent of Hashish. *J. Am. Chem. Soc.* 86:1646–1647. doi:10.1021/ja01062a046.

Garrido, J.J., F. Fernandes, P. Giraud, I. Mouret, E. Pasqualini, M.P. Fache, F. Jullien, and B. Dargent. 2001. Identification of an axonal determinant in the C-terminus of the sodium channel Na(v)1.2. *Embo J.* 20:5950–5961. doi:10.1093/emboj/20.21.5950.

Gebremedhin, D., A.R. Lange, W.B. Campbell, C.J. Hillard, and D.R. Harder. 1999. Cannabinoid CB1 receptor of cat cerebral arterial muscle functions to inhibit L-type Ca $^{2+}$ channel current. *Am. J. Physiol. Circ. Physiol.* 276:H2085–H2093. doi:10.1152/ajpheart.1999.276.6.H2085.

Gérard, C.M., C. Mollereau, G. Vassart, and M. Parmentier. 1991. Molecular cloning of a human cannabinoid receptor which is also expressed in testis. *Biochem. J.* 279 (Pt 1):129–34. doi:10.1042/bj2790129.

Girach, F., T.J. Craig, D.L. Rocca, and J.M. Henley. 2013. RIM1α SUMOylation Is Required for Fast Synaptic Vesicle Exocytosis. *Cell Rep.* 5:1294–1301. doi:10.1016/J.CELREP.2013.10.039.

Glass, M., and C.C. Felder. 1997. Concurrent Stimulation of Cannabinoid CB1 and Dopamine D2 Receptors Augments cAMP Accumulation in Striatal Neurons: Evidence for a Gs Linkage to the CB1 Receptor. *J. Neurosci.* 17:5327–5333. doi:10.1523/JNEUROSCI.17-14-05327.1997.

González, C., J. Cánovas, J. Fresno, E. Couve, and A. Couve. 2016. Axons provide the secretory machinery for trafficking of voltage-gated sodium channels in peripheral nerve. *Proc. Natl. Acad. Sci.* 113:1823–1828.

González, C., V.H. Cornejo, and A. Couve. 2018. Golgi bypass for local delivery of axonal proteins, fact or fiction? *Curr. Opin. Cell Biol.* 53:9–14. doi:10.1016/J.CEB.2018.03.010.

Goodman, O.B., J.G. Krupnick, F. Santini, V. V. Gurevich, R.B. Penn, A.W. Gagnon, J.H. Keen, and J.L. Benovic. 1996. β-Arrestin acts as a clathrin adaptor in endocytosis of the β2-adrenergic receptor. *Nature*. 383:447–450. doi:10.1038/383447a0.

Gopala Krishna, A., S.T. Menon, T.J. Terry, And, and T.P. Sakmar*. 2002. Evidence That Helix 8 of Rhodopsin Acts as a Membrane-Dependent Conformational Switch†. doi:10.1021/BI025534M.

Graham, T.R., P.A. Scott, and S.D. Emr. 1993. Brefeldin A reversibly blocks early but not late protein transport steps in the yeast secretory pathway. *EMBO J.* 12:869–877. doi:10.1002/j.1460-2075.1993.tb05727.x.

Grimsey, N.L., E.S. Graham, M. Dragunow, and M. Glass. 2010. Cannabinoid Receptor 1 trafficking and the role of the intracellular pool: Implications for therapeutics. *Biochem. Pharmacol.* 80:1050–1062. doi:10.1016/J.BCP.2010.06.007.

Gu, C., Y.N. Jan, and L.Y. Jan. 2003. A Conserved Domain in Axonal Targeting of Kv1 (Shaker) Voltage-Gated Potassium Channels. *Science (80-.).* 301:646–649. doi:10.1126/SCIENCE.1086998.

Guardia, C.M., R. De Pace, R. Mattera, and J.S. %J C. opinion in neurobiology Bonifacino. 2018. Neuronal functions of adaptor complexes involved in protein sorting. 51:103–110.

Guerriero, C.J., and J.L. Brodsky. 2012. The Delicate Balance Between Secreted Protein Folding and Endoplasmic Reticulum-Associated Degradation in Human Physiology. *Physiol. Rev.* 92:537–576. doi:10.1152/physrev.00027.2011.

Guggenhuber, S., A. Alpar, R. Chen, N. Schmitz, M. Wickert, T. Mattheus, A.E. Harasta, M. Purrio, N. Kaiser, M.R. Elphick, K. Monory, W. Kilb, H.J. Luhmann, T. Harkany, B. Lutz, and M. Klugmann. 2016. Cannabinoid receptor-interacting protein Crip1a modulates CB1 receptor signaling in mouse hippocampus. *Brain Struct. Funct.* 221. doi:10.1007/s00429-015-1027-6.

Gulyas, A.I., B.F. Cravatt, M.H. Bracey, T.P. Dinh, D. Piomelli, F. Boscia, and T.F. Freund. 2004. Segregation of two endocannabinoid-hydrolyzing enzymes into pre- and postsynaptic compartments in the rat hippocampus, cerebellum and amygdala. *Eur. J. Neurosci.* 20:441–458. doi:10.1111/j.1460-9568.2004.03428.x.

Gyombolai, P., E. Boros, L. Hunyady, and G. Turu. 2013. Differential β-arrestin2 requirements for constitutive and agonist-induced internalization of the CB1 cannabinoid receptor. *Mol. Cell. Endocrinol.* 372:116–127. doi:10.1016/J.MCE.2013.03.013.

Haar, E. Vander, S. Lee, S. Bandhakavi, T.J. Griffin, and D.-H. Kim. 2007. Insulin signalling to mTOR mediated by the Akt/PKB substrate PRAS40. *Nat. Cell Biol.* 9:316–323. doi:10.1038/ncb1547.

Hájková, A., Š. Techlovská, M. Dvořáková, J.N. Chambers, J. Kumpošt, P. Hubálková, L. Prezeau, and J. Blahos. 2016. SGIP1 alters internalization and modulates signaling of activated cannabinoid receptor 1 in a biased manner. *Neuropharmacology*. doi:10.1016/j.neuropharm.2016.03.008.

Han, M., V. V Gurevich, S.A. Vishnivetskiy, P.B. Sigler, and C. Schubert. 2001. Crystal Structure of β-Arrestin at 1.9 Å: Possible Mechanism of Receptor Binding and Membrane Translocation. *Structure*. 9:869–880. doi:10.1016/S0969-2126(01)00644-X.

Hangen, E., F.P. Cordelières, J.D. Petersen, D. Choquet, and F. Coussen. 2018. Neuronal Activity and Intracellular Calcium Levels Regulate Intracellular Transport of Newly Synthesized AMPAR. *Cell Rep.* 24:1001-1012.e3. doi:10.1016/J.CELREP.2018.06.095.

Hanson, S.R., E.K. Culyba, T.-L. Hsu, C.-H. Wong, J.W. Kelly, and E.T. Powers. 2009. The core trisaccharide of an N-linked glycoprotein intrinsically accelerates folding and enhances stability. *Proc. Natl. Acad. Sci.* 106:3131–3136. doi:10.1073/PNAS.0810318105.

Hanus, C., H. Geptin, G. Tushev, S. Garg, B. Alvarez-Castelao, S. Sambandan, L. Kochen, A.-S. Hafner, J.D. Langer, and E.M. Schuman. 2016. Unconventional secretory processing diversifies neuronal ion channel properties. *Elife*. 5.

Hastings, M.H., and H.-Y. Man. 2018. Synaptic Capture of Laterally Diffusing AMPA Receptors - An Idea That Stuck. *Trends Neurosci.* 41:330–332. doi:10.1016/j.tins.2018.03.016.

Häusser, M., G. Stuart, C. Racca, and B. Sakmann. 1995. Axonal initiation and active dendritic propagation of action potentials in substantia nigra neurons. *Neuron*. 15:637–647. doi:10.1016/0896-6273(95)90152-3.

Hebert-Chatelain, E., T. Desprez, R. Serrat, L. Bellocchio, E. Soria-Gomez, A. Busquets-Garcia, A.C. Pagano Zottola, A. Delamarre, A. Cannich, P. Vincent, M. Varilh, L.M. Robin, G. Terral, M.D. García-Fernández, M. Colavita, W. Mazier, F. Drago, N. Puente, L. Reguero, I. Elezgarai, J.-W. Dupuy, D. Cota, M.-L. Lopez-Rodriguez, G. Barreda-Gómez, F. Massa, P. Grandes, G. Bénard, and G. Marsicano. 2016. A cannabinoid link between mitochondria and memory. *Nature*. 539:555–559. doi:10.1038/nature20127.

Hebert-Chatelain, E., L. Reguero, N. Puente, B. Lutz, F. Chaouloff, R. Rossignol, P.-V. Piazza, G. Benard, P. Grandes, and G. Marsicano. 2014. Studying mitochondrial CB1 receptors: Yes we can. *Mol. Metab.* 3:339. doi:10.1016/j.molmet.2014.03.008.

von Heijne, G. 2006. Membrane-protein topology. *Nat. Rev. Mol. Cell Biol.* 7:909–918. doi:10.1038/nrm2063.

Henquet, C., R. Murray, D. Linszen, and J. van Os. 2005. The Environment and Schizophrenia: The Role of Cannabis Use. *Schizophr. Bull.* 31:608–612. doi:10.1093/schbul/sbi027.

Henry, D.J., and C. Chavkin. 1995. Activation of inwardly rectifying potassium channels (GIRK1) by co-expressed rat brain cannabinoid receptors in Xenopus oocytes. *Neurosci. Lett.* 186:91–94. doi:10.1016/0304-3940(95)11289-9.

Herde, M.K., K.J. Iremonger, S. Constantin, and A.E. Herbison. 2013. GnRH neurons elaborate a long-range projection with shared axonal and dendritic functions. *J. Neurosci.* 33:12689–97. doi:10.1523/JNEUROSCI.0579-13.2013.

Herkenham, M., A.B. Lynn, M.R. Johnson, L.S. Melvin, B.R. de Costa, and K.C. Rice. 1991. Characterization and localization of cannabinoid receptors in rat brain: a quantitative in vitro autoradiographic study. *J. Neurosci.* 11:563–83. doi:10.1523/JNEUROSCI.11-02-00563.1991.

Hermann, H., G. Marsicano, and B. Lutz. 2002. Coexpression of the cannabinoid receptor type 1 with dopamine and serotonin receptors in distinct neuronal subpopulations of the adult mouse forebrain. *Neuroscience*. 109:451–460. doi:10.1016/S0306-4522(01)00509-7.

Heydorn, A., B.P. Søndergaard, B. Ersbøll, B. Holst, F.C. Nielsen, C.R. Haft, J. Whistler, and T.W. Schwartz. 2004. A library of 7TM receptor C-terminal tails. Interactions with the proposed post-endocytic sorting proteins ERM-binding phosphoprotein 50 (EBP50), N-ethylmaleimide-sensitive factor (NSF), sorting nexin 1 (SNX1), and G protein-coupled receptor-associated sorting protein (GASP). *J. Biol. Chem.* 279:54291–303. doi:10.1074/jbc.M406169200.

Hildick, K.L. 2013. Mechanisms underlying the trafficking and distribution of cannabionid receptor type 1 in primary hippocampal neurons. PhD. University of Bristol.

Hillard, C.J., S. Manna, M.J. Greenberg, R. DiCamelli, R.A. Ross, L.A. Stevenson, V. Murphy, R.G. Pertwee, and W.B. Campbell. 1999. Synthesis and characterization of potent and selective agonists of the neuronal cannabinoid receptor (CB1). *J. Pharmacol. Exp. Ther.* 289:1427–33.

Ho, B.Y., Y. Uezono, S. Takada, I. Takase, and F. Izumi. 1999. Coupling of the expressed cannabinoid CB1 and CB2 receptors to phospholipase C and G protein-coupled inwardly rectifying K+ channels. *Receptors Channels*. 6:363–74.

Hollopeter, G., J.J. Lange, Y. Zhang, T.N. Vu, M. Gu, M. Ailion, E.J. Lambie, B.D. Slaughter, J.R. Unruh, L. Florens, and E.M. Jorgensen. 2014. The membrane-associated proteins FCHo and SGIP are allosteric activators of the AP2 clathrin adaptor complex. *Elife*. 3. doi:10.7554/eLife.03648.

Holt, C.E., and E.M. Schuman. 2013. The central dogma decentralized: new perspectives on RNA function and local translation in neurons. *Neuron*. 80:648–57. doi:10.1016/j.neuron.2013.10.036.

Horton, A.C., and M.D. Ehlers. 2003. Dual modes of endoplasmic reticulum-to-Golgi transport in dendrites revealed by live-cell imaging. *J. Neurosci.* 23:6188–99. doi:10.1523/JNEUROSCI.23-15-06188.2003.

Horton, A.C., and M.D. Ehlers. 2004. Secretory trafficking in neuronal dendrites. *Nat. Cell Biol.* 6:585–591.

Howlett, A.C. 1984. Inhibition of neuroblastoma adenylate cyclase by cannabinoid and nantradol compounds. *Life Sci.* 35:1803–1810. doi:10.1016/0024-3205(84)90278-9.

Howlett, A.C. 1987. Cannabinoid inhibition of adenylate cyclase: Relative activity of constituents and metabolites of marihuana. *Neuropharmacology*. 26:507–512. doi:10.1016/0028-3908(87)90035-9.

Howlett, A.C. 2005. Cannabinoid receptor signaling. *Handb Exp Pharmacol*. 53–79.

Howlett, A.C., F. Barth, T.I. Bonner, G. Cabral, P. Casellas, W.A. Devane, C.C. Felder, M. Herkenham, K. Mackie, B.R. Martin, R. Mechoulam, and R.G. Pertwee. 2002. International Union of Pharmacology. XXVII. Classification of cannabinoid receptors. *Pharmacol Rev*. 54:161–202.

Howlett, A.C., and R.M. Fleming. 1984. Cannabinoid inhibition of adenylate cyclase. Pharmacology of the response in neuroblastoma cell membranes. *Mol. Pharmacol.* 26.

Howlett, A.C., J.M. Qualy, and L.L. Khachatrian. 1986. Involvement of Gi in the inhibition of adenylate cyclase by cannabimimetic drugs. *Mol. Pharmacol.* 29.

Hsieh, C., S. Brown, C. Derleth, and K. Mackie. 2002. Internalization and Recycling of the CB1 Cannabinoid Receptor. *J. Neurochem.* 73:493–501. doi:10.1046/j.1471-4159.1999.0730493.x.

Hunter, M.R., D.B. Finlay, and M. Glass. 2017. Signaling and Regulation of the Cannabinoid CB1 Receptor. *Handb. Cannabis Relat. Pathol.* 564–572. doi:10.1016/B978-0-12-800756-3/00069-7.

Hunziker, W., J. Andrew Whitney, and I. Mellman. 1991. Selective inhibition of transcytosis by brefeldin A in MDCK cells. *Cell*. 67:617–627. doi:10.1016/0092-8674(91)90535-7.

Hunziker, W., J.A. Whitney, and I. Mellman. 1992. Brefeldin A and the endocytic pathway Possible implications for membrane traffic and sorting. *FEBS Lett.* 307:93–96. doi:10.1016/0014-5793(92)80908-Y.

Irannejad, R. 2014. GPCR signaling along the endocytic pathway. *Curr. Opin. Cell Biol.* 27:109–116. doi:10.1016/J.CEB.2013.10.003.

Irving, A.J., A.A. Coutts, J. Harvey, M.G. Rae, K. Mackie, G.S. Bewick, and R.G. Pertwee. 2000. Functional expression of cell surface cannabinoid CB1 receptors on presynaptic inhibitory terminals in cultured rat hippocampal neurons. *Neuroscience*. 98:253–262. doi:10.1016/s0306-4522(00)00120-2.

Irving, A.J., N.A. McDonald, and T. Harkany. 2008. CB1 Cannabinoid Receptors: Molecular Biology, Second Messenger Coupling and Polarized Trafficking in Neurons. *In* Cannabinoids and the Brain. Springer US, Boston, MA. 59–73.

Janda, C.Y., J. Li, C. Oubridge, H. Hernández, C. V. Robinson, and K. Nagai. 2010. Recognition of a signal peptide by the signal recognition particle. *Nature*. 465:507–510. doi:10.1038/nature08870.

Jarrahian, A., V.J. Watts, and E.L. Barker. 2004. D2 Dopamine Receptors Modulate Gα-Subunit Coupling of the CB1 Cannabinoid Receptor. *J. Pharmacol. Exp. Ther.* 308:880–886. doi:10.1124/JPET.103.057620.

Jensen, C.S., S. Watanabe, J.I. Stas, J. Klaphaak, A. Yamane, N. Schmitt, S.-P. Olesen, J.S. Trimmer, H.B. Rasmussen, and H. Misonou. 2017. Trafficking of Kv2.1 Channels to the Axon Initial Segment by a Novel Nonconventional Secretory Pathway. *J. Neurosci.* 37:11523–11536. doi:10.1523/JNEUROSCI.3510-16.2017.

Jin, W.Z., S. Brown, J.P. Roche, C. Hsieh, J.P. Celver, A. Kovoor, C. Chavkin, and K. Mackie. 1999. Distinct domains of the CB1 cannabinoid receptor mediate desensitization and internalization. *J. Neurosci.* 19:3773–3780.

Jo, K., R. Derin, M. Li, and D.S. Bredt. 1999. Characterization of MALS/Velis-1, -2, and -3: a family of mammalian LIN-7 homologs enriched at brain synapses in association with the postsynaptic density-95/NMDA receptor postsynaptic complex. *J. Neurosci.* 19:4189–99. doi:10.1523/JNEUROSCI.19-11-04189.1999.

Johansson, K., K. Neovius, S.M. DeSantis, S. Rössner, and M. Neovius. 2009. Discontinuation due to adverse events in randomized trials of orlistat, sibutramine and rimonabant: a meta-analysis. *Obes. Rev.* 10:564–575. doi:10.1111/j.1467-789X.2009.00581.x.

Johnson, B., A.N. Leek, L. Solé, E.E. Maverick, T.P. Levine, and M.M. Tamkun. 2018. Kv2 potassium channels form endoplasmic reticulum/plasma membrane junctions via interaction with VAPA and VAPB. *Proc. Natl. Acad. Sci. U. S. A.* 115:E7331–E7340. doi:10.1073/pnas.1805757115.

Jong, Y.-J.I., S.K. Harmon, and K.L. O'Malley. 2018. GPCR signalling from within the cell. *Br. J. Pharmacol.* 175:4026–4035. doi:10.1111/bph.14023.

Kano, M., T. Ohno-Shosaku, Y. Hashimotodani, M. Uchigashima, and M. Watanabe. 2009. Endocannabinoid-Mediated Control of Synaptic Transmission. *Physiol. Rev.* 89:309–380. doi:10.1152/physrev.00019.2008.

Kapitein, L.C., and C.C. Hoogenraad. 2011. Which way to go? Cytoskeletal organization and polarized transport in neurons. *Mol. Cell. Neurosci.* 46:9–20. doi:10.1016/J.MCN.2010.08.015.

Katona, I. 2009. Endocannabinoid receptors: CNS localization of the CB1 cannabinoid receptor. *In* Behavioral Neurobiology of the Endocannabinoid System. Springer. 65–86.

Katona, I., and T.F. Freund. 2012. Multiple Functions of Endocannabinoid Signaling in the Brain. *In* Annual Review of Neuroscience, Vol 35. S.E. Hyman, editor. 529–558.

Katona, I., B. Sperlágh, A. Sík, A. Käfalvi, E.S. Vizi, K. Mackie, and T.F. Freund. 1999. Presynaptically located CB1 cannabinoid receptors regulate GABA release from axon terminals of specific hippocampal interneurons. *J. Neurosci.* 19:4544–58. doi:10.1523/JNEUROSCI.19-11-04544.1999.

Kaufman, R.J., M. V. Davies, L.C. Wasley, and D. Michnick. 1991. Improved vectors for stable expression of foreign genes in mammalian cells by use of the untranslated leader sequence from EMC virus. *Nucleic Acids Res.* 19:4485–4490. doi:10.1093/nar/19.16.4485.

Kaur, R., S.R. Ambwani, and S. Singh. 2016a. Endocannabinoid System: A Multi-Facet Therapeutic Target. *Curr. Clin. Pharmacol.* 11:110–7.

Kaur, R., P. Sidhu, and S. Singh. 2016b. What failed BIA 10-2474 Phase I clinical trial? Global speculations and recommendations for future Phase I trials. *J. Pharmacol. Pharmacother.* 7:120–6. doi:10.4103/0976-500X.189661.

Kearn, C.S., K. Blake-Palmer, E. Daniel, K. Mackie, and M. Glass. 2005. Concurrent stimulation of cannabinoid CB1 and dopamine D2 receptors enhances heterodimer formation: a mechanism for receptor cross-talk? *Mol. Pharmacol.* 67:1697–704. doi:10.1124/mol.104.006882.

Keefe, A.D., D.S. Wilson, B. Seelig, and J.W. Szostak. 2001. One-Step Purification of Recombinant Proteins Using a Nanomolar-Affinity Streptavidin-Binding Peptide, the SBP-Tag. *Protein Expr. Purif.* 23:440–446. doi:10.1006/PREP.2001.1515.

Keren, O., and Y. Sarne. 2003. Multiple mechanisms of CB1 cannabinoid receptors regulation. *Brain Res.* 980:197–205. doi:10.1016/s0006-8993(03)02970-6.

Khurana, L., K. Mackie, D. Piomelli, and D.A. Kendall. 2017. Modulation of CB1 cannabinoid receptor by allosteric ligands: Pharmacology and therapeutic opportunities. *Neuropharmacology*. 124:3–12. doi:10.1016/J.NEUROPHARM.2017.05.018.

Klumperman, J. 2011. Architecture of the mammalian Golgi. *Cold Spring Harb. Perspect. Biol.* 3:a005181. doi:10.1101/cshperspect.a005181.

Kneussel, M., and T.J. Hausrat. 2016. Postsynaptic Neurotransmitter Receptor Reserve Pools for Synaptic Potentiation. *Trends Neurosci.* 39:170–182. doi:10.1016/j.tins.2016.01.002.

Koch, M., L. Varela, J.G. Kim, J.D. Kim, F. Hernández-Nuño, S.E. Simonds, C.M. Castorena, C.R. Vianna, J.K. Elmquist, Y.M. Morozov, P. Rakic, I. Bechmann, M.A. Cowley, K. Szigeti-Buck, M.O. Dietrich, X.-B. Gao, S. Diano, and T.L. Horvath. 2015. Hypothalamic POMC neurons promote cannabinoid-induced feeding. *Nature*. 519:45–50. doi:10.1038/nature14260.

Kogan, N.M., and R. Mechoulam. 2007. Cannabinoids in health and disease. *Dialogues Clin Neurosci*. 9:413–430.

Kornfeld, R., and S. Kornfeld. 1985. Assembly of Asparagine-Linked Oligosaccharides. *Annu. Rev. Biochem.* 54:631–664. doi:10.1146/annurev.bi.54.070185.003215.

Kouznetsova, M., B. Kelley, M. Shen, and S.A. Thayer. 2002. Desensitization of cannabinoid-mediated presynaptic inhibition of neurotransmission between rat hippocampal neurons in culture. *Mol. Pharmacol.* 61:477–85. doi:10.1124/mol.61.3.477.

Kreitzer, A.C., and W.G. Regehr. 2001. Retrograde Inhibition of Presynaptic Calcium Influx by Endogenous Cannabinoids at Excitatory Synapses onto Purkinje Cells. *Neuron*. 29:717–727. doi:10.1016/S0896-6273(01)00246-X.

Ladarre, D., and Z. Lenkei. 2017. Cell-Autonomous Endocannabinoid Production Shapes Polarized and Dynamic Distribution and Signaling Patterns of Cannabinoid CB1 Receptors in Neurons. *In* Endocannabinoids and Lipid Mediators in Brain Functions. Springer. 79–107.

Ladarre, D., A.B. Roland, S. Biedzinski, A. Ricobaraza, and Z. Lenkei. 2015. Polarized cellular patterns of endocannabinoid production and detection shape cannabinoid signaling in neurons. *Front. Cell. Neurosci.* 8:426. doi:10.3389/fncel.2014.00426.

Langhans, M., T. Meckel, A. Kress, A. Lerich, and D.G. Robinson. 2012. ERES (ER exit sites) and the “Secretory Unit Concept.” *J. Microsc.* 247:48–59. doi:10.1111/j.1365-2818.2011.03597.x.

Laporte, S.A., R.H. Oakley, J. Zhang, J.A. Holt, S.S.G. Ferguson, M.G. Caron, and L.S. Barak. 1999. The β2-adrenergic receptor/βarrestin complex recruits the clathrin adaptor AP-2 during endocytosis. *Proc. Natl. Acad. Sci.* 96:3712–3717. doi:10.1073/PNAS.96.7.3712.

Lasiecka, Z.M., and B. Winckler. 2011. Mechanisms of polarized membrane trafficking in neurons - Focusing in on endosomes. *Mol. Cell. Neurosci.* 48:278–287. doi:10.1016/j.mcn.2011.06.013.

Lauckner, J.E., B. Hille, and K. Mackie. 2005. The cannabinoid agonist WIN55,212-2 increases intracellular calcium via CB1 receptor coupling to Gq/11 G proteins. *Proc. Natl. Acad. Sci. U. S. A.* 102:19144–9. doi:10.1073/pnas.0509588102.

Lee, S.-E., S. Jeong, U. Lee, and S. Chang. 2019. SGIP1α functions as a selective endocytic adaptor for the internalization of synaptotagmin 1 at synapses. *Mol. Brain*. 12:41. doi:10.1186/s13041-019-0464-1.

Leterrier, C., D. Bonnard, D. Carrel, J. Rossier, and Z. Lenkei. 2004. Constitutive endocytic cycle of the CB1 cannabinoid receptor. *J. Biol. Chem.* 279:36013–36021. doi:10.1074/jbc.M403990200.

Leterrier, C., N. Clerc, F. Rueda-Boroni, A. Montersino, B. Dargent, and F. Castets. 2017. Ankyrin G Membrane Partners Drive the Establishment and Maintenance of the Axon Initial Segment. *Front. Cell. Neurosci.* 11:6. doi:10.3389/fncel.2017.00006.

Leterrier, C., and B. Dargent. 2014. No Pasaran! Role of the axon initial segment in the regulation of protein transport and the maintenance of axonal identity. *Semin. Cell Dev. Biol.* 27:44–51. doi:10.1016/J.SEMCDB.2013.11.001.

Leterrier, C., J. Laine, M. Darmon, H. Boudin, J. Rossier, and Z. Lenkei. 2006. Constitutive activation drives compartment-selective endocytosis and axonal targeting of type 1 cannabinoid receptors. *J. Neurosci.* 26:3141–3153. doi:10.1523/jneurosci.5437-05.2006.

Li, P., S.A. Merrill, E.M. Jorgensen, and K. Shen. 2016. Two Clathrin Adaptor Protein Complexes Instruct Axon-Dendrite Polarity. *Neuron*. 90:564–580. doi:10.1016/j.neuron.2016.04.020.

Live, D.H., R.A. Kumar, X. Beebe, S.J. Danishefsky, J.W. Kelly, and E.T. Powers. 1996. Conformational influences of glycosylation of a peptide: A possible model for the effect of glycosylation on the rate of protein folding. *Proc. Natl. Acad. Sci.* 93:12759–12761. doi:10.1073/pnas.93.23.12759.

Lorincz, A., and Z. Nusser. 2010. Molecular identity of dendritic voltage-gated sodium channels. *Science*. 328:906–9. doi:10.1126/science.1187958.

Lu, H.C., and K. Mackie. 2016. An introduction to the endogenous cannabinoid system. *Biol. Psychiatry*. 79. doi:10.1016/j.biopsych.2015.07.028.

Luarte, A., V.H. Cornejo, F. Bertin, J. Gallardo, and A. %J D. neurobiology Couve. 2018. The axonal endoplasmic reticulum: One organelle—many functions in development, maintenance, and plasticity. 78:181–208.

Ludányi, A., S.S.-J. Hu, M. Yamazaki, A. Tanimura, D. Piomelli, M. Watanabe, M. Kano, K. Sakimura, Z. Maglóczky, K. Mackie, T.F. Freund, and I. Katona. 2011. Complementary synaptic distribution of enzymes responsible for synthesis and inactivation of the endocannabinoid 2-arachidonoylglycerol in the human hippocampus. *Neuroscience*. 174:50–63. doi:10.1016/J.NEUROSCIENCE.2010.10.062.

Luini, A. 2011. A brief history of the cisternal progression-maturation model. *Cell. Logist.* 1:6–11. doi:10.4161/cl.1.1.14693.

Mackie, K. 2005. Distribution of Cannabinoid Receptors in the Central and Peripheral Nervous System. *In* Cannabinoids. Springer-Verlag, Berlin/Heidelberg. 299–325.

Mackie, K. 2008. Signaling via CNS cannabinoid receptors. *Mol. Cell. Endocrinol.* 286:S60–S65. doi:10.1016/j.mce.2008.01.022.

Mackie, K., and B. Hille. 1992. Cannabinoids inhibit N-type calcium channels in neuroblastoma-glioma cells. *Proc. Natl. Acad. Sci. U. S. A.* 89:3825–9. doi:10.1073/pnas.89.9.3825.

Mackie, K., Y. Lai, R. Westenbroek, and R. Mitchell. 1995. Cannabinoids activate an inwardly rectifying potassium conductance and inhibit Q-type calcium currents in AtT20 cells transfected with rat brain cannabinoid receptor. *J. Neurosci.* 15:6552–61. doi:10.1523/JNEUROSCI.15-10-06552.1995.

Maejima, T., K. Hashimoto, T. Yoshida, A. Aiba, and M. Kano. 2001. Presynaptic Inhibition Caused by Retrograde Signal from Metabotropic Glutamate to Cannabinoid Receptors. *Neuron*. 31:463–475. doi:10.1016/S0896-6273(01)00375-0.

Mahavadi, S., W. Sriwai, J. Huang, J.R. Grider, and K.S. Murthy. 2014. Inhibitory signaling by CB_1 receptors in smooth muscle mediated by GRK5/β-arrestin activation of ERK1/2 and Src kinase. *Am. J. Physiol. Liver Physiol.* 306:G535–G545. doi:10.1152/ajpgi.00397.2013.

Margeta, M.A., G.J. Wang, and K. Shen. 2009. Clathrin adaptor AP-1 complex excludes multiple postsynaptic receptors from axons in C. elegans. *Proc. Natl. Acad. Sci.* 106:1632–1637. doi:10.1073/PNAS.0812078106.

Marsicano, G., and R. Kuner. 2008. Anatomical Distribution of Receptors, Ligands and Enzymes in the Brain and in the Spinal Cord: Circuitries and Neurochemistry. *In* Cannabinoids and the Brain. Springer US, Boston, MA. 161–201.

Martina, M., I. Vida, and P. Jonas. 2000. Distal initiation and active propagation of action potentials in interneuron dendrites. *Science*. 287:295–300. doi:10.1126/science.287.5451.295.

Martínez-Alonso, E., M. Tomás, and J.A. Martínez-Menárguez. 2013. Morpho-functional architecture of the Golgi complex of neuroendocrine cells. *Front. Endocrinol. (Lausanne).* 4:41. doi:10.3389/fendo.2013.00041.

Martini, L., D. Thompson, V. Kharazia, and J.L. Whistler. 2010. Differential Regulation of Behavioral Tolerance to WIN55,212-2 by GASP1. *Neuropsychopharmacology*. 35:1363–1373. doi:10.1038/npp.2010.6.

Martini, L., M. Waldhoer, M. Pusch, V. Kharazia, J. Fong, J.H. Lee, C. Freissmuth, and J.L. Whistler. 2007. Ligand-induced down-regulation of the cannabinoid 1 receptor is mediated by the G-protein-coupled receptor-associated sorting protein GASP1. *FASEB J.* 21:802–811. doi:10.1096/fj.06-7132com.

Di Marzo, V. 2009. The endocannabinoid system: Its general strategy of action, tools for its pharmacological manipulation and potential therapeutic exploitation. *Pharmacol. Res.* 60:77–84. doi:10.1016/J.PHRS.2009.02.010.

Mascia, F., L. Klotz, J. Lerch, M.H. Ahmed, Y. Zhang, and R. Enz. 2017. CRIP1a inhibits endocytosis of G-protein coupled receptors activated by endocannabinoids and glutamate by a common molecular mechanism. *J Neurochem*. 141:577–591.

Matsuda, L.A., S.J. Lolait, M.J. Brownstein, A.C. Young, and T.I. Bonner. 1990. Structure of a Cannabinoid Receptor and Functional Expression of the Cloned cDNA. *Nature*. 346:561–564. doi:10.1038/346561a0.

Matsuda, S., E. Miura, K. Matsuda, W. Kakegawa, K. Kohda, M. Watanabe, and M. Yuzaki. 2008. Accumulation of AMPA Receptors in Autophagosomes in Neuronal Axons Lacking Adaptor Protein AP-4. *Neuron*. 57:730–745. doi:10.1016/J.NEURON.2008.02.012.

Matsumoto, A., M. Mizuno, N. Hamada, Y. Nozaki, E.F. Jimbo, M.Y. Momoi, K. Nagata, and T. Yamagata. 2014. LIN7A Depletion Disrupts Cerebral Cortex Development, Contributing to Intellectual Disability in 12q21-Deletion Syndrome. *PLoS One*. 9:e92695. doi:10.1371/journal.pone.0092695.

McAllister, S.D., G. Griffin, L.S. Satin, and M.E. Abood. 1999. Cannabinoid receptors can activate and inhibit G protein-coupled inwardly rectifying potassium channels in a xenopus oocyte expression system. *J. Pharmacol. Exp. Ther.* 291:618–26.

McDonald, N.A., C.M. Henstridge, C.N. Connolly, and A.J. Irving. 2007a. An essential role for constitutive endocytosis, but not activity, in the axonal targeting of the CB1 cannabinoid receptor. *Mol. Pharmacol.* 71:976–984. doi:10.1124/mol.106.029348.

McDonald, N.A., C.M. Henstridge, C.N. Connolly, and A.J. Irving. 2007b. Generation and functional characterization of fluorescent, N-terminally tagged CB1 receptor chimeras for live-cell imaging. *Mol. Cell. Neurosci.* 35:237–248. doi:10.1016/j.mcn.2007.02.016.

Mechoulam, R., S. Ben-Shabat, L. Hanus, M. Ligumsky, N.E. Kaminski, A.R. Schatz, A. Gopher, S. Almog, B.R. Martin, D.R. Compton, R.G. Pertwee, G. Griffin, M. Bayewitch, J. Barg, and Z. Vogel. 1995. Identification of an endogenous 2-monoglyceride, present in canine gut, that binds to cannabinoid receptors. *Biochem. Pharmacol.* 50:83–90. doi:10.1016/0006-2952(95)00109-D.

Mendizabal-Zubiaga, J., S. Melser, G. Bénard, A. Ramos, L. Reguero, S. Arrabal, I. Elezgarai, I. Gerrikagoitia, J. Suarez, F. Rodríguez De Fonseca, N. Puente, G. Marsicano, and P. Grandes. 2016. Cannabinoid CB1 Receptors Are Localized in Striated Muscle Mitochondria and Regulate Mitochondrial Respiration. *Front. Physiol.* 7:476. doi:10.3389/fphys.2016.00476.

Mikasova, L., L. Groc, D. Choquet, and O.J. %J P. of the N.A. of S. Manzoni. 2008. Altered surface trafficking of presynaptic cannabinoid type 1 receptor in and out synaptic terminals parallels receptor desensitization. pnas. 0805959105.

Miller, S.G., L. Carnell, and H.H. Moore. 1992. Post-Golgi membrane traffic: brefeldin A inhibits export from distal Golgi compartments to the cell surface but not recycling. *J. Cell Biol.* 118:267–83. doi:10.1083/jcb.118.2.267.

Morgan, D.J., B.J. Davis, C.S. Kearn, D. Marcus, A.J. Cook, J. Wager-Miller, A. Straiker, M.H. Myoga, J. Karduck, E. Leishman, L.J. Sim-Selley, T.A. Czyzyk, H.B. Bradshaw, D.E. Selley, and K. Mackie. 2014. Mutation of Putative GRK Phosphorylation Sites in the Cannabinoid Receptor 1 (CB1R) Confers Resistance to Cannabinoid Tolerance and Hypersensitivity to Cannabinoids in Mice. *J. Neurosci.* 34:5152–5163. doi:10.1523/jneurosci.3445-12.2014.

Morozov, Y.M., M.H. Dominguez, L. Varela, M. Shanabrough, M. Koch, T.L. Horvath, and P. Rakic. 2013. Antibodies to cannabinoid type 1 receptor co-react with stomatin-like protein 2 in mouse brain mitochondria. *Eur. J. Neurosci.* 38:2341–2348. doi:10.1111/ejn.12237.

Moser, E., J. Kargl, J.L. Whistler, M. Waldhoer, and P. Tschische. 2010. G Protein-Coupled Receptor-Associated Sorting Protein 1 Regulates the Postendocytic Sorting of Seven-Transmembrane-Spanning G Protein-Coupled Receptors. *Pharmacology*. 86:22–29. doi:10.1159/000314161.

Mousavi, S.A., L. Malerød, T. Berg, and R. Kjeken. 2004. Clathrin-dependent endocytosis. 377. 1–16 pp.

Munro, S., and H.R.B. Pelham. 1987. A C-terminal signal prevents secretion of luminal ER proteins. *Cell*. 48:899–907. doi:10.1016/0092-8674(87)90086-9.

Munro, S., K.L. Thomas, and M. Abu-Shaar. 1993. Molecular characterization of a peripheral receptor for cannabinoids. *Nature*. 365:61–65. doi:10.1038/365061a0.

Murakami, M., and T. Kouyama. 2008. Crystal structure of squid rhodopsin. *Nature*. 453:363–367. doi:10.1038/nature06925.

Nakatsu, F., M. Okada, F. Mori, N. Kumazawa, H. Iwasa, G. Zhu, Y. Kasagi, H. Kamiya, A. Harada, K. Nishimura, A. Takeuchi, T. Miyazaki, M. Watanabe, S. Yuasa, T. Manabe, K. Wakabayashi, S. Kaneko, T. Saito, and H. Ohno. 2004. Defective function of GABA-containing synaptic vesicles in mice lacking the AP-3B clathrin adaptor. *J. Cell Biol.* 167:293–302. doi:10.1083/jcb.200405032.

Navarrete, M., and A. Araque. 2008. Endocannabinoids Mediate Neuron-Astrocyte Communication. *Neuron*. 57:883–893. doi:10.1016/J.NEURON.2008.01.029.

Navarrete, M., and A. Araque. 2010. Endocannabinoids Potentiate Synaptic Transmission through Stimulation of Astrocytes. *Neuron*. 68:113–126. doi:10.1016/J.NEURON.2010.08.043.

Navarrete, M., A. Diez, and A. Araque. 2014. Astrocytes in endocannabinoid signalling. *Philos. Trans. R. Soc. B-Biological Sci.* 369. doi:10.1098/rstb.2013.0599.

Niehaus, J.L., Y. Liu, K.T. Wallis, M. Egertova, S.G. Bhartur, S. Mukhopadhyay, S. Shi, H. He, D.E. Selley, A.C. Howlett, M.R. Elphick, and D.L. Lewis. 2007. CB1 Cannabinoid Receptor Activity Is Modulated by the Cannabinoid Receptor Interacting Protein CRIP 1a. *Mol. Pharmacol.* 72:1557–1566. doi:10.1124/mol.107.039263.

Nogueras-Ortiz, C., and G.A. Yudowski. 2016. The Multiple Waves of Cannabinoid 1 Receptor Signaling. *Mol. Pharmacol.* 90:620–626. doi:10.1124/mol.116.104539.

Nordström, R., and H. Andersson. 2006. Amino-Terminal Processing of the Human Cannabinoid Receptor 1. *J. Recept. Signal Transduct.* 26:259–267. doi:10.1080/10799890600758252.

Nyathi, Y., B.M. Wilkinson, and M.R. Pool. 2013. Co-translational targeting and translocation of proteins to the endoplasmic reticulum. *Biochim. Biophys. Acta - Mol. Cell Res.* 1833:2392–2402. doi:10.1016/J.BBAMCR.2013.02.021.

Nyíri, G., C. Cserép, E. Szabadits, K. MacKie, and T.F. Freund. 2005. CB1 cannabinoid receptors are enriched in the perisynaptic annulus and on preterminal segments of hippocampal GABAergic axons. *Neuroscience*. 136:811–822. doi:10.1016/J.NEUROSCIENCE.2005.01.026.

Oddi, S., E. Dainese, F. Fezza, M. Lanuti, D. Barcaroli, V. De Laurenzi, D. Centonze, and M. Maccarrone. 2011. Functional characterization of putative cholesterol binding sequence (CRAC) in human type-1 cannabinoid receptor. *J. Neurochem.* 116:858–865. doi:10.1111/j.1471-4159.2010.07041.x.

Oddi, S., E. Dainese, S. Sandiford, F. Fezza, M. Lanuti, V. Chiurchiù, A. Totaro, G. Catanzaro, D. Barcaroli, V. De Laurenzi, D. Centonze, S. Mukhopadhyay, J. Selent, A.C. Howlett, and M. Maccarrone. 2012. Effects of palmitoylation of Cys415 in helix 8 of the CB1 cannabinoid receptor on membrane localization and signalling. *Br. J. Pharmacol.* 165:2635–2651. doi:10.1111/j.1476-5381.2011.01658.x.

Oddi, S., T.M. Stepniewski, A. Totaro, J. Selent, L. Scipioni, B. Dufrusine, F. Fezza, E. Dainese, and M. Maccarrone. 2017. Palmitoylation of cysteine 415 of CB1 receptor affects ligand-stimulated internalization and selective interaction with membrane cholesterol and caveolin 1. *Biochim. Biophys. Acta - Mol. Cell Biol. Lipids*. 1862. doi:10.1016/j.bbalip.2017.02.004.

Oddi, S., A. Totaro, L. Scipioni, B. Dufrusine, T.M. Stepniewski, J. Selent, M. Maccarrone, and E. Dainese. 2018. Role of palmitoylation of cysteine 415 in functional coupling CB 1 receptor to Gα i2 protein. *Biotechnol. Appl. Biochem.* 65:16–20. doi:10.1002/bab.1575.

Odorizzi, G., C.R. Cowles, and S.D. Emr. 1998. The AP-3 complex: a coat of many colours. *Trends Cell Biol.* 8:282–288. doi:10.1016/S0962-8924(98)01295-1.

Ohno-Shosaku, T., T. Maejima, and M. Kano. 2001. Endogenous Cannabinoids Mediate Retrograde Signals from Depolarized Postsynaptic Neurons to Presynaptic Terminals. *Neuron*. 29:729–738. doi:10.1016/S0896-6273(01)00247-1.

Ohno, H., R.C. Aguilar, D. Yeh, D. Taura, T. Saito, and J.S. Bonifacino. 1998. The medium subunits of adaptor complexes recognize distinct but overlapping sets of tyrosine-based sorting signals. *J. Biol. Chem.* 273:25915–21. doi:10.1074/jbc.273.40.25915.

Pan, X., S.R. Ikeda, and D.L. Lewis. 1996. Rat brain cannabinoid receptor modulates N-type Ca2+ channels in a neuronal expression system. *Mol. Pharmacol.* 49.

Pandey, A., D.M. LeBlanc, H.B. Parmar, T.T.T. Phạm, M. Sarker, L. Xu, R. Duncan, X.-Q. Liu, and J.K. Rainey. 2019. Structure, amphipathy, and topology of the membrane-proximal helix 8 influence apelin receptor plasma membrane localization. *Biochim. Biophys. Acta - Biomembr.* 1861:183036. doi:10.1016/J.BBAMEM.2019.183036.

van de Pavert, S.A., A. Kantardzhieva, A. Malysheva, J. Meuleman, I. Versteeg, C. Levelt, J. Klooster, S. Geiger, M.W. Seeliger, P. Rashbass, A. Le Bivic, and J. Wijnholds. 2004. Crumbs homologue 1 is required for maintenance of photoreceptor cell polarization and adhesion during light exposure. *J. Cell Sci.* 117:4169–77. doi:10.1242/jcs.01301.

Pavlos, N.J., and P.A. Friedman. 2017. GPCR Signaling and Trafficking: The Long and Short of It. *Trends Endocrinol. Metab.* 28:213–226. doi:10.1016/J.TEM.2016.10.007.

Pelham, H.R.., and J.E. Rothman. 2000. The Debate about Transport in the Golgi—Two Sides of the Same Coin? *Cell*. 102:713–719. doi:10.1016/S0092-8674(00)00060-X.

Penn, A.C., C.L. Zhang, F. Georges, L. Royer, C. Breillat, E. Hosy, J.D. Petersen, Y. Humeau, and D. Choquet. 2017. Hippocampal LTP and contextual learning require surface diffusion of AMPA receptors. *Nature*. 549:384–388. doi:10.1038/nature23658.

Perego, C., C. Vanoni, S. Massari, R. Longhi, and G. Pietrini. 2000. Mammalian LIN-7 PDZ proteins associate with β-catenin at the cell-cell junctions of epithelia and neurons. *EMBO J.* 19:3978–3989. doi:10.1093/emboj/19.15.3978.

Perez, S.M., J.J. Donegan, A.M. Boley, D.D. Aguilar, A. Giuffrida, and D.J. Lodge. 2019. Ventral hippocampal overexpression of Cannabinoid Receptor Interacting Protein 1 (CNRIP1) produces a schizophrenia-like phenotype in the rat. *Schizophr. Res.* 206:263–270. doi:10.1016/J.SCHRES.2018.11.006.

Pertwee, R.G. 2005. Inverse agonism and neutral antagonism at cannabinoid CB1 receptors. *Life Sci.* 76:1307–1324. doi:10.1016/J.LFS.2004.10.025.

Pertwee, R.G. 2015. Endocannabinoids. Springer.

Pertwee, R.G., A.C. Howlett, M.E. Abood, S.P.H. Alexander, V. Di Marzo, M.R. Elphick, P.J. Greasley, H.S. Hansen, G. Kunos, K. Mackie, R. Mechoulam, and R.A. Ross. 2010. International Union of Basic and Clinical Pharmacology. LXXIX. Cannabinoid Receptors and Their Ligands: Beyond CB1 and CB2. *Pharmacol. Rev.* 62:588–631. doi:10.1124/pr.110.003004.

Peters, A., C.C. Proskauer, and I.R. Kaiserman-Abramof. 1968. The small pyramidal neuron of the rat cerebral cortex. The axon hillock and initial segment. *J. Cell Biol.* 39:604–19. doi:10.1083/jcb.39.3.604.

Pierce, K.L., R.T. Premont, and R.J. Lefkowitz. 2002. Seven-transmembrane receptors. *Nat. Rev. Mol. Cell Biol.* 3:639–650. doi:10.1038/nrm908.

Piomelli, D. 2003. The molecular logic of endocannabinoid signalling. *Nat. Rev. Neurosci.* 4:873–884. doi:10.1038/nrn1247.

Piserchio, A., V. Zelesky, J. Yu, L. Taylor, P. Polgar, and D.F. Mierke. 2005. Bradykinin B2 receptor signaling: Structural and functional characterization of the C-terminus. *Biopolymers*. 80:367–373. doi:10.1002/bip.20220.

Quassollo, G., J. Wojnacki, D.A. Salas, L. Gastaldi, M.P. Marzolo, C. Conde, M. Bisbal, A. Couve, and A. Cáceres. 2015. A RhoA Signaling Pathway Regulates Dendritic Golgi Outpost Formation. *Curr. Biol.* 25:971–82. doi:10.1016/j.cub.2015.01.075.

Rabouille, C., and J. Klumperman. 2005. The maturing role of COPI vesicles in intra-Golgi transport. *Nat. Rev. Mol. Cell Biol.* 6:812–817. doi:10.1038/nrm1735.

Rajagopal, S., and S.K. Shenoy. 2018. GPCR desensitization: Acute and prolonged phases. *Cell. Signal.* 41:9–16. doi:10.1016/J.CELLSIG.2017.01.024.

Rappoport, J.Z. 2008. Focusing on clathrin-mediated endocytosis. *Biochem. J.* 412:415–23. doi:10.1042/BJ20080474.

Razani, B., S.E. Woodman, and M.P. Lisanti. 2002. Caveolae: from cell biology to animal physiology. *Pharmacol. Rev.* 54:431–67.

Reid, D.W., and C. V. Nicchitta. 2015. Diversity and selectivity in mRNA translation on the endoplasmic reticulum. *Nat. Rev. Mol. Cell Biol.* 16:221–231. doi:10.1038/nrm3958.

Rey, A.A., M. Purrio, M.-P. Viveros, and B. Lutz. 2012. Biphasic Effects of Cannabinoids in Anxiety Responses: CB1 and GABAB Receptors in the Balance of GABAergic and Glutamatergic Neurotransmission. *Neuropsychopharmacology*. 37:2624–2634. doi:10.1038/npp.2012.123.

Rinaldi-Carmona, M., A. Le Duigou, D. Oustric, F. Barth, M. Bouaboula, P. Carayon, P. Casellas, and G. Le Fur. 1998. Modulation of CB1 cannabinoid receptor functions after a long-term exposure to agonist or inverse agonist in the Chinese hamster ovary cell expression system. *J. Pharmacol. Exp. Ther.* 287:1038–47.

Ritter, S.L., and R.A. Hall. 2009. Fine-tuning of GPCR activity by receptor-interacting proteins. *Nat. Rev. Mol. Cell Biol.* 10:819–830. doi:10.1038/nrm2803.

Robin, L.M., J.F. Oliveira da Cruz, V.C. Langlais, M. Martin-Fernandez, M. Metna-Laurent, A. Busquets-Garcia, L. Bellocchio, E. Soria-Gomez, T. Papouin, M. Varilh, M.W. Sherwood, I. Belluomo, G. Balcells, I. Matias, B. Bosier, F. Drago, A. Van Eeckhaut, I. Smolders, F. Georges, A. Araque, A. Panatier, S.H.R. Oliet, and G. Marsicano. 2018. Astroglial CB1 Receptors Determine Synaptic D-Serine Availability to Enable Recognition Memory. *Neuron*. 98:935-944.e5. doi:10.1016/J.NEURON.2018.04.034.

Roche, J.P., S. Bounds, S. Brown, and K. Mackie. 1999. A mutation in the second transmembrane region of the CB1 receptor selectively disrupts G protein signaling and prevents receptor internalization. *Mol. Pharmacol.* 56:611–8. doi:10.1124/mol.56.3.611.

Rothman, J., and K. Simons. 1981. The golgi apparatus: two organelles in tandem. *Science (80-.).* 213:1212–1219. doi:10.1126/science.7268428.

Rozenfeld, R. 2011. Type I cannabinoid receptor trafficking: All roads lead to lysosome. *Traffic*. 12:12–18. doi:10.1111/j.1600-0854.2010.01130.x.

Rozenfeld, R., and L.A. Devi. 2008. Regulation of CB 1 cannabinoid receptor trafficking by the adaptor protein AP-3. *FASEB J.* 22:2311–2322. doi:10.1096/fj.07-102731.

Ruiz-Canada, C., D.J. Kelleher, and R. Gilmore. 2009. Cotranslational and Posttranslational N-Glycosylation of Polypeptides by Distinct Mammalian OST Isoforms. *Cell*. 136:272–283. doi:10.1016/J.CELL.2008.11.047.

Salazar, G., R. Love, M.L. Styers, E. Werner, A. Peden, S. Rodriguez, M. Gearing, B.H. Wainer, and V. Faundez. 2004. AP-3-dependent mechanisms control the targeting of a chloride channel (ClC-3) in neuronal and non-neuronal cells. *J. Biol. Chem.* 279:25430–9. doi:10.1074/jbc.M402331200.

Sampo, B., S. Kaech, S. Kunz, and G. Banker. 2003. Two Distinct Mechanisms Target Membrane Proteins to the Axonal Surface. *Neuron*. 37:611–624. doi:10.1016/S0896-6273(03)00058-8.

Sánchez-Fernández, G., S. Cabezudo, C. García-Hoz, C. Benincá, A.M. Aragay, F. Mayor, and C. Ribas. 2014. Gαq signalling: The new and the old. *Cell. Signal.* 26:833–848. doi:10.1016/J.CELLSIG.2014.01.010.

Sarnataro, D., C. Grimaldi, S. Pisanti, P. Gazzerro, C. Laezza, C. Zurzolo, and M. Bifulco. 2005. Plasma membrane and lysosomal localization of CB1 cannabinoid receptor are dependent on lipid rafts and regulated by anandamide in human breast cancer cells. *FEBS Lett.* 579:6343–6349. doi:10.1016/j.febslet.2005.10.016.

Scales, S.J., M. Gomez, and T.E. Kreis. 1999. Coat Proteins Regulating Membrane Traffic. *Int. Rev. Cytol.* 195:67–144. doi:10.1016/S0074-7696(08)62704-7.

Sensoy, O., and H. Weinstein. 2015. A mechanistic role of Helix 8 in GPCRs: Computational modeling of the dopamine D2 receptor interaction with the GIPC1–PDZ-domain. *Biochim. Biophys. Acta - Biomembr.* 1848:976–983. doi:10.1016/J.BBAMEM.2014.12.002.

Shimamura, T., K. Hiraki, N. Takahashi, T. Hori, H. Ago, K. Masuda, K. Takio, M. Ishiguro, and M. Miyano. 2008. Crystal structure of squid rhodopsin with intracellularly extended cytoplasmic region. *J. Biol. Chem.* 283:17753–6. doi:10.1074/jbc.C800040200.

Simon, A.C., C. Loverdo, A.L. Gaffuri, M. Urbanski, D. Ladarre, D. Carrel, I. Rivals, C. Leterrier, O. Benichou, P. Dournaud, B. Szabo, R. Voituriez, and Z. Lenkei. 2013. Activation-dependent plasticity of polarized GPCR distribution on the neuronal surface. *J. Mol. Cell Biol.* 5:250–265. doi:10.1093/jmcb/mjt014.

Simonin, F., P. Karcher, J.J.-M. Boeuf, A. Matifas, and B.L. Kieffer. 2004. Identification of a novel family of G protein-coupled receptor associated sorting proteins. *J. Neurochem.* 89:766–775. doi:10.1111/j.1471-4159.2004.02411.x.

Sloper, J.J., and T.P.S. Powell. 1979. A Study of the Axon Initial Segment and Proximal Axon of Neurons in the Primate Motor and Somatic Sensory Cortices. *Philos. Trans. R. Soc. B Biol. Sci.* 285:173–197. doi:10.1098/rstb.1979.0004.

Smith, T.H., L.C. Blume, A. Straiker, J.O. Cox, B.G. David, J.R.S. McVoy, K.W. Sayers, J.L. Poklis, R.A. Abdullah, M. Egertova, C.-K. Chen, K. Mackie, M.R. Elphick, A.C. Howlett, and D.E. Selley. 2015. Cannabinoid Receptor-Interacting Protein 1a Modulates CB1 Receptor Signaling and Regulation. *Mol. Pharmacol.* 87. doi:10.1124/mol.114.096495.

Song, A., D. Wang, G. Chen, Y. Li, J. Luo, S. Duan, and M. Poo. 2009. A Selective Filter for Cytoplasmic Transport at the Axon Initial Segment. *Cell*. 136:1148–1160. doi:10.1016/J.CELL.2009.01.016.

Song, C., and A.C. Howlett. 1995. Rat brain cannabinoid receptors are N-linked glycosylated proteins. *Life Sci.* 56:1983–1989. doi:10.1016/0024-3205(95)00179-A.

Sönnichsen, B., S. De Renzis, E. Nielsen, J. Rietdorf, and M. Zerial. 2000. Distinct membrane domains on endosomes in the recycling pathway visualized by multicolor imaging of Rab4, Rab5, and Rab11. *J. Cell Biol.* 149:901–14. doi:10.1083/jcb.149.4.901.

Spomer, L., C.G.W. Gertzen, B. Schmitz, D. Häussinger, H. Gohlke, and V. Keitel. 2014. A membrane-proximal, C-terminal α-helix is required for plasma membrane localization and function of the G Protein-coupled receptor (GPCR) TGR5. *J. Biol. Chem.* 289:3689–702. doi:10.1074/jbc.M113.502344.

Stadel, R., K.H. Ahn, and D.A. Kendall. 2011. The cannabinoid type-1 receptor carboxyl-terminus, more than just a tail. *J. Neurochem.* 117:1–18. doi:10.1111/j.1471-4159.2011.07186.x.

Stagg, S.M., C. Gürkan, D.M. Fowler, P. LaPointe, T.R. Foss, C.S. Potter, B. Carragher, and W.E. Balch. 2006. Structure of the Sec13/31 COPII coat cage. *Nature*. 439:234–238. doi:10.1038/nature04339.

Steindel, F., R. Lerner, M. Häring, S. Ruehle, G. Marsicano, B. Lutz, and K. Monory. 2013. Neuron-type specific cannabinoid-mediated G protein signalling in mouse hippocampus. *J. Neurochem.* 124:795–807. doi:10.1111/jnc.12137.

Stornaiuolo, M., L. V. Lotti, N. Borgese, M.-R. Torrisi, G. Mottola, G. Martire, and S. Bonatti. 2003. KDEL and KKXX Retrieval Signals Appended to the Same Reporter Protein Determine Different Trafficking between Endoplasmic Reticulum, Intermediate Compartment, and Golgi Complex. *Mol. Biol. Cell*. 14:889–902. doi:10.1091/mbc.e02-08-0468.

Straiker, A., and K. Mackie. 2005. Depolarization-induced suppression of excitation in murine autaptic hippocampal neurones. *J. Physiol.* 569:501–517. doi:10.1113/jphysiol.2005.091918.

Straiker, A., J. Wager-Miller, J. Hutchens, and K. Mackie. 2012a. Differential signalling in human cannabinoid CB1 receptors and their splice variants in autaptic hippocampal neurones. *Br. J. Pharmacol.* 165:2660–2671. doi:10.1111/j.1476-5381.2011.01744.x.

Straiker, A., J. Wager-Miller, and K. Mackie. 2012b. The CB1 cannabinoid receptor C-terminus regulates receptor desensitization in autaptic hippocampal neurones. *Br. J. Pharmacol.* 165:2652–2659. doi:10.1111/j.1476-5381.2011.01743.x.

Sugiura, H., K. Iwata, M. Matsuoka, H. Hayashi, T. Takemiya, S. Yasuda, M. Ichikawa, T. Yamauchi, P. Mehlen, T. Haga, and K. Yamagata. 2004. Inhibitory role of endophilin 3 in receptor-mediated endocytosis. *J. Biol. Chem.* 279:23343–8. doi:10.1074/jbc.M312607200.

Sugiura, T., S. Kondo, A. Sukagawa, S. Nakane, A. Shinoda, K. Itoh, A. Yamashita, and K. Waku. 1995. 2-Arachidonoylgylcerol: A Possible Endogenous Cannabinoid Receptor Ligand in Brain. *Biochem. Biophys. Res. Commun.* 215:89–97. doi:10.1006/BBRC.1995.2437.

Tang, L.T.-H., T.J. Craig, and J.M. Henley. 2015. SUMOylation of synapsin Ia maintains synaptic vesicle availability and is reduced in an autism mutation. *Nat. Commun.* 6:7728. doi:10.1038/ncomms8728.

Tappe-Theodor, A., N. Agarwal, I. Katona, T. Rubino, L. Martini, J. Swiercz, K. Mackie, H. Monyer, D. Parolaro, J. Whistler, T. Kuner, and R. Kuner. 2007. A molecular basis of analgesic tolerance to cannabinoids. *J. Neurosci.* 27:4165–4177. doi:10.1523/JNEUROSCI.5648-06.2007.

Thibault, K., D. Carrel, D. Bonnard, K. Gallatz, A. Simon, M. Biard, S. Pezet, M. Palkovits, and Z. Lenkei. 2013. Activation-dependent subcellular distribution patterns of CB1 Cannabinoid Receptors in the Rat Forebrain. *Cereb. Cortex*. 23:2581–2591. doi:10.1093/cercor/bhs240.

Thome, C., T. Kelly, A. Yanez, C. Schultz, M. Engelhardt, S.B. Cambridge, M. Both, A. Draguhn, H. Beck, and A. V. Egorov. 2014. Axon-Carrying Dendrites Convey Privileged Synaptic Input in Hippocampal Neurons. *Neuron*. 83:1418–1430. doi:10.1016/J.NEURON.2014.08.013.

Trevaskis, J., K. Walder, V. Foletta, L. Kerr-Bayles, J. McMillan, A. Cooper, S. Lee, K. Bolton, M. Prior, R. Fahey, K. Whitecross, G.J. Morton, M.W. Schwartz, and G.R. Collier. 2005. Src homology 3-domain growth factor receptor-bound 2-like (endophilin) interacting protein 1, a novel neuronal protein that regulates energy balance. *Endocrinology*. 146:3757–3764. doi:10.1210/en.2005-0282.

Turu, G., and L. Hunyady. 2010. Signal transduction of the CB1 cannabinoid receptor. *J. Mol. Endocrinol.* 44:75–85. doi:10.1677/JME-08-0190.

Twitchell, W., S. Brown, and K. Mackie. 1997. Cannabinoids Inhibit N- and P/Q-Type Calcium Channels in Cultured Rat Hippocampal Neurons. *J. Neurophysiol.* 78:43–50. doi:10.1152/jn.1997.78.1.43.

Uezu, A., A. Horiuchi, K. Kanda, N. Kikuchi, K. Umeda, K. Tsujita, S. Suetsugu, N. Araki, H. Yamamoto, T. Takenawa, and H. Nakanishi. 2007. SGIP1□Is an Endocytic Protein That Directly Interacts with Phospholipids and Eps15. *J. Biol. Chem.* 282:26481–26489. doi:10.1074/jbc.M703815200.

Valenzuela, J.I., and F. Perez. 2015. Diversifying the secretory routes in neurons. *Front. Neurosci.* 9:358. doi:10.3389/fnins.2015.00358.

Vershinin, M., B.C. Carter, D.S. Razafsky, S.J. King, and S.P. Gross. 2007. Multiple-motor based transport and its regulation by Tau. *Proc. Natl. Acad. Sci.* 104:87–92. doi:10.1073/PNAS.0607919104.

Weingarten, M.D., A.H. Lockwood, S.Y. Hwo, and M.W. Kirschner. 1975. A protein factor essential for microtubule assembly. *Proc. Natl. Acad. Sci. U. S. A.* 72:1858–62. doi:10.1073/pnas.72.5.1858.

Whistler, J.L., J. Enquist, A. Marley, J. Fong, F. Gladher, P. Tsuruda, S.R. Murray, and M. Von Zastrow. 2002. Modulation of postendocytic sorting of G protein-coupled receptors. *Science*. 297:615–20. doi:10.1126/science.1073308.

Wickert, M., K.L. Hildick, G.L. Baillie, R. Jelinek, A. Aparisi Rey, K. Monory, M. Schneider, R. Ross, J. Henley, and B. Lutz. 2018. The F238L point mutation in the cannabinoid type-1 receptor enhances basal endocytosis via lipid rafts. *Front. Mol. Neurosci.* 11:230.

Wilhelm, B.G., S. Mandad, S. Truckenbrodt, K. Kröhnert, C. Schäfer, B. Rammner, S.J. Koo, G.A. Claßen, M. Krauss, V. Haucke, H. Urlaub, and S.O. Rizzoli. 2014. Composition of isolated synaptic boutons reveals the amounts of vesicle trafficking proteins. *Science*. 344:1023–8. doi:10.1126/science.1252884.

Wilson, R.I., and R.A. Nicoll. 2001. Endogenous cannabinoids mediate retrograde signalling at hippocampal synapses. *Nature*. 410:588–592. doi:10.1038/35069076.

Wilson, R.I., and R.A. Nicoll. 2002. Endocannabinoid signaling in the brain. *Science*. 296:678–82. doi:10.1126/science.1063545.

Wisco, D., E.D. Anderson, M.C. Chang, C. Norden, T. Boiko, H. Fölsch, and B. Winckler. 2003. Uncovering multiple axonal targeting pathways in hippocampal neurons. *J. Cell Biol.* 162:1317–1328. doi:10.1083/JCB.200307069.

Wockner, L.F., E.P. Noble, B.R. Lawford, R.M. Young, C.P. Morris, V.L.J. Whitehall, and J. Voisey. 2014. Genome-wide DNA methylation analysis of human brain tissue from schizophrenia patients. *Transl. Psychiatry*. 4:e339–e339. doi:10.1038/tp.2013.111.

Wood, S.A., J.E. Park, and W.J. Brown. 1991. Brefeldin A causes a microtubule-mediated fusion of the trans-Golgi network and early endosomes. *Cell*. 67:591–600. doi:10.1016/0092-8674(91)90533-5.

Wu, D.-F., L.-Q. Yang, A. Goschke, R. Stumm, L.-O. Brandenburg, Y.-J. Liang, V. Höllt, and T. Koch. 2008. Role of receptor internalization in the agonist-induced desensitization of cannabinoid type 1 receptors. *J. Neurochem.* 104:1132–1143. doi:10.1111/j.1471-4159.2007.05063.x.

Yako, Y.Y., J.B. Echouffo-Tcheugui, E. V. Balti, T.E. Matsha, E. Sobngwi, R.T. Erasmus, and A.P. Kengne. 2015. Genetic association studies of obesity in Africa: a systematic review. *Obes. Rev.* 16:259–272. doi:10.1111/obr.12260.

Yamada, M., A. Inanobe, and Y. Kurachi. 1998. G protein regulation of potassium ion channels. *Pharmacol. Rev.* 50:723–60.

Yap, C.C., R.L. Nokes, D. Wisco, E. Anderson, H. Fölsch, and B. Winckler. 2008a. Pathway selection to the axon depends on multiple targeting signals in NgCAM. *J. Cell Sci.* 121:1514–25. doi:10.1242/jcs.022442.

Yap, C.C., D. Wisco, P. Kujala, Z.M. Lasiecka, J.T. Cannon, M.C. Chang, H. Hirling, J. Klumperman, and B. Winckler. 2008b. The somatodendritic endosomal regulator NEEP21 facilitates axonal targeting of L1/NgCAM. *J. Cell Biol.* 180:827–42. doi:10.1083/jcb.200707143.

Zastrow, M. von. 2003. Mechanisms regulating membrane trafficking of G protein-coupled receptors in the endocytic pathway. *Life Sci.* 74:217–224. doi:10.1016/J.LFS.2003.09.008.

Zavitsanou, K., T. Garrick, and X.F. Huang. 2004. Selective antagonist [3H]SR141716A binding to cannabinoid CB1 receptors is increased in the anterior cingulate cortex in schizophrenia. *Prog. Neuro-Psychopharmacology Biol. Psychiatry*. 28:355–360. doi:10.1016/J.PNPBP.2003.11.005.

Zerial, M., and H. McBride. 2001. Rab proteins as membrane organizers. *Nat. Rev. Mol. Cell Biol.* 2:107–117. doi:10.1038/35052055.

Zhang, J., M. Tan, Y. Yin, B. Ren, N. Jiang, G. Guo, and Y. Chen. 2015. Distinct Functions of Endophilin Isoforms in Synaptic Vesicle Endocytosis. *Neural Plast.* 2015:1–10. doi:10.1155/2015/371496.

Zheng, N., and L.M. Gierasch. 1996. Signal Sequences: The Same Yet Different. *Cell*. 86:849–852. doi:10.1016/S0092-8674(00)80159-2.

Zhou, Y., F. V. Howell, O.O. Glebov, D. Albrecht, G. Williams, and P. Doherty. 2016. Regulated endosomal trafficking of Diacylglycerol lipase alpha (DAGLα) generates distinct cellular pools; implications for endocannabinoid signaling. *Mol. Cell. Neurosci.* 76:76–86. doi:10.1016/J.MCN.2016.08.011.

Zhu, B., R.E. Carmichael, L. Solabre Valois, K.A. Wilkinson, and J.M. Henley. 2018. The transcription factor MEF2A plays a key role in the differentiation/maturation of rat neural stem cells into neurons. *Biochem. Biophys. Res. Commun.* 500:645–649. doi:10.1016/J.BBRC.2018.04.125.

Chapter 8 – APPENDIX I: PUBLICATION